Optimization of Critical Metals Recycling Processes : Localized Spectroscopy and Insight into Extraction Processes using Ionic Liquids

Antonio de Braga Souza Neto

ÉCOLE DOCTORALE 388
CHIMIE PHYSIQUE ET CHIMIE ANALYTIQUE DE PARIS CENTRE

THÈSE DE DOCTORAT

pour l'obtention du titre de

Docteur en Sciences de Sorbonne Université
Mention : Chimie

Présentée et soutenue par

Antonio De Souza Braga Neto

Optimization of Critical Metals Recycling Processes: Localized Spectroscopy and Insight into Extraction Processes using Ionic Liquids

Thèse dirigée par Juliette Sirieix-Plénet et co-encadrée par
Anne-Laure Rollet, Baptiste Rigaud et Guillaume Mériguet

soutenue le 28 septembre 2023 devant un jury composé de :

Mario Ávila Rodríguez ..... President du Jury
Maria Boltoeva ..... Rapporteure
Sabine Bouguet-Bonnet ..... Rapporteure
Michel Bardet ..... Examinateur
Juliette Sirieix-Plénet ..... Directrice de thèse
Baptiste Rigaud ..... Invité

Acknowledgments

I wish to express my profound gratitude to everyone who played a role, small or large, in materializing this thesis.

I want to express my deep appreciation to Mario Ávila Rodríguez for accepting the position of president for my thesis jury and for providing me with valuable feedback on my work. I would also like to sincerely thank Maria Boltoeva and Sabine Bouguet-Bonnet for agreeing to review my thesis and for their invaluable insights. Additionally, I am grateful to Michel Bardet for his dedication to examining my thesis and for his genuine interest in my research.

My most profound appreciation goes to my thesis director, Juliette Sirieix-Plénet, for entrusting me with this endeavor; support, patience, and invaluable advice have been essential. A special acknowledgment to Baptiste Rigaud for his expertise and dedicated guidance on the NMR technique. Anne-Laure Rollet's precious guidance, expert insights, and ever-present humor have been foundational. Equally, I'm thankful to Guillaume Mériguet for his thorough feedback and consistent support throughout my thesis.The collective wisdom, dedication, and enriching discussions of this team have been instrumental, and I am eternally grateful.

Further gratitude is extended to Natalie Malikova and Laurent Michot for their instrumental assistance with the SAXS experiments and succeeding discussions. My scientific collaborations with Stella and Ousmane were pleasing, and I thank them enthusiastically. Delphine Talbot, Ana Porras-Gutierrez, and Sandrine Leclerc were helpful in their hands-on support with experiments and sourcing materials. I must also recognize intern Marie for her dedicated work and interest in my thesis project.

The PHENIX laboratory has been a special place for me over these thesis years, and my gratitude is infinite. I express my deepest thanks to the entire NMR platform of Sorbonne University, especially Imane Senoussaou, for their support during exhaustive experiment hours. My office and corridor mates have cheered many lunches, coffee breaks and have taught me some French. Special thanks to Alice, Gérard, Cynara, Stella, Alexandros, Laurent Gaillon, Cécile Rizzi, Véronique Peyre, and Alex for making every day brighter.

The friendship and support from friends I made and those far away who stayed close have encouraged me during this journey. Thais, François-Xavier, Nicolas, Vanessa, Carlos, Flavia, Mateus, Anna, Douglas, Ari, Carol, Vivian, Adrien, and everyone from Maison du Brésil and Fondation Suisse, your companionship has been essential to me.

I thank the non-permanent group for the insightful scientific exchanges and lively bar discussions. Names such as Ana Alice, Guilherme, Sarrah, Roxanne, Minh-thé, Claire, Tzu-Yao, Jeanne, Camille, Loic, Sivagen, Ali, Pierre, Maxime, Lydia, and so many others will always remind me of the vibrant atmosphere and shared experiences.

Lastly, my deepest love and thanks go to my family back in Brazil. To my parents, Vania and Antonio, who have consistently supported my academic pursuits. My grandmothers, Filomena and Dejanira, who embarked on this journey with me, always kept me in their prayers and thoughts and will forever be in my heart.

In reflection, every individual mentioned, and those inadvertently left out, have played an integral role in my journey. Their contributions, support, and relationships have indelibly impacted my academic and personal growth.

Contents

List of Acronyms

ABS aqueous biphasic system

[C_4mim][TFSI] 1-butyl-3-methylimidazolium bis(trifluoromethylsulfonyl)imide

[Chol] cholinium

[Chol][TFSI] choline bis(trifluoromethylsulfonyl)imide

D distribution ratio

D_2O deuterium oxide

[D2EHP] bis(2-ethyhexyl) phosphate

D2EHPA di-2-ethylhexylphoshoric acid

DMSO dimethylsulfoxide

DOSY Diffusion Ordered Spectroscopy

ξ correlation length

% E percentage extraction

EDX Energy-Dispersive X-ray Analysis

EU European Union

EXAFS Extended X-ray Absorption Fine Structure

HLLE Homogeneous Liquid-Liquid Extraction

HOESY Heteronuclear Overhauser Effect SpectroscopY

[Hbet] betainium

[Hbet][TFSI] betainium bis(trifluoromethylsulfonyl)imide

ICP-OES inductively-coupled plasma optical emission spectroscopy

IL ionic liquid

IL:aq ionic liquid and aqueous phase mass ratio

K_a acid dissociation constant

LCST Lower Critical Solution Temperature

LOCSY LOCalized SpectroscopY

NMR nuclear magnetic resonance

NOESY Nuclear Overhauser Effect Spectroscopy

PGE platinum-group element

%S percentage stripping

SAXS Small-angle X-ray scattering

τ_C correlation time associated with the local Brownian motion

T_1 spin-lattice (or longitudinal) relaxation time

T_2 spin-spin (or transverse) relaxation time

TGA Thermal gravimetric analysis

TBP tri-n-butylphosphate

[TFSI] bis(trifluoromethylsulfonyl)imide

[TOPO]
Trioctylphosphine oxide

TXRF Total-Reflection X-ray Fluorescence

UCST Upper Critical Solution Temperature

UV-VIS ultraviolet-visible

XRD X-ray diffraction

General Introduction

The liquid-liquid extraction (LLE), a fundamental element in hydrometallurgical processing, plays a pivotal role in the recycling of critical metals. This process is integral to these valuable resources' recovery and sustainable use. In recent years, developing and applying Ionic Liquids (ILs) have marked a significant advancement in this field. These substances have risen as superior alternatives to the traditional volatile organic solvents typically employed in such processes. The growing preference for ILs is rooted in their numerous advantageous properties. These include a marked reduction in toxicity, a non-flammable nature, and significantly lower volatility. Such characteristics render ILs environmentally safer and more efficient and effective in operational contexts.

Within the broad scope of LLE, a specific category of ILs, known as thermomorphic ILs, has demonstrated exceptional functionality. These ILs are particularly noted for their Homogeneous Liquid-Liquid Extraction (HLLE) capabilities. A defining feature of thermomorphic ILs is their unique temperature-dependent miscibility with aqueous solutions. This allows for a complete and thorough mixing of the phases involved in the extraction process. Such a characteristic is highly beneficial as it eliminates the interface barriers often encountered in conventional extraction setups. The result is a more streamlined and efficient process, enhancing both the efficacy and yield of the extraction.

This thesis delves into the nuanced roles and applications of these innovative ILs within the context of LLE. By exploring the chemical and physical properties of thermomorphic ILs, we aim to elucidate their mechanisms of action and the resulting implications for metal extraction processes. The focus on temperature-dependent miscibility offers a window into understanding how these ILs can be manipulated and optimized for specific extraction requirements. Moreover, the study highlights the environmental benefits of using ILs, considering their reduced toxicity and lower environmental impact than traditional solvents.

Nuclear Magnetic Resonance spectroscopy (NMR) has transformed the study of LLE processes. NMR stands out as a sophisticated analytical technique, enabling comprehensive investigation of all entities within the extraction system, including the ionic liquid, extractant, water, and specific metal ions. This thesis contributes significantly to the field by providing detailed insights and methodologies for enhancing the understanding and efficiency of these extraction systems, focusing on both the chemical and environmental aspects.

The thesis is structured into several chapters, each addressing key aspects of LLE with ILs:

- The first chapter presents an overview of the latest developments in the application of ionic liquids for solvent extraction in the recycling of metals. It emphasizes the role of ILs in promoting sustainable and safer extraction practices.

- The second chapter offers an in-depth look into the production of ILs, detailing the synthesis processes, HLLE experimental protocols, and the theoretical underpinnings of NMR. It also explores how nuclear resonance spectroscopy is applied in studying analogous extraction systems, underscoring its critical role in advancing the field.

- In the third chapter, the focus shifts to applying localized spectroscopy (LOCSY). This section delves into how this technique enhances our understanding of the dynamics and mechanics of liquid-liquid extraction processes.
- The fourth chapter investigates lithium extraction from aqueous solutions using thermomorphic IL systems. This section evaluates the process's effectiveness and considers its environmental impacts and sustainability.
- The fifth chapter thoroughly explores platinum extraction using thermomorphic IL systems. This involves an analysis of both the technical mechanisms and the practical, real-world applications of these systems.
- The concluding chapter synthesizes the principal findings of the research, discussing the broader implications and suggesting future research directions. This final section aims to provide a holistic view of the advancements made in the field and the potential pathways for further exploration and application.

Through this approach, the thesis aims to deepen the understanding of ILs in hydrometallurgical processes, specifically focusing on the innovative application of thermomorphic ILs in liquid-liquid extraction. The comprehensive treatment of topics ranging from chemical synthesis to practical applications reflects the multifaceted nature of this field and underscores the potential of ILs in metal recycling processes. In the broader perspective of metal recovery and recycling, this research contributes to the ongoing efforts to develop more sustainable and eco-friendly industrial practices. By harnessing the unique properties of ILs, we can pave the way for more efficient and less harmful extraction techniques. This benefits the environment and supports the sustainable management of metal resources, which are crucial in various industries and technologies.

Chapter 1

State of the art

Contents

1.1 Critical metals

The continuous growth of the global population, industrialization, and the use of electronic devices have been boosting the demand for metal resources. Terms such as critical raw material (CRM) or critical metals appear to describe resources with a combined high supply risk and high economic importance. Figure 1.1 shows the overall results of the criticality assessment made by the European Commission in 2020 [1].

The economic importance of these metals is linked to their applications and possible substitution. Critical metals are essential in modern society for technological advancement in strategic sectors and for enhancing the quality of life. Besides, they are associated with low-carbon technologies, which are vital for achieving carbon neutrality goals. Raw materials are necessary for solar panels, wind turbines, energy-efficient lighting, and electric vehicles [2–4]

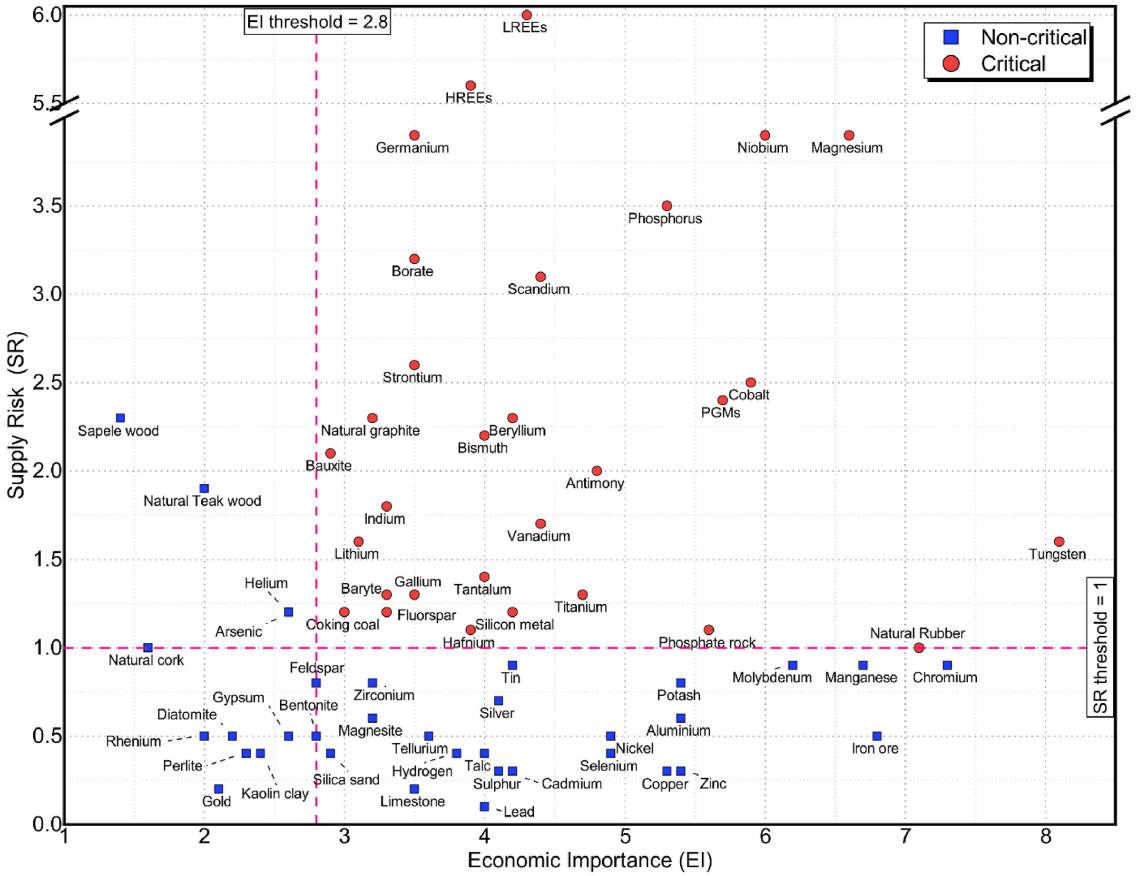

Figure 1.1: Economic importance and supply risk results of 2020 criticality assessment by the European Commission [5].

Moreover, the supply risk is related to supply concentration in determined countries, poor governance in these countries, recycling rates, existence, and the criticality of possible substitutes. Figure 1.2 presents the countries accounting for the largest share of the global supply of CRMs. As observed, several critical raw materials appear in China. Russia and South Africa are the most significant global suppliers of platinum group metals (PGM), and Chile for Lithium.

Circular economy strategies, such as end-of-life collection and recycling, can assist the

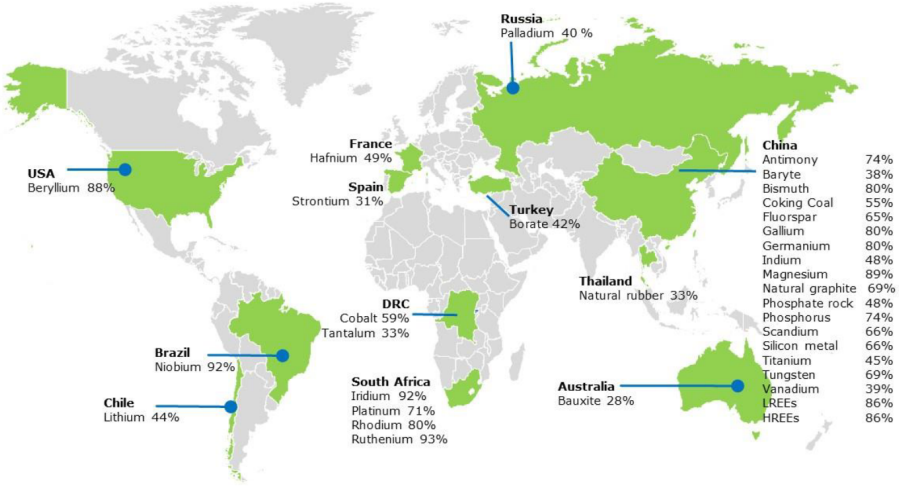

Figure 1.2: Countries accounting for the largest share of the global supply of CRMs [1].

supply chain for many critical metals. Figure 1.3 shows the recycling rates for several metals, and critical metals have low recycling rates. For example, the recycling rate for lithium is lower than 1 %. According to Karali and Shah, end-of-life collection and recycling could allow some secondary resources to fulfill 37 % to 91 % of the demand for CRMs in clean technologies in 2050 [4]. Secondary resources refer to the context of technospheric mining, in other words, the secondary mining of raw materials from the technosphere, which is part of the environment made or modified by humans. In contrast, primary resources refer to primary mining, which extracts raw materials from the Earth's crust. Lithium and platinum included in the larger platinum group metals (PGMs), that are placed in the critical metal quadrant (figure 1.1) and which are very insufficiently recycled (figure 1.3), are the main metallic species studied in the present work.

1.1.1 Lithium

Lithium is an alkali metal and the lightest of the metals. It plays a crucial role in the energy transition to reduce global warming. Lithium-ion batteries allow the storage of energy from renewable sources, for example, hydroelectric and solar, reducing fossil fuel burn emissions. Besides, there is a growing market for portable electronic devices and the rising use of electric tools. The estimated global primary lithium reserves are around 26 million tons [7]. However, more than this amount of resources is needed to meet the projected demand by 2100. Only the EU by itself would need almost 60 times more Li in 2050, compared to the 2020 production, to meet its low carbon emission goals [1].

Nowadays, the main primary sources of lithium are brines pumped from beneath arid sedimentary basins and granitic pegmatite ores. Chile is the leading producer of lithium from brine, while Australia is the primary producer of lithium from pegmatites. Other potential sources of primary lithium include clays, geothermal brines, oilfield brines, and zeolites [8].

The increased utilization of lithium-ion batteries (LIBs) is expected to result in increased recycling of lithium from batteries. Lithium-ion battery recycling is expected to play an essential role in the lithium supply in the future, being the main secondary source of this metal [9, 10].

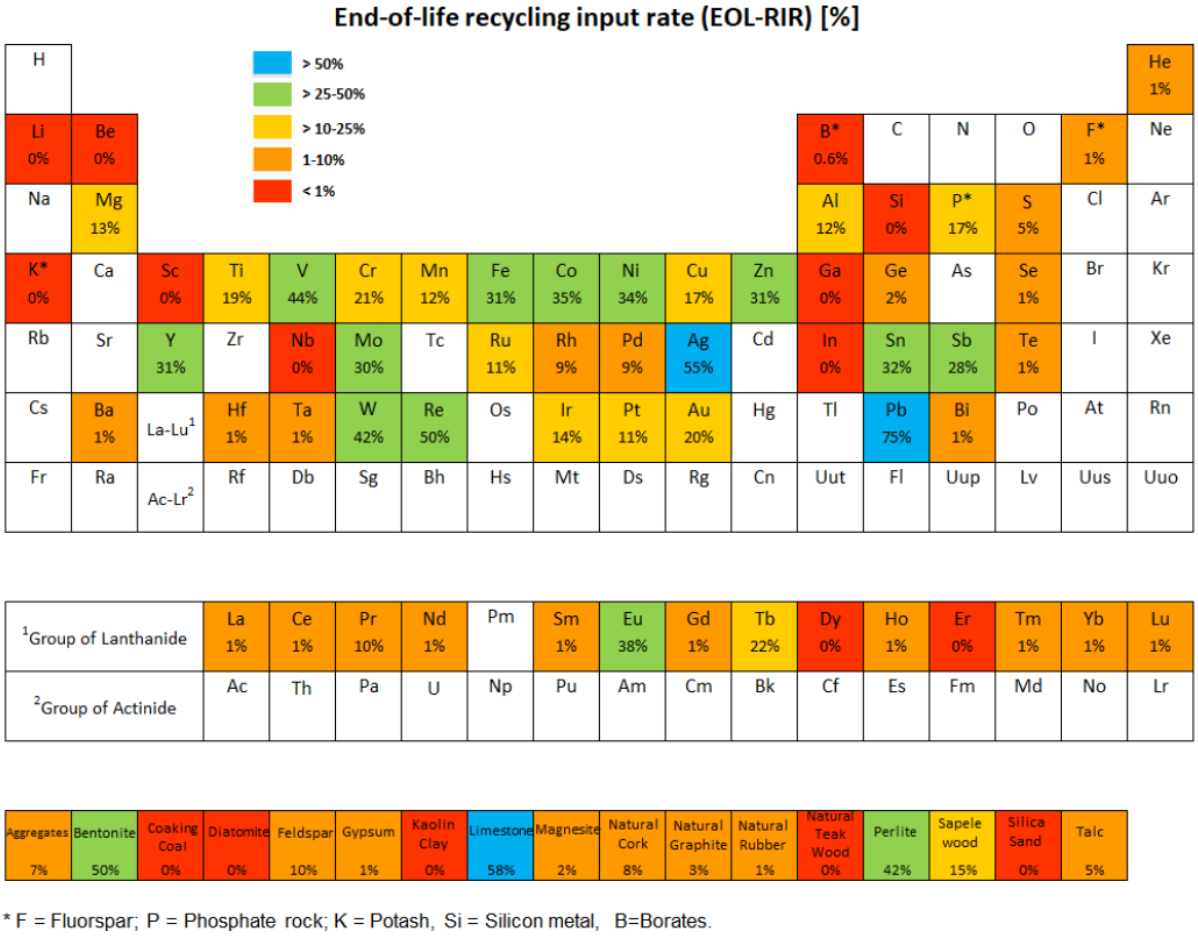

Figure 1.3: End-of-life recycling rates for different metals [6].

1.1.2 Platinum

The platinum-group elements or metals (PGEs or PGMs), platinum, palladium, rhodium, ruthenium, iridium, and osmium, share comparable physical and chemical characteristics and are typically found co-existing naturally. Their critical role in numerous industrial applications is undeniable, yet their extraction is restricted to a few locations. Economic conditions, environmental concerns, and political and social issues can potentially interrupt the supply and accessibility of these precious metals.

PGMs, among the rarest metals, are found in very low concentrations in the Earth's upper crust, with only approximately 0.05 parts per billion of platinum present. Ores primarily mined for their PGM concentrations typically have an average grade ranging from 5 to 15 ppm. However, the best ore specimens may contain significantly higher concentrations, ranging from tens to hundreds of parts per million [11].

These metals play a crucial role in various industries. For instance, they are utilized in catalytic converters to effectively reduce harmful emissions like carbon monoxide, hydrocarbons, and nitrous oxide from automobile exhaust. The production of explosives, fertilizers, and nitric acid, specifically nitric oxide, relies on using platinum or platinum-rhodium alloys. Platinum catalysts are essential in refining crude oil and producing aromatic compounds and high-octane gasoline. PGMs alloys demonstrate exceptional toughness and durability, making them highly desirable for coating industrial crucibles used in manu-

facturing chemicals and synthetic materials. The glass manufacturing industry relies on PGMs for the production of fiberglass, as well as flat-panel and liquid crystal displays. Moreover, PGMs find applications in the electronics industry, where they are utilized in computer hard disks, hybridized integrated circuits, and multilayer ceramic capacitors. In addition, platinum is utilized in medical implants like pacemakers, and PGMs play a role in developing cancer-fighting drugs. The white color, strength, and tarnish resistance of platinum alloys make them a popular choice for jewelry. Furthermore, platinum, palladium, and rhodium in the form of coins and bars serve as investment commodities, and financial instruments linked to the value of these PGMs are traded on significant exchanges [11].

Platinum group metals can be found in more than 100 minerals and occur as native metals. They can be found in combination with various other elements, including transition metals, post-transition metals, and metalloids, such as copper, iron, mercury, nickel, silver, bismuth, lead, tin, antimony, arsenic, and tellurium, as well as non-metals such as selenium and sulfur. South Africa, Zimbabwe, and Russia have the three geologic deposits that together account for almost all production and identified resouces [11].

Around 90% of PMGs' global production can be attributed to South Africa and Russia. Recycled catalytic converters from end-of-life vehicles, jewelry, and electronic equipment are a substantial secondary source of platinum, palladium, and rhodium. These recycled materials contribute to a considerable part of the total global supply. The volume derived from these secondary sources effectively fills the disparity between the global mining production and its consumption demand [12, 13]. Therefore, it is essential to recycle these metals to ensure a sustainable supply.

1.1.3 Recovery of critical metals from secondary sources

Recycling metals is a way to improve society's resource efficiency. Various metal recycling processes can be divided into pyrometallurgical, hydrometallurgical, and hybrid routes. The industrial pyrometallurgical process used on primary and secondary ores does not fulfill the required criteria of waste control and low energy consumption [14]. Hydrometallurgy is an interesting alternative that still needs improvements in reducing effluents, operation costs, efficiency, and selectivity. In that process, recovery of metal ions is usually obtained after the first leaching of the scraps. Leaching involves dissolving the material in acid media and occurs after mechanical pretreatment. Leaching is followed by a solvent extraction step that should be able to extract each type of ion to recover them separately selectively. Both leaching and extraction steps require incremental processes, relying on precise experimental conditions tuning that depends on the material's chemical composition and particle size distribution for efficient recycling [3, 15, 16].

The main secondary source for lithium, LIBs, contains valuable metals besides lithium, such as cobalt, nickel, manganese, and more, making their recycling more economically feasible. Their recycling process is carried out in a series of stages, comprising hydrometallurgical and pyrometallurgical operations. However, lithium is usually not the main metal focus in the process. For instance, in LIBs recycling, cobalt, manganese, and nickel are extracted preferably, and lithium is left in the leaching solution [3, 9, 17]. Therefore, providing tools specifically aimed at this metal is crucial to encourage and enhance its recycling and primary mining.

Platinum from catalytic converters in end-of-life vehicles is the main secondary source

of this metal. Jewelry and electronic equipment can also be recycled to obtain platinum. Recycling this precious metal and other PGMs plays a crucial role in meeting global demand, as the secondary sources might contribute significantly to filling the gap between world mine production and consumption [11].

1.2 Liquid-liquid extraction

Solvent or liquid-liquid extraction is a broadly used technique because of its simplicity, speed, and wide application. Commonly, it is assumed to be an ideal method of separating trace constituents from large amounts of other substances [15, 16, 18]. The process is regularly very selective, and the separation of the solute of interest can usually be made as complete as desired by several repetitions of the extraction procedure. Solvent extraction kinetics is a function of the rates of chemical changes in the system and the rates of diffusion of the various species that control the chemical reactions. Different chemical interactions can arise where the formation of new coordination compounds, dissociation or association, and aggregation are possible [15]. The solvent extraction finds utility in various sectors, such as pharmaceutical and biomedical industries, for organic solute separation. It's also employed in environmental waste treatment and metal separation industries. Solvent extraction is a fundamental technique, especially in the field of metal extraction.

In a classic view of metal separation, solvent extraction is the distribution of a solute or solutes between two immiscible liquids or phases. This allocation of a solute or solutes usually occurs within aqueous and organic solutions at ambient pressures and temperatures. Typically, solvent extraction involves dissolving extractants in an organic solvent like kerosene or toluene and then bringing it in contact with the aqueous phase containing the metal. The effectiveness of these extraction systems is high [15]. However, the safety and environmental concerns arising from the volatility and flammability of organic solvents are significant. As a result, the utilization of ionic liquids as substitute solvents for solvent extraction has been studied [19–21]. The distribution of the solute is influenced by interactions between the solute and solvent, such as interactions between metal and water in the aqueous phase. It also depends on the reactions of the solute with other species in either the organic or aqueous phase, for example, complex formation and interactions of the complex or solute with the organic phase. The properties of liquids, such as viscosity, surface tension, vapor pressure, density, polarity, and dielectric constant, are essential in solvent extraction techniques [16].

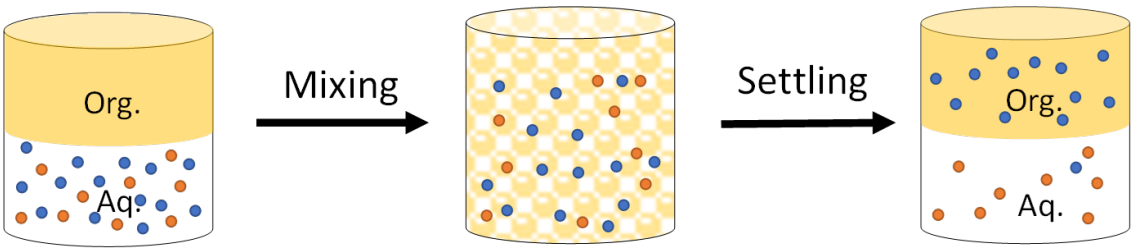

Figure 1.4: Liquid-liquid extraction simplified scheme.

In liquid-liquid extraction processes, one of the fundamental steps is recycling the organic phase. After extracting the desired component from the feed solution into the or-

ganic phase and subsequent stripping or back-extraction to recover the solute, the organic phase, now essentially free of the extracted solute, is recycled and reintroduced into the extraction system. This recycling not only significantly reduces operational costs but also contributes to the sustainability of the process. It minimizes the consumption of solvents, which can be expensive and environmentally impactful. Furthermore, reducing the need for fresh solvent inputs curtails environmental risks and the potential hazards associated with the transport and storage of volatile or toxic solvents [15, 16].

1.2.1 Terms and variables

The solvent enriched phase in one or more solutes is called an *extract*. The feed solution in which the solute, or solutes, are removed is called the *raffinate*. The feed aqueous phase comprises acids dissolved in water, solute, or a mixture of solutes and contamination compounds. While the organic phase usually contains an extractant dissolved in a diluent and, in some cases, a phase modifier. The diluent is mainly used to reduce viscosity and dilute the extractant. The phase modifier is combined to enhance the system's physical properties, avoiding, for example, third phase formation and improvement of extractant [15, 16]. Solvent extraction has received considerable attention because of its high efficiency in metal recovery and has been widely used to separate and purify metals.

The *distribution ratio*, D (eq. 1.1), is a thermodynamic indicator of how the solute is distributed between the two phases. It is defined as the ratio of the analytical concentration of the solute in the organic phase ($[M]_{\text{org}}$) to the analytical concentration in the aqueous phase ($[M]_{\text{aq}}$):

$$D = \frac{[M]_{\text{org}}}{[M]_{\text{aq}}} \tag{1.1}$$

A more practical quantitative view on the amount of solute extracted to the organic phase can be given by the *extraction efficiency* or percentage extraction, $\%E$ (eq.1.2), is defined as the amount of solute in the organic phase over the total amount of solute in both phases.

$$\%E = \frac{\text{Amount of solute in the organic phase}}{\text{Total amount of solute in both phases}} \tag{1.2}$$

The efficiency of extraction, $\%E$, can be related to the distribution ratio, D, with the volumetric phase ratio, v. This relationship is shown in Equation 1.3 bellow.

$$\%E = \frac{D \cdot v}{1 + D \cdot v} \tag{1.3}$$

The volumetric phase ratio is defined as the volume ratio of the organic phase to the aqueous phase, Equation 1.4. V_{org} is the volume of the organic phase, and V_{aq} volume of the aqueous phase.

$$v = \frac{V_{org}}{V_{aq}} \tag{1.4}$$

The extraction efficiency is not only influenced by D but also by v. In many instances, as v changes, it can affect the equilibrium of the extraction process, subsequently impacting the value of $\%E$.

1.2.2 Extraction Mechanisms

Solvent extraction allows the separation of organic and inorganic species. Organic compounds are usually easily dissolved in organic solvents, but inorganic substances do not. Then, they must be modified to be extracted by reaction with an organic compound, extractants, or extracting agents. This process is described as a reactive extraction or extraction with complexation [15]. Extraction can occur through solvation, anion, and cation exchange. Solvation is the interaction of a solute with the solvent, stabilizing the solute species in a solution.

Anion Exchange. In solvent extraction by anion exchange, metal ions react with inorganic ligands to form negatively charged complexes extracted into organic solvents with basic extractants, usually large organic cations. Basic extractants are mainly primary, secondary, and tertiary amines in their protonated form. Still, quaternary ammonium salts are also classified as basic extractants. Usually, long alkyl chains are added to the nitrogen center to decrease the water solubility of the salts. This process can work with various anions ligands, but Cl^-, NO_3^-, SO_4^{2-} are mainly studied. The complex formation can be very diverse for each metal ion in a mixture, then high selectivity can be obtained if a proper anion ligand is selected for a specific metal. The equation 1.5 generally represents an anion extraction process, where M represents the metal, X is a ligand, and B is an extractant.

$$\mathrm{MX_{x_{aq}}^{n-}} + n\ HX_{\mathrm{aq}}^- + n\mathrm{B_{org}} \rightarrow [\mathrm{BH}]_n[\mathrm{MX_x}]_{\mathrm{org}} + n\ X_{\mathrm{aq}}^- \tag{1.5}$$

How well the metal complex is extracted into the organic phase depends on the aggregation of extracted species, the dipole moment of the complex, and the polarity of the solution. Due to the concentration effects, the complexes can form aggregates or not, and the preference of these aggregates for one of the two phases can be modified. For example, aggregates with low dipole moments will preferably be extracted to an organic phase with a low dielectric constant. Other factors, such as electrostatic interactions and hydrogen bonding, also affect distribution and selectivity, but these mechanisms are still not fully understood. Lastly, stripping can be achieved by contacting the loaded organic phase with a low-concentration solution of the coordinating anion or increasing the pH to deprotonate the extractant in the case of amines.

Cation Exchange. Cation exchangers or acidic extractants can replace their acidic protons with metal cations in this mechanism. Thus, they can extract the metal as cations, M^{z+}. Simultaneously, these extractants release their acidic protons to the aqueous phase. The extraction mechanism can be described by the following simplified equation:

$$\mathrm{M_{aq}^{z+}} + z\ \mathrm{HA_{org}} \rightarrow \mathrm{MA}_{z\,\mathrm{org}} + z\ \mathrm{H_{aq}^+} \tag{1.6}$$

As denoted in equation 1.6 that extraction is pH dependent. High pH values are beneficial in this type of metal extraction, but the solvent and the concentrations can also influence the extraction. Simplistically, in this mechanism, interactions between the extractant and diluent have to be diminished, and the extractant in the organic phase comes into equilibrium with the aqueous phase. Once present in the aqueous phase, the acidic extractant should be able to dissociate into a proton and the corresponding anion, which

depends on the acidity of the extractant (K_a). The deprotonated extractant needs to be dehydrated to coordinate with the metal ion. Once the metal-ion interaction occurs and forms a metal complex, it is distributed between the phases [15]. The common idea is that the metal is usually extracted by a dimer $(HA)_2$, not by the single extractant, creating the $M(HA_2)_n$ mix in the organic phase. However, even more complicated oligomeric structures can be formed, which can occur in the organic phase. These structures in the organic phase have a coordinating sphere comprising the extractant A^- after losing a proton, the extractant HA after gaining a proton, and water. The type of structure formed depends on the extractant and diluent used [22]. Finally, stripping can be achieved by putting the loaded organic phase in an acidic solution. Commercial acidic extractants are generally carboxylic acids, organophosphorus acids such as mono and dialkylphosphoric acids, dialkylphosphonic acids and dialkylphosphinic acids, and chelating acidic extractants such as β-diketones [15, 16].

Solvation. Neutral extractants are organic compounds that efficiently dissolve and transport metal ions, along with their related ions, to the organic phase. These metal ions, highly hydrated in the water phase, don't naturally interact with the organic phase. Neutral extractants have the ability to substitute the hydration water around the metal ions, creating a water-repelling compound and moving the metal to the organic phase. This process of dissolving metal salts is why neutral extractants are also known as solvating extractants. The extraction mechanism for a metal salt (MX_z) is represented below. Where S is the neutral extractant, and X represents an anion.

$$M^{x+}_{aq} + n\ S_{org} + x{X^-}_{org} \rightarrow MS_nX_{xorg} \tag{1.7}$$

Common examples of neutral extractants include phosphate esters like tri-n-butyl phosphate (TBP), phosphine oxides like tri-n-octylphosphine oxide (TOPO), and solvating solvents like ethers and ketones [15, 16].

1.3 Ionic Liquids

Some authors might have a more extensive definition of an Ionic liquid (IL) as: '*A liquid comprised entirely of ions*'. In a practical way, Room Temperature Ionic liquids (RTILs) are often shortened to Ionic Liquids and are traditionally defined as salts that are liquid below 100 °C [23, 24].

The definition of the word "ion" in this context necessitates further discussion once metal ion and ionic complexes are involved in this work. Certain species, like Cl^-, are easily identifiable as simple molecular ions such as $[NO_3]^-$. However, the situation becomes more intricate when metal coordination complex ionic species are analyzed, such as $[AlCl_4]^-$. These are ionic species, and as long as they remain bound in the actual liquid for extended periods, they align with the IL definition. Nevertheless, there is always an equilibrium process through which such complex species form, and thus, we must always acknowledge the presence of some amount of the component species in equilibrium. In the case of $[AlCl_4]^-$, these components could be Al^{3+} and Cl^-. As long as these involved components are also ionic, it is still an IL, although this speciation, along with its response to variables like temperature, can significantly influence the properties of the IL [23].

The structure of an ionic liquid can be abbreviated as [Cation]Anion]. Most ionic liquids consist of bulky organic cations and organic or inorganic anions. Millions of different simple ionic liquids can be prepared by combining other cations and anions. Some common IL cations and anions are presented below, Figure 1.5.

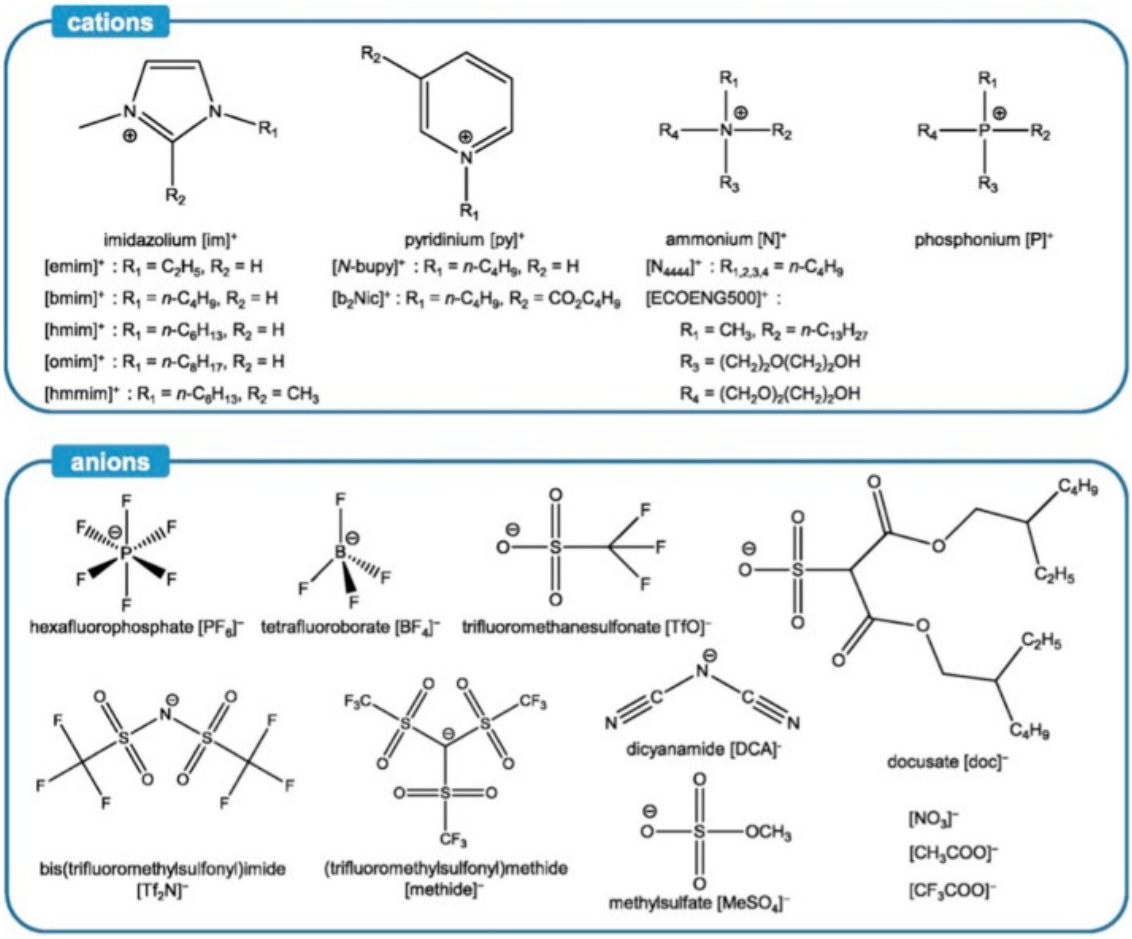

Figure 1.5: Common cations and anions found in the structures of ILs [25].

ILs have unique properties that make them suitable for various applications. Their low melting points and stability make them ideal for pharmaceutical applications, mainly as pharmaceutical salts. ILs are also used in synthetic reactions, materials processing, and gas separation, where their unique solvation environments are advantageous [24, 26]. In biomass processing, ILs aid in dissolving and processing complex biomaterials. They also find applications in biotechnology, as they can dissolve and stabilize enzymes, proteins, DNA, and RNA [27].

The excellent electrochemical stability of certain ILs makes them valuable in electrochemical devices, electrowinning processes, water splitting, and metal-air batteries [28]. ILs are used as catalysts and synthetic media in various synthetic reactions, including organic, inorganic, and biological synthesis [29]. Their ability to dissolve insoluble materials and stabilize nanoparticle dispersions is beneficial in materials synthesis [30]. Chiral ILs are employed in stereoselective synthesis, chromatography, and spectroscopy [24].

ILs are also utilized as heat transfer fluids, lubricants, and in the field of energetic materials [31]. They offer advantages in sensors, particularly electrochemical sensors, due

to their wide electrochemical window and nonvolatility.

The main disadvantage of ionic liquids is their high viscosity at room temperature. Still, their density drops significantly at higher temperatures or when water-saturated. There are also significant differences between individual ionic liquids, with viscosities ranging from 10 cP to above 10000 cP depending on the nature of their ions [23]. The anion and cation choice also significantly affect other physical properties, such as the miscibility with water, the density, and the melting point. This tunability offers the opportunity to tune the properties of a given ionic liquid for a specific application. Therefore, ionic liquids are often called *designer solvents* [32].

The wide range of applications highlights the versatility and potential of ILs in various fields, showcasing their unique properties and potential for further development. The field of ILs has seen rapid expansion since their discovery, and their applications continue to grow from laboratory-scale research to industrial utilization [23, 24, 33, 34].

1.3.1 Properties

Vapor Pressure. Ionic liquids have unique properties that make them advantageous for various applications. One significant characteristic is their low volatility, which stems from the ionic nature of ILs and the reduced Coulombic interactions between ions. This nature limits the formation of ion pairs necessary for volatilization, resulting in minimal vapor phase transfer. Instead, ILs tend to decompose before reaching the vapor phase. The low volatility of ILs simplifies purification after synthesis since volatile by-products can be evaporated. Additionally, ILs are often considered eco-friendly alternatives to volatile organic solvents (VOCs) due to their low vapor pressure. As they usually do not evaporate, they do not contribute directly to air pollution. However, it is essential to note that not all ILs are inherently green, as some can be highly toxic and harmful to the environment when improperly disposed of. Moreover, the decomposition products and waste of ILs may be volatile and indirectly affect the atmosphere [35, 36]. The property of negligible vapor pressure in ILs is widely acknowledged as advantageous for their applications. However, it remains one of the least explored physical properties. More extensive investigations into the vapor pressure of different ILs and an understanding of the gas-phase structures are seen as important future study areas [23].

Thermal stability. In addition to low volatility, ILs exhibit a wide liquid range due to their low tendency to crystallize. The lower limit of the liquid range is typically the glass transition temperature. In contrast, the upper limit is determined by the maximum operating temperature beyond which the IL undergoes thermal decomposition or reverts to its starting components [23].

Electrochemical Properties. Electrochemically, ILs demonstrate good stability, electrical conductivity, and a broad electrochemical window, allowing for electrochemical processes that are not achievable in aqueous media due to the limited electrochemical window [37]. This property enables their use in applications such as batteries, supercapacitors, fuel cells, and more. Another advantage of this material is its inherent safety compared to traditional organic solvents. Traditional solvents often accumulate static electricity, increasing the risk of solvent fires triggered by a small spark. In contrast, ILs possess

intrinsic electrical conductivity, preventing the accumulation of static electricity. Furthermore, their low volatility and flammability reduce the chances of a fire in the presence of a spark [23].

Viscosity. The viscosity of ILs is generally higher than that of common organic solvents due to their strong intermolecular interactions, such as van der Waals forces and hydrogen bonding. Viscosity can vary depending on the choice of cation and anion, with alkyl chains increasing viscosity and fluorinated anions decreasing it. The high viscosity of ILs can slow down mass transfer and complicate solvent pumping during scale-up processes. However, in solvent extraction processes, where ILs are water-saturated, the viscosity is significantly lower [19, 23]. Temperature also plays a role in viscosity, as increasing it reduces viscosity, allowing for improved processability of ILs [38, 39].

density. Density is another important property to consider in the context of solvent extraction. The relative densities of ILs and water determine the phase separation and settling speed in biphasic mixtures. Long alkyl chains in IL structures decrease density, while fluorinated anions increase it. This property influences the design of industrial setups and the separation of ILs from aqueous phases.

Nanostructure. The formation of nanostructure represents a complex characteristic of ionic liquids. While this aspect is not commonly recognized as an advantage, it possesses unique properties and exerts a significant influence on the behavior and properties of ILs, as well as the reactions occurring within them. Moreover, the structural characteristics of ILs at interfaces, including solid surfaces such as inorganic nanoparticles immersed in ILs, and at liquid/liquid or liquid/gas interfaces, are even more intricate but equally essential, given their profound impact on the performance of ILs in various applications [23, 40].

Water solubility. The hydrophobicity of ILs determines their behavior with water. Some ILs are hydrophilic and completely miscible with water, while others are hydrophobic and form two phases when in contact with water. Due to their polar and hygroscopic nature, ILs can easily absorb water. The presence of water in hydrophobic ILs affects the solvent polarity to a limited extent, as the nanodomains within the IL structure maintain interactions with solutes[41, 42]. Dissolution of ILs in water can lead to losses in industrial solvent extraction processes, necessitating research on IL separation techniques from metal-containing waste streams.

Solvation in ILs. ILs can accommodate ionic species, unlike molecular solvents, which only accommodate neutral complexes. The solvation of metal ions in ILs differs from traditional solvents, and their solubility is often limited due to weak coordination in commercial ILs. However, the solubility of inorganic compounds in ILs can be improved by introducing coordinating functional groups in the IL structure, such as in functionalized ILs [43, 44].

1.3.2 Application of ionic liquids in liquid-liquid extraction

Ionic liquids have emerged as an important category of solvents for metal processing, particularly in the field of metal extraction in the last decades. One of the key advan-

tages of ionic liquids in metal extraction is their unique properties compared to traditional organic solvents [20]. Ionic liquids have gained interest in the solvent extraction community due to their low flammability, low volatility, and wide liquid range. They also offer structural flexibility, allowing for functionalization and customization for specific applications [23, 24, 33, 34]. Ionic liquids can incorporate extractants directly into their structure, eliminating the need for separate solvent and extractant phases [45, 46]. While the initial motivation was their perceived green nature, their low vapor pressure alone cannot classify them as green solvents due to their toxicity [47].

Various water-immiscible ionic liquids have been used as acidic, neutral, or basic extractants in solvent extraction experiments. Ionic liquids with hydrophobic anions or hydrophobic cations in combination with hydrophilic anions have been used for metal extraction. The hydrophobicity of the ionic liquid is an important factor in determining its applicability in solvent extraction systems. Nevertheless, some highly viscous ionic liquids may require dilution in an organic solvent. Most ionic liquids can be used in their pure form as the organic phase. This simplifies the design of solvent extraction setups and opens up possibilities for new extraction systems. Undiluted ionic liquids are often operated at higher temperatures to reduce viscosity and enable industrial-scale extraction. However, the viscosity of non-fluorinated ionic liquids is generally higher than that of fluorinated ones, even when the latter are water-saturated [42, 48]. While fluorinated ionic liquids offer advantages in terms of reduced viscosity, they have higher costs and may require the addition of extractants to the organic phase.

Early studies focused on using ionic liquids as diluents for metal extractants and comparing their extraction behavior with traditional systems. Subsequent research explored the use of functionalized ionic liquids with coordinating functions. Neutral, acidic, and basic extractants have been investigated in combination with ionic liquids for metal extraction, each involving different extraction mechanisms. Strategies to mitigate solvent losses due to ion exchange have been proposed, including ion recovery from the aqueous phase and using sacrificial cation exchangers.

The extraction of metals using ionic liquids involves various mechanisms, which can differ from those in organic solvents. Ionic liquids can enable anion exchange processes when using acidic extractants or cation exchange processes when using solvating extractants. Basic extractants can be used as both diluents and extractants in ionic liquids, but the absence of an apolar diluent alters the solvation of the complex in the organic phase. Undiluted basic extractants can absorb significant amounts of water, creating a distinct environment compared to nonpolar diluents [49, 50]. The extraction mechanisms of metals in ionic liquids are influenced by factors such as extractant concentration, metal concentration, and the presence of salting-out agents. The use of ionic liquids in metal extraction offers new possibilities in the academic field. Careful selection of extractants, ionic liquids, and extraction mechanisms is essential for specific metal separations[41, 43]. The goal is to develop efficient and sustainable extraction processes while minimizing solvent losses.

Table 1.1 provides an overview of various extraction systems for lithium as reported in the literature. Each of these systems incorporates a phosphorus-based extractant, an ionic liquid cation, and/or anion. Some systems combine an extractant with an ionic liquid, serving as a diluent. Tributyl phosphate (TBP) and trioctylphosphine oxide (TOPO) emerge as the most frequently employed extractants, diluted in ionic liquids or volatile organic solvents, such as kerosene. The ILs used as diluents are usually composed of imidazolium cations and fluorinated anions. Commercial extractants

like Cyanex® 936P, 923, and LIX 54 are typically diluted in volatile organic solvents. Other notable extractants include benzoyltrifluoroacetone (HBTA), tri-n-octyl phosphine oxide (TOPO), thenoyltrifluoroacetone (TTA), and tetrabutylphosphonium (TBPH). The ionic liquids bis(2,4,4-trimethylpentyl)phosphinate ([P_{4444}][BTMPP]) and tetrabutylammonium 2-ethylhexyl phosphate mono-2-ethylhexyl ([N_{4444}][EHEHP]) serve as examples of ionic liquids possessing extraction capabilities for lithium.

Table 1.1: Lithum extraction liquid-liquid systems.

Ionic Liquid	**Extractant**	**Initial [Li]**	**Source**	**Ref.**
[C_{10}mim][TFSI], [C_4mim][TFSI]	TBP	2.8 mg/L	Batteries	Zante, 2019 [51]
[N_{4444}][EHEHP]		0.5 g/L		Shi, 2020 [52]
[P_{4444}][BTMPP]		0.5 g/L		Shi, 2017 [53]
[C_4mim][TFSI]	TBP	2.02 g/L	Brine	Shi, 2016 [54]
[C_4mim][TFSI], [C_2mim][TFSI], [C_4mim][PF_6]	TBP	2.30 g/L	Brine	Gao, 2015 [55]
	TTA–TOPO	0.17 mg/L	Seawater	Harvianto, 2016 [56]
	Cyanex® 936P		Brine	Solvay, 2021 [57]
	Cyanex® 923 and LIX 54	1 g/L	Brine	Pranolo, 2015 [58]
	HBTA-TOPO	1.6 g/L	Brine	Zang, 2017 [59]

An overview of the Pt liquid-liquid extraction system is presented in Table 1.2. Platinum extraction primarily relies on amine and phosphorus based extractants. Solvent extraction offers a high recovery rate, but it involves multistage separation and the utilization of organic solvents, which can have negative implications for health and the environment. However, the use of ILs for platinum extraction offers an alternative that helps minimize or eliminate the need for these potentially harmful organic solvents.

Binnemans and Jones have discussed the reasons behind the limited impact of ionic liquids (ILs) and deep eutectic solvents (DESs) in the metallurgical industry. The same authors have studied solvent extraction using ILs extensively [38, 39, 39, 41, 43, 72–76]. The authors point to several factors that contribute to this failed impact of IL in the metallurgical industry, including the challenges associated with high viscosity, the limited

Table 1.2: Platinum extraction liquid-liquid systems.

Extractant	**Diluent**	**Initial [metal]**	**Efficiency**	**Ref.**
Cyphos® IL 101	Toluene	0.5 Mm	97 to 100%	Paiva, 2022 [13]
Cyanex® 923	Toluene	0.5 mM		Gupta, 2013 [60]
[TON][Dca], [THN][Dca]		4 mM	100%	Boudesocque, 2019 [61]
[OMIM][TFSI]		8.2 mM	99%	Génand-Pinaz, 2013 [62]
[C_{14}pyr][TFSI]			98%	Gras, 2020 [63]
Secundary Amine	Solvesso 150 (ASCC)	24g/L	98%	Kriel, 2015 [64]
Aliquat 336 , Alamine 336, D2EPA and TBP	kerosene		99%	Marinho, 2010 [65]
TOA	[P2225][TFSI]	5 mM		Matsumiya, 2019 [66]
DMDCHTDGA	toluene	500 mg/L	98%	Méndez, 2021 [67]
[OMIM][TFSI], Cyphos® 102		1 mM		Papaiconomou, 2015 [68]
Aliquat® 336	kerosene	364 mg/L		Raju, 2012 [69]
MTAA, TOA, TODGA, TBP	toluene	372 mg/L		Rudik, 2020 [70]

chemical stability of ILs and DESs in metallurgical processes, difficulties in recycling and reusing these solvents, the absence of established unit processes and flowsheets on a pilot scale, a lack of comprehensive material-property data for engineering purposes, the administrative burden of obtaining licenses and safety permits, high costs for large-scale

operations, and minimal added value compared to existing hydrometallurgical processes. Despite these limitations, the authors note that the research conducted on ILs has resulted in the accumulation of extensive expertise in studying complex fluids through innovative approaches. They propose that this expertise should be redirected toward the investigation of speciation and the chemical thermodynamics of hydrometallurgical solutions. By doing so, the problem-solving capabilities of IL and DES researchers can play a crucial role in facilitating the ongoing shift from linear to low-energy-input, circular economy hydrometallurgy. This aligns with the aim of this study, which is to provide tools for investigating and enhancing the performance of liquid-liquid extraction systems.

1.3.3 Homogeneous liquid-liquid extraction

The viscosity of ionic liquids presents a challenge in solvent extraction processes without dilution in an organic solvent, as it slows down the extraction kinetics by impeding mass transfer [19, 23]. Typically, the metal ion extractant reaction occurs at the interphase of the biphasic mixture, requiring vigorous stirring to increase the interphase and facilitate extraction. However, stirring becomes more energy-intensive with a more viscous mixture, and pumping the solvent through the system becomes more difficult [15]. To address the issue of high viscosity, homogeneous liquid-liquid extraction (HLLE) has been explored as an alternative ionic liquid solvent extraction technique. HLLE utilizes thermomorphic ionic liquids that exhibit temperature-dependent phase behavior in water.

In HLLE, instead of stirring the viscous biphasic mixture, the temperature is adjusted above the *upper critical solution temperature* (UCST) or below the *lower critical solution temperature* (LCST) to achieve a single homogeneous phase [77, 78]. UCST systems become homogeneous upon heating, while LCST systems become homogeneous upon cooling [79]. The temperature at which this occurs is called the *cloud point* temperature (T_{cp}). By achieving a homogeneous phase, complex formation between the metal ion and the extractant can occur throughout the solution without the interphase barrier. Subsequently, the mixture is returned to its initial temperature, leading to phase separation, with the hydrophobic metal complex settling in the ionic liquid phase [38, 39]. In summary, HLLE involves temperature adjustments to achieve a homogeneous state, followed by phase separation and metal extraction upon returning to the initial temperature. Figure 1.6 illustrates the stages of the HLLE process.

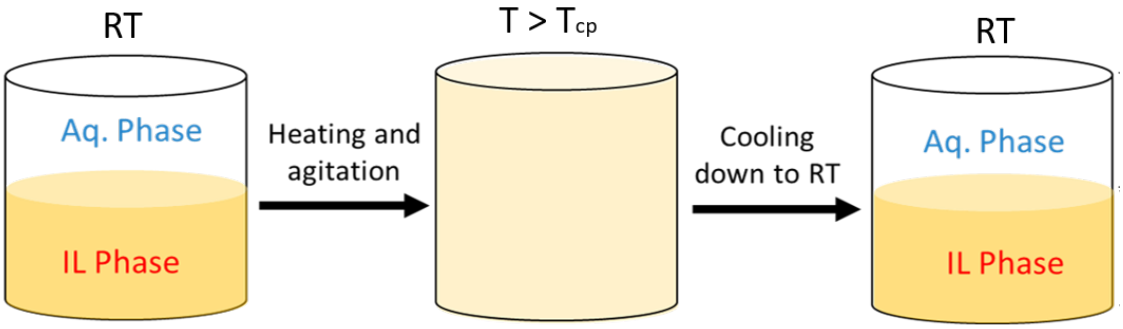

Figure 1.6: Homogemeous Liquid-liquid extraction simplified scheme for IL/aqueous phase system with a UCST.

The concept of HLLE was introduced by Murata et al. [80], who used thenoyltri-

fluoroacetone in propylene carbonate to extract Fe(III) in a water/propylene carbonate mixture with a UCST of 73 °C. pH change or addition of modifiers can also induce phase separation and influence the composition and interactions of the organic or aqueous phase. The miscibility of two liquids depends on their nature, temperature, and composition. Some two or more component biphasic systems (e.g., liquid-liquid extraction systems) show thermomorphic behavior, meaning that a transition is observed between a homogeneous system and a two-phase system at a specific temperature.

Researchers have explored HLLE extensively since its introduction, applying it to extract and separate various metal ions. For example, Wang et al. [81] studied the recycling of Au(III), Pd(II), and Pt(IV) from the acidic medium using UCST-type ionic liquids. Wang et al. [81] achieved phase separation in the extraction of Ag(I) by lowering the temperature below 50 °C using a mixture of 1-hexyl-3-methylimidazolium tetrafluoroborate, water, and a complexing agent. Nd(II) was extracted using choline hexafluoroacetylacetonate, [Chol][hfac], in the ionic liquid choline bis(trifluoromethylsulfonyl)imide, [Chol][TFSI] by Onghena et al. [72].

In this thesis two thermomorphic ionic liquids are mainly investigated: cholinium bis(trifluoromethylsulfonyl)imide [Chol][TFSI] and betaine bis(trifluoromethylsulfonyl)imide [Hbet][TFSI].

The thermomorphic ionic liquid used here is cholinium bis(trifluoromethylsulfonyl)imide, [Chol][TFSI]. Additionally, in the aqueous solution, betaine (trimethylglycine) is added. Figure 1.7 presents the chemical structure of the different molecules. [Chol][TFSI] ionic liquid and water, in a mass fraction of 1:1, form a biphasic system at room temperature and become monophasic above $T_{cp} = 72$ °C, its upper critical transition temperature [82].

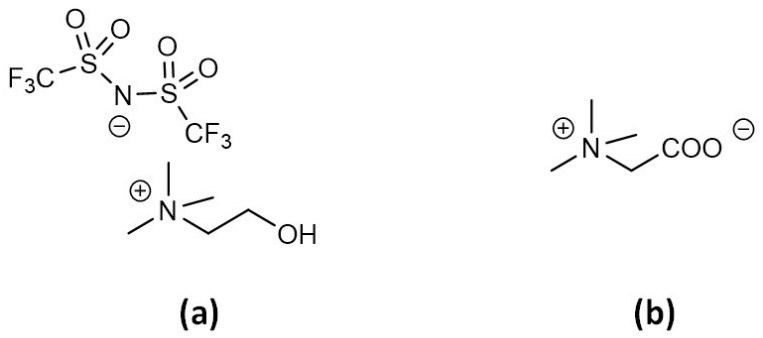

Figure 1.7: Chemical structure of (a) [Chol][TFSI] and (b) betaine.

The HLLE system with [Hbet][TFSI] has gained attention from other researchers, who have investigated its performance in applications such as scandium removal and neodymium extraction. Sasaki et al. [83] explored the extraction of U(IV), Pd(II), Rh(III), and Ru(III) from nitrate media to [Hbet][TFSI]. However, they did not achieve a homogeneous state due to low-temperature elevation. Onghena and Binnemans [84] have recovered Scandium(III) from aqueous solutions by [Hbet][TFSI]. Vander Hoogerstraete et al. [38] extracted rare earths with betaine in [Hbet][TFSI]. The structure of the IL is shown in Figure 1.8.

The ionic liquid betaine bis(trifluoromethylsulfonyl)imide [Hbet][TFSI] shows high solubility in water and is a promising candidate for HLLE. At room temperature, approx-

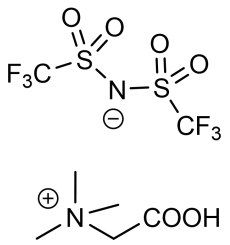

Figure 1.8: Chemical structure of [Hbet][TFSI].

imately 12 % of the ionic liquid dissolves in the aqueous phase, while 16 % of water dissolves in the IL phase. The miscibility of the [Hbet][TFSI]/H_2O system is temperature and composition-dependent [36]. Above the UCST of 55 °C, the mixture becomes homogeneous, facilitating improved reaction kinetics and molecular-scale mixing. This system can be employed in HLLE or temperature-induced phase separation for metal extraction [78].

Objectives

The central objective of this thesis is to develop methodologies to elucidate the processes involved in the extraction of metal ions by ionic liquids (ILs) in the context of recycling operations employing liquid-liquid extractions. The goal is to provide an empirical foundation for further optimization of these processes.

A significant difficulty in this area is the necessity to comprehend the underlying mechanisms during the solvation of metal ions in ILs and to determine the roles of the aqueous phase and the extractant. Most investigations into liquid-liquid extraction processes are hinged on analytical methods that predominantly focus on the metal species dissolved pre- and post-extraction.

Enhancing the efficiency of these extraction procedures potentially necessitates a comprehensive understanding of the interactions among all the species implicated in the process. Despite substantial progress in characterizing these systems, knowledge gaps and conceptual ambiguities remain to be addressed.

In light of this, the present research proposes an investigative approach that studies the processes at play for all the participating species (solvents, counterions, extractants) during liquid-liquid extraction. Employing nuclear magnetic resonance (NMR) techniques facilitates the observation of solvent extractants, mainly through hydrogen, carbon, and fluorine nuclei. This provides a mechanism for simultaneous monitoring of all the molecules involved, including the ionic liquids' water, extractant, cation, and anion.

The current research offers a diverse range of tools for studying these systems. NMR spectroscopy, a commonly employed and potent tool, is extensively used for probing localized dynamics and structure within materials—the thesis endeavors to explore and demonstrate tools specifically applicable to the investigation of extraction systems. The primary NMR techniques selected for the research include localized spectroscopy, quantitative NMR, structural experiments reliant on the nuclear Overhauser effect (NOE), and diffusion experiments.

A key focus of the thesis is the investigation of the processes of metal extraction using thermomophic ionic liquids. In conjunction with metallurgical extraction parameters, this study aspires to gain a more profound understanding of solvent extraction processes.

Chapter 2

Ionic liquids: synthesis and NMR methods for Ionic Liquids

Contents

This chapter is designed to provide a comprehensive overview of the methodologies employed throughout this research, particularly emphasizing the synthesis of ionic liquids (ILs) and the procedural steps followed during the extraction experiments. Subsequently, the analytical instruments and methodologies utilized throughout this study are presented. The final section of this chapter presents a general introductory exposition on Nuclear Magnetic Resonance (NMR) theory. This elucidation serves as a precursor to a more detailed discussion of the specific NMR experimental protocols adopted in this work. This chapter aims to provide theoretical background and methodological details to understand the research processes fully.

2.1 Synthesis of the Ionic liquids

2.1.1 Materials

Betaine (BioUltra, $\geq$ 99.0 %, Sigma-Aldrich) was used as an extractant. High-purity grade lithium bis(trifluoromethanesufonyl), imide, Ultrapure (Type 1) water (Direct-Q 5UV Millipore), LiTFSI (99.9 %, Solvionic), choline chloride ($\geq$ 98.0%, Sigma-Aldrich), Choline hydroxide solution (46 wt.% in H_2O, Sigma-Aldrich) and di-2-ethylhexyl phosphoric acid, D2EHPA ($>$ 90.0 %, Baysolvex), Betaine hydrochloride, ($>$ 99.0 %, Alpha Aesar), and ethanol ($>$ 99.8 %,VWR chemicals), were used for the synthesis of the ionic liquids.

2.1.2 Synthesis of choline bis(trifluoromethanesufonyl)imide [Chol][TFSI]

Choline bis(trifluoromethanesufonyl)imide [Chol][TFSI] was prepared following a literature procedure [82]. LiTFSI (36.33 g, 0.26 mol) dissolved in ultrapure water(25 mL) was added to a solution of choline chloride (74.71 g, 0.26 mol) in water (25 mL). The mixture was vigorously stirred for one hour at room temperature, and two phases were observed. After stopping agitation and letting the phases settle, they were separated. The IL phase was washed with ultrapure water to remove chloride impurities. The presence of chloride in the water layer after the addition of a small aliquot of a concentrated silver nitrate solution to the washing solution verified washing. The [Chol][TFSI] IL was freeze-dried overnight, and a white solid was obtained. Synthesis was confirmed with ^{1}H NMR A.2 in Annexe A. ^{1}H NMR (500 MHz, [D6]DMSO, TMS): δ = 5.29 (t, 1H), 3.84 (m, 2H), 3.39 (m, 2H), 3.10 (s, 9H). All NMR experiments in this chapter were performed in a 500 MHz (11.7 T) Bruker AV III spectrometer equipped with a 5 mm Double Resonance Broadband Probe (BBI).

2.1.3 Synthesis of choline bis(2-ethyhexyl) phosphate [Chol][D2EHP]

Equimolar quantities of di-2-ethylhexyl phosphoric acid D2EHPA (14.07 g, 0.0415 mol) and choline hydroxide (11.02 g, 0.0415 mol) were mixed to reduce the viscosity of the mixture, 25 mL of ethanol were added. The mixture was agitated for one hour at room temperature, and a pH= 7 was obtained. The ethanol and water were eliminated by heating the mixture to 80 °C. Afterward, the product was freeze-dried to eliminate the residual water, obtaining neat [Chol][D2EHP], a transparent dark orange viscous liquid. NMR spectroscopy was used to confirm the structure. ^{1}H and ^{13}C NMR spectra are shown in Figure A.2 and A.3. Thermal gravimetric analysis (TGA) was done to characterize the

ionic liquid A.4. ^{1}H NMR (500 MHz, [D6]DMSO, TMS): δ = 0.80 - 0.81 (m, 12H, 4CH3), 0.91 - 0.91 (m, 12H, 4CH_3), 1.19 - 1.44 (m, 32H, 16CH_2), 1.59 (m, 2H, 2CH), 3.63 (m, 4H, 2OCH_2) 3.81 (m, OCH_2), 3.47 (m, NCH_2), 3.16 (s, 3NCH_3). ^{13}C NMR (500 MHz, [D6]DMSO, TMS): δ = 11.12 (4CH_3), 13.66 (2CH_3), 14.01 (2CH_3), 19.71 (4CH_2), 23.14 (2CH_2), 23.32 (2CH2), 24.07 (4CH_2), 29.06 (2CH3), 30.12 (2CH_2), 40.43 (2CH), 58.70 (3NCH_3), 53.41 (OCH_2), 56.35 (NCH_2), 67.27 (2OCH_2).

2.1.4 Synthesis betanium bistrifluoromethanesufonyl)imide [Hbet][TFSI]

A betaine hydrochloride solution (1 mol, 153.61 g) in 250 mL of water was combined, under agitation, with 500 mL of an aqueous solution of lithium bis(trifluoromethylsulfonyl)imide (1 mol, 287.08 g). The combined solutions were then agitated for one hour at ambient temperature, separating the aqueous phase from the ionic liquid. Post-separation, the ionic liquid phase underwent three washes with small water quantities until the silver nitrate test no longer indicated the presence of chloride impurities. Subsequently, the product underwent freeze-drying to remove any remaining water. A white solid was obtained. Synthesis was confirmed with ^{1}H NMR A.5. ^{1}H NMR (500 MHz, [D6]DMSO, TMS): δ = 4.29 (s, 2H), 3.22 (s, 9H).

2.2 Liquid-Liquid Extraction Experiments

Liquid-liquid experiments are done by putting an ionic liquid (IL) phase in contact with an aqueous phase. This section describes the preparation of the main IL phases and aqueous phase for the studied systems.

2.2.1 preparation of the ionic liquid phase

The three ILs presented in the previous section were used in different extraction systems.

[Chol][TFSI] The IL [Chol][TFSI] is used in our systems as a diluent; thus, it is necessary to use an extractant in these systems. The preparation of the IL phase may vary according to the extractant added.

- **Betaine** When betaine is used as an extractant, the IL phase is composed only of [Chol][TFSI] saturated in water. Dry [Chol][TFSI] without water is solid at room temperature. Saturating [Chol][TFSI] of water facilitates the handling of the IL and avoids uncontrolled water uptake in the IL phase during extraction experiments. The IL was saturated in water, mixing the same masses of ultra-pure water and IL to the phase and heating to 80 °C. In this particular system, the extractant is added to the aqueous phase.
- **[Chol][D2EHP]** The second IL phase is composed of [Chol][D2EHP] with [Chol][TFSI]. Since the extraction studies described in this study do not require dry [Chol][D2EHP], but [Chol][D2EHP] dissolved in the ionic liquid phase, [Chol][D2EHP] was prepared directly in the ionic liquid [Chol][TFSI]. Choline hydroxide and di-2-ethylhexyl phosphoric acid D2EHPA were added to [Chol][TFSI] saturated in water in equimolar quantities to obtain a desired concentration of 50 %

w/w [Chol][D2EHP]. A similar preparation was described by other authors [72]. Different concentrations of [Chol][D2EHP] were obtained by dissolving this solution in [Chol][TFSI] saturated in water. Before the extraction, the ionic liquid phase obtained was also saturated in water, as described before.[Chol][D2EHP] has the role of metal extractant, while [Chol][TFSI] is the diluent of the phase. Phosphorous extractants are generally used in lithium LLE, such as the anion of [Chol][D2EHP].

[Hbet][TFSI] The IL [Hbet][TFSI] can be used as a diluent and extractant at the same time. Then, the IL phase was composed of [Hbet][TFSI] saturated in water as described for the IL [Chol][TFSI]. This temperature is above 72 °C, the upper critical solution temperature (UCST), where the system passes from biphasic to monophasic [82].

The masses of the aqueous and IL phases change during extraction due to the mutual solubility of IL and water. In particular, the mass of the aqueous phase increases because of the migration of the IL into this phase [39, 73, 74].

2.2.2 preparation of the aqueous phase for extraction

The aqueous phase was prepared by dissolving a metallic salt in ultrapure water (purification system Direct-Q 5UV Millipore). Also, when mentioned, a certain amount of betaine was added to these solutions. The betaine in these systems plays the role of metal extractant for different metals.

2.2.3 Extraction experiments

Liquid-liquid experiments are done by putting an ionic liquid phase in contact with an aqueous phase. Extraction experiments were performed by adding a mass of the aqueous phase (upper phase) to a mass of the ionic liquid phase (bottom phase). The mixture was then heated in a silicone bath above the UCST of the system and was stirred 600 rpm to obtain one homogeneous phase. Once a homogeneous phase was obtained, the heating and agitation were maintained for 30 min. The system was cooled down at room temperature, and the phases were let to settle for at least 2 hours. Finally, the two phases were separated for analysis.

As depicted in Chapter § 1, the percentage extraction is defined as the amount of metal extracted from the organic phase over the total amount of metal in both phases. It can be defined as:

Liquid-liquid extraction can be evaluated by the distribution ratio (D) and the extraction percentage (%E), which can be defined as:

$$D = \frac{[M]_{\mathrm{IL}}}{[M]_{\mathrm{aq}}} \tag{2.1}$$

$$\%E = \frac{[M]_{\mathrm{IL}}\, m_{\mathrm{IL}}}{[M]_{\mathrm{IL}}\, m_{\mathrm{IL}} + [M]_{\mathrm{aq}}\, m_{\mathrm{aq}}} \times 100 \tag{2.2}$$

Where $[M]_{\mathrm{IL}}$ (mg/kg) and $[M]_{\mathrm{aq}}$ (mg/kg) are the metal concentrations after extraction of the IL and the aqueous phase and m_{IL} and m_{aq} are the masses of the IL and the aqueous phase after extraction, respectively. Usually, the m_{IL} and m_{aq} are considered equal to the initial mass of the corresponding phase. For this reason, the values of D and $\%E$ might be slightly overestimated because of the change of masses in both phases due to the mutual

water-IL solubility [39, 73]. D and $\%E$ can be related throughout the phase ratio as shown in Equation 1.3. In this work, the mass phase ratio (IL:aq ratio) is defined as presented in Equation 2.3.

$$IL : aq = \frac{m_{IL}}{m_{aq}} \tag{2.3}$$

2.3 Nuclear Magnetic Resonance

Nuclear Magnetic Resonance (NMR) spectroscopy is a technique used in analytical chemistry for research and quality control purposes. It's a valuable tool for understanding the composition and purity of a sample and determining its molecular structure. For instance, NMR can be used to analyze mixtures qualitatively and quantitatively containing known substances.

Several studies highlight the advancements in employing NMR spectroscopy for analyzing ionic liquids [85–88]. Beyond the conventional structural elucidation of these synthesized liquids, the NMR methods available allow for an in-depth exploration of these substances' structure and dynamic behavior. Given that numerous ionic liquids contain NMR-responsive nuclei, they are appropriately suitable for multinuclear NMR studies. NMR techniques, such as pulsed field gradient, relaxometry, electrophoretic NMR, and others, are used to examine pure ionic liquids and their interactions with diverse salts and solvents. NMR spectroscopy has emerged as an indispensable tool in comprehending ionic liquids. NMR techniques offer profound insights into their molecular architecture, dynamics, and the origins of their physicochemical attributes.

Regarding unidentified compounds, NMR can be employed to infer their basic structure directly. NMR can further reveal the molecular conformation in a solution and study molecular-level physical properties. These properties might include changes in conformation, phase transitions, solubility, and diffusion. According to the research issue, a wide range of NMR techniques can be used for different finalities. The NMR principles are presented in the following sections [89, 90].

2.3.1 Principles

For NMR spectroscopy analysis, the need for magnetic nuclei is essential. These nuclei will interact with the magnetic field. Within the NMR magnet, the nucleus will engage with the main magnetic field, denoted as $\vec{B}_0$ [89, 90].

The nucleus magnetic moment, represented by $\vec{\mu}$, interacts with $\vec{B}_0$, and the energy produced from this interaction can be described by Equation 2.4. Each nucleus within a sample has a distinct magnetic moment that points in a unique direction.

$$E = -\vec{\mu} \cdot \vec{B}_0 \tag{2.4}$$

This magnetic moment originates from the nuclear spin $\vec{S}$, a quantum property. There is a direct proportionality between the magnetic moment and the spin, with γ representing the gyromagnetic ratio (Equation 2.5).

$$\vec{\mu} = \gamma \hbar \vec{S} \tag{2.5}$$

Upon subjecting these magnetic nuclei to a magnetic field, the Zeeman effect incites the nuclear spins to align along the longitudinal axis of $\vec{B}_0$. The transverse components of the magnetization precess around the direction of the imposed magnetic field. This precession occurs at a specific frequency ω_0 for each nucleus, known as the Larmor frequency, which can be detailed by Equation 2.6.

$$\omega_0 = \gamma B_0 \tag{2.6}$$

In a bulk sample, the initial spin orientations are random. Still, in a magnetic field $\vec{B}_0$, each nucleus's individual magnetic moment will be influenced by internal magnetic fields, such as those from neighboring nuclei, altering their magnetic moment orientation. Over time, an uneven distribution of orientations will form, with magnetic moments in the field's direction being slightly more probable than those against the field. This leads to a bulk magnetization, M_{eq}, in the direction of the magnetic field, a state known as thermal equilibrium. This is illustrated in Figure 2.1.

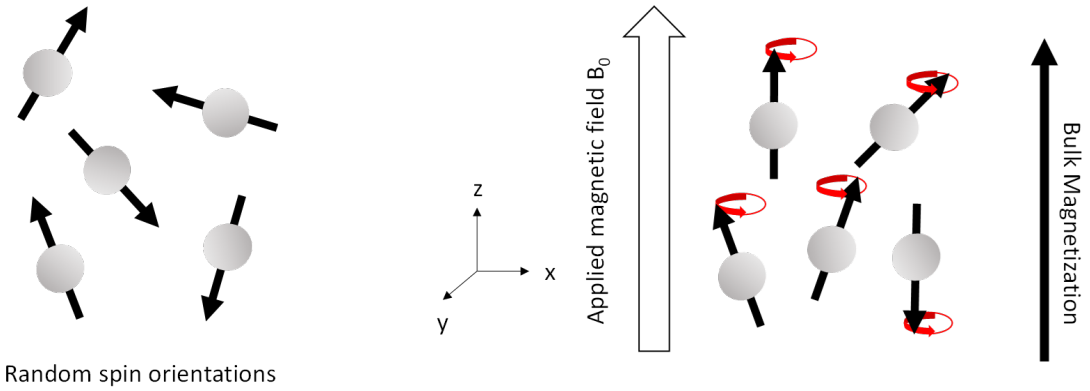

Figure 2.1: Net magnetization along the external magnetic.

2.3.2 Relaxation

This reconfiguration process of magnetic moments to achieve thermal equilibrium is characterized by a time referred to as T_1, also known as the longitudinal relaxation or spin-lattice relaxation time (Equation 2.7).

$$M(t) = M_{\text{eq}}\left(1 - \mathrm{e}^{-t/T_1}\right) \tag{2.7}$$

NMR's principle involves applying a radio frequency (RF) pulse at the Larmor frequency to generate a rotation of the net magnetization away from the external magnetic field. The RF field changes the orientation of spins, which in turn changes the net magnetization angle. After a 90° pulse, the magnetization rotates around $\vec{B}_0$, producing an electric current in a coil near the sample. This tiny oscillating current can be detected using a sensitive detector, with the detected signal known as the FID (*free induction decay*). The Fourier transform of this signal gives the NMR spectrum on a frequency scale.

As equilibrium conditions have a magnetization of amplitude M_0, along the z-axis and no transverse (x or y magnetization), applying an electromagnetic pulse to tip the longitudinal magnetization vector through a 90° angle creates transverse magnetization.

Over time, fluctuating internal magnetic fields will cause this transverse magnetization to diminish to zero. This decay process, known as transverse relaxation, happens in the xy plane and is characterized by a time T_2. The transverse T_2 relaxation timeline is described by the following Equation 2.8:

$$M(t) = M_{\text{eq}} \text{e}^{-t/T_2} \tag{2.8}$$

Inversion recovery experiment A commonly utilized experiment for estimating the longitudinal relaxation time, T_1, is the inversion-recovery experiment as depicted in Figure 2.2.

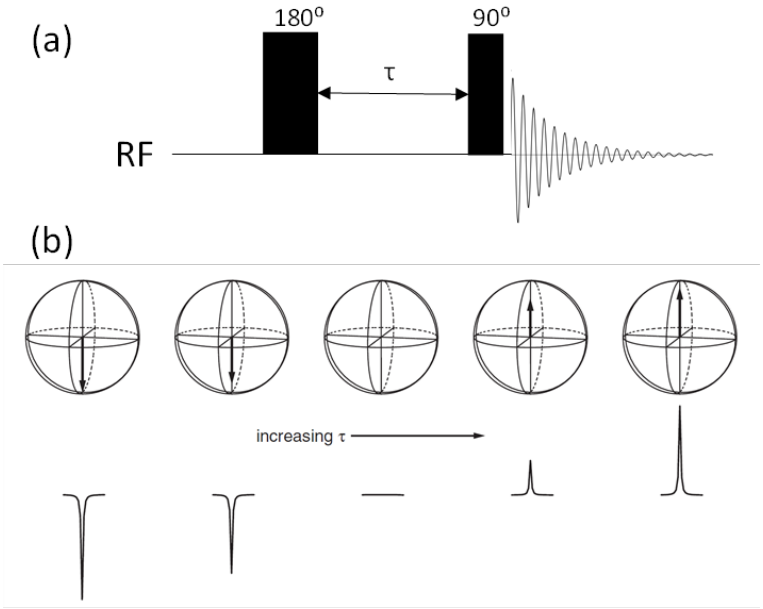

Figure 2.2: (a)Inversion recovery pulse program and (b) visual scheme of inversion recovery experiment. The spectra, illustrated, capture the magnitude and orientation of the z-magnetization. By studying the variation in peak heights corresponding to the τ_i delay, the recovery rate of the z-magnetization can be determined. [89]

The experiment involves an initial 180° pulse, which flips the magnetization. This change in magnetization is followed by a variable delay (τ_i) before implementing an excitation pulse. T_1 can be measured by incrementing the τ_i delay. During τ_i, the magnetization relaxes along the z-axis, and the size of the magnetization vector can be determined using the excitation pulse. For brief τ_i durations, an inverted signal materializes, and as the recovery time lengthens, the signal transitions through zero, then to positive phases, as presented in Figure 2.2(b).

In the inversion-recovery pulse sequence, the recycle delay between individual experiments allows the magnetization to return to equilibrium before the following scan.

Endo et al. [91] employed relaxation NMR to investigate the rotational dynamics brought about by methylation, drawing comparisons between rotational correlation times in [C_4mim][Br] and [C_4C_1mim][Br]. Allen et al. [92] studied ^{1}H and ^{13}C T_1 and T_2 relaxation evaluations to shed light on the formation of expansive hydrogen-bonded networks in water-infused [EMIM][acetate] mixtures. The way solvents, particularly water, interact with ILs has been a significant focus due to the intricacies they introduce and the

subsequent implications in their usage. Relaxometry can also assist in assessing the local-scale dynamics of high-temperature inorganic molten salts and room-temperature ionic liquids [93]. Relaxation techniques provided insights into the intermolecular structural features of low-molecular-weight organogel fibers [94]. This research employed proton nuclear spin relaxation to investigate the structure and dynamics of organogels derived from a phenylalanine amino acid modified with a naphthalimide moiety. The discerned relaxation parameters highlighted the organogel fibers' flexibility and hinted at cluster formations. Supplementary NMR methodologies corroborated the intimate intermolecular contacts, underscoring the distinctive structural configurations of the molecules.

Some general principles of NMR are presented in this section. The phenomena underlying NMR form the backbone of a sophisticated characterization technique. The NMR technique relies on manipulating coherences with a sequence of pulses, allowing to probe effects across bonds and space. The following sections briefly explore how some core principles can be employed as a hands-on investigative tool.

2.3.3 Quantitative NMR Internal standard

Quantitative Nuclear Magnetic Resonance (qNMR) technique features one of the fundamental applications of NMR spectroscopy. The principal correlation of qNMR postulates that the integrated signal area, denoted as I_x, in a spectrum, is directly proportional to the number of spins (specifically, protons) responsible for this resonance, N_x, that contribute to the corresponding resonance line, as shown in Equation 2.9 [95]

$$I_x = K_s \times N_x \tag{2.9}$$

with K_s symbolizing a spectrometer constant, which depends on the sequence and acquisition parameters. Generally, the NMR signal from an individual compound is characterized by multiple resonance lines. Nevertheless, selecting one unique resonance line is sufficient for a sample composition. This proportional relationship serves as the fundamental basis for quantification in NMR studies.

2.3.3.1 Internal standard

The selection of a specific resonance peak, alongside knowing its associated number of spins, facilitates its comparison with a peak originating from a standard substance added with a predetermined concentration. In proton NMR experiments, the constant K_s is shared among all resonances within the same spectrum under correctly calibrated acquisition parameters. Consequently, this constance cancels out when considering ratios between these resonances. The concentration C of a component x can be calculated with a known standard concentration C_{std}, as described in Equation 2.10.

$$C_x = C_{std} \times \frac{I_x}{I_{std}} \frac{N_{std}}{N_x} \tag{2.10}$$

Where I_{std} and N_{std} are the integrated area and the respective number of protons relative to the integration peak.

This method of quantification through NMR employs the use of an internal chemical standard. However, this approach encounters numerous challenges as the selected reference chemical must fulfill a broad range of criteria concerning solubility, stability, relaxation

time, chemical shift, and lack of interaction with the sample under quantification. Other quantitative methods appear as an alternative method to face these issues.

2.3.3.2 ERETIC Digital Method

The ERETIC digital method (*Electronic REference To access In vivo Concentrations*) is based on generating a signal that will be calibrated against a known reference then integrated into the molecule's spectrum to be quantified. This method avoids most of the problems traditional quantification methods face by adding a standard substance. The ERETIC method was first described by Akoka et al. [96], where the ERETIC signal was created electronically and used for concentration measurement by proton NMR. Also, this method was applied to obtain precise quantitative data in 2D NMR spectroscopy in homonuclear and heteronuclear spectra and diffusion-ordered NMR as a diffusion reference [97, 98]. This method was improved by the addition of a broadband antenna inside the NMR probe [99]. It was used for quantifications in different systems, in particular for proton NMR [100, 101].

The main difference between the ERETIC digital method and the traditional ERETIC method is that the ERETIC signal is created electronically in the original version and digitally, using the `TopSpin` software in the new ERETIC digital version. The ERETIC digital method can be utilized in two basic steps, calibration and quantification, described as follows.

Calibration When employing the ERETIC method for quantification, the initial step necessitates calibrating the synthetic signal through a reference sample of known concentration. Calibrating the synthetic signal requires recording a spectrum of the reference sample with suitably adjusted parameters such as tuning, shimming, and 90° pulse optimization, which is performed using parameters specifically optimized for quantification.

The synthetic signal must be incorporated following this spectrum's recording and appropriate processing (via Fourier transform, phase, and baseline correction). Subsequently, the digital signal is added at a chosen chemical shift, and its intensity can be altered.

Post-addition of this signal and the reference and synthetic signals should be inserted. After integrating the reference and synthetic signal, the integral of the reference signal is calibrated considering the proton concentration. The integral value of the synthetic signal must be noted for later use in the quantification step.

Quantification The subsequent step involves quantifying the sample of interest. For this, a new experiment must be created. Ideally, this experiment should be created from the calibration experiment to preserve the calibration acquisition settings. However, parameters such as number of scans, receiver, and the duration of the 90° pulse can be modified, as a correction factor exists to account for any changes.

The synthetic signal is added once the spectrum is recorded and processed, like the calibration experiment. The synthetic signal becomes visible, and its intensity can be adjusted concerning the calibration spectrum due to potential changes in the parameters mentioned. The synthetic signal should be inserted and calibrated according to the value obtained during calibration. Subsequently, the signal of interest is integrated, and the integral value will represent the concentration multiplied by a factor equal to the number of atoms corresponding to the selected signal.

2.3.4 Structure and Dynamics

Nuclear Magnetic Resonance has emerged as the method of choice for studying both structure and dynamics. The quantification of diffusion coefficients can provide insights into large-range dynamics of molecules. One of the principal features of NMR spectroscopy is the capacity to examine site-specific molecular associations [102, 103]. This capability can improve the comprehension of intermolecular proximities, thereby offering comprehensive information on ion associations and interactions.

2.3.4.1 Nuclear Overhauser Effect

The Nuclear Overhauser Effect (NOE) was initially proposed by Albert W. Overhauser in 1953 [104]. NOE is essentially a transfer of spin polarization via cross-relaxation through dipole-dipole interactions. This transfer occurs through space rather than through chemical bonds.

The most elementary experiment to observe the NOE is the steady-state experiment, which involves the selective saturation of a spin, followed by the implementation of a 90° pulse to monitor the change in polarization on a different spin. To comprehend the NOE effect, a system of two coupled spins sharing a spatial (dipolar) coupling must be taken into account. The NOE effect concerns changes in spin polarization, that is, the differences in populations between energy states.

In equilibrium, the discrepancies in populations between energy levels are governed by the Boltzmann distribution. Figure 2.3 presents a two-spin system energy level transitions diagram.

NOE experiments are powerful NMR techniques used to determine through-space interactions, but careful experimental design and data interpretation are crucial to obtaining accurate information. When analyzing NOESY and HOESY data, care must be taken due to the complex interplay of several factors. These include the influence of intensity dependence on various conditions, the potential for spin diffusion causing cross-peaks between non-adjacent spins, the possibility of negative enhancements leading to inverted cross-peaks, dynamic effects impacting molecular conformation, and the influence of relaxation processes on spectral interpretation. These intricacies require detailed analysis and a solid understanding of the relaxation characteristics of the studied system.

The NOE corresponds to the combination of only two of these transitions - the double quantum ($\alpha\alpha \leftrightarrow \beta\beta$, $\Delta E = 2\omega_0$) and the zero quantum transition ($\alpha\beta \leftrightarrow \beta\alpha$, $\Delta E = 0$). The cross-relaxation rate (σ) is the difference of the two transition probabilities $W_{2\mathrm{IS}}$ and $W_{0\mathrm{IS}}$

$$\sigma = W_{2\mathrm{IS}} - W_{0\mathrm{IS}}$$

and depends both on the Larmor frequency (ω_0) of the nuclei under study and the molecular dynamics of spins. For fast dynamics (correlation time small compared to $1/\omega_0$) $\sigma > 0$, for slow dynamics (correlation time large compared to $1/\omega_0$) $\sigma < 0$ [106].

Another significant contributor to the cross-relaxation rates is the distance, r, between the spins since the dipole-dipole interaction strongly depends on it. The cross-relaxation rates scale as $1/r^6$. Hence, the closer the spins are to each other, the higher the cross-relaxation rate σ will be, and it vanishes for distances larger than a few ångströms.

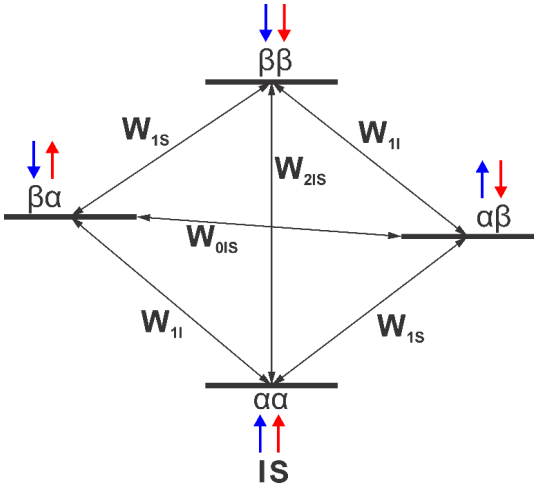

Figure 2.3: Energy level and possible transitions of a two spins system [105].

NOESY Nuclear Overhauser Effect Spectroscopy (NOESY) is a two-dimensional nuclear magnetic resonance technique that provides information about the spatial proximity of nuclear spins in a molecule. It is a powerful tool used to study molecular structures, interactions, and dynamics in solution.

The key principle behind the NOESY experiment involves irradiating proton nuclear spins with a selective radiofrequency pulse, exciting a specific resonance frequency. During the subsequent relaxation period, the magnetization from this excited spin is transferred to other nearby spins through the NOE mechanism.

The basic NOESY pulse sequence, depicted in Figure 2.4, mirrors a traditional two-dimensional exchange experiment. After an initial 90° pulse generating the transverse magnetization, which evolves during a variable interval t_1, a subsequent 90° pulse causes the chemical shift-encoded longitudinal magnetization. Following this, during a duration denoted as T_m (the mixing time), the magnetization undergoes transfer between nuclei via cross-relaxation or chemical exchange. The final 90° pulse generates a transverse magnetization that can be detected [107]. In the NOESY spectrum, one axis represents the chemical shift of the directly excited nuclear spin, while the other axis represents the chemical shifts of the neighboring spins that have experienced NOE-mediated enhancements. The cross-peaks in the NOESY spectrum indicate the correlations between spins that are spatially close to each other. Cross-peaks imply close spatial proximity, providing valuable information about the 3D structure of the molecule.

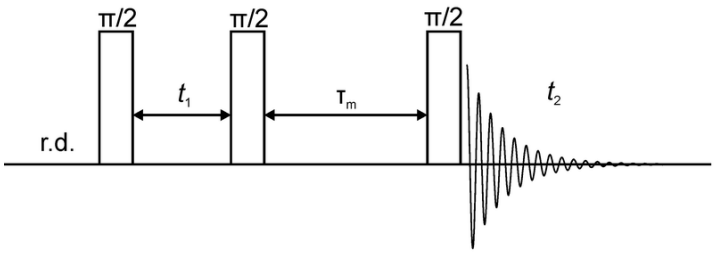

Figure 2.4: Basic NOESY pulse sequency [105].

Pantoja et al. [108] used NOESY experiments to develop an NMR-based approach to

determine dynamical component exchange in a phase-separating system. NOESY was also applied to study the interaction between ionic liquids and water. In a study by Santos et al. [109], non-linear behavior and the presence of the Nuclear Overhauser Effect in some systems indicate the formation of supramolecular aggregates. The experiment was also used to evidence spin diffusion in an imidazolium tetrafluoroborate ionic liquid [110]. Kurteva et al. [111] investigated possible interactions between imidazolium-based ionic liquids and extractants used in solvent extraction by employing NOESY.

HOESY The 2D Heteronuclear NOESY and HOESY, experiments allow detecting heteronuclear through-space NOE (nuclear Overhauser effect) vicinities between nuclei. HOESY is the heteronuclear version of the NOESY experiment.

The most critical parameter to optimize is the mixing time. These experiments have also been applied to pure ILs, mixed IL/solvent, IL/solute, and IL/salt systems [102]. HOESY experiment enables the observation of the NOE between disparate nuclear isotopes, potentially yielding insights about the relative arrangements of anions and cations in an ionic liquid.

Through heteronuclear through-space NOE experiments, such as ^{19}F-^{1}H HOESY, it is possible to gain insights into the interactions between cations and anions in ionic liquids [112, 113]. This technique has also been utilized to study the aggregation influence of polyethyleneglycol organic solvents with ILs [114]. NOE is also an excellent choice to investigate interionic interactions to understand ion-pair dynamics. Examination of liquid structures was done on high-temperature inorganic molten salts and room-temperature ionic liquids using chemical shifts and magnetization transfer experiments combined with local-scale dynamics assessed via relaxometry, and long-range dynamics probed with pulsed field gradient NMR [93]. Martin et al. [115] utilized a combination of quantitative HOESY analysis and molecular dynamics simulations to test the theory that intermolecular NOEs will be sensitive to long-range distances for nuclei with similar resonance frequencies compared to those with significantly different frequencies.

2.3.4.2 Diffusion experiments

Diffusion refers to the random, translational movement of molecules, often called Brownian motion. This process is primarily propelled by internal thermal energy but can also be influenced by spatial molecular distributions and the intrinsic molecular motion within a substance. The study of diffusion in ionic liquids is critical, given its central role in ion transport. Furthermore, this process is intrinsically linked to inter-ionic and molecular interactions, thus making it a key aspect to understand in the context of ionic liquids. The diffusion NMR methodology is implemented through the integration of NMR pulses and pulsed field gradients (PFG) directed across the vertical axis of the sample to encode spatial data. The most frequently employed diffusion experiment is termed Pulse Field Gradient Spin Echo (PFGSE) [116].

Diffusion-Ordered Spectroscopy (DOSY) is a 2D NMR experiment that provides valuable information about how molecules move and interact with each other in a solution. It is based on nuclear magnetic resonance (NMR) principles and utilizes PFGSE experiment. A magnetic field gradient is applied during the experiment to understand the diffusion behavior. The strength of this gradient is gradually increased, and as a result, the NMR signal from each molecule starts to experience different decay rates. The faster

the molecule diffuses, the more quickly its NMR signal decays. By measuring the decay rates at different gradient strengths, it is possible to analyze the self-diffusion behavior of individual molecules in the solution. The DOSY experiment provides a 2D plot, where one axis represents the chemical shift, giving information about the molecular structure, and the other axis represents the diffusion behavior of the molecules. This behavior allows us to differentiate and characterize different species in a mixture, determine molecular sizes, and even study interactions between molecules in a solution.

The diffusion behavior is associated with the properties of a particular molecule, such as size, shape, mass, and charge, as well as its surrounding environment, such as solution, temperature, and aggregation state. Each component in a mixture can be pseudo-separated, based on its own diffusion coefficient [116, 117]. A 2D NMR spectrum, with one dimension corresponding to the chemical shifts and the other to the diffusion coefficient, can be obtained with the experimental data set.

These types of experiments produce stacked spectra with increasing pulsed magnetic field gradient strength. Pulsed field gradients (PFGs) establish a linear spatial variation in the magnetic field, which induces a linear variation of the nuclear Larmor frequencies. Figure 2.5 depicts a fundamental diffusion NMR pulse sequence. The rectangles with diagonal stripes symbolize the field gradient pulses. In Figure 2.5, an initial 90° pulse is applied. During the initial interval τ at point t_1, a gradient pulse with a duration of δ and strength g is introduced, causing spin i to undergo a phase change by the end of τ. Subsequent to this period, a 180° radiofrequency pulse is employed, which serves to reverse the precessional motion. This implies a switch in the phase angle or, equivalently, a change in the direction of the applied gradients and the static field. When the time reaches $t_1 + \Delta$, a gradient pulse of identical magnitude and length is applied.

Refocusing is accomplished only for those nuclei that have not significantly moved along the direction of the gradient, as demonstrated in Figure 2.5. If a nucleus moves along the applied field gradient during the diffusion time Δ, the precession frequencies during the dephasing and refocusing periods will not be identical. Consequently, the spin won't be perfectly refocused, resulting in signal attenuation.

By iteratively conducting this experiment with gradual increases in the magnetic field gradient strength or pulse duration, a 2D map depicting the decay of peak intensity will be generated. The obtained signal is an integral over the entire sample volume, with the NMR signal intensity experiencing attenuation based on the diffusion time Δ, the gradient strength g, and the gradient pulse length δ. This decay can be subsequently fitted using the Stejskal-Tanner equation [119, 120]:

$$I = I_0 e^{-D\delta^2\gamma^2 g^2\left(\Delta - \frac{\delta}{3} - \frac{\tau}{2}\right)} \tag{2.11}$$

is the observed intensity, I_0 the reference intensity obtained for null gradient, D the diffusion coefficient, and γ the gyromagnetic ratio of the observed nucleus.

Mazan and Boltoeva [121] investigated the transport properties of ionic liquids using DOSY NMR, revealing diffusion trends influenced by alkyl chain length. They also studied the ionic interaction between cation and anion in ionic liquids, and combining DOSY and NOE, they investigated the structure of some ionic liquids [122, 123]. Also, using the pulse gradient spin-echo (PGSE) method in NMR diffusion assessments, it is possible to determine the diffusion coefficient of solvent within organogel [124].In another study, the aqueous acidic solution and ionic liquid biphasic system were examined using

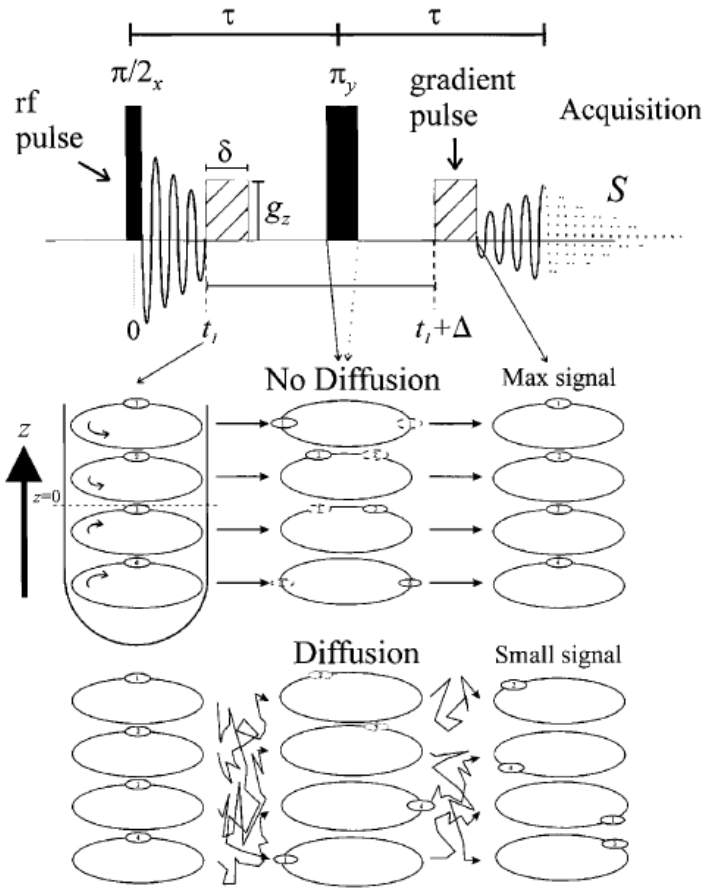

Figure 2.5: Basic scheme of Stejskal-Tanner (PFG) pulse sequence diffusion measure and flow [118].

NOE and DOSY NMR measurements to observe interactions between cations, anions, water, and nitrate species [125]. DOSY, combined with NOE experiments, was employed to study molecular interactions in systems for the extraction of polyphenols [126]. Li et al. [127] utilized multinuclear DOSY NMR techniques to characterize reactive intermediates and determine their aggregation number and solvation state. Additionally, DOSY was employed to investigate the dynamic-structural behavior of imidazolium ionic liquids with different anions, revealing the influence of ion structure and IL concentration on the maintenance of contact ion pairs or aggregates [128].

2.4 Conclusion

In conclusion, this chapter presents the ionic liquid synthesis methods and the use of Nuclear Magnetic Resonance (NMR) methods in their analysis. The synthesis of several ionic liquids, [Chol][TFSI], [Chol][D2EHP], and [Chol][TFSI], was detailed. These specific syntheses set the groundwork for more complex experiments and the understanding of ionic liquids. The protocol of liquid-liquid extraction experiments with thermomorphic ionic liquids was presented, highlighting the preparation of both ionic liquid and aqueous phases. The chapter explored the principles and applications of Nuclear Magnetic Resonance in

the context of ionic liquids. An overview of the NMR principles, relaxation, quantitative NMR, and experiments to probe structure and dynamics was provided, emphasizing the relevance of NMR methods for analyzing ionic liquids. Notably, the presentation of specific experiments like the Inversion recovery experiment, NOESY, HOESY, and DOSY emphasizes the important role of NMR in the ionic liquid investigation. Overall, the chapter arranges some foundation for further studies and experiments in this thesis, showing the preparation of liquid/liquid systems and elucidating the potential uses and benefits of NMR in the context of investigating ionic liquids, and in particular liquid-liquid extraction thermomorphic ionic liquids.

Chapter 3

LOCalized SpectroscopY (LOCSY) as tool for the Study of Liquid-liquid Extraction

Contents

3.1 Introduction

For the study of liquid-liquid extraction, slice selective NMR experiments are particularly worthwhile. They make it possible to record spectra at different positions within the sample; in other words, they give access to in situ spectral mapping, which is highly valuable information for a better understanding of the process. This chapter explores a radio frequency selective pulse method, the NMR LOCalized SpectrocopY (LOCSY), for this purpose [129]. This slice-selective NMR experiment offers a rapid and easy technique to obtain qualitative and quantitative data on the different species' spatial distribution and monitor them over time.

Most of the studies regarding solvent extraction are mainly focused on the metallic species and the study of the phase involved separately. Initially, LOCSY was used to observe different biphasic systems at equilibrium at room temperature, and chemical shift maps were obtained according to position along the tube's z-axis.

Afterward, a homogenization setup was built to promote agitation through a gas insert into the NMR tube inside the spectrometer. This method was validated using the LOCSY experiment. The 2D mapping of the samples is also compared with 1D images of the samples obtained with the echograd pulse sequence.

Finally, LOCSY was used to observe the process of the settling phase in the same system during cooling down.

These efforts have the objective of a better understanding of extraction systems at macro and molecular levels.

3.2 Experimental

In this section, the LOCSY technique is presented with experimental details, and the echograd pulse sequence is described.

3.2.1 Echograd

The Echograd pulse sequence, showing in Figure 3.1, is employed for implementing ultra-fast 2D experiments on a Bruker Avance Spectrometer [130, 131]. This sequence is used for gradient and chirp pulse calibration. It allows us to determine the gradient-induced frequency dispersion and calibrate the encoding pulse power. The Echograd sequence results in a spin echo, which, following Fourier Transform (FT) and phase correction, displays a 1D image of the profile of the sample.

Although the pulse sequence described is shown for the proton ^{1}H it can be applied to other nuclei. The delay d5 should be fine-tuned to position the echo at the center of the acquisition window approximately. A Gaussian function is used, and the center of this function (parameter GB in Topspin) must be adjusted based on the echo's position. Typically, GB is set to 0.5 if the echo is perfectly centered in the acquisition window (default value).

The following Topspin commands are used to process the FID: GM to apply the Gaussian multiplication, FT for Fourier Transform, and phase the spectrum starting with first-order phase correction. Since gradients induce phase dispersion, a considerable first-order phase correction is usually necessary. However, a small zero-order phase correction can be applied to obtain a symmetric image.

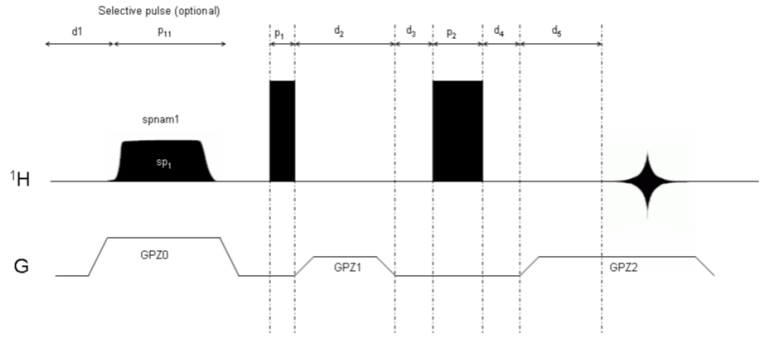

Figure 3.1: Echograd pulse sequence for proton. d1: 1-5 T1 d2: 10 ms d3: 1 ms d4: 1 ms d5: 5 ms, sp1: encoding pulse power (120 dB for the gradients calibration, then calibrated) p11: duration of the encoding pulse (15 ms here) spnam1: encoding pulse name [131]

3.2.2 LOCSY Nuclear Magnetic Resonance

Chemical shift imaging (CSI) and LOCSY are methods of spectral localization. The CSI method employs a series of pulsed field gradients to capture the Fourier transform of the targeted distribution across a rectangular grid space. Then, straightforward Fourier inversion subsequently retrieves the initial distribution [132]. CSI integrates the spatial data derived from standard NMR imaging with the spectral details obtained from NMR spectroscopy related to chemical shifts, and the gradient pulse mainly imposes its resolution.

Comparing the two techniques, LOCSY allows one to choose directly the region of interest one wants to investigate. Meanwhile, CSI is also more susceptible to motion artifacts due to the longer acquisition times, potentially degrading image quality.

However, CSI can offer advantages, such as more extensive sample coverage and the visualization of spatial distributions across larger regions of interest [133, 134].

The CSI technique has been recently used to study microstructural growth in solid electrolytes in solid-state batteries using ^{7}Li NMR [135]. Also, with ^{7}Li NMR, aqueous biphasic systems (ABSs) have been investigated for potential applications for aqueous-based battery systems using CSI [136].

The LOCSY (*LOCalized SpectroscopY*) has been proposed by Mantel et al. [129] to study different species in samples that are heterogeneous at a macroscopic scale. The essence of the sequence is similar to STEAM (*STimulated Echo Acquisition Mode*) sequence [137], although the spatial resolution is only achieved along one direction. In the LOCSY sequence, a pulsed field gradient is applied on the vertical axis (z), i.e., along the NMR tube, allowing the spatial encoding of a sample in this direction. The spins experience different magnetic fields as $B(z) = B_0 + Gz$, where G is the strength of the applied gradient, B_0 is the static magnetic field, and z is the position. As a result, the resonance frequencies, ω, vary along the direction z according to equation 3.1. Simultaneously, a frequency selective excitation pulse is applied, which excites only selected a narrow frequency range and thus only a spatial slice of the sample.

$$\omega(z) = \gamma\,[B_0 + Gz] \tag{3.1}$$

where ω_0 is the resonance frequency in the static field and where γ is the gyromagnetic ratio.

The LOCSY pulse sequence is presented in Figure 3.2. A 2D map is generated by col-

lecting a set of 1D spectra acquired by systematically changing the excitation frequencies of the selective pulses, as exemplified in Figure 3.3 for a system that will be studied further in this thesis. The frequency deviation of the selective pulses was achieved by applying a frequency ramp to the pulses.

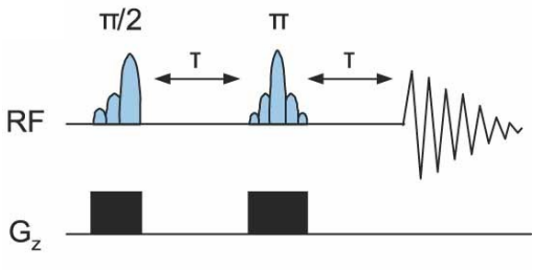

Figure 3.2: LOCSY pulse sequence. The delay T is maintained constant during the experiment. RF represents the radio frequency pulses and G_z the gradient pulse [129].

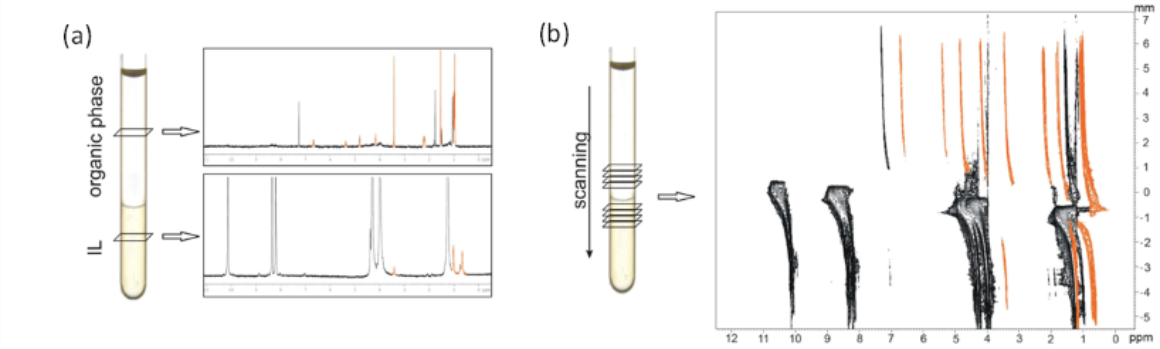

Figure 3.3: LOCSY experiment scheme. (a) Proton NMR 1D spectra were obtained in different regions of the z-axis of the tube, and the resulting (b) 2D NMR map of the tube resonances was obtained by scanning the z-axis. NMR study investigated the peptide transition from the ionic liquid (IL) phase to the organic solvent. Figure (b) presents a 2D plot of the vertical NMR scan for the two-phase sample, providing valuable insights into the molecular interactions and structural changes occurring at the IL-organic solvent interface. This figure represents the IL signals in black and the peptide signals in orange [138].

The sample's slice size Δz is defined by the excitation pulse bandwidth BW according to equation 3.2 [129, 139]. It is essential to notice that the size of the slice is limited by the gradient strength G.

$$\Delta z = \frac{BW}{\gamma G} \tag{3.2}$$

The coil size limits the maximum observable area of a sample in this technique. While it provides the flexibility to select specific regions of interest for observation, areas outside the coil detection zone remain unobserved.

Nonetheless, artefacts can be observed in biphasic systems due to changes in the magnetic susceptibility near the interfaces (liquid/liquid, liquid/air, liquid/glass). The presence of a refocusing pulse surrounded by two spoil gradients can significantly reduce this kind of artefacts. Also, one effect of a pulsed magnetic field gradient is introducing a

dephasing for the coherences associated with different spatial locations along the sample [129, 140]. To reduce dephasing effects and get a better resolution, the pulse sequence *Double Pulse Field Gradient Selective Echo* can be used, Figure 3.4 [141, 142]. This sequence uses one excitation pulse and two refocalization pulses. The spacial encoding pulse field gradients, during the refocalization pulses, are between two coherent selection pulse field gradients, as shown in Figure 3.4. Keeping the echo delay (τ) minimal can prevent undesired dephasing effects [143].

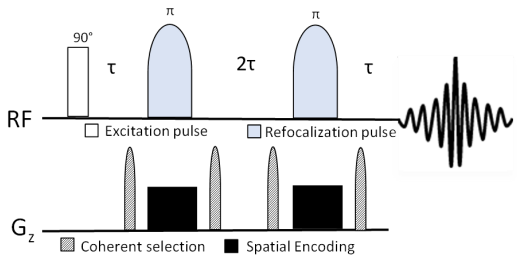

Figure 3.4: Double Pulse Field Gradient Selective Echo pulse sequence [141].

Spatially resolved NMR experiments have been utilized to access Fick and mutual diffusion coefficients [142, 144]. In a study by Wisniewska and Seland [145], the relationship between structure and diffusion in hydrogels was investigated using spatially resolved NMR spectroscopy. This method was also employed in studying the extraction process of peptides in a biphasic system composed of an ionic liquid and an organic solvent [138]. Lambert et al. [146] investigate liquid-liquid interfaces using volume-selective. This study shows a potential for resolutions down to 10 nm. However, a significant consideration is the effect of diffusion at the interface when applying the selective impulse. Diffusion near these interfaces is anisotropic, with a reduction of diffusion coefficient at the interface compared to the bulk. This reduced diffusion coefficient effectively enhances the spatial resolution, minimizing the traditionally anticipated diffusion limitations during volume-selective NMR experiments.

The LOCSY experiments were performed using a 500 MHz Bruker Avance III spectrometer with a 5 mm BBI probe and a maximum 55 G/cm uniaxial z gradient. The recorded NMR data were processed and analyzed using the Bruker software `TopSpin` (version 3.6.2) to extract relevant information and perform data interpretation.

NMR tube preparation The NMR tubes were prepared adding a capillary D_2O inside for the lock. The IL phase, the denser phase, was added first to the capillary, and the aqueous phase, the lighter phase.

Acquisition parameters The acquisition parameters for the biphasic samples were optimized with a T_1 inversion recovery experiment for the determination of the recovery delay ($D_1 = 5 \times T_1$) and the determination of the 90°pulse duration. The echo delay was set to 1 ms.

Gradient These experiments used a pulsed field gradient of 5.5 G/cm, corresponding to 10 % of gradient-amplifier power.

Selective pulses The LOCSY experimental parameters were determined initially, deciding the region along the z-axis to be observed and the size of the slices. Once they are defined and know the gradient strength along the z-axis, G_z, the excitation pulse bandwidth of the selective pulse BW is related to the thickness of the slice δz by the Equation 3.3.

$$G_z = \frac{BW}{\gamma \times \Delta z} \tag{3.3}$$

The center frequency of the selective pulse (offset) corresponds to the desired location on the z-axis. The Bruker `Topspin` software shape tool was used to create RF shapes for the slices and determine the power level for these pulses.

3.3 Mapping of biphasic Liquid/Liquid distribution

The LOCSY technique enables the study of regions near the interface as well as the bulk of biphasic systems at the same time. This technique facilitates the mapping of chemical shifts based on the position along the z-axis of the NMR tube. In this investigation, liquid-liquid extraction systems are observed when the aqueous and ionic liquid phases are brought into contact within the NMR tube without agitation or heating.

3.3.1 TBP in [C_4mim][TFSI]/water

Initially, the LOCSY sequence was applied to a solvent extraction system for lithium composed of the ionic liquid 1-butyl-3-methylimidazolium bis(trifluoromethylsulfonyl)imide [C_4mim][TFSI], with TBP extractant. The IL and aqueous phases in the system were prepared based on the conditions proposed by Zante et al. [51], mixing 60 % w/w of the extractant TBP and 40 % w/w of the IL [C_4mim][TFSI]. The aqueous lithium concentration was 0.4 mM, and the pH of the aqueous phase was adjusted to 2 by adding small aliquots of sulfuric acid. The pH was measured with a Sension+ PH3 pH meter. Approximately 0.25 mL of each phase was added to the NMR tube.

Figure 3.5 shows the system's 2D ^{1}H NMR map, corresponding to a region of 1.45 cm in the z-axis of the NMR tube. The colors on the map indicate the intensity. The color flow goes from blue for low intensities to red for high intensities. The chemical shifts are assigned on the map. The mapping of chemical shifts according to the position along the tube's z-axis was obtained with a refocusing pulse of RE-BURP type with a bandwidth of 2000 Hz. The frequency offset of the pulses was incremented in steps of 2500 Hz from -20000 to $+20000$ Hz, corresponding to 17 slices of 845 µm.

A clear separation between the phases is seen in the 2D NMR spectrum. In the bottom part of the spectrum, the organic/IL phase is observed, which is the denser phase, with the chemical shifts corresponding to the IL and extractant. On the top of the spectrum, the aqueous phase is marked by the peak of water. [C_4mim][TFSI] and TBP have large aliphatic groups, as shown in the structure, and the presence of LiCl and H_2SO_4 dissolved in the aqueous phase tends to reduce the miscibility of ionic liquid/water systems [147]. Thus, a defined interface and separation of the two phases are observed in the map. Even though similar volumes of the phases were added to the tube, the higher volume of the ionic phase is due to the selected frequency offset range, which is not centered in the interface. Additionally, because of the size of the slice, an overlapping region of the organic and

aqueous phases in the interface region is expected due to the excitation of protons from the two regions.

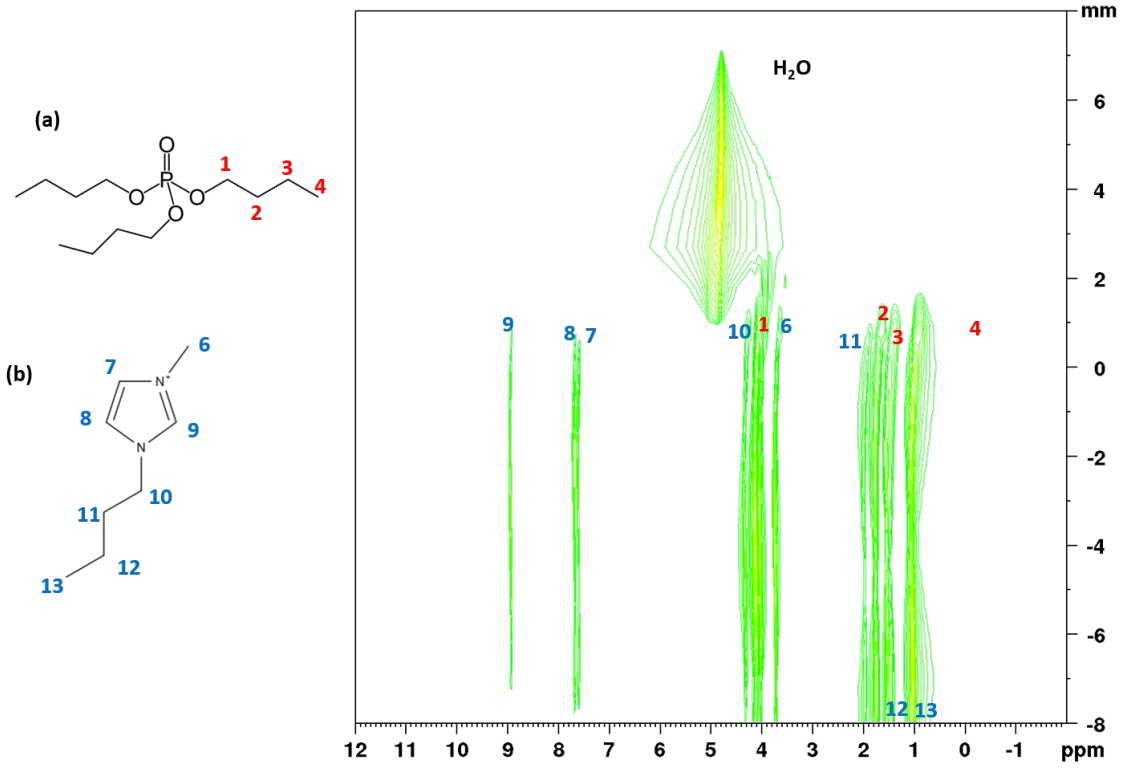

Figure 3.5: Chemical structure of (a) TBP (b)$[C_4mim]^+$ and 2D ^1H mapping of chemical shift according to position along the tube's z-axis. The map was acquired with 8 scans for each slice, a $D_1 = 5$ s RF pulse duration of 8.5 µs. The color indicates the intensity, from green for low intensities to red for high intensities.

The LOCSY technique is also suitable for different nuclei. In this case, the ^{31}P nucleus present in the TBP was observed (Figure 3.6). The same region was maintained, but due to the change in the gyromagnetic ratio, the shape pulse bandwidth and frequency offset had to be adjusted to keep this region, as implied in Equation 3.3. A refocusing pulse of RE-BURP type with a bandwidth of 800 Hz was applied. The frequency offset of the pulses was incremented from −6400 to +6400 Hz in steps of 800 Hz, equivalent to slices of approximately 845 µm. The map shows, as expected that TBP is only present in the IL phase, and the chemical shift corresponds well to the chemical environment of the TBP functional group [148, 149].

No significant change is observed along the z-axis for this system at the scale observed, except during the phase change. A closer look at the interface can be performed with other sequences that can get a better spatial resolution [146]. However, it demonstrates the possibility of obtaining coherent spatially resolved chemical shift information for different nuclei. Practical insights can be extracted from systems with high metal/TBP concentration ratio, where significant chemical shift changes of ^{31}P are observed [148], or from systems with increased miscibility between the ionic liquid and aqueous phase, enabling proton NMR analysis.

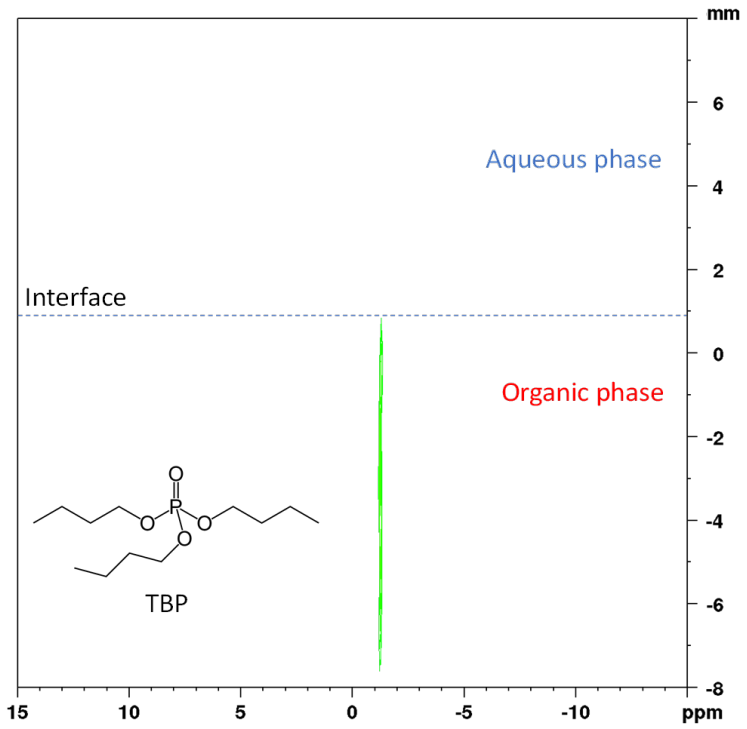

Figure 3.6: Chemical structure of TBP and ^{31}P 2D mapping of chemical shift according to position along the tube's z-axis.

3.3.2 [Chol][D2EHP] in [Chol][TFSI]/water

This work also investigated a second system developed for lithium extraction using ^{1}H LOCSY NMR. This system was composed of the ionic liquid [Chol][D2EHP] and [Chol][TFSI] (saturated with water) and an aqueous phase with only LiCl.

The concentration of [Chol][D2EHP] diluted in [Chol][TFSI] saturated in water was 25 % w/w, and a concentration of 0.1 M of LiCl was used in the aqueous phase. Similar masses of IL and aqueous phase were added to the NMR tube. The LOCSY 2D map is shown in Figure 3.7. A refocusing pulse of RE-BURP type with a bandwidth of 1170 Hz was applied to obtain this map. The frequency offset of the pulses was incremented in steps of 1170 Hz from −30420 to +37100 Hz. It corresponds to 40 slices of 500 µm.

The bottom phase corresponds to the IL phase, and the top phase corresponds to the aqueous phase of the system. Both ionic liquids are partially miscible with water. This miscibility can be seen in the map, where low-intensity lines are observed in the contour plot, around 4.1 and 4.6 ppm, at position in the z-axis corresponding to -1 and 4 mm . It is possible to see a concentration gradient in the system, in particular in the IL phase close to the interface, due to the change in H_2O–OH chemical shift. The progress of the H_2O–OH peak with increased water content appears gradually to the interface. Reducing hydrogen bonding is usually associated with an upfield shift. This chemical shift might appear due to the water concentration gradient in the tube. This observation could be attributed to the fact that $[D2EHP]^-$ is an amphiphilic molecule and might form inverse micelles and assist in dissolving more water in the ionic liquid phase, causing the concentration gradient seen on the spectrum [150, 151]. Another potential cause might be the increased dissolution of $[D2EHP]^-$ in water with the reduction of pH or formation

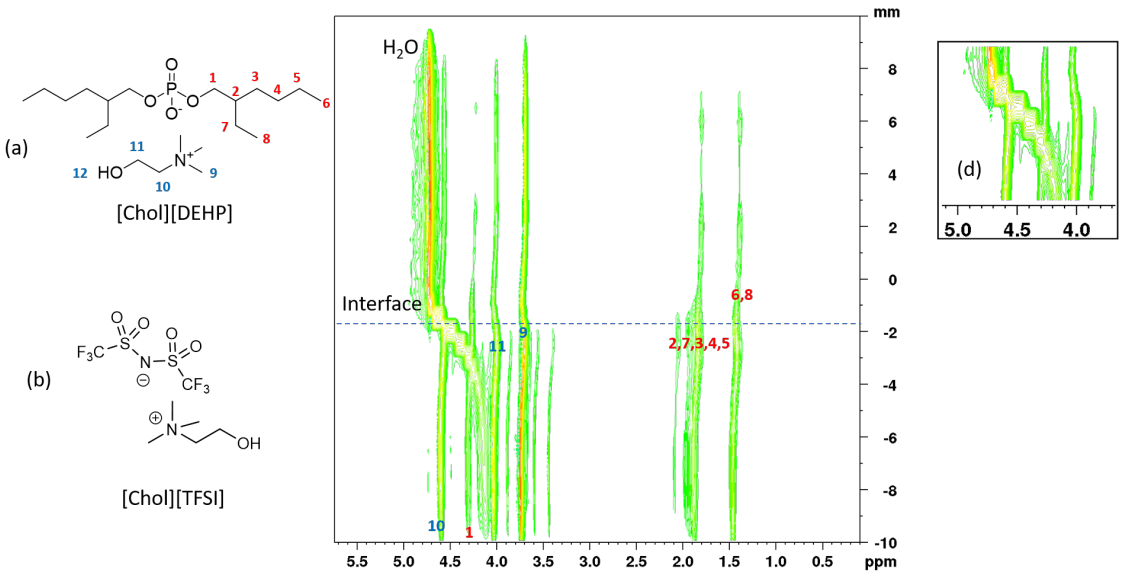

Figure 3.7: Chemical structure of (a) [Chol][D2EHP], (b)[Chol][TFSI] and ^{1}H 2D mapping of chemical shift according to position along the tube's z-axis. The map was acquired with 16 scans for each slice, a $D1 = 5$ s RF pulse duration of 8.5 µs.

of metal extractant complexes [152]. The solubility of D2EHPA increases considerably when the pH exceeds 4, which corresponds to the deprotonation of D2EHPA at pH levels higher than 4. In our IL, the extractant is deprotonated, which could contribute to the dissolution of the extractant in the IL phase. This effect in the interface may not be due to magnetic field gradient since it is not seen in other peaks, even at lower intensities. In the map in Figure 3.7, the interface region is not as straightforward as in the previous system and is marked by a slight chemical shift change, reduction of the intensity of the contours, and mainly because of the appearance of a prominent water peak.

This effect in the interface may not be due to magnetic field gradient since it is not seen in other peaks, even at lower intensities. In the map in Figure 3.7, the interface region is not as straightforward as in the previous system and is marked by a slight chemical shift change, reduction of the intensity of the contours, and mainly because of the appearance of a prominent water peak. The 2D map shows that water concentration in the IL phase increases when it is close to the interface.

3.3.3 Betaine in [Chol][TFSI]/water

Finally, the system composed by [Chol][TFSI] saturated in H_2O with an aqueous phase constituted of 24 % w/w of betaine and 0.1 M of LiCl was studied. Similar IL and aqueous phase masses were added into the NMR tube (approximately 300 mg). The map was obtained with a refocusing pulse of RE-BURP type with a bandwidth of 1170 Hz. The frequency offset of the pulses was incremented in steps of 1170 Hz from −14040 to +16380 Hz. That corresponds to 26 slices of 500 µm with a total length of approximately 1.3 cm in the tube z-axis.

A well-defined interface region is observed in the ^{1}H LOCSY NMR, Figure 3.8. Also, it is observed that the distributions of the proton containing species between the two phases can be differentiated only by the intensity of the peaks and their chemical shift.

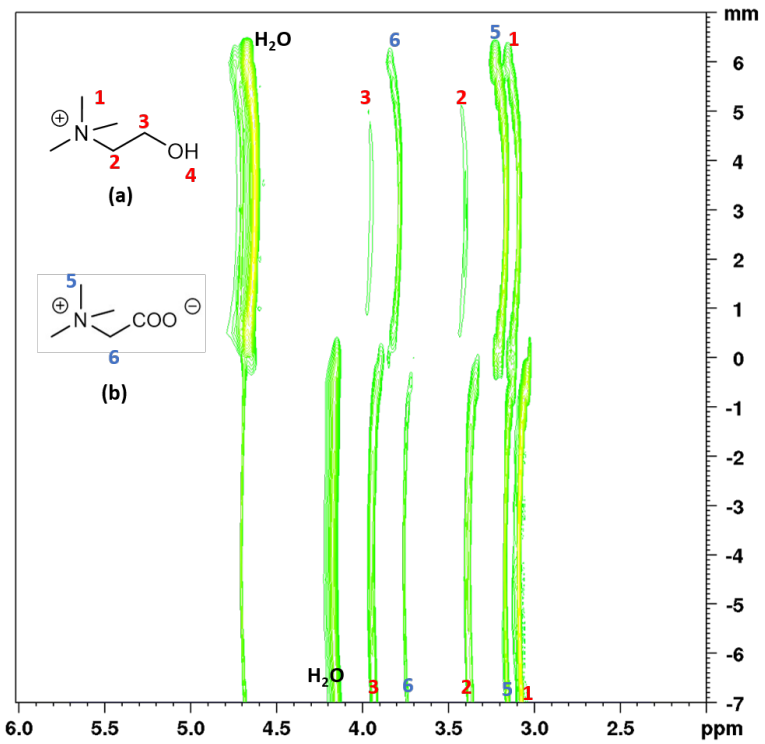

Figure 3.8: 2D ^{1}H LOCSY spectrum of biphasic system composed of [Chol][TFSI], betaine and H_2O. The peak around 4.7 ppm corresponds to D_2O in the capillary tube.

Additionally, no concentration gradients are observed along the tube z-axis a few hours after the tube preparation. The betaine extractant is soluble in both the aqueous and IL phases (peaks 5 and 6). The cholinium cation is also miscible with water (peaks 1, 2, and 3). All the species are presented in both phases. Mechanical mixing might occur during sample preparation and handling. Together with diffusion, it might contribute to the species' observed distribution in the two phases.

The nucleus ^{7}Li was observed for the same system, Figure 3.9. For the LOCSY experiments, the selective pulses RE-BURP had a bandwidth of 910 Hz, which corresponds to 0.1 cm slices. The frequency offset was incremented from -2730 to $+2730$ Hz incremented in 910 Hz steps. Only 7 slices were acquired due to the long recycling delay ($D_1 = 65$ s) required.

The LOCSY map shows that lithium is present in both phases, even after a few hours, without intentional mechanical agitation or heating applied to the sample. As anticipated, the lithium concentration is higher in the top phase, i.e., the aqueous phase, as depicted in the map. Additionally, there is a slight difference in the chemical shift of lithium between the two phases, as shown in Figure 3.9(b). The observed chemical shifts correspond to lithium in water or aromatic solvents [153]. In Figure 3.9(a), it is possible to observe the presence of an interface in the system. In this interfacial region, more artifacts are observed than on the proton map. This occurrence may be attributed to the dephasing of the lithium peak caused by the pulsed magnetic field and the magnetic field inhomogeneities generated in this particular region, which could be attributed to the meniscus in the interface.

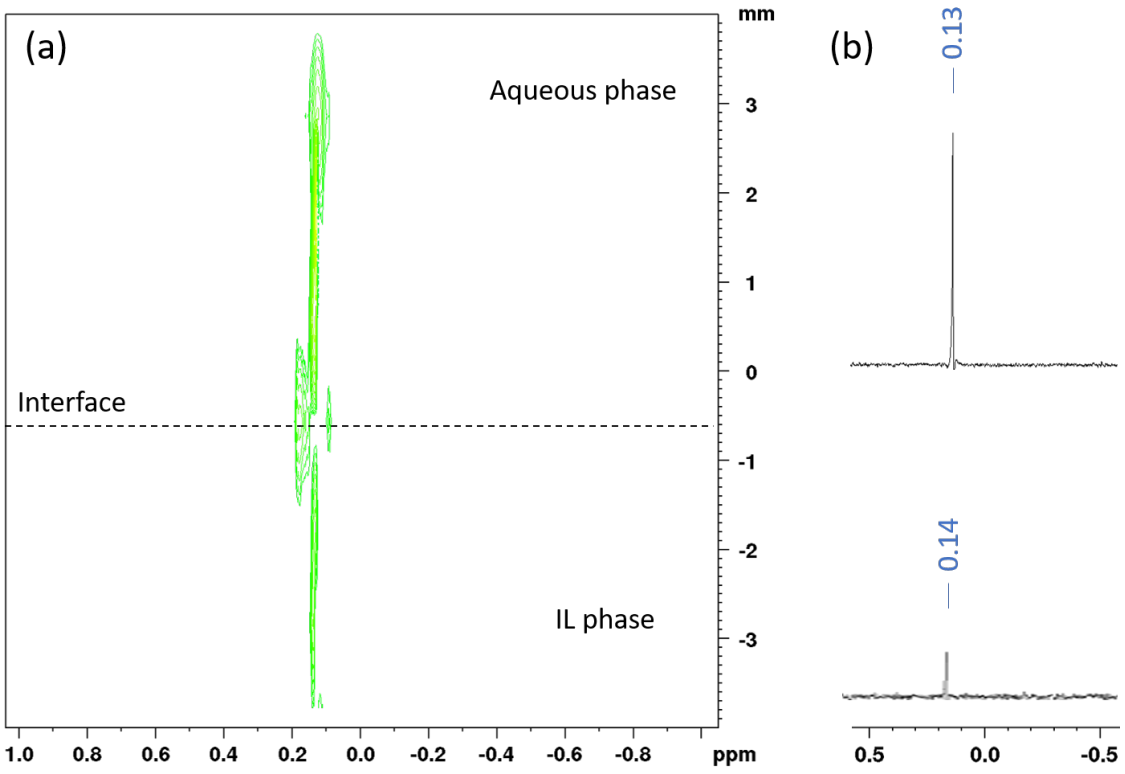

Figure 3.9: (a) ^{7}Li 2D mapping of chemical shift according to position along the tube's z-axis and (b) ^{7}Li 1D spectra of the aqueous phase (top) and the IL phase (bottom) extracted from the 2D LOCSY map.

3.4 Heating and Homogenization of a Thermomorphic System

Homogeneous liquid-liquid extraction processes require heating and homogenizing a thermomorphic system composed of an ionic liquid and an aqueous phase.

To follow the heating and homogenization of an extraction system, approximately 300 mg of IL [Chol][TFSI] saturated in water and an aqueous phase with 0.1 M of LiCl and 24 % w/w of betaine in a mass phase ratio IL:aq of 1:1 in 5 mm NMR tube. First, Figure 3.10 (a) shows the resulting ^{1}H NMR 2D map of the biphasic system at room temperature; the top of the map part corresponds to the aqueous phase of the system and the bottom part to the ionic liquid phase, as described before. Nevertheless, these spectra were recorded with a wider range of offset frequencies than in Figure 3.8, which results in a shift of resonances and a broadening observed at the interface of the biphasic system at the meniscus and the extremities of the coil. Magnetic susceptibility variations might be the cause of these observations. The magnetic field heterogeneity can be challenging to compensate fully by magnet shimming. Second, Figure 3.10 (b) and (c) show the system at 80 °C without agitation for 2 h and 10 h, respectively. A shift of resonances and the start of phases mixing are observed. Despite these long heating times, complete mixing of phases is not seen, and the sample remains heterogeneous even after more than 20 h under 80 °C (data not shown). This fact confirms the absence of convection on the systems since otherwise, it would yield a faster biphasic to monophasic transition.

As the biphasic/monophasic transition appears to be limited by diffusion. There are two options for in situ NMR study of such systems. The first one is to heat the mixture inside the spectrometer and wait for the equilibrium, which is excessively time-consuming. The second option is to agitate the mixture outside the spectrometer during the heating or cooling times and insert it in the spectrometer afterward. In addition to convenience, the temperature is not controlled during the tube transfer. It appears that an easy-to-use setup for in situ agitation inside the spectrometer must be developed [154].

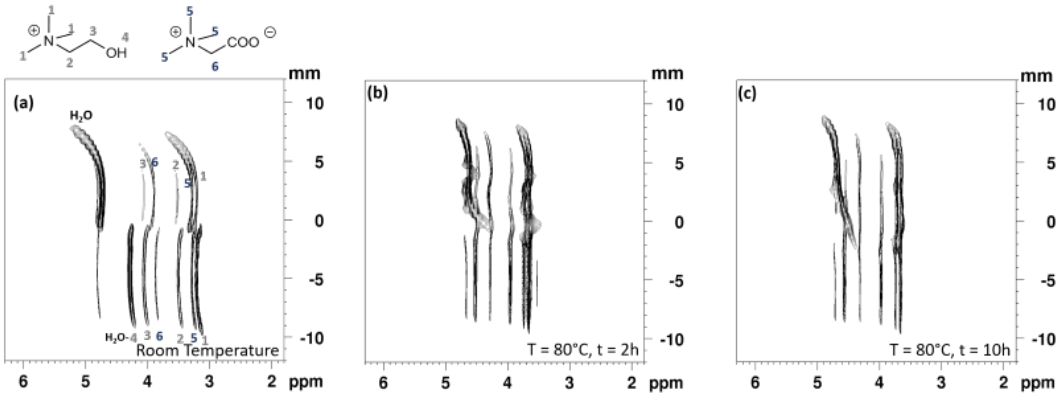

Figure 3.10: LOCSY 2D map of [Chol][TFSI] and aqueous phase biphasic system at (a) room temperature (b) heated at 80 °C after 2 h and, (c) after 10 h at 80 °C. The maps were obtained with a pulsed field gradient of 5.5 G/cm was used, corresponding to 10 % of gradient-amplifier power in a 5 mm BBI probe. A refocusing pulse of RE-BURP type with a bandwidth of 1170 Hz was applied. The frequency offset of the pulses was incremented from −30420 to +35100 Hz in steps of 1170 Hz.

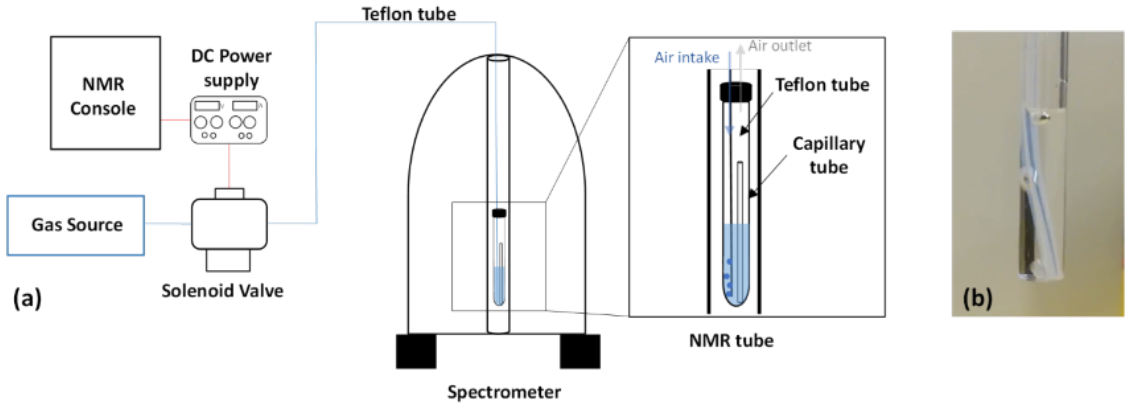

Figure 3.11: Agitation setup components and scheme. The complete schema of the agitation setup is presented in (a). The gas bubbling inside the NMR tube can be seen in (b).

3.4.1 Homogenization setup

The schema of the system and its components are presented in Figure 3.11. The opening of the solenoid valve (Swagelok sc00015) allows the release of gas bubbles (N_2) through a Teflon tube located inside the NMR tube.

The solenoid valve is itself connected to a compressed gas line, allowing a quick switch. Its power supply is provided by a 24 V DC current (Iso-Tech IPS 2303DD). The spectrometer software (`Topspin` 3.6.2) controls the switching of the solenoid valve via a 1 V electrical signal which is retrieved from the Bruker Avance III NMR spectrometer console. This electrical signal acts as a switch to control the closing and opening of the solenoid valve. A specific pulse program drives the electrical signal. To activate the gas outlet, the console transmits a current to open the valve, which allows gas injection into the tube. The pulse program used is shown below.

```
1 ze
    30s setnmr3^20
2 30m
    30s setnmr3|20
exit
```

The pulse program instruction to turn the electrical output signal on or off is `setnmr`. The circumflex (gas in the tube) and vertical bar (no gas flow) characters define the activation or deactivation of the 1 V signal, respectively. The `setnmr` instruction must be specified behind a delay. The bubble time is therefore defined between the two `setnmr` instructions. In particular, it is set to 30 min in this program. In this way, it is possible to correlate precisely the stirring time and the recording of the NMR spectra. A macro controls a series of different programs and pulse programs. In this macro, in the first step, the gas injection is deactivated to avoid the effects of disturbances caused by the gas flow in the tube and, consequently, the inhomogeneity of the magnetic field. The second step starts the pulse program, which determines the duration of the gas passage inside the tube during a given time. After this agitation, it turns off again to perform automatic tuning, shimming, and finally executes the NMR experiment. The gas flux is controlled manually in the gas line outlet and the valve in a way that provides the appropriate agitation for the studied systems. Figure 3.11 (b) presents an image of the gas flow inside the NMR tube. The complete schema of the agitation setup can be seen in Figure 3.11 (a).

NMR tube preparation for homogenization A 10 mm tube was used to have enough space to fit both the Teflon tube and the glass capillary for the lock of the magnetic field. The different components are introduced in the following order: (1) the ionic liquid that is the densest phase, (2) the sealed capillary of 1.7 mm diameter, filled with deuterium oxide, and (3) the aqueous phase. Two holes were made in the NMR tube cap, one larger of approximately 2.5 mm to insert the Teflon tube of an outer diameter of 3.17 mm and an inner diameter of 1.58 mm, for the intake of gas, and finally one smaller of 0.5 mm to work as a gas outlet. To avoid capillary effects inside the Teflon tube and, consequently, the formation of interfaces at different positions in the NMR tube, the Teflon tube was perforated at several points in the part that was immersed in the ionic liquid.

3.4.2 Biphasic system homogenization

Figure 3.12 presents the same system (described in § 3.4) but with the homogenization setup, which permits the agitation of the sample inside the spectrometer. The acquisition, at room temperature and without agitation, is started just right after the contact with the two phases, IL and aqueous phase (Figure 3.12(a)). For this reason, the betaine diffuses

progressively during the acquisition from the aqueous phase into the ionic liquid phase. In consequence, a shift of resonances of the OH–H_2O peak (see the fork shape around 4.7 ppm in Figure 3.12(a)) in the IL phase along the z-axis in the NMR tube, is observed. This change is related to the concentration difference of the betaine in the IL phase. This shift means that the betaine concentration is higher close to the interface.

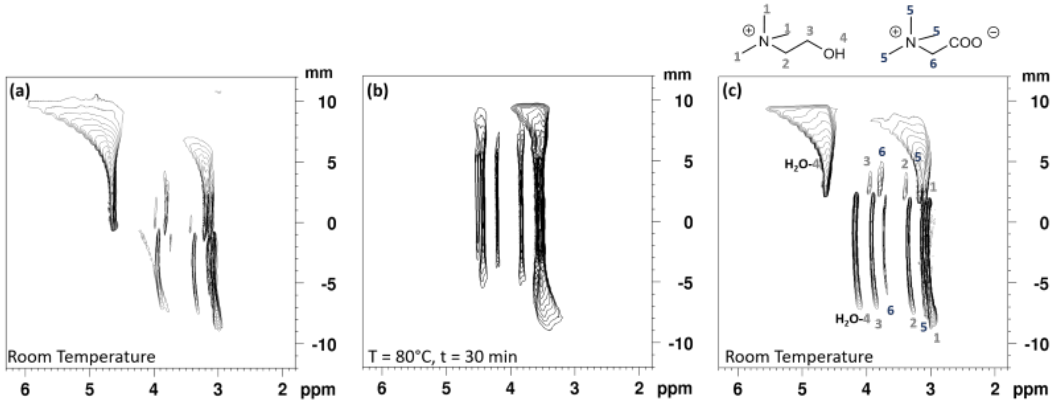

Figure 3.12: LOCSY 2D map of [Chol][TFSI] and aqueous phase biphasic system at (a) room temperature, (b) heated at 80°C after agitation during 30 min, (c) return at room temperature. The vertical axis origin was arbitrarily set to the position of the interface. The maps were obtained with a pulsed field gradient of 5.5 G/cm was used in a 10 mm BBO probe. A refocusing pulse of RE-BURP type with a bandwidth of 1170 Hz was applied. The frequency offset of the pulses was incremented from −10800 to +6750 Hz in steps of 450 Hz, equivalent to 400 µm slices.

In the second step, the system is heated at 80 °C, reaching this temperature within 15 min. The agitation starts immediately when the temperature reaches 80 °C. Notably, after only 30 min of agitation, the complete mixing of the phase and the homogenization are achieved (Figure 3.12 (a)). The homogenization of the system can also be confirmed with a 1D image of the sample acquired by an echograd sequence[130]. This experiment makes it possible to obtain a 1D image of the sample. Figure 3.13 (a) shows the Echograd profile of the tube at 80 °C after agitation. The plateau observed confirms a homogeneous distribution all over the sample. On the contrary, without agitation, a heterogeneous distribution is observed even after 20 h at 80 °C (Figure 3.13 (b)). Furthermore, the echograd indicates that no convection occurs at high temperatures. Note that the spectra' edges correspond to the coil's edge effects.

The return of the sample to room temperature is observed in Figure 3.12 (c). Due to

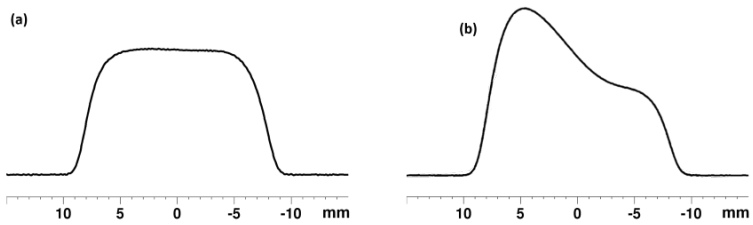

Figure 3.13: Echograd spectra of the sample heated at 80 °C after (a) 30 min of agitation and (b) 20 h, without agitation setup.

the mass transfer between the phases during the process, a phase change in the interface height might occur in the tube. An increase in volume is observed in the IL phase and bottom phase. However, no significant change is observed in the interface level of the system when the experiment is done outside the spectrometer. The opposite is observed for systems without lithium: an increase in the aqueous phase volume. One possible reason for this observation could be the influence of salts on ionic liquid IL and water mixtures is significant. Studies have been conducted to explore how salts impact the mutual solubility and subsequent changes in the cloud point temperature of thermomorphic systems. Certain salts can either promote increased solubility, salting-in, or decreased solubility, salting-out, depending on the specific type of salt introduced to the system [147, 155]. Dupont presents a sequence for salting-out in ionic liquids, where Li^+ and Cl^- ions appear to decrease the miscibility of the phases IL/water. On the other hand, the solubility of water could be increased in the ionic liquid due to the presence of betaine [156]. The increase in the volume of the ionic liquid phase might be explained by a more significant increase in water solubility in the ionic liquid and a decrease in IL solubility in the aqueous phase. Once in the NMR tube, this change in the interface would be more visible than in the experiments done in a bigger dimensions flask in the laboratory bench. Another potential cause might be air in the Teflon tube after bubbling, which could shift the liquid level in the NMR tube upwards. It is also worth considering that liquid projections, some water evaporation, or changes in the tube position inside the spectrometer may contribute to what is seen on the map.

Resonance shifts and peak broadening are also observed in the spectra on Figure 3.12 due to the boundaries of the excitation volume of the coil.

To insert the NMR tube in the spectrometer, the airlift cannot be used alone, but the Teflon tube has to be guided carefully through the bore in a way that allows the NMR tube to go down to the probe, avoiding that the tube stays stuck in the upper parts of the spectrometer bore. The hole in the NMR tube stopper must be tight enough to keep the Teflon tube fixed in the NMR tube. Once the experiment is done, it might be necessary to pull gently the Teflon tube to lift the NMR tube. For these reasons, flexible tubes that don't interfere with the NMR signal are recommended in this method.

The macro was used to facilitate the experiments, but it is not necessary. Only the pulse program to operate the valve is required, although the use of a macro to unlock during agitation, lock, shim, and tune after the agitation is convenient for the user.

Making a small vent in the stopper for the gas outlet and checking visually the gas flow inside the NMR tube is fundamental to prevent liquid projections inside the spectrometer. This method makes it possible to successfully perform agitation thanks to the gas bubbling setup in the NMR tube located inside the spectrometer and, hence, homogenize the sample. The validation of our method has been carried out using homogeneous liquid-liquid extraction processes and slice-selective NMR experiments. It has been evidenced that clean homogenization was rapidly achieved, whereas, without agitation, the system is still heterogeneous after 20 h. This method can be applied for various purposes, such as macroscopically nonstable samples or inserting operando gas within a liquid sample.

3.5 Phase Separation of Thermomorphic System

Phase separation or settling is crucial in solvent extraction processes as it facilitates efficient extraction, selectivity, purification, and the recovery of solute species from the extract phase. Ensuring clear phase separation enables better process control and optimization. In a thermomorphic system, phase settling starts with decreasing temperature to room temperature. Once the system was homogenized inside the spectrometer at 80 °C, it was set back to the room temperature 25 °C. For the LOCSY experiments, the selective proton pulses RE-BURP used had a bandwidth of 1170 Hz, which is equal to 0.5 mm slices. Their frequency offset was incremented from −7980 to +8400 Hz incremented in 1170 Hz steps, 14 slices in total.

One LOCSY spectrum was obtained as the system returned to room temperature. The Auto shimming tool was turned on during all experiments to improve lineshape quality. This 2D experiment takes around 45 min. Figure 3.14(a) shows the first spectrum obtained during phase separation.

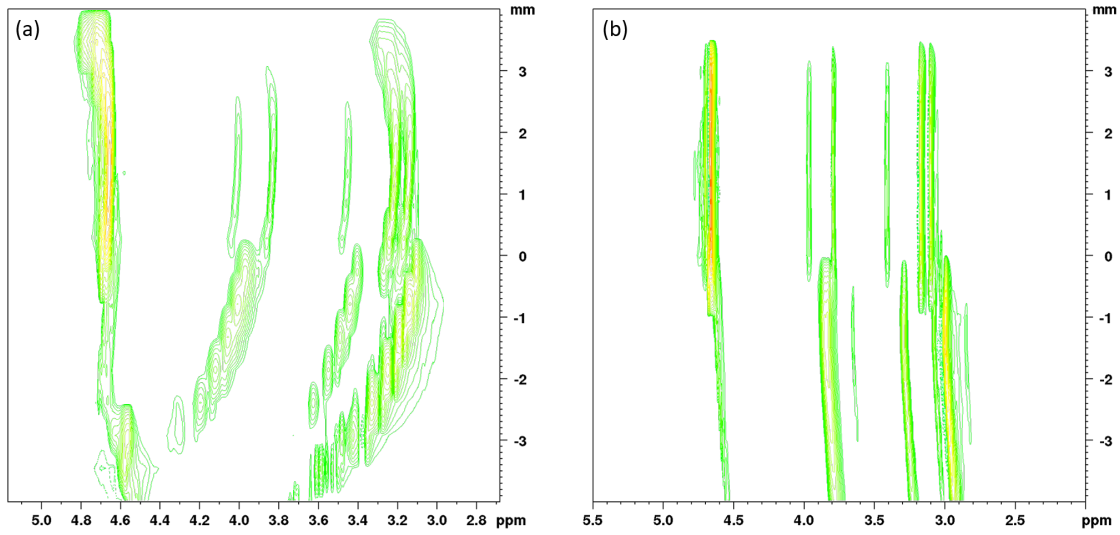

Figure 3.14: 2D LOCSY map obtained (a) during cooling down from 80°C to 25° C, system not in equilibrium; (b) map obtained after phases settled.

Chemical shift variations are particularly noticeable in the region where the ionic liquid (IL) settles, which coincides with the starting point of spectrum recording. These changes in chemical shift and broadening could be attributed to temperature, concentration, and structural variations resulting from the settling process. The spectrum acquisition commenced from the bottom of the tube and progressed towards the top. Consequently, the chemical shifts at the bottom of the spectrum resemble those observed in the system at 80 °C (Figure 3.10). As the phases cool and settle, the chemical shifts tend to shift towards lower frequencies. The presence of inhomogeneities in the system, such as the formation, growth, and precipitation of nanodroplets, contributes to peak broadening due to associated variations in the magnetic field. Upon reaching the aqueous phase after approximately twenty minutes of acquisition, the observed effects on the IL phase diminish. This could be attributed to the stability of the system at room temperature and the faster separation of the lower viscosity aqueous phase compared to the IL. Subsequent spectra recorded after the initial one did not show significant changes in peak intensities.

Similar systems have demonstrated only slight changes in extraction efficiency after 50 minutes at room temperature, suggesting complete phase settling at this time [38].

3.5.1 Monitoring the time evolution of phase separation with LOCSY

The LOCSY pulse program offers the advantage of selectively observing specific regions along the tube without recording the entire tube volume. To monitor the early stages of phase separation, one spectrum was recorded for the initial region of the IL phase and another for the initial region of the aqueous phase. These slices were approximately centered at 2 mm and −2 mm on the scale presented in Figure 3.10. Thus, spectra were obtained for each phase at approximately five minutes intervals. Spectra obtained before 35 minutes were challenging to analyze due to peak broadening, peak overlap, and inadequate shimming caused by inhomogeneities resulting from phase separation. To mitigate peak overlap issues, the CH_2 peak of betaine, the lowest frequency CH_2 peak of cholinium, and the water peak intensity were plotted in figure 3.15. However, in the ionic liquid phase, the overlapping peaks of the higher frequency cholinium CH_2 and H_2O-OH hindered their deconvolution before 90 minutes, resulting in a decrease of the water content only visible after 90 minutes in the IL phase.

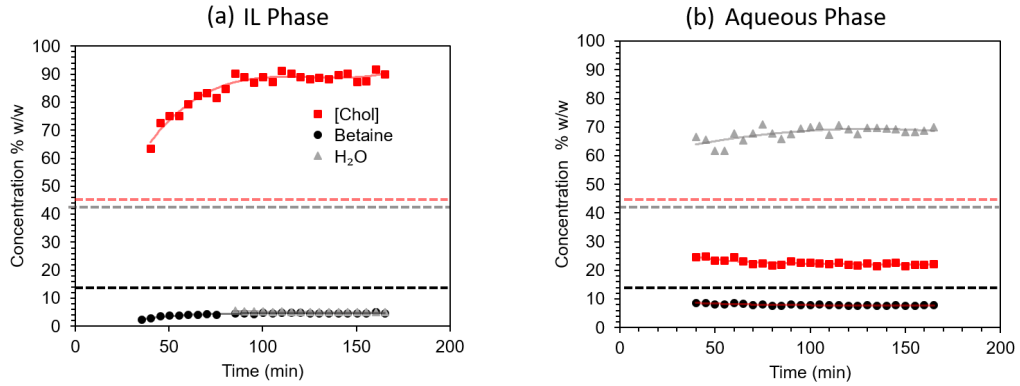

Figure 3.15: Intensities of cholinium, betaine and H_2O overtime during phase separation for (a) IL and (b) aqueous phase, from 25°C. The dashed lines represent the concentration of the monophasic system at 80°C.

Figure 3.15 shows that the intensity changes in the IL phase are more significant than in the aqueous phase for the time range analyzed. No significant changes in peak intensities are observed after 100 minutes, as depicted in the 2D maps. Given their linked compositions, the aqueous phase composition should be almost established within 35 minutes, as observed in the aqueous phase. The disparity observed may stem from the varied viscosity, affecting the uniformity of each phase at the observed slice. The higher intensity changes in the IL phase can be attributed to the difference in viscosity between the phases. As the IL phase is more viscous than the aqueous phase, the transfer of material within this phase takes longer. The graph shows a decrease in water content and an increase in IL cation and betaine content in the IL phase. There was a decrease in betaine and cholinium and an increase in the water content. Both graphs show that betaine and cholinium appear to follow the same trend. The method for analyzing the evolution of the system over time may have limitations, as concentration trends in the aqueous phase are more challenging to observe despite changes in the IL phase.

In the homogeneous system at 80 °C, the components distribute themselves to attain a mean concentration, shown in the graph as dashed lines. Consequently, the concentration of betaine in the aqueous phase is expected to increase while decreasing in the ionic liquid phase compared to the mean composition, which is consistent with the graph observation.

However, it is important to notice that these experiments need to be run for a certain time range, which can limit the temporal resolution of the experiments, making it challenging to capture rapid changes in peak intensities that occur on short time scales. The individual spectra of the phases at 40 minutes and 160 minutes are shown in Figure 3.16. It is important to note that distorted lineshapes can be caused by inhomogeneities in the system, such as meniscus and dephasing, due to the pulsed magnetic field, which can affect the accuracy of the analysis.

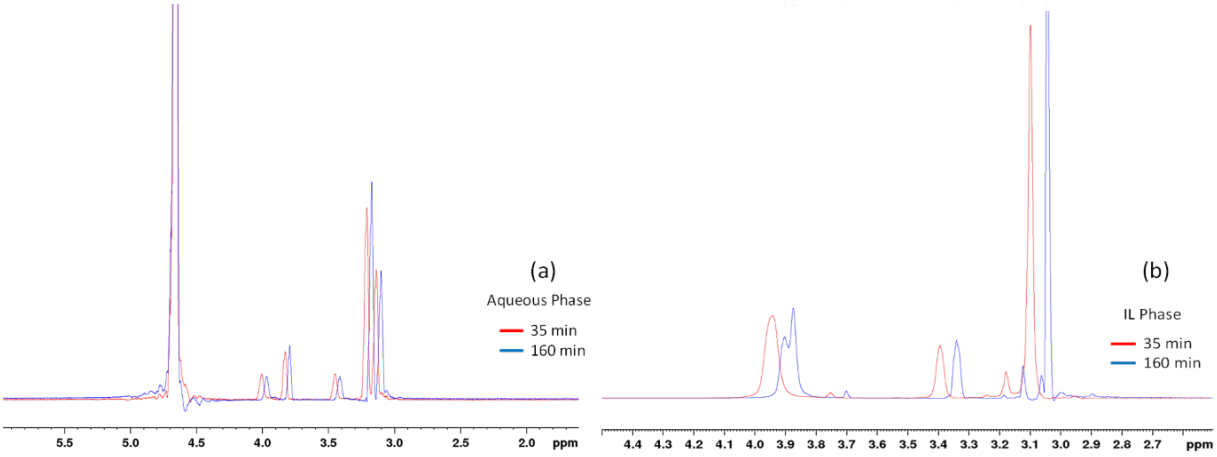

Figure 3.16: 1D spectra the for (a) aqueous and (b) IL phase, at 35 minutes and 160 minutes.

3.6 Conclusion

The LOCSY technique was applied to study biphasic liquid-liquid extraction systems. Clear phase separation and interface regions were observed in the NMR spectra of different nuclei. Concentration gradients and differences in chemical shifts were identified, providing insights into different systems' composition and behavior. In further investigations, it is important to prioritize proper sample preparation and handling to minimize artifacts and enhance data reproducibility. Maintaining precise temperature control during experiments will be essential to mitigate temperature-induced effects and ensure data accuracy. Further optimizing gradient coil shimming to minimize inhomogeneities will also lead to more accurate and precise gradient performance, ultimately improving spatial resolution. These perspectives can contribute to improving the localized technique, particularly in biphasic systems.

The homogeneous liquid-liquid extraction process typically requires heating and homogenization. However, implementing an in situ agitation setup using gas bubbling inside the NMR tube can achieve rapid and efficient system homogenization. The method was validated through slice-selective NMR experiments, demonstrating that clean homogenization can be achieved quickly. This approach offers potential applications for studying macroscopically unstable samples or introducing operando gas into liquid samples. The homogenization process makes it easy and fast to homogenize and insert gas into the spectrometer. However, improving the gas flow in the system would enhance the method. To improve spatially resolved results interpretations when needed, studies on the effects of gas bubbling in the tube's position and liquid could be considered for the current setup.

Phase separation during the cooling process was investigated for the [Chol][TFSI]/aqueous phase system. Chemical shifts and peak intensities showed variations as the system transitioned from 80 °C to room temperature. The settling process was more pronounced in the ionic liquid phase, with significant intensity changes observed. Betaine exhibited higher affinity in both phases, while water content decreased in the ionic liquid phase. After 100 minutes, no significant changes were observed in peak intensities.

Since LOCSY can measure concentration profiles with reasonable time and space resolution, it is an interesting tool for investigating phase transfer dynamics or mutual diffusion in these complex phases. For instance, Pantoja et al. [157] proposed to fit the concentration profile of each species obtained in the slice selective experiment to determine mutual diffusion coefficients in a system presenting a LCST. Such an approach seems promising for the systems of the present study.

Refining data processing techniques to remove artifacts or advanced deconvolution methods to enhance spectral resolution and sensitivity could be considered as perspectives for further improving the LOCSY technique. Besides, the data obtained from localized spectroscopy experiments can be used to validate and improve computational models and simulations of solvent extraction systems. This approach helps in gaining a comprehensive understanding of the processes.

The examples in this chapter provide a glimpse into the potential applications of the LOCSY sequence, showcasing its ability to investigate extraction systems. These findings can contribute to a better understanding of thermomorphic systems and their applications in solvent extraction processes.

Chapter 4

Lithium Extraction using Thermomorphic Ionic Liquids

Contents

This chapter discusses the potential use of the ionic liquid cholinium bis(trifluoromethylsulfonyl)imide, [Chol][TFSI], for the homogeneous liquid-liquid extraction (HLLE) of lithium ions. This IL has been successfully applied for metal extraction with different extractants [39, 72]. [Chol][TFSI] exhibits thermomorphic behavior in water, with an upper critical solution temperature (UCST) of 72 °C [82]. Since [Chol][TFSI] lacks specific chelating functions, an extractant is usually necessary [72]. Due to their polarity, polar extractants could be combined with [Chol][TFSI], while nonpolar extractants have low solubility in this ionic liquid. The chosen extractant was betaine, meeting the requirements of higher affinity for the ionic liquid phase. Betaine is a zwitterionic molecule with a quaternary ammonium group and a carboxylic group in its structure. This molecule was applied for the HLLE of several metals (Ag, Cu, Zn, Fe, Co, Ni, In, Ga and several rare earths) [73].

Most studies of the liquid-liquid extraction process are based on analytical techniques focused mainly on metal ions. NMR spectroscopy is used to fill the gaps in the understanding of the liquid-liquid extraction process since this technique allows the observation of the different species present in the system, such as extractant, cation, and anion of the IL, and some metal ions following other nuclei. Besides its criticality, lithium was chosen because it has isotopes relatively easy to access by NMR.

The chapter begins by evaluating the effects of various parameters on lithium extraction efficiency, and assessing concentrations using the ERETIC digital method. The potential of [Chol][D2EHP] as a lithium extractant is also studied.

Furthermore, a detailed NMR investigation is conducted into the solvation of Li^+ ions in pure [Chol][TFSI]. The chapter delves into diffusion characteristics and longitudinal relaxation time measurements to provide a molecular-level understanding of Li^+ behavior in this ionic liquid environment.

The focus then shifts to a comprehensive NMR study of the extraction system, including the construction and analysis of the [Chol][TFSI]/water/betaine ternary phase diagram and the examination of chemical shift changes in the ^{1}H NMR spectrum under varying water and betaine contents. The exploration extends to observing the ^{1}H NMR spectrum of the [Chol][TFSI] phase post-lithium extraction. Furthermore, NOE correlation analysis, including both NOESY and HOESY experiments, is incorporated to elucidate intermolecular interactions. Diffusion experiments are also used to provide insights into molecular mobility within the system. Finally, small-angle X-ray scattering (SAXS) is used for the investigation of structural organization in the studied systems.

This work intends to investigate the interaction of Li ions in HLLE systems and to understand the mechanism at play.

4.1 Quantification of Extraction Efficiency and Effects of Parameters

To assess the extraction efficiency of lithium using the [Chol][TFSI]-betaine system, several extraction parameters were evaluated, including the initial concentration of betaine in the aqueous phase, the IL:aq mass phase ratio, and the initial lithium concentrations in the aqueous phase. The procedure for the homogeneous liquid-liquid extraction is described in the previous chapter. The quantification of lithium concentrations was performed using a quantitative NMR technique, ERETIC Digital (see § 2.3.3.2), and these results were

compared with the Inductively Coupled Plasma Optical Emission spectroscopy (ICP-EOS) measurements. The replacement of betaine for another extractant is also briefly studied in this section by investigating some extraction parameters.

4.1.1 Effect of Betaine Concentration and Evaluation with ERETIC Digital Method

The influence of betaine concentration was examined for two different initial aqueous lithium solutions with concentrations of 0.05 mg/g and 0.005 mg/g by varying the initial betaine concentration in the aqueous phase.

Experimental details *The aqueous phases for extraction experiments in this chapter were prepared with lithium chloride (> 99 %, Prolabo) and ultrapure (Type 1) water (Direct-Q 5UV Millipore). A mass ratio of 1:1 for IL:aq was maintained, and the concentration efficiencies were determined based on the final lithium concentration in the aqueous phase. The NMR measurements were performed in a 500 MHz (11.7 T) Bruker AV III spectrometer equipped with 5 mm Double Resonance Broadband Probe (BBI). The NMR tubes were prepared by adding approximately 0.3 mL of aqueous phases after extraction and a 1.7 mm Bruker NMR capillary filled with deuterium oxide (Sigma AldrichL, 99.9 atom % D). Unless stated otherwise, all the NMR tubes in this work were prepared similarly. Simultaneously, the concentrations in the final aqueous phase were measured using the ERETIC digital method and ICP-EOS. A 100 µg/mL lithium and Geo elements aqueous solution (diluted in a 5 % HNO_3 aqueous solution, SM60A-100, VHG Labs) were used as calibration standards for inductively coupled plasma optical emission spectroscopy (ICP-OES). The aqueous phase samples were diluted by approximately a factor of 12 in a 5 % HNO_3 aqueous solution. The equipment standard deviation gave the ICP-EOS error bars. The ERETIC digital measurement uncertainties are estimated from linearity tests by comparing the initial values of known LiCl concentration and those calculated following the measurements. The NMR measurement uncertainties are estimated at 8 % for lithium.*

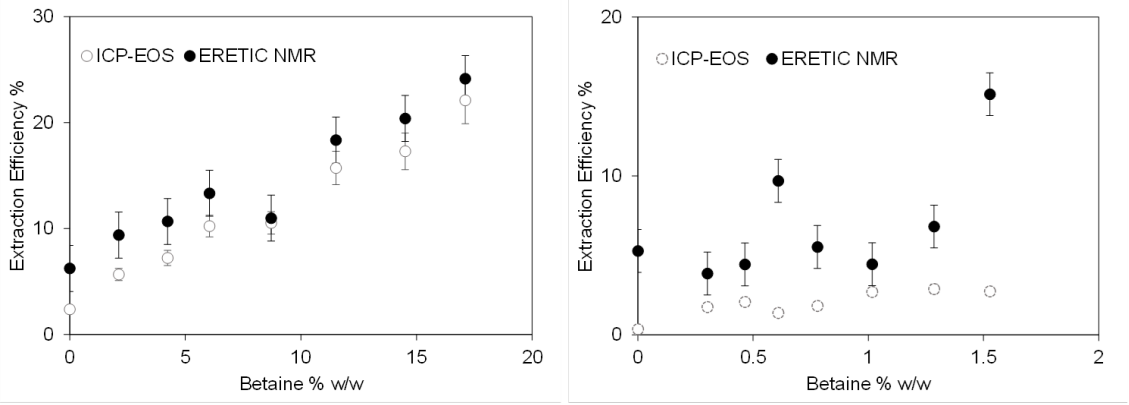

Figure 4.1: Effect of betaine concentration on Li extraction efficiency in two different initial Li concentrations (a) 0.05 mg/g and (b) 0.005 mg/g, IL:aq mass ratio 1:1 and comparison between two quantitative techniques, ERETIC NMR and ICP-EOS.

The results obtained by these two techniques are displayed in Figure 4.1. The exact aqueous solutions after extraction were used for NMR and ICP-EOS analysis. At

the highest initial Li concentration (0.05 mg/g), there is a good agreement of the NMR method and the ICP-EOS measurements. Figure 4.1(b) shows a discrepancy between the results of the two techniques at low lithium concentration (0.005 mg/g). The quantitative NMR yielded higher concentrations compared to ICP-EOS. This discrepancy can be mitigated by increasing the number of scans and improving the integration process. However, a good agreement was observed between the results obtained from both techniques at higher lithium concentrations. This agreement suggests that, with the parameters used, the ERETIC digital method is suitable for evaluating lithium concentrations in NMR. Furthermore, with an appropriate choice of acquisition parameters, the ERETIC method could assess lower concentrations accurately. The ERETIC digital method is an efficient, non-invasive analytical technique for quantifying Li concentrations, thus simplifying the process by eliminating the need for sample dilution or adding a reference compound.

In assessing the impact of betaine concentration, betaine concentration reveals a positive correlation with extraction efficiency. The highest Li concentration presented an overall higher extraction efficiency. However, the highest extraction efficiency reached was around 24 % with approximately 16 % w/w betaine in the initial aqueous phase. Despite this, the absence of a plateau for the initial lithium concentration of 0.05 mg/g implies there may be room for further optimization of extraction efficiency. In contrast, a plateau is noticeable in the ICP-EOS results corresponding to the lowest initial metal concentration, Figure 4.1(b). Consequently, the betaine concentration was further raised, approaching the maximum concentration that could be reached without leading to a complete mixing of the two phases at room temperature. The lithium concentration after extraction in the aqueous phase was measured using the ERETIC digital NMR method, a technique also utilized for the measurements discussed in this chapter. An increase in lithium extraction efficiency to nearly 33 % was achieved with an initial betaine concentration of 24 % w/w. However, this efficiency is still low. To improve the lithium extraction efficiency, a study of other extraction parameters linked with this system is done. Additionally, the potential of alternative extractants was explored to improve the overall efficiency of the extraction process.

4.1.2 Effect of the IL:aq phase ratio

The influence of the IL:aq mass ratio was investigated using an initial betaine concentration of 24 % w/w and 0.06 mg/g of Li in the aqueous phase. The mass phase ratio IL:aq was varied from 1:1 to 5:1. The results are shown in Figure 4.2. The extraction efficiency increases until the phase ratio of 3:1, reaching an extraction efficiency of 64%. The extraction efficiency did not increase when more mass of the ionic liquid phase was added while keeping the same mass of the aqueous phase. This lack of change in efficiency could be attributed to the betaine extractant quantity remaining constant in the aqueous phase. The increase of the IL phase might increase the extractant transfer into the phase. However, as the quantity of extractant is limited, the extraction efficiency of lithium is limited. Although the IL:aq phase ratio of 3:1 was more efficient, especially for NMR analysis, the ratio 2:1 was preferable for further analysis to save IL and maintain sufficient mass of the aqueous phase.

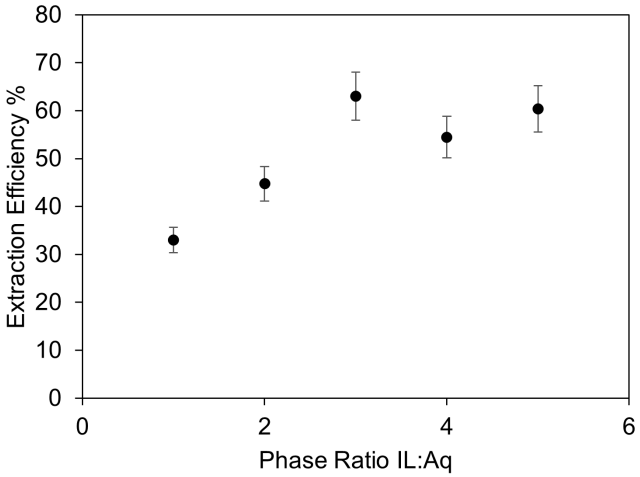

Figure 4.2: Effect of the mass phase ratio IL:aq in the Li extraction efficient. Initial Li concentration was maintained 0.06 mg/g and betaine concentration of 24% w/w.

4.1.3 Effect of Initial Metal Concentration

The effect of initial lithium concentration in the aqueous phase was studied using an IL:aq mass ratio of 2:1 and an initial betaine concentration of 24 % w/w. Results are shown in Figure 4.3. The initial lithium concentration was varied from 0.06 to 2.2 mg/g.

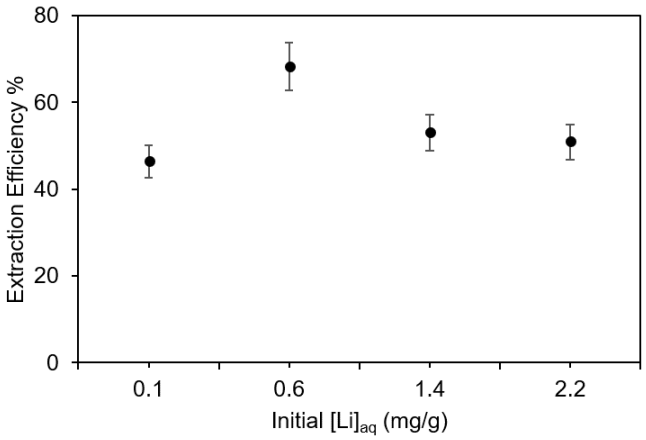

Figure 4.3: Effect of initial Li concentration in the Li extraction efficiency and final lithium concentration in the IL phase. IL:aq mass ratio of 2:1 and an initial betaine concentration of 24 % w/w.

The extraction efficiency increases until a certain point, reaching a maximum of 67% at 1.2 mg/g. The initial increase in lithium concentration appears to increase the extraction efficiency. However, considering the associated error bars, the extraction efficiency remains consistent despite the increased Li concentration. Nevertheless, the efficiency declines after a certain point, which can be attributed to the decreasing miscibility of the two phases as the concentration of lithium and chloride ions in the aqueous phase increases. The change of masses in both phases due to the mutual water-IL solubility could cause an overestimation of the %E. When this solubility is reduced, this overestimation might also be reduced. This apparent plateau might indicate a saturation of the IL with Li ions as the lithium concentration in the IL phase appears constant in the last metal concentrations, as observed in Figure 4.3.

4.1.4 ^{7}Li LOCSY for the determination of Li extraction efficiency

Another significant application of the LOCSY experiment lies in assessing extraction efficiencies within the extraction system. For this purpose, a phase ratio (IL:aq) of 2:1, an initial lithium concentration of 0.1 mg/g, and a betaine concentration of 24% w/w were used. The IL phase was composed of [Chol][TFSI] saturated in water. The homogenization procedure outlined in Section 3.4 was employed within the spectrometer. For the LOCSY experiments, the selective proton pulses RE-BURP had a bandwidth of 910 Hz, which corresponds to 0.1 cm slices. Frequency offset was incremented from −2730 to +2730 Hz incremented in 910 Hz steps.

Figure 4.4 showcases the spectra at room temperature, post-agitation at 80 °C, and after settling back to room temperature. Figure 4.4(a) reveals that some lithium had already migrated to the aqueous phase, a phenomenon potentially attributable to inadvertent mechanical disturbances during sample preparation and manipulation.

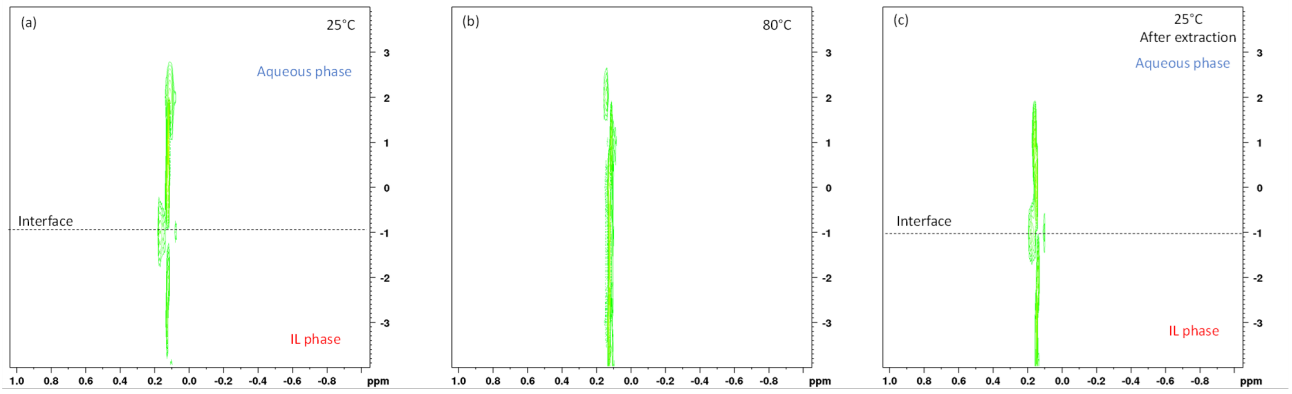

Figure 4.4: ^{7}Li LOCSY maps for [Chol][TFSI]/betaine extraction system. (a) at 25°C before heating and agitation, (b) after heating at 80 °C and (c) the return to the system to 25°C. Initial extraction conditions IL:aq = 2:1, lithium concentration of 0.1 mg/g, and a betaine concentration of 24% w/w.

The extraction efficiency, denoted as %E, was ascertained by averaging the absolute intensities of slices in the IL phase between -3 and -2 mm on the $z - axis$ and between 0 and 1 mm in the aqueous phase after extraction. The derived extraction efficiency stood at 51%. When compared with a system under identical initial conditions measured using ERETIC, which displayed an extraction efficiency of 48%, the results exhibit congruence when error margins are considered.

4.1.5 [Chol][D2EHP] as Lithium Extractant

As lithium extraction with betaine appears to have some limitations, other extractants were explored for lithium extraction with [Chol][TFSI]. Tributyl phosphate (TBP) and di-(2-ethylhexyl)phosphoric acid (D2EHPA) are utilized as a common extractant for lithium ions, along with ketones, crown ethers, and other organophosphorus compounds [158, 159]. However, it was observed in this work that TBP and D2EHPA have low solubility in [Chol][TFSI].

TBP is a neutral extractant with one hydrogen acceptor site per molecule. While, D2EHPA operates as an acidic extractant, providing both hydrogen bond donor and acceptor sites. This extractant tends to form dimers. In non-polar diluents, acid extractants typically exist in the form of hydrogen-bonded dimers. These extractants require neutralization through an acid/base saponification reaction to enhance their extraction capabilities to prevent a rise in the acidity of the aqueous phase due to the release of hydrogen ions during extraction. The acid/base saponification reaction can generate environmentally warmful residues [160]. An alternative to face these issues is to convert this extractant into an IL [161]. This conversion can also facilitate the solubility of the extractant in [Chol][TFSI]. Thus, [Chol][D2EHP] was synthesized with acid-base coupling. This new IL was completely soluble in [Chol][TFSI].

Initially, the effect of [Chol][D2EHP] concentration in the IL phase was studied using an IL:aq mass ratio of 1:1 and an initial lithium concentration of 0.07 mg/g. The concentrations of [Chol][D2EHP] were varied from 5 to 50 % w/w. However, for concentrations above 25 %, the IL and aqueous phases are completely miscible. Figure 4.5 presents the results. Lithium exctraction efficiency increases until a maximum 17 % with 10 % w/w of

[Chol][D2EHP] in [Chol][TFSI] saturated in water. Nevertheless, the extraction efficiency from 10 to 25 % w/w does not show improvement.

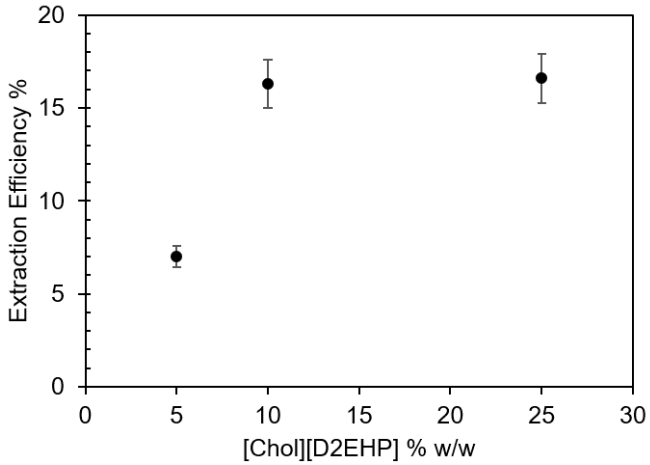

Figure 4.5: Extraction efficiency of Lithium as a function of the initial [Chol][D2EHP] extractant concentration. IL:aq mass ratio of 1:1 and an initial lithium concentration of 0.07 mg/g.

Subsequently, the influence of the phase ratio was also investigated. The phase ratio varied from 1:1 to 5:1, as shown in Figure 4.6. The extraction efficiency reached a plateau at 2:1 with an extraction efficiency of 45%.

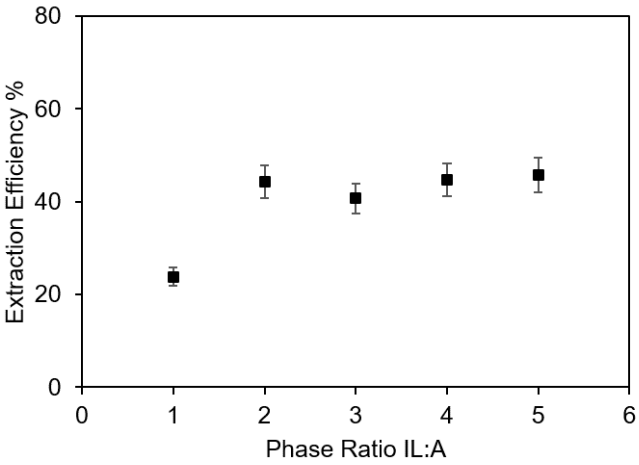

Figure 4.6: Extraction efficiency of Lithium as a function of the mass phase ratio IL:aq, for initial lithium concentration of 0.07mg/g and 10 % w/w of [Chol][D2EHP].

This behavior might be due to the increasing loss of extractant [Chol][D2EHP] into the aqueous phase. Indeed, this extractant increases the solubility of the IL in the aqueous phase. It could be observed in Figure 4.7 with the ^{1}H spectra of the IL and aqueous phase after liquid-liquid extraction. Once the aqueous phase is saturated with the ionic liquid phase, no extraction efficiency changes are observed.

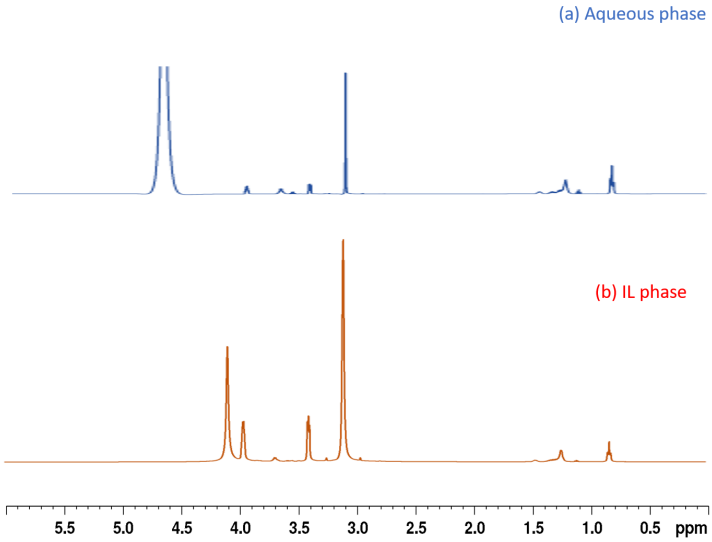

Figure 4.7: ^{1}H spectra of the (b) IL and (a) aqueous phase after liquid-liquid extraction. Initial extraction conditions of IL:aq = 2:1, lithium concentration of 0.07mg/g, and 10 % w/w of [Chol][D2EHP].

In conclusion, for [Chol][D2EHP] as the extractant, we have evidenced a lower extraction efficiency for lithium, most probably due to the transfer of [Chol][D2HEP] and [Chol][TFSI] from IL phase to the aqueous phase. Consequently, we have chosen the system [Chol][TFSI] and water with betaine as an extractant, for further investigations in HLLE. Nevertheless, some structural investigations with [Chol][D2EHP] are presented later in this chapter to understand its behavior better.

4.2 NMR investigation of the solvation of Li^+ in pure [Chol][TFSI]

The extraction processes involve several species interacting, possibly modifying a system's phase diagram. In this regard, it is interesting to study the different parts of this complex system separately. At first, neat [Chol][TFSI] with lithium at different concentrations, are important building blocks for the understanding of the extraction processes. Moreover, little information is available in the literature. In this section, we investigate the dynamics of [Chol][TFSI] with lithium using pulsed field gradients NMR and NMR relaxometry.

To investigate the impact of lithium ions solvation in an ionic liquid environment, samples with varying concentrations of Li were prepared by adding LiTFSI salt (99.9 %, Solvionic) to the ionic liquid [Chol][TFSI] within an inert atmosphere glove box. Before being introduced into the glove box, the salt, and ionic liquid were dried overnight in a freeze dryer, then in a vacuum furnace at 80 °C, and finally in the furnace connected to the glove box under vacuum. The resulting samples were placed into a 5 mm NMR tubes, and a DMSO capillary was added for locking in each tube. The NMR experiments were performed at 40 °C to ensure all samples were liquid, as concentrations below 0.1 molal were solid at room temperature. In this section, these samples are studied using NMR spectroscopy, mainly longitudinal relaxation times and diffusion coefficient determination under varying lithium concentrations.

The exclusion of water in this initial exploration offers a unique perspective on the interplay between lithium ions and the ionic liquid in isolation, without the influences that water may present. The following sections will study the system in the presence of water. This comparative study holds great significance as it enables us to interpret the role of water in modulating the metal ions solvation process, thereby contributing to a comprehensive understanding of the system's behavior under diverse conditions.

4.2.1 Diffusion

It is known that lithium has a great impact on ionic liquids dynamical properties [162–174]. It is important to characterize how lithium impact our ionic liquid, and particularly the dynamical properties. Hence, the diffusion coefficient of each species have been measured using the pulsed field gradients NMR technique.

Experimental details. *NMR Pulsed Field Gradient (PFG) measurements were performed on a 300 MHz and a 500 MHz Bruker spectrometers at 40 °C. The 300 MHz spectrometer is equipped with a probe capable of producing magnetic field gradient pulses up to 50 G cm^{-1}, for ^{19}F and 120 G cm^{-1}, for ^{7}Li and ^{19}F experiments, and the 500 MHz spectrometer with a probe of maximum strength gradient of 55 G cm^{-1}, for ^{1}H experiments.*

The diffusion measurement was conducted with a 2D sequence using stimulated echo, bipolar gradients, and eddy current delay (Bruker ledbpgp2s pulse program). The gradient pulse duration δ and the diffusion time Δ were in the range of 1 to 10 ms and 0.2 to 2 s, respectively. The gradient strength G was varied from 2 to 98 % of the maximum strength in 16 steps. The diffusion coefficients D were determined by fitting the echo signal decay with the Stejskal-Tanner equation 2.11.

The self-diffusion coefficients of cholinium (^{1}H), $TFSI^-$ (^{19}F), and lithium (^{7}Li) ions decrease with the molality of LiTFSI (Figure 4.8) about two orders of magnitude from the initial dilution to 3 mol/kg. Such decrease when adding lithium salt in ionic liquids has been observed, along with an increase of the viscosity, for all the studied system: imidazolium type with LiTFSI [164, 166, 167, 169, 171, 173], $LiBF_4$ [162, 172, 174] or $LiPF_6$ [164], pyrrolidinium kind with LiTFSI [163, 170] or $LiPF_6$, ammonium kind [165, 168], and other less common ionic liquids [169]. The density of the liquid also often increases upon lithium salt addition.

Nevertheless, the self-diffusion coefficients decrease depending on the ionic liquids. In the case of [Chol][TFSI], it is by far the strongest observed, as it is usually less than one order of magnitude. It has been related to a modification of the structure of the liquid through the solvation of lithium [175]. In the case of $TFSI^-$ anion, lithium cation interacts more strongly with the oxygen [176, 177] and is surrounded by approximately three $TFSI^-$. Experimentally, the solvation of lithium cation by $TFSI^-$ anion is expressed by the evolution of $D(TFSI^-)$ that tends to come closer to $D(Li^+)$ when Li^+ concentration is increased. In this regard, the effect of anion on transport in lithium/ionic liquid systems has been more often investigated. The very symmetric BF_4^- anion yields a very slow diffusion of Li^+, despite $D(BF_4^-)$ remains close to the diffusion value of the ionic liquid cation [162, 172, 174]. In contrast, for $TFSI^-$, lithium diffusion remains close to other ionic species [164, 166, 167, 169, 173]. This idea of asymmetry has been pushed forward by mixing asymmetric anions [177], leading to better transport performance for lithium.

Another interesting observation in Figure 4.8, is the crossing of $D(Li^+)$ and $D(TFSI^-)$ around 1.5 mol/kg: below 1.5 mol/kg $D(TFSI^-) > D(Li^+)$ and above $D(Li^+) > D(TFSI^-)$. Note that in pure molten lithium bis(fluorosulfonyl)imide and lithium fluorosulfonyl(trifluoromethylsulfonyl)imide $D(Li^+) > D(\text{anion})$ with the respective values of $D(Li^+) = 1.4 \times 10^{-11}$ m^2/s, $D(FSI^-) = 5.5 \times 10^{-12}$ m^2/s and $D(Li^+) = 7 \times 10^{-12}$ m^2/s, $D(TFSI^-) = 0.7 \times 10^{-12}$ m^2/s [178]. Again, the structure of the ionic liquid mixtures can be questioned. Lithium cations at low concentrations are isolated and mainly coordinated by the two groups of oxygens of $TFSI^-$ (bidentate) [177]. At high concentrations, lithium cations form agregates sharing $TFSI^-$ anions, leading to monodentate coordination [177]. This structure modification operates a switch between a vehicle transport mechanism, i.e., lithium moves with its solvation sphere, to a hoping mechanism, i.e., lithium jumping from $TFSI^-$ site to $TFSI^-$ site. The cross-over observed in Figure 4.8 would be experimental evidence of this phenomenon.

To better understand the phenomenon at play, this long-distance transport study (PFG NMR investigates micrometer scale diffusion) needs to be completed by studying at a more local scale.

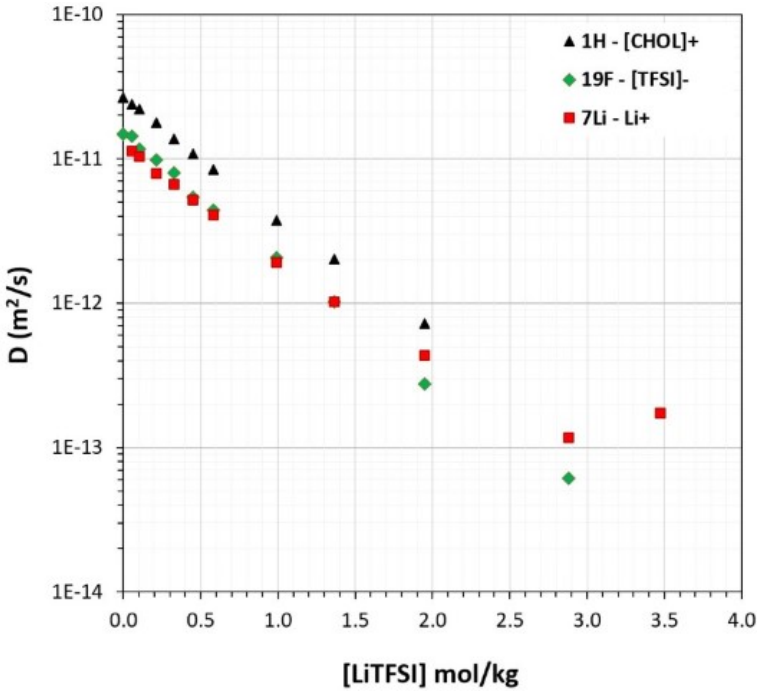

Figure 4.8: Self-diffusion coefficient of choline (black triangle), TFSI (green diamond), and lithium (red square) versus the molality of LiTFSI in the molten salt.

4.2.2 Longitudinal relaxation time measurements

To understand how lithium impacts the dynamics of the ionic liquids at short timescale, the NMR relaxation times T_1 of ^{7}Li, ^{19}F and ^{1}H of all chemical groups have been measured. Indeed, T_1 gives insight into to the dynamics at timescale about $1/\omega_0$, i.e. in the present case at the nanosecond timescale [179]. The idea is to see how local motions affect long-range motions.

The longitudinal relaxation times T_1 were determined using Inversion Recovery sequence on a 500 MHz and a 300 MHz Bruker spectrometers for ^{1}H, ^{19}F and ^{7}Li. For ^{1}H and ^{7}Li nuclei, the T_1 values at 11.7 T (500 MHz) are always larger than those at 7.0 T (300 MHz) over the entire lithium molality range studied (our 500 MHz spectrometer is not equipped with a suitable probe for ^{19}F measurement). Furthermore, their variation versus LiTFSI molality is similar at both magnetic fields. Consequently, the results at only one field (300 MHz) are plotted in the figures, but all the values are gathered in table 4.1, together with the self-diffusion coefficients presented in the previous section.

Table 4.1: Self-diffusion coefficients of choline (^{1}H), TFSI (^{19}F) and lithium (^{7}Li) ions determined by NMR Pulsed Field Gradient (PFG) diffusion measurements.

[LiTFSI]	**Choline**									**TFSI**		**Lithium**		
molality (mol/kg)	T_1 (ms)								D $\times 10^{11}$ m^2/s	T_1 (ms)	D $\times 10^{11}$ m^2/s	T_1 (ms)		D $\times 10^{11}$ m^2/s
	(a) CH_3		(b) CH_2		(c) CH_2		(d) OH			CF_3		Li^+		
	300 MHz	500 MHz	300 MHz	500 MHz	300 MHz	500 MHz	300 MHz	500 MHz		300 MHz		300 MHz	500 MHz	
0	600.9	734.6	588.7	761.6	578.6	835.9	1239.0	1727	2.67	855.2	1.44			
0.05	552.8	688.5	544.7	740.1	610.6	817.6	1090.0	1720	2.39	782.9	1.17	319.6	497.2	1.13
0.10	504.8	720.1	542.5	711.6	597.8	790.5	989.6	1484	2.23	802.7	0.99	335.8	538.8	1.04
0.21	409.1	701.7	549.0	654.2	575.7	717.7		1284	1.79	770.8	0.80	329.8	516.1	0.794
0.33	504.8	637.5	507.5			715.45		981.0	1.38	727.9	0.54	324.5	520.9	0.668
0.45	402.4	581.1	427.9	596.5	406.8	655.7	804.9	1049	1.09	684.4	0.44	309.6	498.2	0.522
0.58	374.7	598.5	383.1	540.4	432.1	604.8	684.2	904.7	0.84	707.3	0.21	330.0	530.1	0.409
0.99	350.9	553.8	374.5	536.1	410.2	576.6	658.8	834.4	0.38	699.5	0.10	355.3	545.6	0.192
1.37	324.5	493.0	325.6	502.8	385.6	534.9	528.8	651.7	0.20	681.5	0.028	377.1	584.4	0.102
1.95	319.9	486.0	348.3	515.5	366.3	531.5	437.9	593.7	0.07	688.0	0.006	445.2	650.9	0.0436
2.88		475.4		499.6		475.7		513.4		675.3		567.1	869.6	0.0118
3.48										675.0		685.8	995.3	0.0173

For both the ^{1}H (all the chemical groups of choline) and ^{19}F, one observes a decrease of T_1 with LiTFSI molality (Figure 4.9). However, significant differences occur. First, the ^{1}H T_1 of OH is much longer than those of CH_2 and CH_3. The source of relaxation for ^{1}H being dipole-dipole interaction, it appears as if either the distances with other ^{1}H or ^{19}F are higher, or the proton dynamics of OH is much faster by exchange with other OH. Also, it is important to point out that the hydroxyl proton is part of the hydrogen bond, which holds together the cation and anion of the ionic liquid. Second and more importantly, the decrease for all the ^{1}H is continuous all over the concentration range, whereas for the ^{19}F, a quasi-plateau is reached around 0.6 mol/kg. This phenomenon shows a different evolution of the dynamics for the cholinium and the $TFSI^{-}$, as already pointed out previously with the diffusion study.

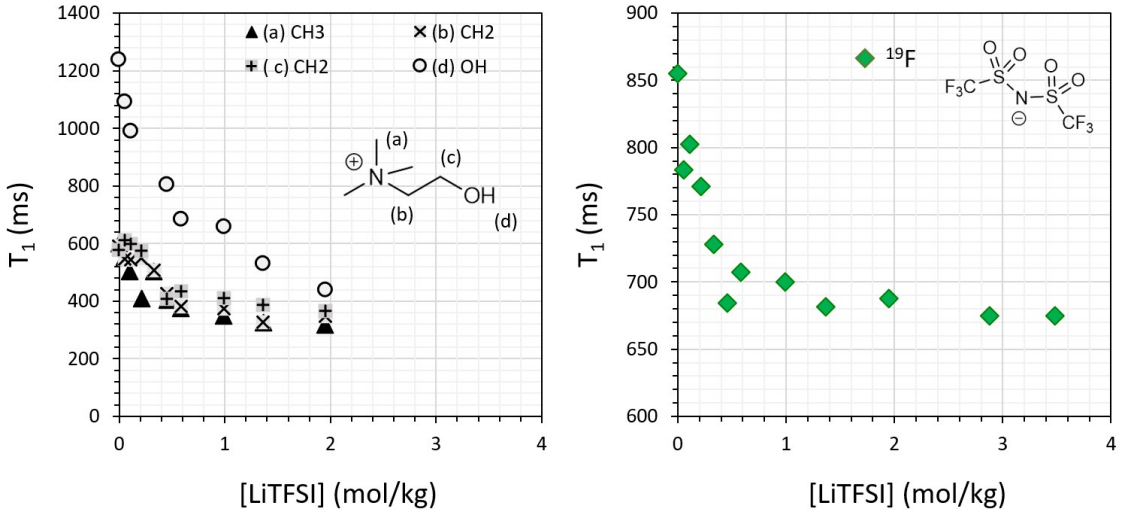

Figure 4.9: ^{1}H and ^{19}F T_1 longitudinal relaxation time at 300 MHz versus LiTFSI molality in dry [Chol][TFSI] ionic liquid.

In this point, the comparison with ^{7}Li T_1 is very interesting (Figure 4.10). The ^{7}Li T_1 is constant up to 0.6 mol/kg and increases above this amount in LiTFSI. This striking concomitant change of ^{19}F T_1 and ^{7}Li T_1 shows how their respective dynamics are convoluted, but in an apparent opposite direction. Here, it is important to recall that ^{19}F has 1/2 spin yielding to NMR relaxation ruled by dipole-dipole interaction, whereas ^{7}Li has 3/2 spin yielding to an NMR relaxation ruled by dipole-dipole interaction and quadrupolar interaction. The complex aspect for ^{7}Li is that none of these interactions dominates, and both must be considered. To be more precise, the dipolar interaction corresponds to the relative fluctuation of two magnetic dipoles. In contrast, the quadrupolar interaction compares the fluctuation to the electric field gradient experienced by the nucleus [180]. Hence, the plateau observed for ^{19}F could correspond to this state of the liquid structure where each TFSI ion coordinates two lithium ions via their oxygens, creating this way a labile network, similar to those evidenced in molten fluoride salts [181, 182]. The TFSI anions, "trapped" in this network, have, in a way, restricted dynamics. At a local scale, the dominant motion of CF_3, from the NMR point of view, is the rotation of the molecular group.

The reverse variation of ^{7}Li T_1, i.e., plateau followed by an increase, suggests the following scene. Lithium is solvated similarly by TFSI anions (same coordination number)

up to approximately 0.6 mol/kg . Above this concentration, TFSI anions are shared between several lithium ions and create a labile network. Lithium ions can then jump from site to site. These jumps increase the lithium mobility leading to an increase of T_1. Nevertheless, the long-range diffusion of lithium continuously decreases with LiTFSI molality (Figure 4.8) and rules out the increase of the lithium mobility but not the jump diffusion. A decrease of the mobility can also yields to an T_1 increase, as in the BPP (Bloembergen-Purcell-Pound) model [183]. In the latter, the dynamics are described by a rotational diffusion of characteristic time τ_C, expressed in the frequency domain by a Lorentzian. When τ_C becomes higher than the Larmor frequency, T_1 increases. In our case, rotational diffusion seems unsuitable, and ^{7}Li T_1 dispersion profile would be important information to reveal the dynamics at the intermediate timescale.

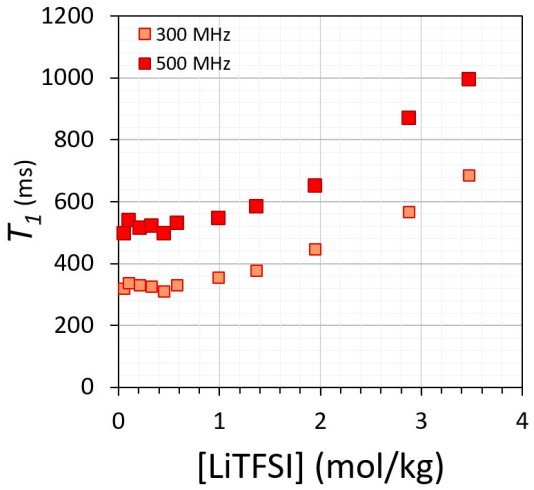

Figure 4.10: ^{7}Li T_1 longitudinal relaxation time at 300 MHz and 500 MHz as function of the LiTFSI molality in dry [Chol][TFSI] ionic liquid.

Despite the NMR relaxation data at 300 and 500 MHz do not fully reveal the dynamics of cholinium, $TFSI^-$, and lithium, they evidence the modification of the dynamics of $TFSI^-$ and lithium due to the change of solvation of lithium by $TFSI^-$. The labile network that progressively leads to an inversion of the self-diffusion coefficients of $TFSI^-$ and lithium, around 1.5 mol/kg, is already built at a lower concentration, around 0.6 mol/kg. In this regard, NMR relaxation measurement brings crucial information to describe the structure and the dynamics of the mixture LiTFSI and [Chol][TFSI] ionic liquid.

4.3 NMR investigation of the extraction system

As highlighted in section § 4.1, the system [Chol][TFSI]/betaine emerges as the most favorable for lithium ion liquid-liquid extraction among all the systems examined in this chapter. This section delves deeper into the local structure and dynamics of the ionic liquid phase used in extraction systems.

Initially, the influence of water and betaine on the structure of [Chol][TFSI] is scrutinized. A more detailed examination of the system's structure and chemical environment is achieved using NOESY, HOESY, and PFG-NMR experiments, focusing mainly on ^{1}H-^{7}Li and ^{1}H-^{19}F HOESY interactions. Furthermore, self-diffusion coefficients are determined for the nuclei ^{1}H, ^{19}F, ^{7}Li, encompassing all the species present in the system.

4.3.1 [Chol][TFSI]/ water/Betaine ternary Phase diagram

To gain a deeper understanding of the interactions among [Chol][TFSI], betaine, and water, a ternary phase diagram was constructed at 25 °C. This study scrutinized the phase behavior of the ternary system [Chol][TFSI]/water/betaine, aiming to comprehend the influence of extractant concentration on the miscibility of the [Chol][TFSI]/water system.

For constructing the ternary diagram, aqueous solutions with varying concentrations of betaine were brought into contact with the IL saturated in water at a phase ratio of IL:aq = 1:1. The mixture was subsequently heated and agitated at 80 °C and then cooled down to room temperature to complete phase separation, as described in section § 2.2.3.

The composition of each separated phase reflects conditions where phase separation is thermodynamically favorable, enabling the determination of tie-lines. These tie lines connect points representing the compositions of the two coexisting phases in equilibrium. Utilizing these data points, binodal curves can be established [184]. These curves demarcate the composition limits where phase separation is thermodynamically preferred, thus defining the biphasic region of the diagram.

The equilibrium compositions of the aqueous and IL phases for the three constituents (IL, betaine, water) were determined using ^{1}H NMR.

The weight fraction, w_x, of each constituent was determined using the relative integrated signal area ratio of the peaks [95]. The calculation of the molar ratio n_x for a compound x and in a mixture of m components:

$$n_x = \frac{\frac{I_x}{N_x}}{\sum_{i=1}^{m} \frac{I_i}{N_i}} \tag{4.1}$$

I_x is the integrated signal area relative to the resonance, and N_x represents the relative number of protons that cause this resonance. Thus, the mass fraction w_x of a specific compound x in a mixture consisting of m components can be determined as follows:

$$w_x = \frac{n_x M_x}{\sum_{i=1}^{m} n_i M_i} = \frac{\frac{I_x}{N_x} M_x}{\sum_{i=1}^{m} \frac{I_i}{N_i} M_i} \tag{4.2}$$

where M_x is the molar mass of the compound x.

Peak picking and integration were performed a `TopSpin` Bruker software. The peaks in the spectra were deconvoluted to reduce errors caused by overlapping peaks in the measurements.

The ternary phase diagram of the [Chol][TFSI]/betaine/water system, inclusive of its tie-lines, is depicted in Figure 4.11. The intersecting tie-lines evident in Figure 4.11(b) may be attributed to inaccuracies in the NMR measurements.

With an increase in betaine concentration, there is a corresponding increase in the miscibility of the aqueous and ionic liquid phases. This culminates in the two phases becoming completely miscible beyond $w = 20$ % w/w for the betaine.

The extraction experiment found that raising the betaine concentration amplified the water concentration in the IL phase, thus improving the system's extraction efficiency. This finding suggests a crucial role of water in the system. Another notable observation is that compared with the phase diagram, the presence of ions (Li^+ and Cl^-) in the

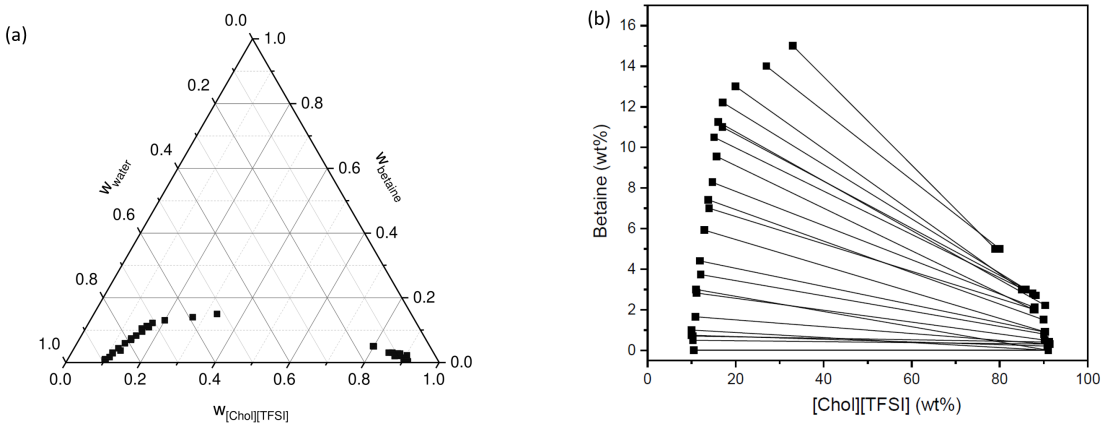

Figure 4.11: (a) Ternary phase diagram and (b) two dimensional with tie-lines for [Chol][TFSI]/betaine(ZW)/water phase diagram at 25 °C.

aqueous phase decreases the mutual solubility of the phases, enabling an increase in betaine concentration without leading to total miscibility of the phases.

4.3.2 Chemical shifts

In the study of nuclear magnetic resonance (NMR), the chemical shift is a crucial factor that provides insights into the electronic environment surrounding specific nuclei. This helps in understanding molecular structures and dynamics. This section of the study focuses on the subtle nuances and shifts within the ^{1}H NMR spectrum of [Chol][TFSI], an ionic liquid, under different conditions. First, the effect of water content on the ^{1}H NMR spectrum is analyzed, revealing the interplay between water molecules and [Chol][TFSI]. Next, the study explores changes in the ^{1}H NMR spectrum caused by adding betaine, shedding light on potential interactions and structural implications. Finally, the ^{1}H NMR spectrum of the post lithium extraction into the ionic liquid phase of [Chol][TFSI] is examined, revealing the impact of lithium-ion integration and its consequences on the ionic liquid.

4.3.2.1 Changes of ^{1}H NMR spectrum of [Chol][TFSI] with water content

The thermomorphic behavior of the system [Chol][TFSI]-water was initially probed by Nockemann et al. [82] using ^{1}H NMR spectroscopy. In their IL crystal structure study, they describe that the anion and cation are held together by hydrogen bonds between the hydroxyl proton and the sulfonyl oxygen. The authors point out that choline bis(trifluoromethylsulfonyl)imide exhibits a tendency to undergo crystallization over glass formation. They attribute this to the low viscosity of the ionic liquid and speculate that hydrogen bonding may play an important role in structuring the ionic liquid, even in the liquid state, then facilitating crystallization.

Hydrogen bonding is accountable for some of the most substantial chemical shift ranges observed. The hydroxyl group itself can present a wide chemical shift range from 1 ppm to around 5 ppm to the reference compound tetramethylsilane [90]. Thus, proton NMR might give some insights into the structure of the extraction system in the study, considering the

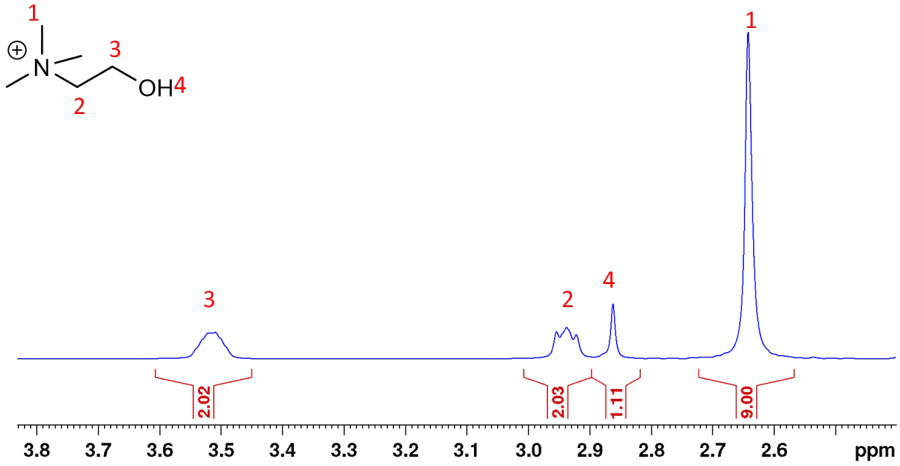

Figure 4.12: ^{1}H NMR spectrum of dry [Chol][TFSI] at 40 °C, with a capillary of DMSO-D6, resonance assignments are indicated by the numbers in red above the spectrum.

presence of hydrogen bonds and a hydroxyl proton in the IL liquid cation.

The ^{1}H NMR spectrum of dry [Chol][TFSI] prepared under an argon atmosphere within a glove box is shown in Figure 4.12. Preparatory steps involved freeze-drying the sample before transferring it into a vacuum furnace linked to the glove box. A DMSO-d6 capillary was introduced in the NMR tube for the NMR lock. The sample was vacuum-sealed post-preparation in the glove box to avoid water absorption. The ^{1}H spectrum was recorded at 40 °C since the pure ionic liquid is in a solid state at room temperature. The resonances for the protons on the cholinium cation are assigned by numbers in the spectrum. The numbers in red below the spectrum indicate the normalized integrals corresponding to each peak's protons. The spectrum also confirms the absence of water in the sample.

For [Chol][TFSI] saturated with water at 25 °C, ^{1}H NMR spectrum indicates (Figure 4.13) a significant difference in the behavior of the OH signal and the apparition of a water signal was observed. In some systems at room temperature, this separation between H_2O and OH peak is not observed, which may indicate fast chemical exchange processes between the protons [185–187]. One hypothesis is that some structural organization may hinder this exchange. Nockemann et al. [82] also observed H_2O/OH peak separation and displacement even at 70 °C for the the system [Chol][TFSI]-water.

As expected, the resonances for the CH_3 groups and two equivalent CH_2 groups shifted to the left, to higher frequencies (i.e., downfield) exhibiting similar chemical shift differences as the "pure" ionic liquid at 40 °C. Nevertheless, the OH peak is also shifted downfield (left), reflecting higher chemical shift differences than the other peaks.

When the electron density around the nucleus decreases, the opposing magnetic field also diminishes. This makes the nucleus more exposed or sensitive to the external magnetic field, resulting in high-frequency shifts, a situation referred to as deshielding. The deshielding of the hydroxyl group in the presence of water in the IL, indicates the strong formation of hydrogen bonds to electronegative atoms, the cation hydroxyl proton, and the H_2O oxygen. This suggests the presence of stronger hydrogen bonds for the cation hydroxyl hydrogen in hydrated samples compared to existing ones formed by the anion and cation alone. At the same time, compared to free water, with a chemical shift of around 4.7 ppm at 25 °C, the H_2O peak in the water saturated IL goes to lower ppm values,

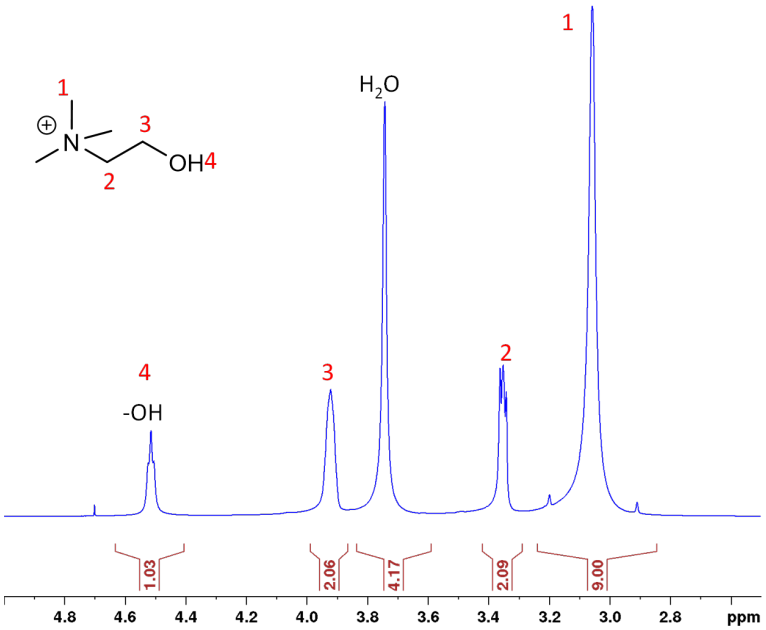

Figure 4.13: Proton NMR spectrum of [Chol][TFSI] saturated with H_2O at 25 °C, resonance assignments are indicated by the numbers. The numbers in red below the spectrum indicate the normalized integrals. The small peak around 4.7 ppm corresponds to the deuterium oxide present in the capillary inside the tube.

indicating the presence of weaker hydrogen bonds for water molecules in the IL network. These shifts are due to changes in the local electric fields derived from charged or polar groups of the water molecules. The cation hydroxyl proton interacts with the negative charge on the oxygen pole, causing its deshielding. On the other hand, the deterioration of the free water network in the IL causes its shielding.

4.3.2.2 Changes of ^{1}H NMR spectrum of [Chol][TFSI] with betaine content

To study the influence of betaine in the extraction system. Aqueous phases containing different betaine concentrations were put in contact with the IL saturated in water. Each sample was heated to 80 °C and agitated for 30 min after a homogeneous phase was obtained. After the samples were cooled down to room temperature, the phases were separated, and the IL phase were analyzed by NMR. The spectra of the IL phases are shown in Figure 4.14.

The water and OH peaks are shifted to higher frequencies. The spectra reveal a broadening of the cholinium –OH and H_2O peaks with the increase of betaine. The concentration of the choline –OH proton is smaller compared to the water protons. Then hydroxyl group proton signal is weaker, and the resonance due to exchange is correspondingly broader. The broadening of the peaks might indicate an increase in the exchange rate.

To facilitate the understanding of the data, the relative shift is employed, denoted as $\delta_{rel} = \delta - \delta_0$, where δ_0 is the chemical shift in the sample without betaine, while δ corresponds to the chemical shift with betaine. The relative chemical shifts are shown in Figure 4.15. The OH and H_2O peaks are shifted to the right. The relative chemical

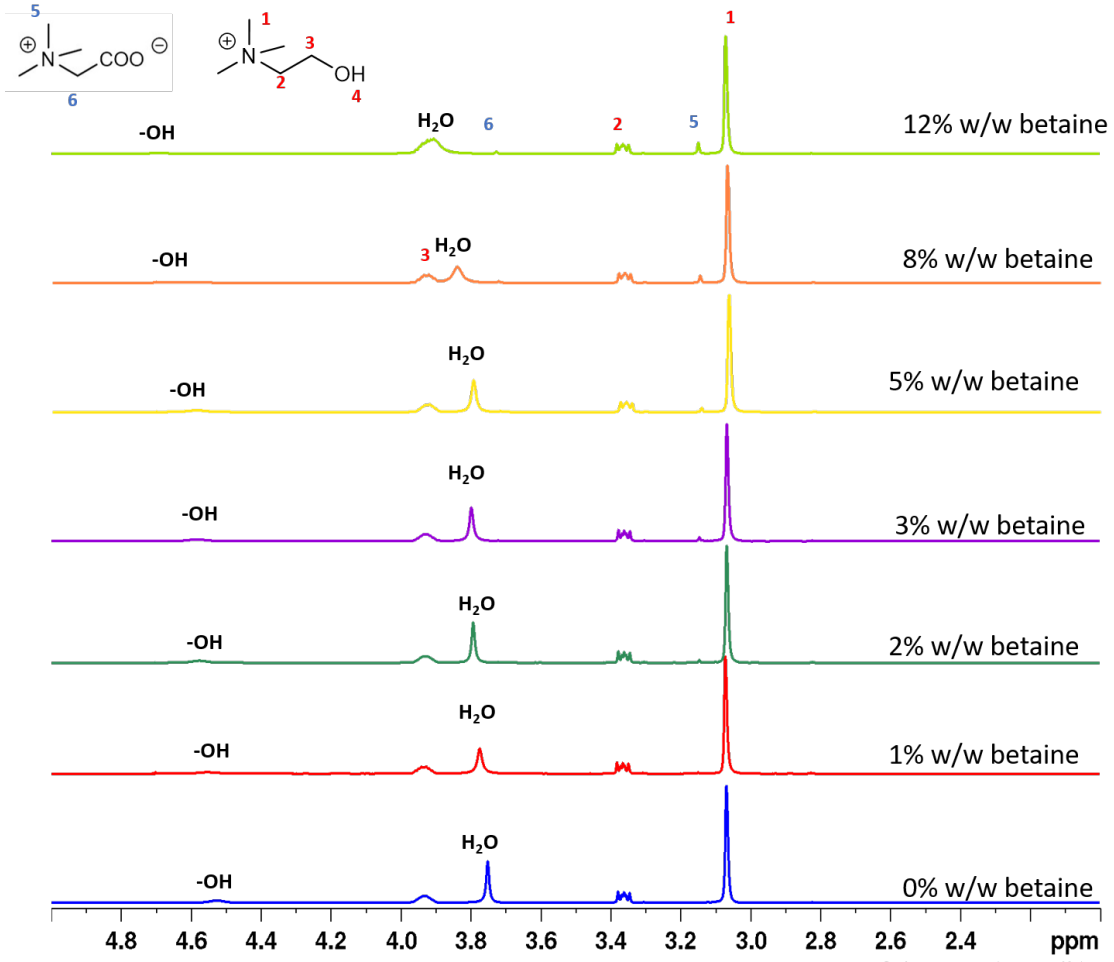

Figure 4.14: ^{1}H spectra of the IL phase with different initial aqueous phase betaine concentrations at 25 °C. The initial betaine concentrations are shown in black in the left of the spectra.

shifts of H_2O is higher than the relative chemical shift of –OH, which may indicate a more significant change in the water chemical environment. The shift in the frequency of H_2O resonances towards the higher end (downfield) serves as an indicator of H-bond formation involving electronegative atoms and enhancement of the water network. Di Gioacchino et al. [188] found evidence of water-mediated aggregates, two betaine molecules connected through their $–COO^-$ groups, bridged by a single water molecule. This structure is reminiscent of the betaine monohydrate crystal [189], and may contribute to the higher relative shift to high frequencies.

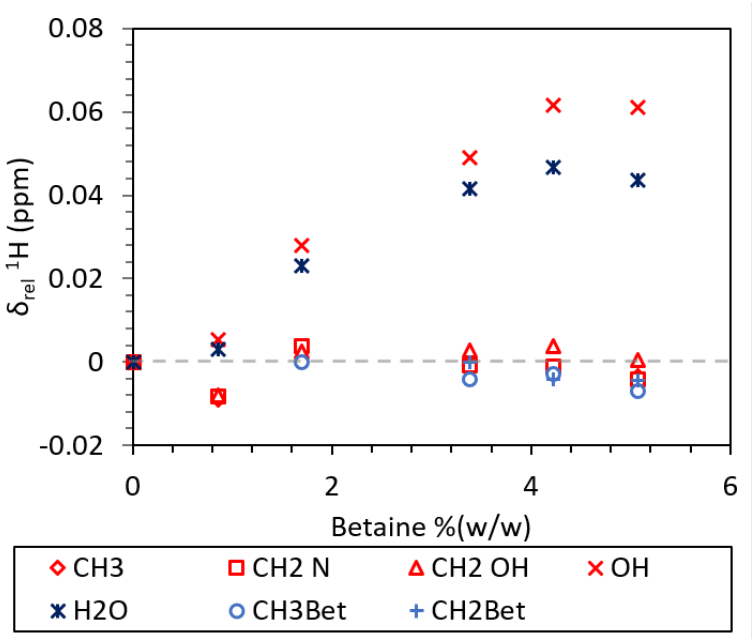

Figure 4.15: ^{1}H relative chemical shifts of cholinium cation upon increase of betaine concentration.

4.3.2.3 ^{1}H NMR spectrum of the [Chol][TFSI] phase after Li^+ extraction

Figure 4.16 shows the spectra of the [Chol][TFSI] saturated in H_2O and an IL phase after extraction. The presence of LiCl dissolved in the aqueous phase could reduce the mutual solubility of the IL aqueous phase system [147].

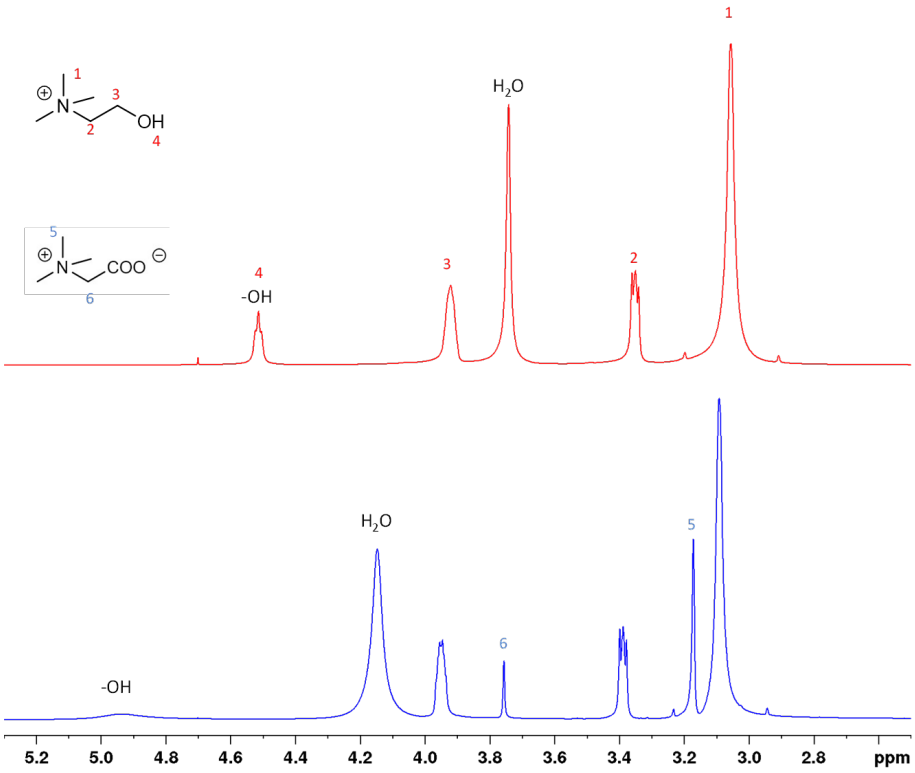

Figure 4.16: ^{1}H NMR spectra for (a) (top) [Chol][TFSI] saturated in H_2O (b) (bottom) ionic liquid phase after extraction with the initial parameters: IL:aq = 2:1, $[Li]_{aq}{}^0$ = 1 M, $[betaine]_{aq}{}^0$ = 24% w/w.

The cholinium –OH and H_2O peaks are shifted to higher frequencies, the concentration of water appears to almost double compared to the ionic liquid saturated in water. The betaine appears to increase the water content in the IL phase, the enhancement of the water network and the formation of stronger H-bonds together with the H_2O betaine interaction described before, might be responsible for the H_2O protons peak deshielding.

This displacement to higher might be due to stronger H-bonds formation due to an enhancement in the water network and also a possible H-bond formation between the betaine carboxyl group oxygen and the cation hydroxyl proton, once it has a negative charge [190]. There is almost no change in the signals CH_2 and CH_3 of choline, meaning they are not particularly affected by adding water or betaine.

There is almost no change in the other signals of choline, meaning they are not particularly affected by the addition of lithium.

Finally, Figure 4.17 presents the IL/aqueous phases system in the presence of lithium ions in the homogeneous state at 80 °C. This suggests that upon an increase of temperature, the hydrogen bonding between the hydroxyl proton of the choline cation and the oxygen atom of the TFSI anion was diminished, allowing the miscibility of the phases. It is not possible to observe anymore a separated peak for the cation hydroxyl proton. The same is

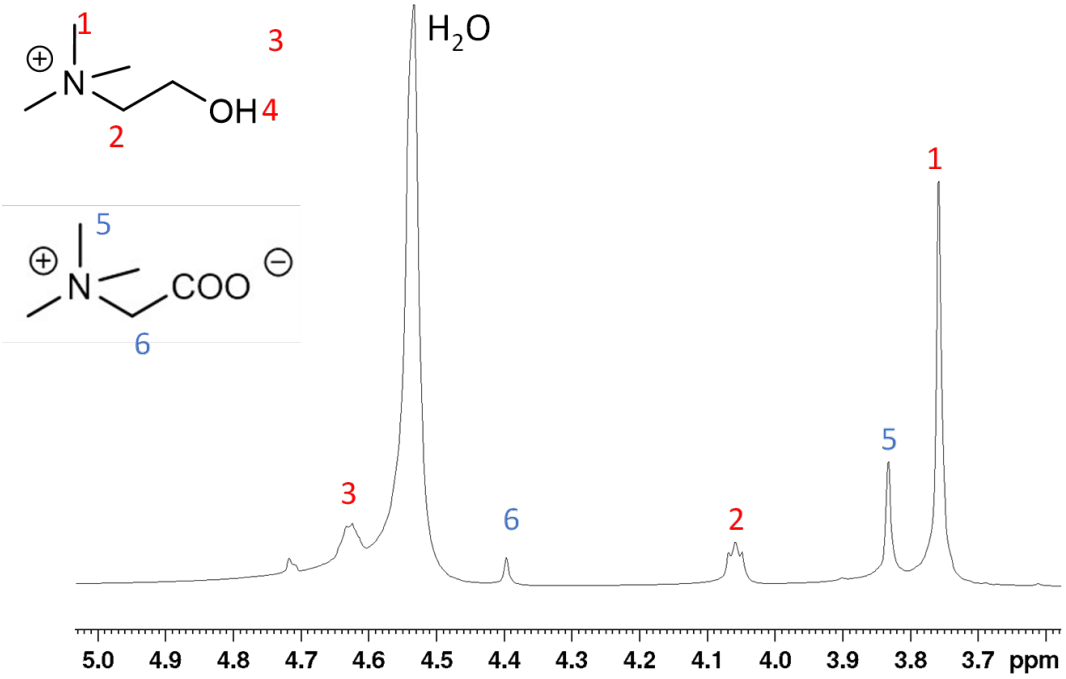

Figure 4.17: ^{1}H spectrum of extraction system IL/aqueous phase homogeneous system at 80 °C. Extraction parameters parameters: IL:aq = 2:1, $[Li]_{aq}^{0}$ = 1 M, $[betaine]_{aq}^{0}$ = 24% w/w. The peak around 4.7 corresponds to the D_2O in the capillary.

observed in a [Chol][TFSI]/water system without the presence of betaine. Upon heating and increase of water content, a gradual breakdown of the hydrogen bonds in the ionic liquids as dilution occurs, leading to increased hydration of the IL [82].

4.3.3 NOE correlation analysis

Understanding the molecular interactions within ionic liquid phases is crucial to better designing and optimizing liquid-liquid extraction processes using these liquids. One tool that allows for an in-depth investigation of such interactions is the Nuclear Overhauser Effect (NOE) correlation analysis. By providing insights into through-space proton-proton and heteronuclear interactions, usually at distances inferior to 5 Å. NOE allows a deeper comprehension of the spatial arrangement of atoms and molecules, particularly in systems like the extraction systems with ionic liquids. This section investigates the NOE correlation analysis of different IL systems through NOESY and HOESY experiments.

4.3.3.1 NOESY

The homonuclear NOE effect was evaluated for the different IL samples to understand the extraction process better. ^{1}H- ^{1}H NOESY experiments were carried out for [Chol][TFSI] saturated in water alone (Sample 1), [Chol][TFSI] with Li^{+} ions (Sample 2), [Chol][TFSI] with betaine (Sample 3), and [Chol][TFSI], betaine and lithium (Sample 4). The samples

Table 4.2: Samples description for NOE experiments.

Sample	**Composition**	**Description**
1	[Chol][TFSI]	[Chol][TFSI] saturated in water.
2	[Chol][TFSI] Li^+	IL phase with Li^+ after homogeneous liquid-liquid extraction (sample heated to 80°C and agitated during 30 min, but no homogeneous system was obtained), the initial aqueous phase had a Li^+ concentration of 0.6 mg/g and IL:A of 1:1.
3	[Chol][TFSI] betaine	IL phase with betaine after homogeneous liquid-liquid extraction (sample heated above the critical temperature and agitated during 30 min); the initial aqueous phase had betaine concentration of 24 % w/w and IL:A of 2:1.
4	[Chol][TFSI] betaine Li^+	IL phase with betaine and Li^+ after homogeneous liquid-liquid extraction (sample heated above the critical temperature and agitated during 30 min); the initial aqueous phase had betaine concentration of 24 % w/w and a Li^+ concentration of 0.6 mg/g and phase ratio IL phase over aqueous phase (IL:aq) of 2:1.

were added to 5 mm NMR tubes, and a D_2O capillary was included in each tube for locking. The samples are detailed in Table 4.2. The NMR experiments were performed in a 500 MHz (11.7 T) Bruker AV III spectrometer equipped with a 5 mm Double Resonance Broadband Probe (BBI). The 2D NOESY was carried out using the standard Bruker pulse program *noesygpph*. Each sample was analyzed at different mixing times to obtain optimal conditions. A series of NOESY experiments were done with different mixing times to determine optimal mixing time. The optimal mixing time was determined as 0.8 s for all the samples.

Figures 4.18 and 4.19 present the ^{1}H- ^{1}H NOESY spectra of the samples at 25 °C. The cross peaks outside the diagonal of the 2D spectra indicate proximity in space of the related nuclei. The numbers assigned to these peaks in the Figure indicate the correlation through space nuclei. In Figure 4.18(a), [Chol][TFSI] saturated with water, correlation peaks of same phase of phase of the diagonal between the cholinium hydroxyl proton and H_2O protons peaks. The same is observed in Figure 4.18(b), for Sample 2. In NOESY experiments, small molecules exhibit cross-peaks with opposite phases compared to the main diagonal, while cross-peaks resulting from chemical exchange display the same phases.

Cross-peaks with the same phase as the main diagonal were observed between the water peak and a broad peak, likely corresponding to the hydroxyl proton, indicating chemical

exchange, in Figure 4.19(c) and (d). Additionally, cross-peaks arising from intramolecular interactions in the cation and zwitterion were observed, although no intermolecular interactions were detected for the ionic liquid cation and betaine.

NOESY experiments were also conducted at a lower temperature with a mixing time of 0.8 s. The spectra for Samples 1 and 2 are shown in Figure 4.20 at 5 °C. The two systems with [Chol][TFSI] without betaine, where the hydroxyl peak appears narrower and more well-defined than at 25°C. The NOESY spectra with and without the presence of lithium are very similar, and it is possible to observe two –OH peaks, both of them presenting cross peaks with H_2O, indicating that chemical exchange occurs with them. This extra –OH signal could come from phase separation at low temperatures. Further Differential Scanning Calorimetry (DSC) analysis would help to confirm this phase separation. The integration areas of the last peaks on the left are similar and could be assigned to the -OH cholinium proton. This may imply that there are two different groups of of –OH undergoing chemical exchange with water at two different rates.

To further investigate Sample 4, NOESY experiments were conducted at lower temperatures. To avoid solidifying the solvent inside the capillary tube, a deuterium oxide capillary tube was replaced with a capillary with deuterated acetone. In Figure 4.21, the system with [Chol][TFSI], betaine, and Li (Sample 4) at 5 °C and −5 °C, still present broader peaks but are more visible than at 25 °C. However, it is possible to observe a broader peak overlapping a narrower one and their cross peaks with water at 5 and −5 °C, similar to the systems without betaine (Figure 4.20). This suggests a potential phase separation again. At −5 °C, the spectrum shows intermolecular chemical exchange for the cholinium and betaine, underlying the proximity of the species at this temperature.

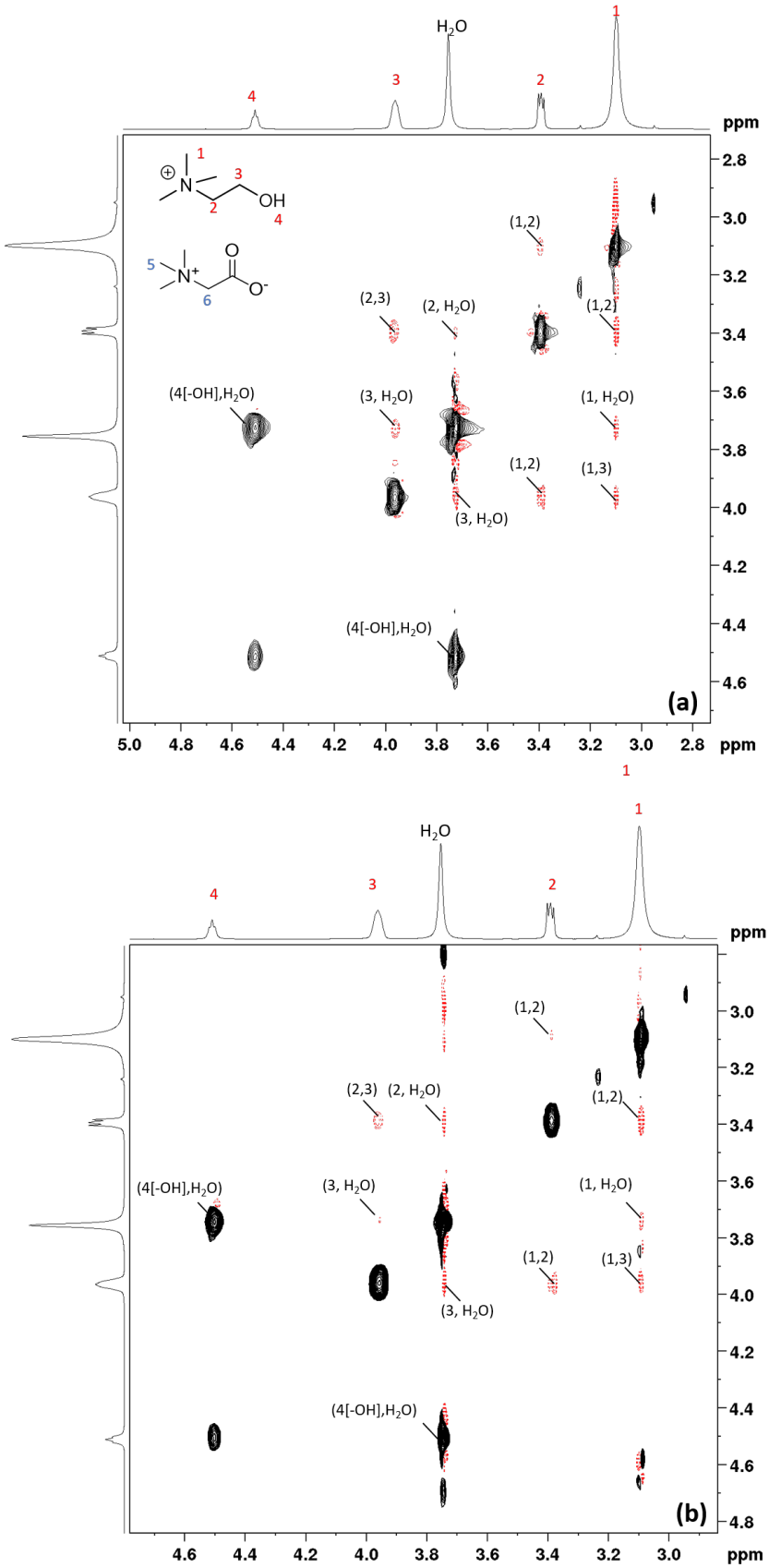

Figure 4.18: ^{1}H- ^{1}H NOESY experiments for different ionic liquids systems t 25 °C with mixing times of 0.8 s. The 2D spectra correspond to Samples (a) 1 and (b) 2 detailed in Table 4.2.

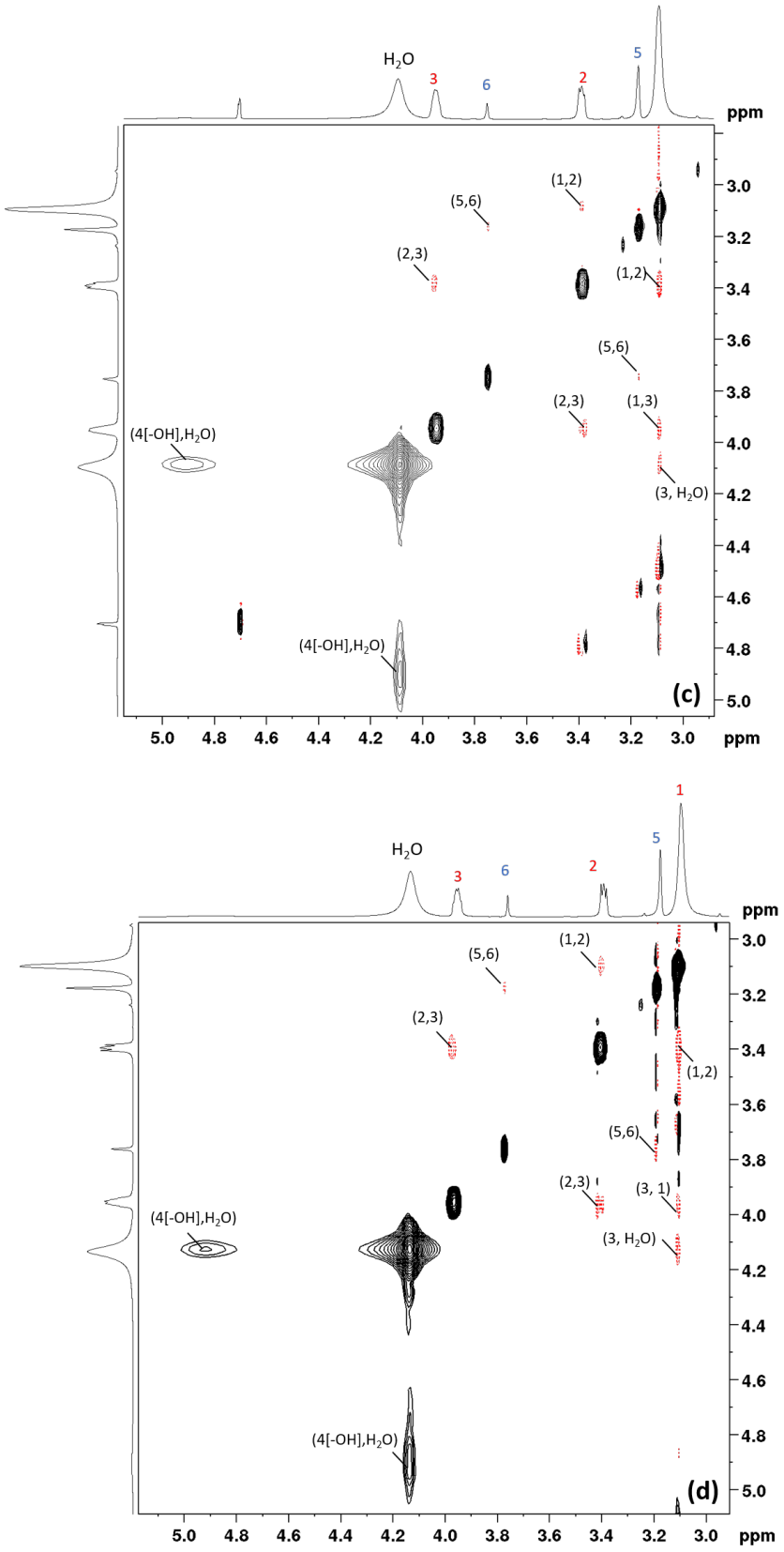

Figure 4.19: ^{1}H- ^{1}H NOESY experiments for different ionic liquids systems t 25 °C with mixing times of 0.8 s. The 2D spectra correspond to Samples (c) 3 and (d) 4 detailed in Table 4.2.

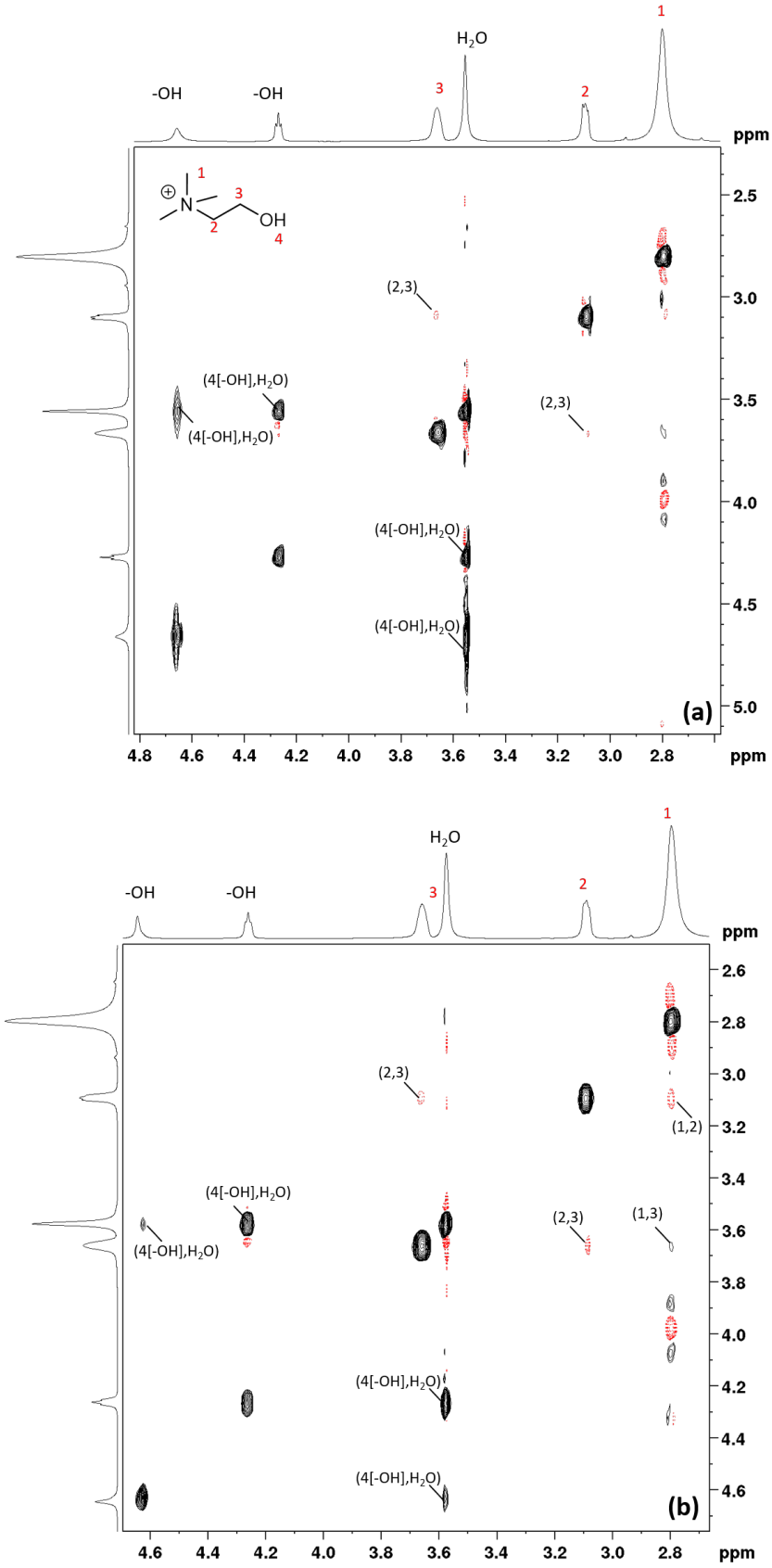

Figure 4.20: ^{1}H- ^{1}H NOESY spectra of the ionic liquid phase at 5 °C (a) without and (b) with lithium ions.

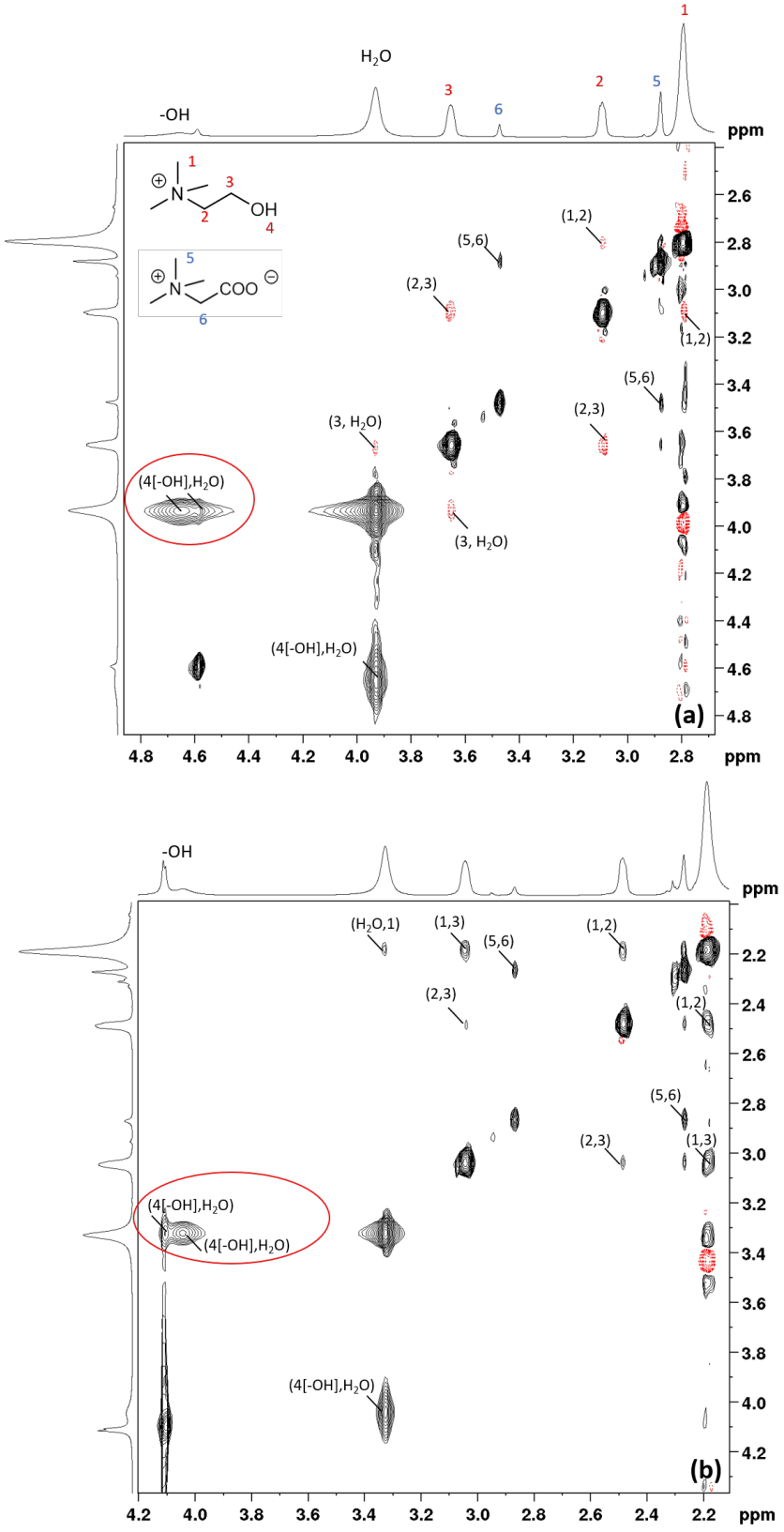

Figure 4.21: ^{1}H- ^{1}H NOESY spectra of the ionic liquid phase with lithium ions and betaine at (a) 5 °C and (b) −5 °C with a mixing time of 0.8 s.

4.3.3.2 HOESY

HOESY (Heteronuclear Overhauser Effect Spectroscopy) plays a pivotal role in understanding the interactions between different nuclei in a molecule or in complex mixtures. This section investigates the HOESY spectra of various samples of [Chol][TFSI] and its combinations with water, betaine, and lithium ions. The intention is to progress from less intricate systems to those more complex, enabling a more straightforward interpretation of the interactions. ^{1}H- ^{19}F and ^{19}F- ^{7}Li HOESY experiments were performed using the 5 mm Jeol JNM-ECZ, Royal HFX probe, at a magnetic field strength of 9.4 T (^{1}H Larmor frequency of 400 MHz) and processed with the JEOL Delta software. Operating this probe at dual tune mode allows us to perform a series of advanced experiments, which includes ^{19}F- ^{7}Li HOESY. ^{1}H- ^{7}Li 2D heteronuclear NOE were carried out in a 500 MHz (11.7 T) Bruker AV III spectrometer equipped with 5 mm Double Resonance Broadband Probe (BBI). The mixing time was varied from 0.1 to 2 seconds for each sample to find the optimal time.

HOESY experiments were performed for a sample of dry [Chol][TFSI] with lithium ions in a molal concentration of 0.05 mol/kg. The 2D spectra are presented in Figure 4.22. The sample was prepared as described in section § 4.2. ^{1}H- ^{19}F HOESY 2D spectrum shows correlating proton-fluorine correlation peaks among all protons in the cholinium, showcasing the adjacency of cation and anion. A correlation peak is also observed in the ^{19}F-^{7}Li HOESY experiment also shows a correlation between these two nuclei, demonstrating the proximity of Li ions and the $TFSI^{-}$. In 2D heteronuclear NOE ^{1}H- ^{7}Li, presented in Figure 4.23 (b) experiments, it is also possible to observe correlation peaks between the lithium and the –OH peak and the closest CH_2 to the hydroxyl. In the case of $TFSI^{-}$ anion, lithium cation tends to interact more strongly with oxygen [176, 177]. Oxygen that forms H-bonds with the cation –OH [82]. These observations could support the correlation observed in ^{1}H- ^{1}Li for the system and showcase a possible impact of the cation in the lithium coordination with $TFSI^{-}$. The ^{1}H- ^{1}H NOESY shown in Figure 4.23 (a) display the intramolecular interaction of cholinium in the system, indicating proximity and even proton exchange due to the cross peaks phase.

Now analyzing a similar system in the presence of water, the ^{1}H- ^{1}Li HOESY experiments were carried for [Chol][TFSI] saturated with water with Li^{+} ions with (Sample 2 in Table 4.2). However, it was not possible to detect any signals from nuclei in close spatial proximity, except for the signal corresponding to water (Figure 4.24). Only a correlation peak arising for the water signal is observed, which implies that the lithium ions are surrounded by water. No correlation for this sample was observed in ^{7}Li- ^{19}F HOESY 2D experiments.

Lastly, upon the inclusion of betaine to the system, ^{1}H- ^{1}F, ^{1}H- ^{1}Li, and ^{1}Li- ^{1}F HOESY experiments were conducted. Specifically, the ^{1}H- ^{1}Li HOESY experiments were executed for [Chol][TFSI] saturated with water, inclusive of Li^{+} and betaine (as detailed in Sample 4 of Table 4.2). For the ^{1}H- ^{1}Li HOESY, no discernible signals from nuclei in close spatial proximity were observed, save for the water signal (as depicted in Figure 4.24). Notably, the sole correlation peak identified was for the water signal, suggesting that water molecules primarily solvate lithium ions. This observation may elucidate the enhanced extraction efficiency observed with heightened water content in the system, further amplified by adding betaine. Thus, it can be inferred that water extensively solvates lithium ions in the IL phase during extraction. Furthermore, water molecules interact with Li^{+} more

intensely than other inorganic ions such as Na^+ and K^+ [191]. Anions like $TFSI^-$ might exhibit weak coordination and do not create an optimal solvation environment for metal ions [192]. The same was observed by Chaumont and Wipff [193] examining the solvation of Eu(III) in both wet and dry [C_4mim][PF_6]. Eu(III) coordinates with $PF_6{}^-$ in the absence of water. However, when water is present, Eu(III) is solvated by water molecules, highlighting the weak coordination properties of $TFSI^-$. Consequently, introducing water to the ionic liquid can enhance the solubility of metals ions in the system. Through these spectra, it is possible to observe that water might be close in space to the cation and anion of the IL. As expected, the cation and anion of the IL are also close in space.

Figure 4.25 presents the ^{1}H- ^{1}F spectra for Sample 4 ([Chol][TFSI] saturated with water, inclusive of Li^+ and betaine). Notably, the spectra reveal correlation peaks between the fluorine a and the protons of the cholinium, aligning with previous crystal structure studies of the IL [82]. Correlations between the betaine, water, and fluorine peaks suggest potential hydrogen bonding interactions between water molecules and $TFSI^-$ anions. Prior literature has also documented spatially close interactions between betaine and $TFSI^-$, exemplified by ammonium hydrogen bonding [44]. The spectra further indicate proximity between certain short-bonded carbon hydrogens and the fluorine or oxygen of the $TFSI^-$ anion, with distances under 300 picometers [194]. The spectra suggest that water is spatially proximate to both the cation and anion of the IL. As anticipated, the cation and anion of the IL exhibit close spatial interaction. However, no correlation was observed for the ^{1}Li- ^{1}F NOE analysis.

It's worth noting that not all close inter-nuclear distances result in observable NOEs. The intensity of an NOE depends on several factors, including the correlation time, the gyromagnetic ratios of the interacting spins, and the distance between them. Thus, the absence of an NOE does not always mean the nuclei are distant from each other. NOE experiments provide valuable spatial information about molecular structures. Careful experimental design and reasonable interpretation of results are essential and were carried out during this study. Thus, combining NOE data with other sources of structural information is often beneficial for a comprehensive understanding of molecular structure and dynamics.

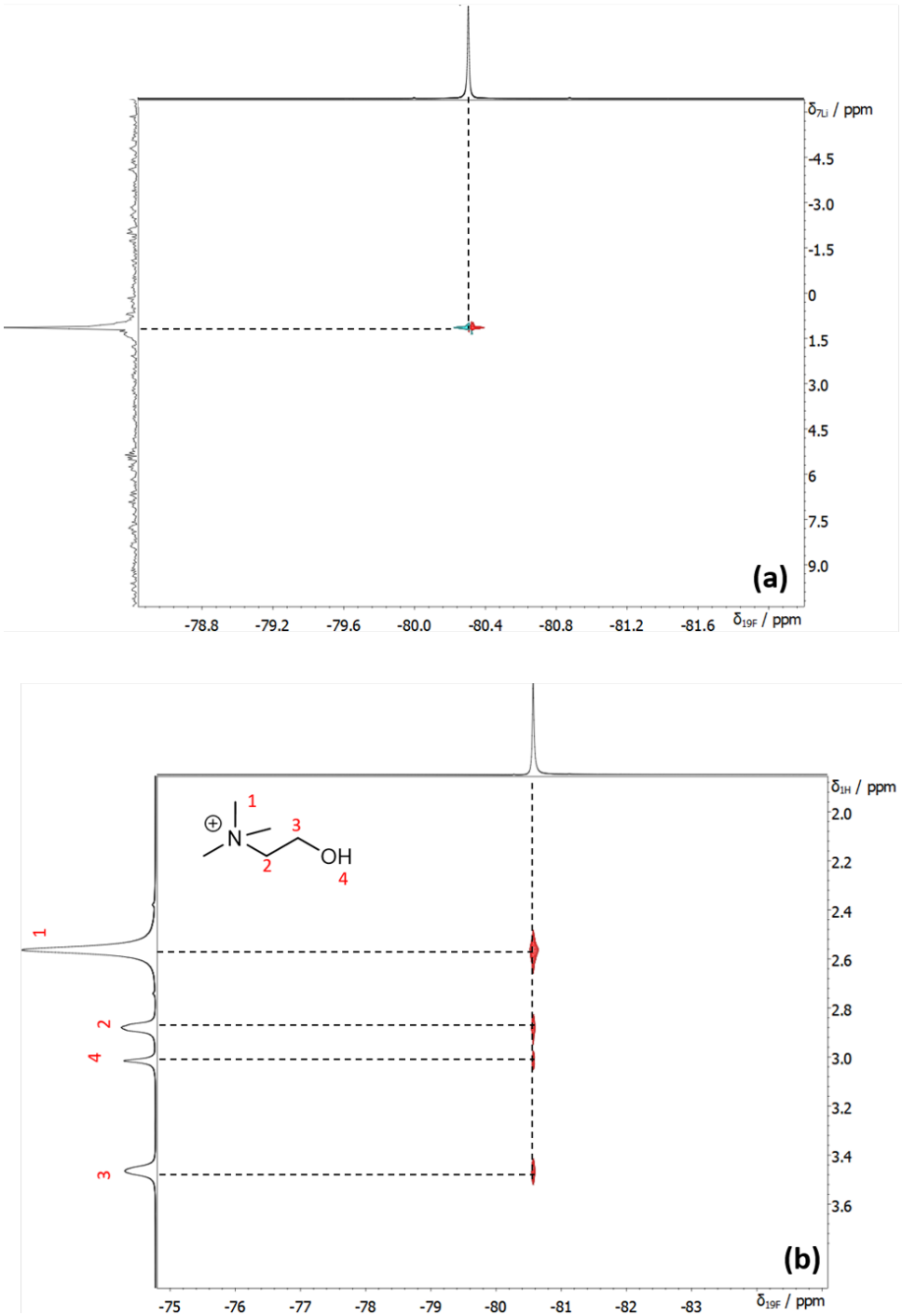

Figure 4.22: ^{7}Li- ^{19}F and ^{1}H- ^{19}F HOESY spectra for 0.05 molal of LiTFSI dissolved in dry [Chol][TFSI] (Jeol JNM-ECZ, Royal HFX probe, 9.4 T).

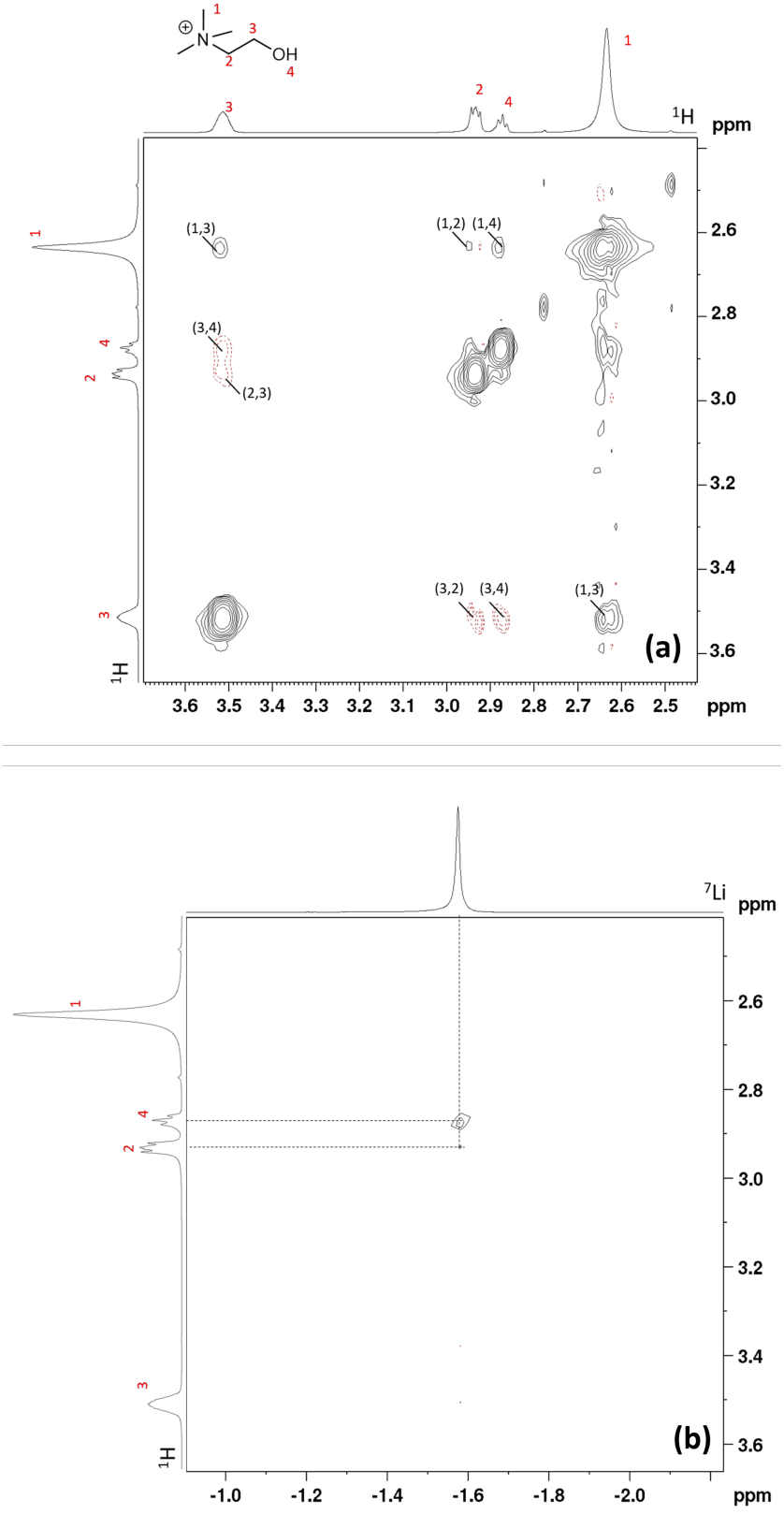

Figure 4.23: Dry [Chol][TFSI] with lithium ions in a molal concentration of 0.05 mol/kg (a) ^{1}H-^{1}H NOESY (b) ^{1}H- ^{1}Li HOESY.(Bruker AV III spectrometer Double Resonance Broadband Probe (BBI), 11.7 T)

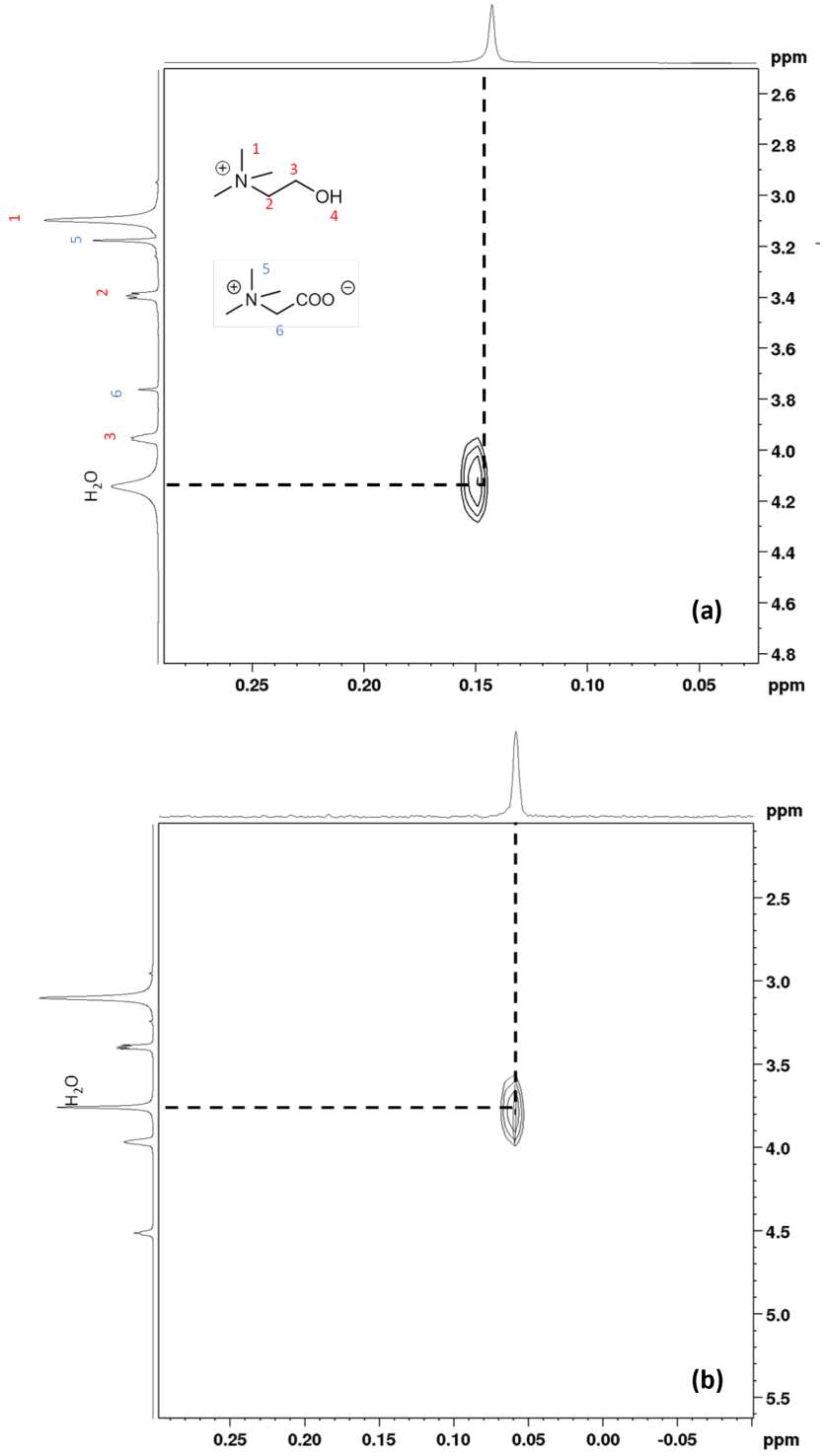

Figure 4.24: ^{1}H- ^{1}Li HOESY experiments for the ionic liquid phase (a) including and (b) not including betaine.

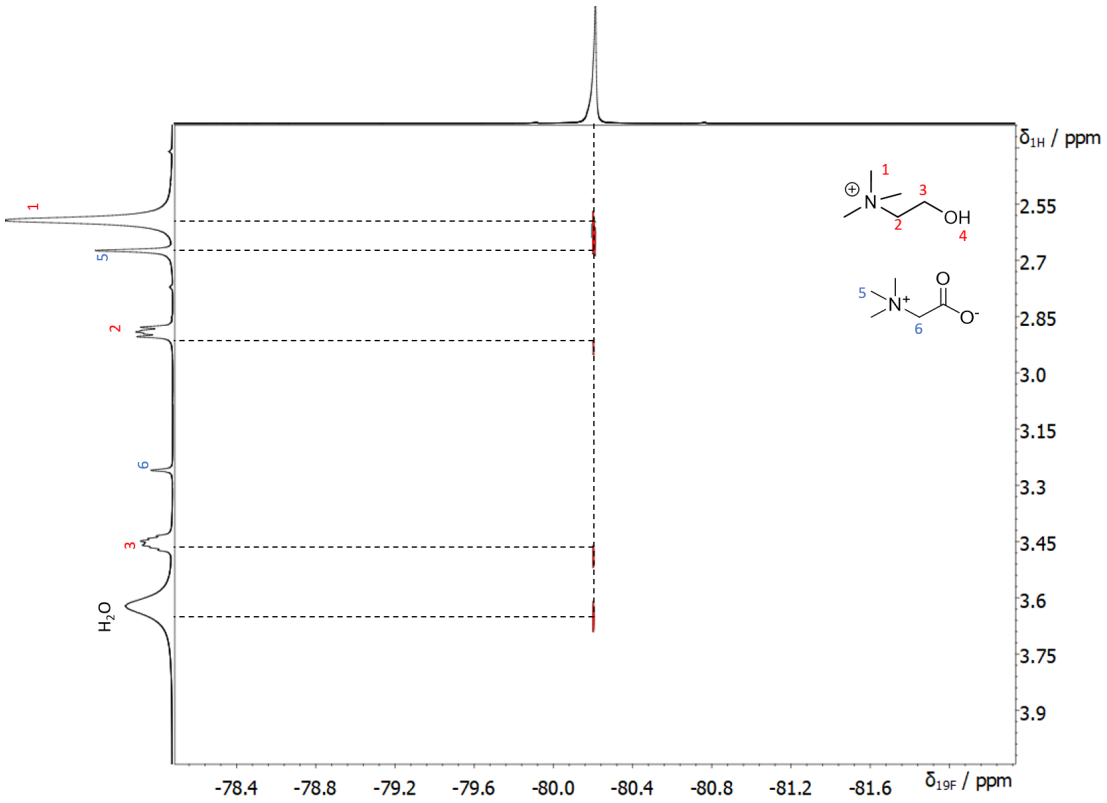

Figure 4.25: ^{1}H- ^{1}F HOESY spectrum of the ionic liquid phase with betaine and lithium.

4.3.4 Diffusion experiments

Understanding molecular mobility becomes fundamental as we investigate the nuances of the [Chol][TFSI]/betaine extraction system. The diffusion NMR experiments presented in this section aim to elucidate the dynamic behavior of various species within our systems. This analysis allows us to gain insights into the diffusion coefficients of different species present, offering a microscopic view of the molecular entities' interplay. Such information complements the chemical shift and NOE correlation analysis detailed earlier and sets the stage for a comprehensive discussion of the system's behavior.

Self diffusion coefficient (D) measurements were performed using Pulsed-field gradient nuclear magnetic resonance (PFG-NMR) on a 300 MHz and a 500 MHz Bruker spectrometers. The first is equipped with a probe capable of producing magnetic field gradient pulses up to of 50 G cm^{-1}, for ^{19}F, and the second is equipped with a probe of maximum strength gradient of 55 G cm^{-1}, for ^{1}H and ^{7}Li experiments. The diffusion measurement was conducted with a 2D sequence using stimulated echo and longitudinal eddy current delay with bipolar gradients (Bruker ledbpgp2s pulse program). The gradient pulse duration δ and the diffusion time Δ were in the range of 1 to 10 ms and 0.2 to 2 s, respectively. The gradient strength G was varied from 2 to 98 % of the maximum strength in 16 steps. The diffusion coefficients D were determined by fitting the echo signal decay with the Stejskal-Tanner equation (Equation 2.11).

Solvation of Li$^+$ in [Chol][TFSI] saturated by water To evaluate the presence of water in the system a sample of 2 molal of LiTFSI dissolved in [Chol][TFSI] saturated in water was prepared. Longitudinal relaxation times and diffusion coefficients for this sample are also determined at 40 °C.

The determined diffusion coefficients for the wet system appear in Table 4.3 in a comparison with the dry system at the same LiTFSI concentration.

Table 4.3: Self-diffusion coefficients for 2 molal of LiTFSI dissolved in [Chol][TFSI] dry and with H_2O systems.

Nucleus	**Species**	**Diffusion Coefficient**	**10^{-11}m^2/s**
		Dry	**with H_2O**
^{1}H	Chol$^+$	0.07	3.34
^{19}F	TFSI$^-$	0.03	2.79
^{7}Li	Li$^+$	0.04	5.77

It has been observed that water can significantly alter the physical and electrochemical properties of hydrophobic ionic liquids [192, 195, 196]. In the presence of water, D is increased more than 40 times for the [Chol] and more than 100 times for the [TFSI] and lithium ions. This increase shows a significant impact of water addition on the translational dynamics of the system. Also, analyzing the DOSY spectra for the wet system, the OH and H_2O peak can not be differentiated, appearing as one peak, and having a non-mono

exponential decay, as appears in Figure 4.26.

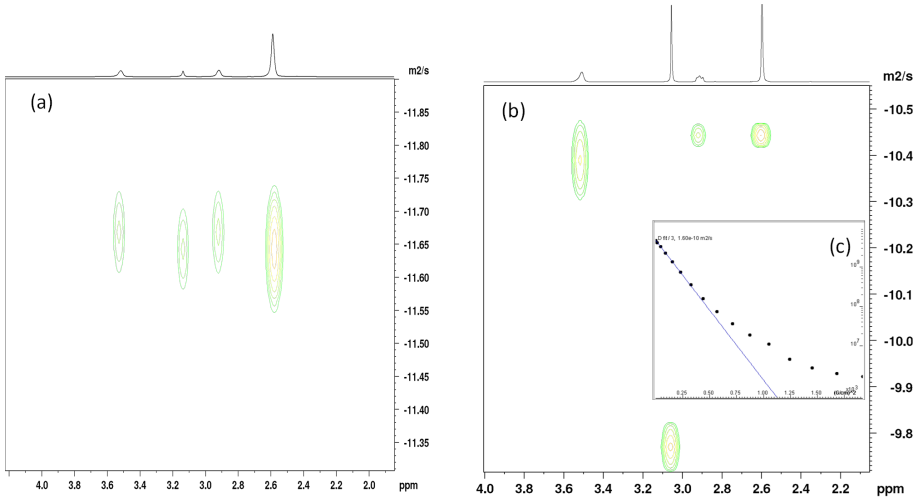

Figure 4.26: ^{1}H DOSY spectra of [Chol][TFSI] (a) dry (b) with water (c) non-mono exponential decay curve peak OH-H_2O

Self-diffusion coefficients were obtained for the samples described in Table 4.2, consisting of the IL and the others involving the ionic liquid after contact with aqueous phases of different compositions. Before measurements, the gradient was calibrated using a DMSO sample.

Before conducting the experiments, the longitudinal relaxation time (T_1) was determined through inversion recovery experiments. For all samples, the recycle delay ($D1$) for the diffusion experiments was set to 6 seconds based on the largest T_1 value ($D1 = 5T_1$), as T_1 did not show significant changes with variations in the system composition. The diffusion data analysis was performed using the `Dynamics Center` software by Bruker.

Below are the 2D NMR spectra obtained for each sample in Figures 4.27 and 4.28. It is possible to observe the different diffusion behaviors of betaine, [Chol][TFSI], and lithium. Both ions have close sizes and appear to be active players in the H-bonding network of the system. However, as observed in NOESY experiments, they appear not to be in close spatial proximity < 5 Å. No significant changes in the diffusion coefficients were observed with the addition of lithium and betaine to the $Chol^+$ cation or betaine in the IL phase. write about exchange effect in dosy [197]

The experimental data for H_2O and –OH display a non-mono-exponential decay with the gradient, Figures 4.29 and 4.30, likely indicating a decay at two different rates, which might describe different populations with the same chemical shift. This peaks present a self diffusion coefficient of around 4×10^{-11} m^2/s which is similar to water confined in IL reported by Saihara et al. [198] for [BMIM][BF_4]/water mixtures.

Tables 4.4 and 4.5 presents a summary of the self diffusion coefficients obtained. As shown, lithium ions have the highest diffusion coefficient for being small and surrounded by water. The diffusion of Li^+ in the dry is much smaller than the diffusion coefficient in the system with the presence of water. After Betaine and and cholinium cation have similar coefficient. Finally, the $TFSI^-$, a weak coordinating anion, presents the lowest diffusion coefficient due to its relatively biggest size and the significant hydrophobic fluorine-fluorine interaction may contribute to its slowest mobility compared to the other species analyzed.

One way to overcome exchange effects observed in DOSY experiments is to use specific

Table 4.4: Self-diffusion coefficients determined for different peaks using proton PFG-NMR.

Sample	$\boldsymbol{D}$ ($\times 10^{-11}$ m^2/s)				
	Choline			Betaine	
Peak	**CH_3**	**CH_2**	**CH_2**	**CH_3**	**CH_2**
1	7.37	7.14	7.25		
2	7.1	7.08	7.12		
3	7.74	7.72	8.17	7.36	7.24
4	7.83	7.9	8.1	7.63	7.35

Table 4.5: Self-diffusion coefficients determined for different peaks using ^{19}F and ^{7}Li PFG-NMR.

Sample	D ($\times 10^{-11}$ m^2/s)	
	$TFSI^-$ (^{19}F)	**Li^+ (^{7}Li)**
1 ([Chol][TFSI])	4.98	-
2 ([Chol][TFSI] and Li^+)	4.88	11.1
3 ([Chol][TFSI], betaine)	5.07	-
4 ([Chol][TFSI], betaine and Li^+	5.1	8.91

sequences that would reduce these effects [199].

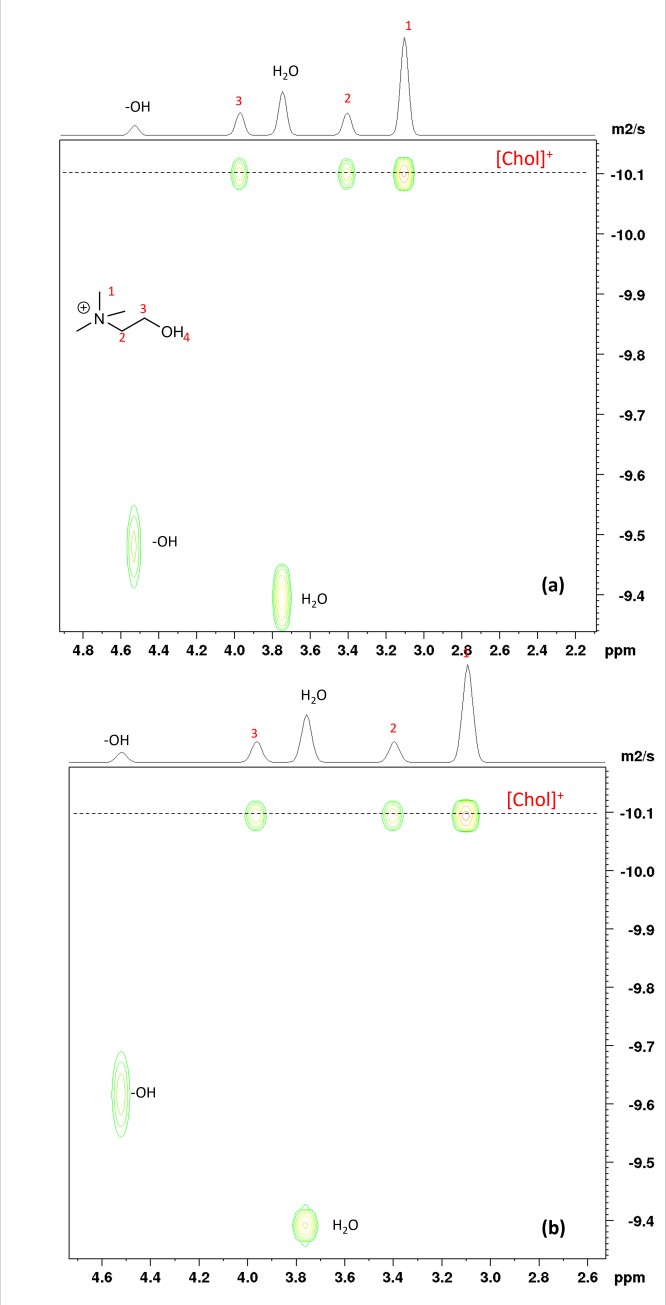

Figure 4.27: ^{1}H DOSY spectra of the ionic liquid phase (a) not accompanied and (b) in the presence of lithium ions.

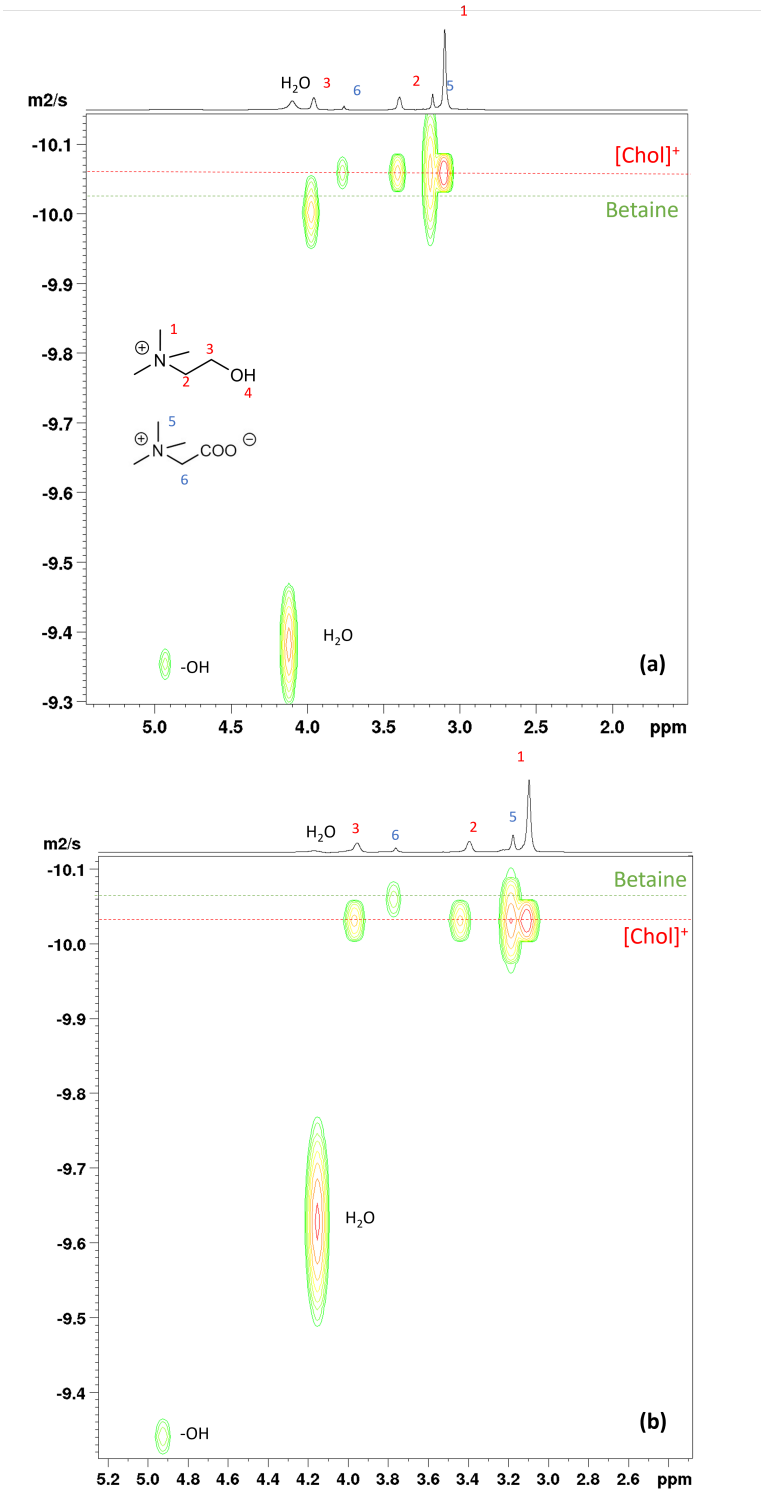

Figure 4.28: ^{1}H DOSY spectra of the ionic liquid phase in the presence of betaine (a) with and (b) without lithium ions.

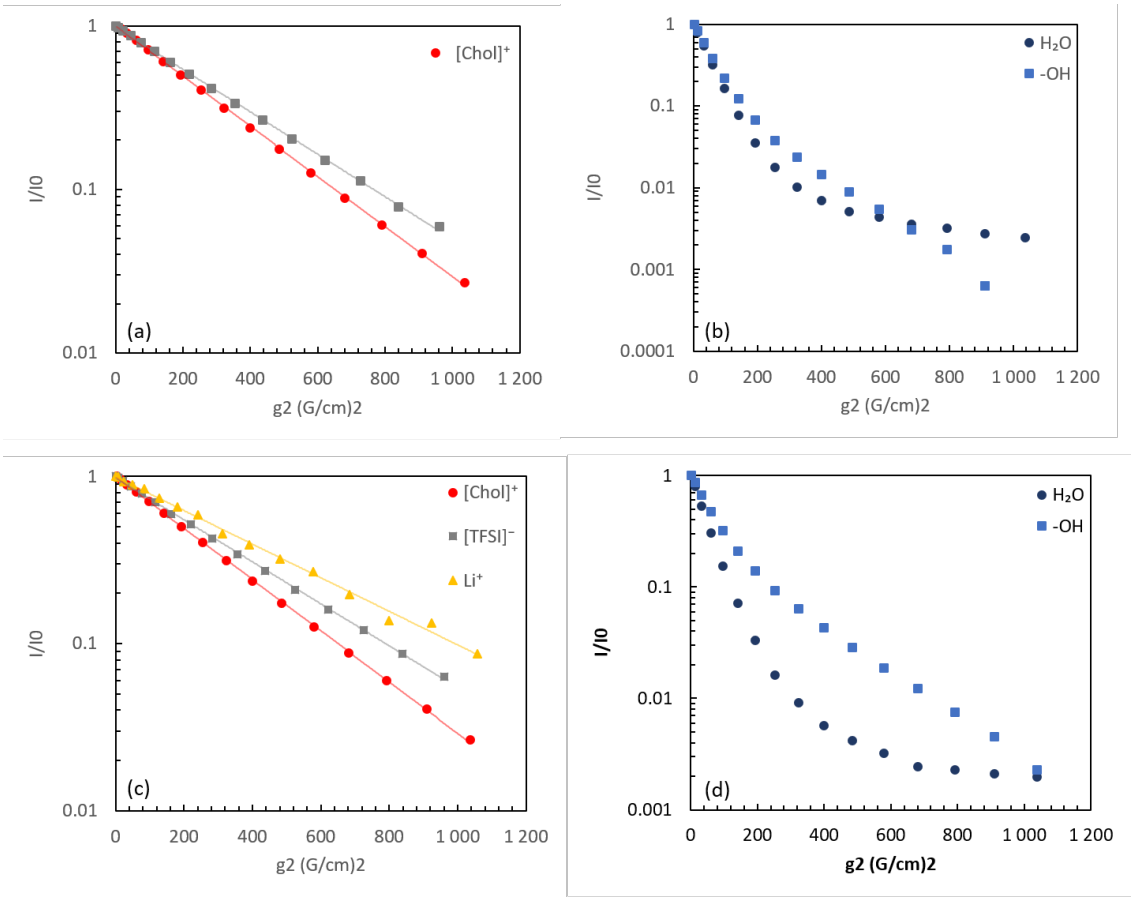

Figure 4.29: Diffusion decay curves for $Chol^+$ (CH_3, CH_2–N and CH_2–O), $TFSI^-$, and lithium and $Chol^+$ (OH) and H_2O. (a) and (b) without the presence of lithium and (c) and (d) with lithium ions.

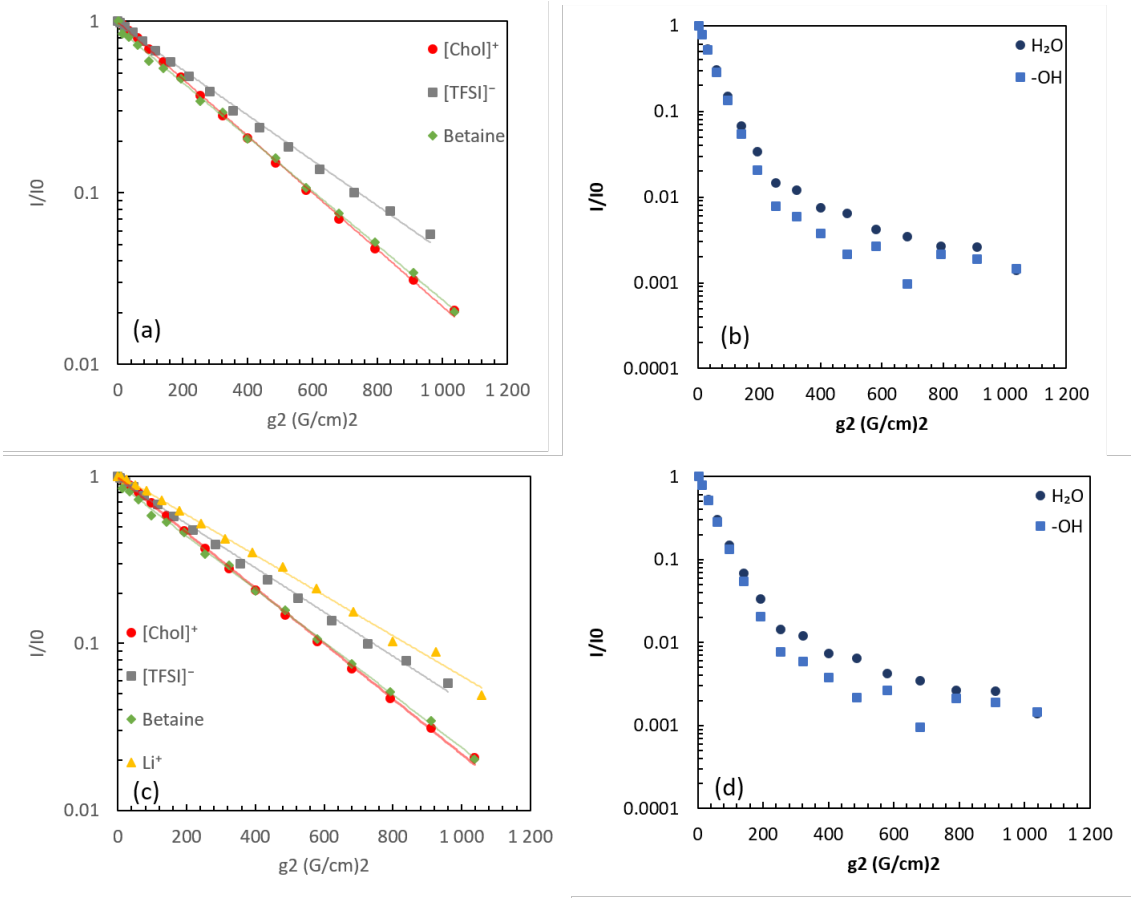

Figure 4.30: Diffusion decay curves for [Chol], betaine, [TFSI], and lithium and [Chol] (OH) and H_2O. (a) and (b) without the presence of lithium and (c) and (d) with lithium ions.

4.4 Nanostructure of the systems (SAXS)

The Small-Angle X-ray Scattering (SAXS) technique is highly valuable when it comes to analyzing ionic liquids and their microstructures. It provides essential data about the shapes, sizes, and spatial distribution of structures and objects, which can reveal how different ionic species are organized within the liquid. This technique can also detect any distinct domains or clusters that may be present. Furthermore, SAXS provides insights into how these ionic liquids interact with other compounds on a nanoscale level, including the formation of complexes or aggregates and changes in the ionic liquid structure [40]. Some theory about this technique is briefly described in Annex B

Through the intensive use of SAXS, Small-Angle Neutron Scattering (SANS), and X-ray Absorption Fine Structure (XAFS) spectroscopy, profound microstructural alterations in ILs targeted for f-block element separations were unraveled. Such changes, modifiable via counterion choices, are further manifested in the emergence of mesoscale patterns depending upon metal content. These revelations promise advancements in efficient separation mechanisms, crucial for tasks like spent nuclear fuel processing [200]. It is increasingly recognized that molecular structures beyond the immediate coordination sphere greatly influence the efficacy of separation processes [201].

Aguilera et al. [175] studied Solvated Ionic Liquids (SILs). This involved the dissolution of Li-salt (LiTFSI) in the solvent tetraglyme, employing SAXS for analysis. A pronounced deviation in structural affiliations was discerned with rising Li-salt concentrations, resembling traditional IL characteristics. A dichotomous response from Li-ions was noted at balanced concentrations, while the majority opted for cationic complex formation via solvation, a separate segment required direct interactions with the TFSI anion.

Mhanna et al. [202], studying binary alcohols, observed that these systems portrayed concentration variations linked with micellar clusters and alcohol-centric domain aggregations. Such dynamics aligned with the prepeak identified in alcohol diffraction studies. Notably, these concentration shifts were inferred to be not a result of mesoscopic domain fluctuations but were intrinsically connected to the micellar entities.

Adopting SAXS, complemented by SANS, has deepened our understanding of ILs and associated systems. These methodologies have elucidated phenomena from micelle-induced concentration variances in binary alcohols to the mesoscale structure of SILs. Such revelations bear significant potential for evolving sophisticated separation methodologies, refining IL behaviors, and enhancing understanding of mesoscale events in soft materials [202, 203].

Recent studies have begun to investigate the microstructure of ternary systems, focusing on the existence and structure of clusters. Prevost et al. [204] studied mixtures of heavy water and short-chain alcohols and found evidence of complex 'micelle-like' structures of alcohol or alcohol-water complexes. These structures were due to fluctuations in density caused by clusters and areas rich in alcohol. Ornstein-Zernike (OZ) equation [205] offers a way to determine correlation lengths linked to the structure, as followed in Equation 4.3.

$$I_{\mathrm{OZ}}(Q) = \frac{I_0}{1 + (Q\xi)^2} \tag{4.3}$$

where ξ is the correlation length.

D'Arrigo *et al.* analyzed spectra of micelle-like structures in small-alcohol solutions by comparing the Ornstein–Zernike approach with the Guinier approximation. Their findings

demonstrated that in the low-q region, these methods are numerically similar, provided the system is made up of spherical particles that interact weakly or not at all. This conclusion was drawn from expanding both the Ornstein–Zernike and Guinier equations quadratically, leading to the equation $Rg^2 = 3\xi^2$, and by then correlating the radius of gyration to a sphere's radius.

Experimental details *For the measured samples, the beam energy was at 12 keV, which corresponds to $\lambda = 1.03$ Å. The Q-range, that we are interested in, is 0.01 and 2 $Å^{-1}$ and the sample-detector distance was set at 536 mm in the high Q-range and 6.2 m in the intermediate and low Q-regime. The samples were measured in borosilicate glass capillary (WJM-Glass-Muller GmbH) with an outside diameter of 1.0 mm, length of 80 mm and wall thickness of 0.01 mm. We do not work in absolute units due to the uncertainty in the capillary diameter. Therefore, we consider the scattered intensity in SAXS in arbitrary units (a.u.). The date*

4.4.1 [Chol][TFSI] with [Chol][D2EHP]

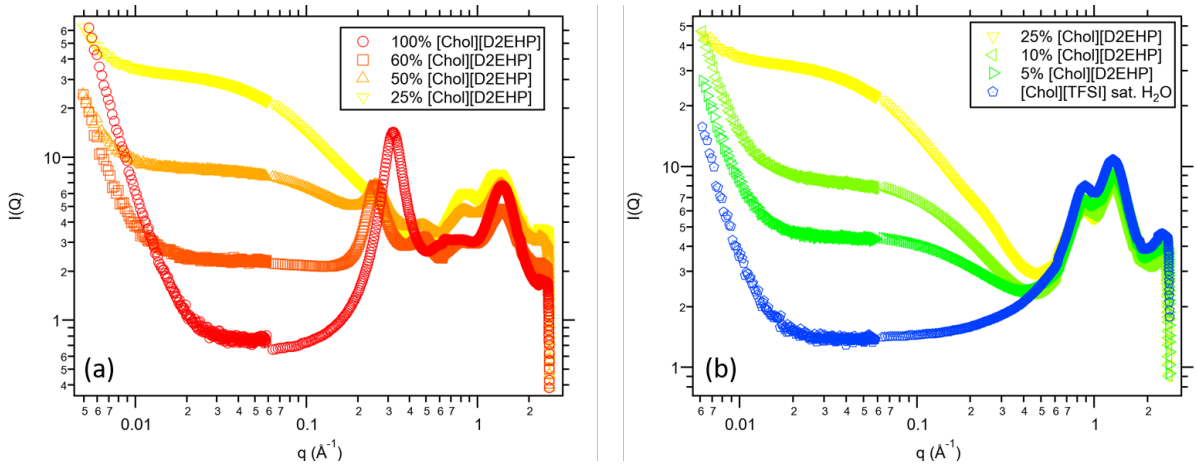

Figure 4.31: All the SAXS experiments presented in this work were run at the SOLEIL Synchrotron (Saint-Aubin, France) on the SWING beamline. Scattering intensity $I(Q)$ as a function of the wave vector Q for [Chol][TFSI] and [Chol][D2EHP] mixtures (a) from neat [Chol][D2EHP] to 25 % w/w [Chol][D2EHP] dissolved in [Chol][TFSI] saturated in water (b) 25 % w/w [Chol][D2EHP] dissolved in [Chol][TFSI] saturated in water to 100 % neat[Chol][TFSI] saturated in water.

Figure 4.31 presents several scattering curves for neat [Chol][D2EHP] dissolved in [Chol][TFSI] saturated in water. For the [Chol][TFSI] saturated in water, which is a viscous liquid at room temperature, it is observed characteristic peaks, at 0.9 and 1.6 $Å^{-1}$, which might link to the cation-anion, cation-cation or anion-anion distances [206]. The neat [Chol][D2EHP] is characterized by peaks at q values of 0.33 and 1.6 $Å^{-1}$. New correlation peaks appear when [Chol][TFSI] is added to [Chol][D2EHP], they might be due to correlation distances linked to the IL liquid added and the neat [Chol][D2EHP].

At the same time, an increase in intensity observed at lower q, a phenomenon that is absent in the pure IL, implying the formation of aggregates [207]. The increase of water content in the system with the increase of the [Chol][TFSI] saturated in water

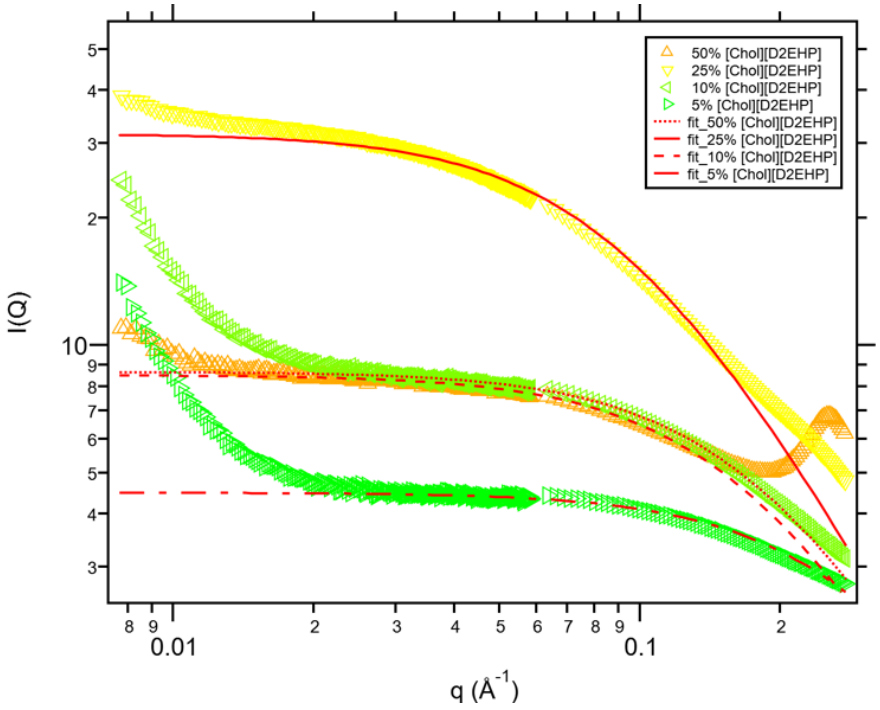

Figure 4.32: Scattering intensity $I(Q)$ as a function of the wave vector Q for [Chol][TFSI] and [Chol][D2EHP] mixtures and Ornstein–Zernike (OZ) function fitting.

concentration might favor the formation of inverse micelles aggregates in the system with water molecules making up the inner core of the aggregate [151]. One can observe in Figure 4.31, that increasing the concentration of [Chol][D2EHP] might favor the formation of bigger structures until 25% w/w [Chol][D2EHP]. However, when it increases more less water is available and there is also the formation of other structures with the correlation peaks of the ILs corresponding to [Chol][TFSI] and [Chol][D2EHP] correlation peaks. These low angle regions were fitted with Ornstein-Zernike (OZ) [205] and Guinier [208] functions to get insights of this aggregate structure size. The Ornstein-Zernike function presented a better agreement for the regions analyzed, as presented in Figure 4.32. The functions were fitted using Iterative Data Fitting (non-linear least-squares / non-linear regression) in Igor Pro software (WaveMetrics, Inc., version 7.08). However, it should be pointed out that the values found might be too small to provide a micro-structure view of the system. One alternative to characterize these structures is the Ornstein–Zernike and the Guinier approximation proposed by D'Arrigo and Teixeira [209][202]). Assuming that the system is composed of spherical particles that interact weakly or not at all, one can determine the diameter of the particle D as in the equation below.

$$D = 2\sqrt{5}\xi \tag{4.4}$$

The OZ correlation distance and its corresponding diameter are shown in Table 4.6, the characteristic diameters determined varied from around 14 to 50 Å. The calculated diameter increases until a certain point with the increase of [Chol][D2EHP], then it decreases when the water concentration is low and the [Chol][D2EHP] concentration is high. The diameters found are similar to the aggregate size of systems with the [D2EHP] anion [210]. Also, the complete miscibility of this mixture of ILs and water observed might

be influenced by this inverse micelles formation behavior.

Table 4.6: Correlation length ξ obtained with the OZ fitted function and derived diameter in of [Chol][D2EHP] % w/w.

[Chol][D2EHP] % w/w	ξ **(Å)**	D **(Å)**
5	3.06	13.70
10	5.22	23.33
25	11.09	49.58
50	5.56	24.86

4.4.2 [Chol][TFSI] with betaine

For a deeper understanding of the ionic liquid structures and their relationship with the liquid-liquid extraction process, we conducted SAXS experiments on the ionic liquid phases from various HLLE systems.

Initially, aqueous phases with different betaine concentrations were put in contact with the ionic liquid [Chol][TFSI] saturated in water. The betaine concentrations in the initial aqueous phases ranged from 1 to 25 % with a same IL:aq phase ratio of 1:1. Each sample was heated and agitated, cooled down, and the phases were separated for analyses. The X-ray scattering curves of the IL phase are shown in Figure 4.33.

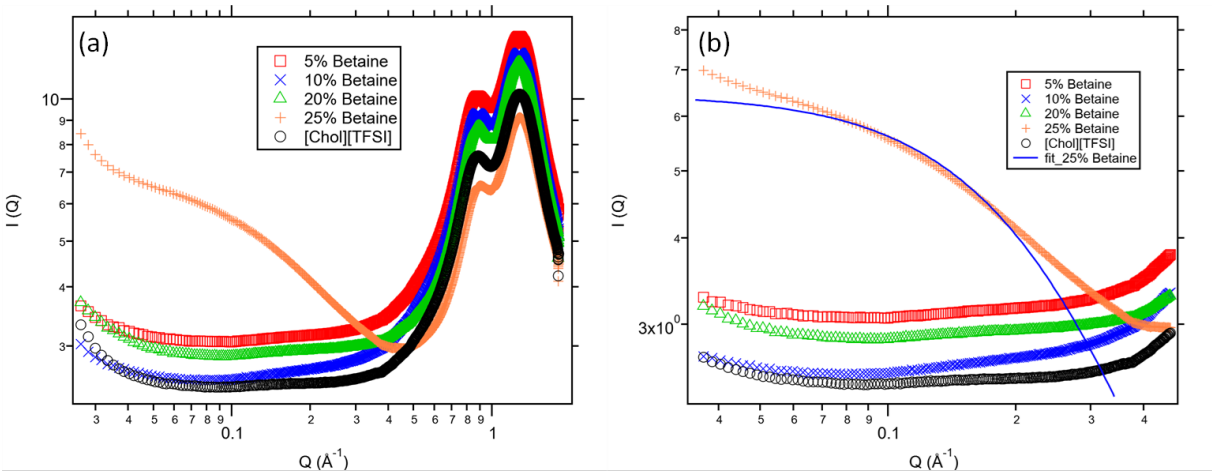

Figure 4.33: (A) Scattering intensity $I(Q)$ as a function of the wave vector Q for the ionic liquid phases after contacting it with aqueous phases with different betaine concentrations (b) Ornstein–Zernike (OZ) function fitting.

The peaks at 0.9 and 1.6 Å^{-1} are typically recognized as correlation peaks that stem from the inherent structure of the IL. They are linked to the anion-anion, anion-cation, and carbon-carbon correlation distances [206]. Also, in this system with an initial betaine concentration of 25 %, an increase of intensity is observed at lower q, a phenomenon that

is absent in the pure [Chol][TFSI] saturated in water and for lower betaine concentrations. The OZ fit gives a correlation length ξ of 4.45 Å and an approximative diameter for the structure of 20 Å for this sample.

The effect of phase ratio was also explored with SAXS. IL:aq phase ratios from 1:1 to 4:1 at a constant initial aqueous phase betaine concentration of 24 % w/w. The results are presented in Figure 4.34 and compared to the IL phase before extraction.

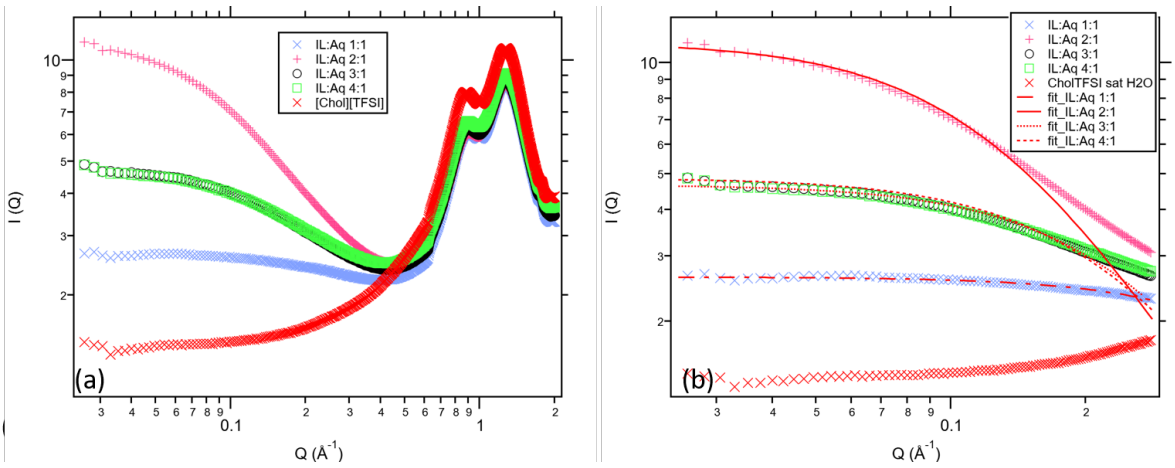

Figure 4.34: (a) Scattering intensity as a function of Q for the ionic liquid phases after extraction with different IL/aq phase ratio (b) Ornstein–Zernike (OZ) function fitting.

High intensities are observed at low q values compared to the initial IL phase, which again may imply aggregation of small molecules [211]. The correlation lengths obtained by OZ plots are reported in Table 4.7. The phase ratio of 2:1 is the highest ξ and D after it decreases to similar lengths. These results imply to have a critical concentration of IL, betaine, and water that leads to aggregation.

Table 4.7: Correlation length ξ obtained with the OZ fitted function.

IL:aq Phase Ratio	ξ **(Å)**	D **(Å)**
1	1.37	6.13
2	7.61	34.02
3	4.00	17.90
4	3.71	16.58

Finally, the influence of initial lithium concentration of the ionic liquid in the scattering curves is presented in Figure 4.35. An IL:aq phase ratio of 2:1 was chosen with an initial betaine concentration of 20 % w/w. Again, it was observed high intensities at low intensity angles compared to the IL saturated in water, indicating aggregation. Correlations distances determined with the OZ function and the approximate diameter are reported in Table 4.8.

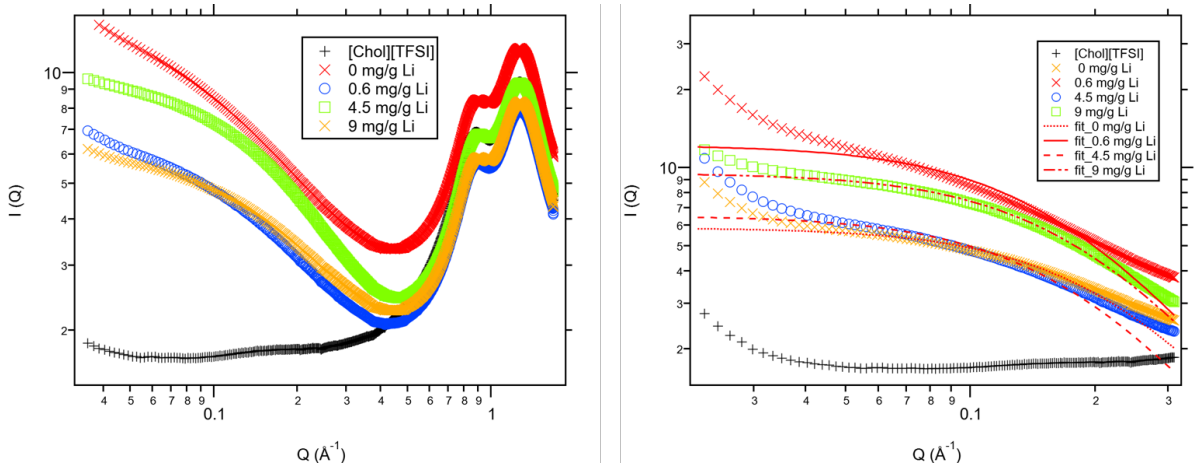

Figure 4.35: (a) Scattering intensity as a function of Q for the ionic liquid phases after extraction with different initial lithium ion concentrations in the aqueous phase with initial betaine concentration of 20 % w/w and (b) Ornstein–Zernike (OZ) function fitting.

Table 4.8: Correlation lenght ξ determined with the OZ fitting.

[Li] mg/g	ξ **(Å)**	D **(Å)**
0.6	6.06	27.09
4.5	5.58	24.97
9.0	5.32	23.80

According to the phase diagram built in this chapter (§section 4.3.1), the maximum betaine concentration in a IL phase for a biphasic system consisting in [Chol][TFSI]/betaine/water is around 6 % w/w betaine and a maximum H_2O concentration of around 18 %. The water concentration in the IL phase increases with betaine concentration. The aggregation is observed close to the limit of betaine concentration in the aqueous phase. The nature of these aggregates is unclear and needs further investigation. However, we can affirm that betaine plays a fundamental role in this structural formation. The intricacy of these systems could arise from an individual or a combination of factors, including the H-bond associations, the self-aggregation leading to H-bonded micellar clusters, and mesoscopic correlations or concentration fluctuations [201, 202, 204].

Another possibility is that these aggregates are formed already in the aqueous phase and then extracted to the IL phase at a critical betaine concentration. Further x-ray studies of the aqueous phase are intended to confirm this hypothesis.

Evaluating the phase ratio aspect, the highest extraction efficiency observed for the phase ratio 3:1, in the conditions studied, might be attributed to the high betaine concentration, chose to it limit together with a bigger mass of [Chol][TFSI], resulting in a big extraction of water mass into the IL phase. At a high phase ratio, the final betaine concentration in the IL is limited, so there is a lower water concentration, and the lithium extraction reaches a limit. Although the extraction of betaine may be favored by the

excess of IL, and it is enough to see bigger aggregation structures. The largest diameter observed in the in 2:1 could be attributed to the highest betaine and water concentration observed in this system, which may have facilitated the aggregation.

Regarding Figure 4.35 and the correlation lengths observed, it is observed that the correlation lengths are similar. They slightly decrease with the increase of the initial Li concentration. The same trend is observed with the extraction efficiency of lithium. These observations might imply that for the LiCl concentration range studied no impact in the IL structure was observed.

4.5 Conclusions

In this chapter, we explored the quantification of extraction efficiency and the effects of various parameters in the context of lithium extraction using thermomorphic ionic liquids. The investigation involved the solvation of Li^+ in pure [Chol][TFSI] and the study of ternary systems comprising [Chol][TFSI], betaine, and water. The structure and dynamics of the IL phase used in HLLE were also analyzed. NMR spectroscopy was the primary tool used in these investigations. Additionally, the nanostructure of the systems was examined using small-angle X-ray scattering (SAXS) technique.

The first section of this chapter focused on assessing the effect of different parameters on extraction efficiency. We examined the influence of betaine concentration IL/aqueous phase ratio and the initial metal concentration on the extraction process for the [Chol][TFSI] saturated in water and betaine. The results showed that betaine concentration, and the phase ratio until the initial lithium concentration influenced extraction efficiency. Considering the parameters used in the individual series, a betaine of concentration of 24 %, a phase ratio of 3:1, and an initial lithium concentration of 0.6 mg/g was obtained as the best condition for lithium extraction positively. Further investigations explored [Chol][D2EHP] as a potential extractant, but it exhibited lower extraction efficiency for lithium than betaine. This extractant has high water solubility, contributing to its loss in the aqueous phase and then lower efficiencies. Simultaneously, another focus of this section is the comparison of the NMR ERETIC digital method for lithium quantification with ICP-EOS measurements. The comparison between the two techniques shows the ERETIC digital method is suitable for accessing lithium concentrations.

In the second section, we explore the NMR investigation of Li^+ solvation in pure [Chol][TFSI]. Longitudinal relaxation time measurements and diffusion experiments were performed to gain insights into the solvation behavior of Li^+ ions in this IL. Nuclei of all species involved are observed. By analyzing the longitudinal relaxation times, a gradual reduction of the T_1 value and the mobility of these species are observed as the lithium concentration and viscosity increase. However, at a certain point, the dynamics change more slowly, indicating a transition to a regime where mobility reaches a limiting value despite further lithium concentration and viscosity increases. The influence of hydrogen bonding in the IL is also observed through the increase of the relaxation times compared to the other protons. ^{7}Li-T_1 results may indicate a significant change in the lithium local rotational dynamics due to the formation of different structures at low and high lithium concentrations. Further, the DOSY measurements indicate a substantial effect of LiTFSI concentration in the diffusion of all species involved that follows a similar decay of self-diffusion coefficient as the lithium concentration increases.

Moving on to the next section, we explored the NMR investigation of the extraction systems, mainly focusing on the ternary system comprising [Chol][TFSI], betaine, and water. A phase diagram was constructed to understand the system behavior, and NOESY and HOESY experiments were conducted to probe the intermolecular interactions. Using NMR is possible to infer the formation of H-bonds with the choline cation and water and observe the intermolecular exchange between the hydroxyl proton and the water, confirmed by HOESY and DOSY experiments. Also, HOESY experiments imply that Li^+ ions are solvated by water in the extraction, the proximity of the IL cation and ion, and the betaine and the IL anion. It is also observed intramolecular interactions in betaine and choline. DOSY experiments confirm the substantial effect of water on system diffusion.

Also, the low influence of betaine and lithium is observed for the system's diffusion.

Based on our analysis of the results, we can infer that betaine is not a suitable extractant for lithium ions. ^{7}Li NMR in both bases, with or without the presence of betaine, allows us to observe that the lithium ions' chemical environment does not change significantly compared to lithium in the water. Also, the chemical environment in the IL and betaine do not present significant changes in the presence of lithium. NOE experiments allow us to observe that lithium ions are extracted surrounded by water molecules. The observed extraction might be mainly due to the components' distributions observed in the in-phase diagram. The bigger the mass transfer of water, the higher the "extraction efficiency" observed for our [Chol][TFSI]/betaine system. This kind of extraction mechanism might be one of the reasons for explaining the difficulty of interpreting the results based on traditional hydrometallurgical studies.

Our findings reveal that the Li extraction system is not notably efficient. Lithium's distribution in the IL phase is suboptimal compared to its distribution in water. Enhancing this distribution is possible by introducing betaine, which augments the miscibility between the phases. As a result, the IL starts mirroring the properties of water. However, there's an essential limitation: the eventual total miscibility of the two phases. At the microscopic level, this behavior originates from lithium's pronounced affinity for water, making it prevalent in the IL phase within its solvation sphere. NMR methods validate this solvation, differentiating it from that observed for lithium without water, as explored in systems. For system enhancement, the route forward involves proposing an IL extraction phase that presents a stronger affinity for lithium than water but maintains limited miscibility with it. Despite this, the study of these systems has raised the interest of using conventional and innovative NMR methods to study liquid-liquid extraction systems.

Further studies with the nitrogen and chloride NMR would be interesting to comprehend better the [Chol][TFSI]/betaine/water/LiCl systems. ^{15}N NMR can reveal the chemical environment of [TFSI] and betaine molecules, indicating interactions within the solution. Chloride NMR can provide insights into chloride ions distribution in the system and capture shifts that might suggest interactions with other molecules in the system. Furthermore, 2D NMR techniques might provide structural insights, and quantitative NMR can capture concentration of the species involved.

Based on the findings presented in this chapter, it is recommended that NMR can be utilized for selecting extractants and diluents in liquid-liquid extraction systems and studying innovative lithium liquid-liquid extraction systems [212–214] In further studies, NMR experiments with, for example, the [Chol][D2EHP] extractant be conducted, in particular, NOE and diffusion experiments to evaluate this IL as a possible extractant and promote further improvement in the system to overcome the issues observed with this extractant in the current study.

Although the limitations in lithium liquid-liquid extraction are observed in the extraction system studied in this work, we can consider that NMR is a suitable technique for studying extraction systems with lithium. The sensibility of this nucleus allows relatively easy implementation of a series of different NMR experiments that, combined with different nuclei, can give important insights into the extraction process. The techniques used in this work can be applied to already-known extraction systems for lithium and have a better understanding of these systems, which could be used for further improvement and design of extraction systems.

The last section involved the investigation of the nanostructure of the system using

SAXS. The structures of [Chol][D2EHP] and [Chol][TFSI] were analyzed, and it is possible to determine the behavior and correlation lengths of aggregates or concentration fluctuations in the system. Also, the effect of betaine on the nanostructure of [Chol][TFSI] was examined. SAXS experiments allowed us to understand better the structural organization of the systems studied. These studies can be used for base system selection and design extraction systems as they give insights into the nanostructural organization of the system. This observation allows us to observe certain phenomena, such as aggregation or concentration fluctuations, which could play an essential role in the extraction processes. One future perspective would be to correlate the observations in SAXS with NMR experiments, for example, with NOE and diffusion experiments.

In conclusion, this chapter explores lithium extraction using thermomorphic ionic liquids. The study sheds light on the effects of parameters on extraction efficiency, ternary system characterization, and solvation behavior. The NMR investigations allowed us to gain deeper insights into the system's molecular interactions and structure, while SAXS techniques provided some insights into the nanostructure.

Chapter 5

Platinum extraction using Thermomorphic ionic liquids

Contents

Platinum (Pt) is a highly valuable and strategically important platinum-group element (PGE) platinum is mostly found in its +II and +IV oxidation state. In this chapter, we investigate the homogeneous liquid-liquid extraction (HLLE) of Pt(IV) using the thermomorphic ionic liquid protonated betaine bis(trifluoromethylsulfonyl)imide [Hbet][TFSI]. [Hbet][TFSI] was initially developed for dissolving metal oxides, utilizing the coordinating ability of betaine [44]. This solubility is attributed to the formation of stoichiometric compounds between the IL and these oxides, as observed by Nockemann et al. [194]. Previous studies showed that an excess of zwitterionic betaine to the aqueous phase, in [Hbet][TFSI] systems, results in significantly higher extraction efficiencies of rare-earth ions [38, 39]. [Hbet][TFSI] is also applied for the selective extraction of uranium and precious metals like palladium, rhodium, and ruthenium [83, 215]. NMR spectroscopy of the ^{195}Pt isotope are relatively convenient due to its moderate abundance and reasonable magnetic moment.

In this chapter, we briefly analyze several extraction parameters of this system, including the addition of betaine as an extractant, phase ratio, selectivity, and back extraction of platinum into the aqueous phase. To gain a better understanding of the system, we employ NMR techniques to study the ^{195}Pt chemical shifts and perform diffusion experiments. Additionally, we present a system for the extraction of Pt(II) with [Chol][TFSI] and betaine, exploring the distribution of the ionic liquid into the two phases using quantitative NMR analysis.

5.1 Pt(IV) extraction with [Hbet][TFSI]

A preliminary study was done in order to choose the most promising systems for platinum extraction study. This studied was performed with Pt in two different oxidation species, Pt(II) and Pt(IV) and two extraction systems. One composed of [Chol][TFSI]/betaine and the other of [Hbet][TFSI]. The [Chol][TFSI]/betaine used in the previous lithium system did not presented visual extraction of Pt(IV). After this preliminary study [Hbet][TFSI] was chosen for Pt(IV).

In order to better understand the extraction mechanism of this system some extraction parameters were analysed. The ionic liquid phase consisted in [Hbet][TFSI] saturated in H_2O. The aqueous phase of the extraction system was prepared with dissolving chloroplatinic acid hydrate $H_2PtCl_6{\cdot}x\ H_2O$ ($\geq$ 99.9 %, Sigma-Aldrich) in Milli-Q water.

To determine the platinum concentration, Total reflection X-ray fluorescence (TXRF) was used. Some theory about this technique is presented in Annex C. The spectrometer used was a S2 PICOFOX (Bruker) equipped with a 50 W X-ray tube using a Mo target and a Peltier-cooled Silicon Drift Detector with an energy resolution below 160 eV.

TXRF Sample preparation *Approximately 100 mg of aqueous phases after extraction were diluted in 5 mL of Milli-Q water. 1 mL of a 15 mg/L Mn standard aqueous solution was added to 1 mL of the diluted aqueous phase solution. Finally, 0.2 mL of a 3 g/L polyvinyl alcohol solution was then added to the final solution. Approximately, 10 µL of this mixture was added onto the sample carrier (polished quartz glass disks) and dried for 60 min in an oven at 60 °C. The manganese was used as internal standard for platinum concentration determination. The Mn solution was prepared with a 1004 mg/L manganese standard for AAS solution (Fluka Analytical, c(HNO_3)=2% w/w) dissolved in Milli-Q*

water. The Polyvinyl alcohol solution was prepared dissolving polyvinyl alcohol (supplier, purity) in Milli-Q water. This solution was added to avoid sample spreading in carrier ensuring a sample droplet of around 5 mm. The IL phase were prepared for TXRF analysis in the same way, however the IL was dissolved in Ethanol absolute (VWR, ≥ 99.8 %) instead of Milli-Q water.

5.1.1 Metal concentration

The effect of metal concentration was studied varying initial feed solutions with different initial Pt(IV) concentrations ranging from [Pt(IV)]= 0.06 to 30 mmol/kg and a mass phase ratio of IL:aq of 1:1. The ionic liquid phase consisted in [Hbet][TFSI] saturated in water.

The Figure 5.1 demonstrates that the extraction percentage is higher at low initial concentrations, reaching 63 % at the lowest concentration, then decreases to 13 % at 30 mmol/kg. At high Pt(IV) concentrations, ranging from 8 to 30 mmol/kg, the percentage of extraction slight reduces with Pt(IV) concentration, remaining relatively constant, around 16 %.

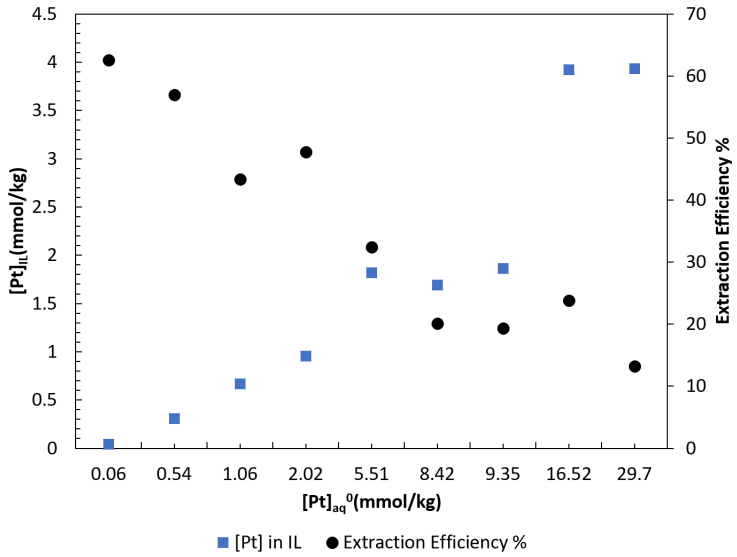

Figure 5.1: Effect of initial Pt concentration on extraction efficiency.

As the initial Pt(IV) concentration in the aqueous phase increases, the concentration in the IL phase after extraction also rises. At low Pt concentrations, the ionic liquid in the ionic liquid phase is present in large excess which favors the loading of the ionic liquid phase influencing the distribution of Pt. At higher Pt concentrations, the ionic liquid phase is no longer present in a large excess so the extraction efficiency is reduced. At the two last initial Pt(IV) concentrations, the final concentration of platinum in the IL phase appears to reach a limit platinum concentration, indicating that we are close to loading capacity of the ionic liquid phase.

The pK_a of 1.83 [216] the betaine cation in [Hbet][TFSI] indicates that it is a relatively weak acid. During extraction, when [Hbet][TFSI] is dissolved in the aqueous phase during the exctraction, it undergoes partial deprotonation, leading to the formation of a pH buffer with a pH value of approximately 1.4. H_2PtCl_6 dissolution leads to an additional decrease of the pH. At 0.05 mmol/kg of H_2PtCl_6 the initial pH is about 4.54 at 40 mmol/kg is 1.27.

However, the addition of a small amount of acid resulting in concentrations of 0.5 M and 1 M of HCl in the initial aqueous phase did not influence the extraction efficiency.

Also, the initial aqueous phase HCl concentrations of 0.5 to 2 M were tested with initial platinum concentration of 0.05 mmol/kg and phase ratio of 1:1. Reducing the pH with the addition in the initial aqueous of HCl did not improve the extraction efficiency for the studied system.

The reduction of initial pH with the addition of acid might reduce the equilibrium pH of the aqueous phase after extraction, maintaining the pH constant during the extraction process [84]. The use of alkaline solutions increase the dissolution of the ionic liquid into the aqueous phase so it was not considered [44].

In the studied system, [Hbet][TFSI] plays a role of the extractant and diluent, it means that there is a significantly higher amount of extractant present in the IL phase compared to the amount of solute Pt. The relatively high concentration of [Hbet] in the aqueous phase is a result of the partial dissolution of the ionic liquid in the aqueous medium and does not change with the initial concentration of platinum in the aqueous phase.

H_2PtCl_6 is a strong acid that undergoes through hydrolysis. Extended X-Ray Absorption Fine Structure (EXAFS) studies show that low chloroplatinic acid concentration (30 ppm, approximately 0.15 mM) favors full hydrolysis by hydroxide ions with precipitation of $H_2Pt(OH)_6$. However, high chloroplatinic acid concentration of 0.01 and 0.1 M H_2PtCl_6 presents higher stability for the Pt -Cl bonds. Also at low pH (1.5 pH) and lower platinum acid concentration, $[PtCl_6]^{2-}$ is also stable [217]. In our system, the low pH of 1.4 reached with the dissolution and deprotonation of [Hbet] might provide the stability of six Pt-Cl bonds at low Pt concentration. Confirmation of the Pt coordination sphere can be done by NMR or Extended X-Ray Absorption Fine Structure (EXAFS).

A formation of a complex with $[PtCl_6]^{2-}$ anion and [Hbet] cation or even its deprotonated form might favor its solubility Pt bearing species into the aqueous phase

5.1.2 Stripping

Stripping or *back-extraction* is the process of removing a solute from a loaded solvent or extract [218]. It is then an important step in the recovery of the solute from the IL phase after it has been extracted from the aqueous phase, allowing recycling of the IL and recover of the target metal in further recovery processes.

In the present study, the back-extraction of platinum loaded in the IL phase was performed using different concentrations of HCl as stripping agent in a concentration range from 0 to 2 M HCl with a phase ratio aq:IL of 1:1. The loaded IL phase was obtained from liquid-liquid extraction with a initial platinum concentration of 5 mM and a phase IL:aq of 1:1. The stripping experiments were conducted the same way as the liquid-liquid extraction, with heating and agitation at 80 °C, cooling down and phase separation. The stripping efficiency is seemingly constant with the concentration of HCl reaching around 65 %, from 0.5 to 2 M HCl as shown in Figure 5.2. Stripping without HCl reduces the stripping efficiency by half.

5.1.3 Selectivity

The selectivity of the system was evaluated for platinum and palladium since these metals can be found together in end of life catalysts [13, 219]. The selectivity of an element A over

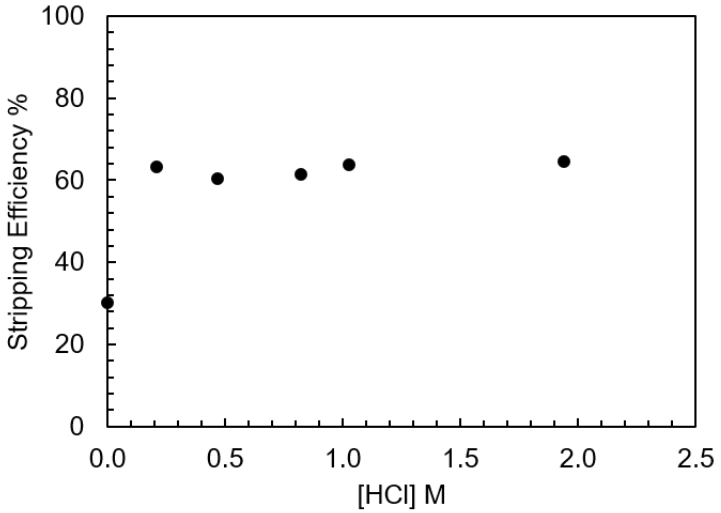

Figure 5.2: Effect of HCl concentration on Pt stripping efficiency.

B, $S_{\mathrm{A/B}}$, can be defined as in Equation 5.1. D_A and D_B are respectively the distribution ratio A and B.

$$S_{\mathrm{A/B}} = \frac{D_A}{D_B} \tag{5.1}$$

In particular, the concentrations ratio Pt/Pd used in this study are similar to concentration ratios in diesel catalysts of light vehicle [219]. The aqueous phase was prepared in the with $PdCl_2$ (Sigma-Aldrich,≥99.9%) and K_2PtCl_6 (Sigma-Aldrich,≥99.9%) dissolved in ultra pure water with a HCl concentration of 2 M. The initial aqueous phase conditions correspond to IL:aq ratio of 1:1, Pt concentration of 5.25 mM, and Pd concentration of of 0.65 mM.

Pd(II) had a higher extraction efficiency of 83% than Pt(IV), that reached the exctraction efficiency of 38%. The selectivity of Pd over Pt is $S_{\mathrm{Pd/Pt}}$= 8.33. Other studies show that Pd(II) is preferably extracted over Rh(III) and Ru(III) from HNO_3 aqueous solutions with [Hbet][TFSI], through a cation exchange reaction, indicates that the formation of $[Pd(bet)_2]^{2+}$, and show high solubility of this complex in the IL [83]. Further enhancing the efficiency of the liquid-liquid extraction process can be achieved through several key strategies, e.g. pH, phase ratios optimization, addition of ligands or diluent, etc... Other strategies can be scrubbing, implementing multiple extraction stages in series which allows for higher solute transfer and improved separation, counter-current flow between the phases enhancing mass transfer. All these strategies can improve the process selectivity and performance.

5.1.4 NMR investigation

After analyzing some liquid-liquid extraction parameters, we proceed to gain further insights into the process by utilizing NMR spectroscopy.

5.1.4.1 ^{195}Pt chemical shift: a sensitive probe?

^{195}Pt is a nuclei with spin $\frac{1}{2}$ with 34 % of natural abundance and a wide range of chemical shifts from −6500 to 200 ppm. Although being a nuclei accessible by NMR spectroscopy, its sensitivity can vary due to NMR instrument and the experimental conditions used [220].

The low concentration of this metal, reported in liquid-liquid extraction experiments might be a practical limit to the study by NMR due to sensitivity issues. Then for NMR investigations, the concentration of Pt was increased, to be easily observable in NMR. In this section, the ^{195}Pt 1D NMR is analyzed in different conditions giving information about chemical environment of the nucleus. ^{195}Pt and ^{1}H diffusion are carried in systems that could represent our extraction process.

Effect of Pt concentration in aqueous solutions The effect of the platinum concentration in aqueous solutions was studied dissolving $H_2PtCl_6{\cdot}x\ H_2O$ ($\geq$ 99.9 %, Sigma-Aldrich) in Deuterium oxide (Sigma-Aldrich). At the lowest platinum concentration prepared of 0.005 M, it was not possible to observe a signal for platinum. Signal from platinum were observed from 0.05 to 0.5 M.

Figure 5.3(a) displays ^{195}Pt spectra of aqueous solutions with increasing concentrations of Pt. They all present similar chemical shifts. Only one peak is observed and the chemical shift do not have significant change with the increase of Pt concentration in the studied range. If we zoom in the peak, it is observed that each Pt peak is formed by five peaks, as in Figure 5.3 (b). This form occurs because chloride can present different isotopes and at high magnetic field ^{35}Cl/^{37}Cl and the isotope shifts can be resolved for the $[PtCl_6]^{2-}$ complex into an approximate five signal pattern recognized as *isotopomers* [221]. The replacement of a Cl^- by and H_2O or OH^- results in a chemical shifts of 600 ppm. The replacement of more chloride ions results in even more higher resonances [222].

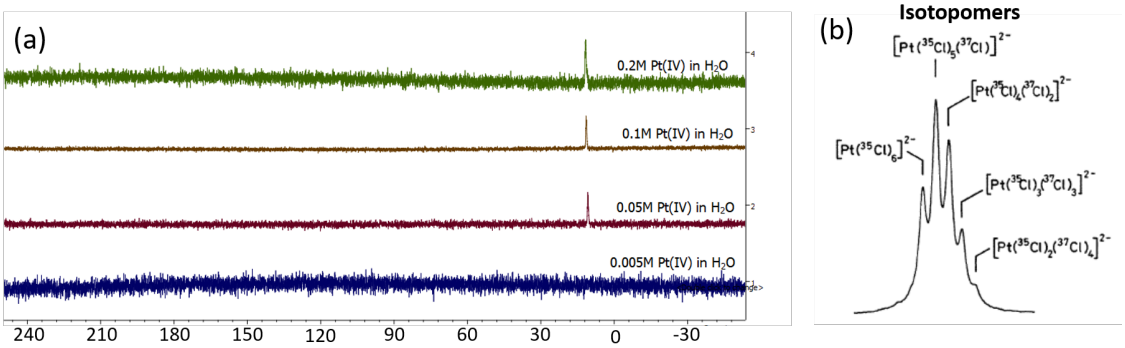

Figure 5.3: ^{195}Pt NMR spectra of aqueous solutions with increasing concentrations of Pt

Effect of betaine The interaction of the platinum anion complex with betaine in aqueous solutions was also investigated. The resulting solution had a betaine concentration of 1.28 mol/kg (approximately 15 % w/w) and 0.2 mol/kg of Pt. Although in the previous studies the betaine zwitterion was not added as an extractant, observing this system may provide some valuable information about the extraction process. Indeed, part of the [Hbet] cation of the IL is deprotonated when dissolved in the aqueous phase during the extraction process and might interact with $[PtCl_6]^{2-}$ as zwitterion. As observed in Figure 5.4 the

peak observed has a chemical shift which indicates that the $[PtCl_6]^{2-}$ might interact with betaine resulting in the change of its chemical environment. The shift to right resonances indicates that the nucleus is more shielded.

Effect of the IL media After HLLE, IL [Hbet][TFSI] saturated with water and loaded with platinum was analysed by ^{195}Pt 1D NMR. The initial conditions of extraction were a phase ratio IL:aq 1:1 and initial Pt concentration of 0.2 M. The spectrum in Figure 5.4 shows that again only one peak is observed and that there is a peak shift to higher resonances indicating the change in the chemical environment of the nucleus. Zooming in the peak, it is still observed that the peak is composed by five other peaks as in Figure 5.5. This fact reveals that the Pt is extracted from the aqueous phase into the IL phase in the form of $[PtCl_6]^{2-}$. This suggest a possible extraction mechanism based on anion exchange with the IL, where $[PtCl_6]^{2-}$ might for complex with $[Hbet]^+$ or the deprotonated cation.

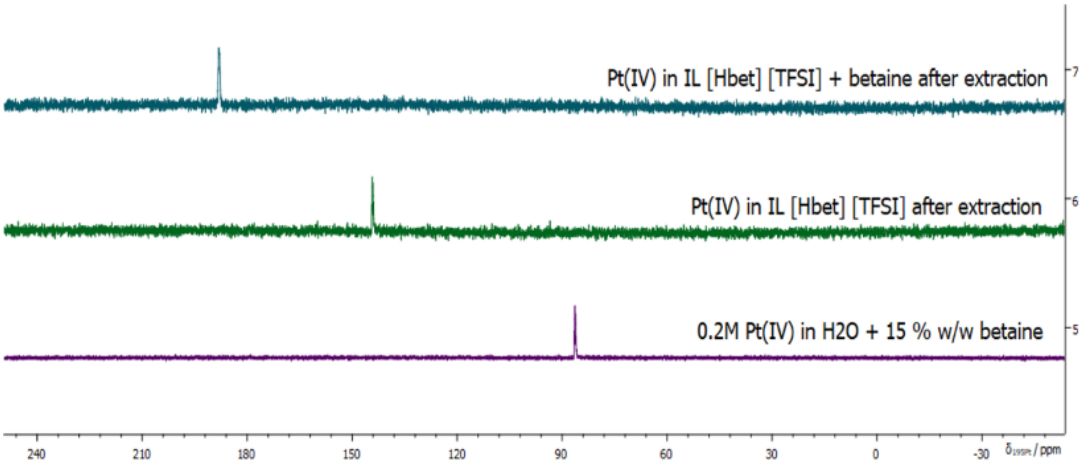

Figure 5.4: ^{195}Pt NMR spectra of the IL phase after Pt extraction.

An even higher chemical shift was observed for platinum in an IL phase loaded with Pt ions with the initial conditions of phase ratio IL:aq 1:1 and aqueous phase with initial betaine concentration of 1.28 mol/kg (approximately 15 % w/w) and 0.1 mol/kg of Pt. The characteristic peak pattern for $[PtCl_6]^{2-}$ is again noticed. Although higher a chemical shift is observed, this chemical shift is still distant from the hydrolysed or substituted $[PtCl_6]^{2-}$ species. This chemical shift change might imply a possible change of the coordination geometry of the complex and the formation of metal complexes with $[PtCl_6]^{2-}$, betaine and $[Hbet]^+$ and described before for other metals in the same IL [223]. The characterization of this metal complex could be done by X-ray diffraction if preciptation of this complex is possible. The solubility of this complexes in the IL and aqueous phase might play an important role in the extraction.

More insights about the chemical environment of $[PtCl_6]^{2-}$ during the extraction process can be obtained from the dynamics in the system.

5.1.4.2 Diffusion

The system dynamics can be studied by determining self-diffusion coefficients using Diffusion Ordered SpectroscopY (DOSY).

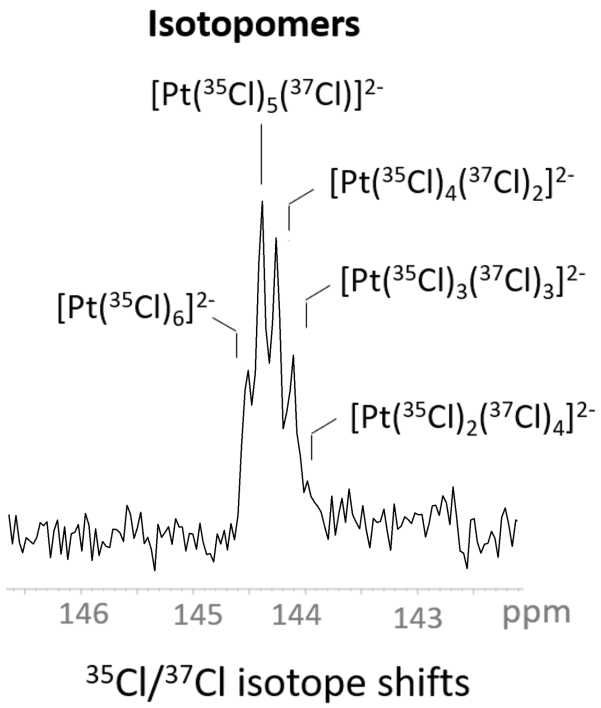

Figure 5.5: ^{195}Pt *isotopomers*. The isotope shifts can be resolved for the $[PtCl_6]^{2-}$ complex into an approximate five signal pattern NMR spectra.

^{1}H DOSY The self diffusion coefficient of the $[Hbet]^+$ cation in the IL phase without Pt and with Pt were compared, Figure 5.7. The IL phase was loaded with the initial conditions of extraction of phase ratio IL:aq 1:1 and initial Pt concentration of 0.2 M. A decrease of about 10 % of is observed for the diffusion coefficient of $[Hbet]^+$ in the presence of Pt, which is significant considering the relative concentrations of $[Hbet]^+$ and $[PtCl_6]^{2-}$. This fact supports the possible formation of platinum metal complexes with $[Hbet]^+$.

^{195}Pt DOSY On the other side, the diffusion coefficient of Pt in aqueous phase with and without the presence of betaine can be compared. We observe a higher than twofold decrease in the diffusion coefficient due to the presence of betaine in Figure 5.6. The reduction in the diffusion coefficient of Pt with the presence of betaine in the aqueous phase suggests pairing and/or aggregation of betaine with $[PtCl_6]^{2-}$.

The study of Pt diffusion in the IL with a high gradient probe is one of the perspectives of future works to get insight into the dynamics of the system and understand better extraction mechanism. Once it was not possible to obtain an adequate decay curve for diffusion coefficient determination with the current gradient condition.

5.2 Pt(II) extraction in [Chol][TFSI]

The presence of different platinum species in these secondary resources depends on various factors, including the original composition of the catalysts, the operating conditions during their use, and the specific methods of recovering and recycling platinum from these sources. The platinum content in these materials may also undergo oxidation and reduction reac-

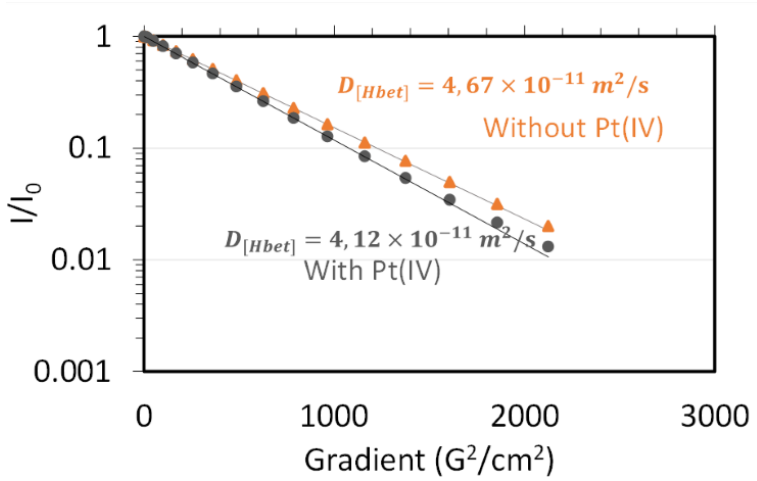

Figure 5.6: ^{1}H Diffusion decay curves of the $[Hbet]^{+}$ cation in the IL phase with and without Pt

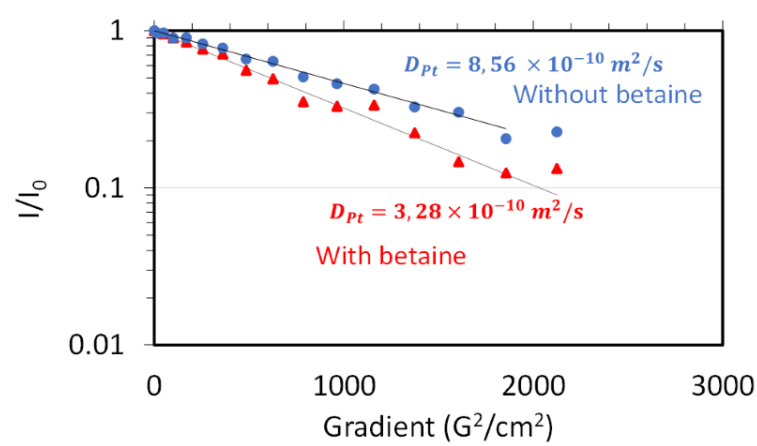

Figure 5.7: Diffusion decay curves of ^{195}Pt in aqueous phase with and without the presence of betaine.

tions during processing and refining. Therefore, it is crucial to carefully characterize and analyze the platinum species in spent automotive catalysts and secondary resources to optimize the recovery and recycling processes. Both Pt(IV) and Pt(II) are described in literature in systems for liquid-liquid extraction. The form of platinum might depend on the source of the platinum-containing material and the specific recycling objectives.

Preliminary studies shown that [Chol][TFSI]/betaine, in opposition to Pt(IV), is a more efficient system to extracted Pt(II) than the system relying on [Hbet][TFSI].

The aqueous phase was prepared dissolving potassium tetrachloroplatinate(II)) in ultra-pure water, K_2PtCl_4 ($\geq$ 99.9 %, Sigma-Aldrich). When K_2PtCl_4 (potassium tetrachloroplatinate(II)) is dissolved in water, it dissociates into its constituent ions, potassium (K^{+}) and tetrachloroplatinate(II)) ($[PtCl_4]^{2-}$). Betaine was dissolved into the aqueous phase to play the role of extractant. While the ionic liquid phase consisted in [Chol][TFSI] saturated in water.

5.2.1 Betaine concentration

The concentration of betaine on the IL phase was varied from 5 to 20 % w/w. For the experiments and IL:aq mass phase ratio of 1:1 was maintained and an initial aqueous phase platinum concentration of approximately 5 mmol/kg was used. In the absence of betaine in the system and for initial betaine concentrations below 5 %, a black precipitate forms. It might indicate that upon the increase of betaine concentration, upon the interaction of betaine and the $[PtCl_4]^{2-}$ or other platinum baring species, a metal complex with betaine is formed and this complex is soluble in the IL and the aqueous phase avoiding the precipitation.

To ensure that no precipitate was in suspension in the IL phase the ionic liquid phase were centrifuged in a Eppendorf MiniSpin Centrifuge during 30 min at 10000 rpm. The extraction efficiency results are presented in Figure 5.8. An extraction efficiency of 80 % was reached for the system at a betaine concentration of 15 % w/w, which is equivalent to a betaine and platinum molar ratio of 230.

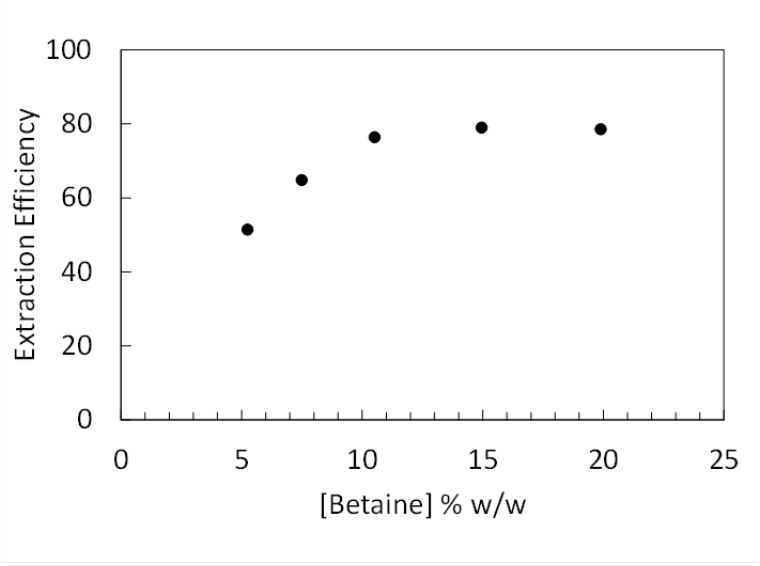

Figure 5.8: Effect of betaine concentration on extraction efficiency of Pt(II).

However thermal decomposition of chlorine complexes were described under different conditions and in temperatures below the one used for the extraction [224, 225]. The study of thermal stability in the experimental conditions may be essential for determining the species present in our system. Preliminary TXRF qualitative analysis of the black precipitate shows that no potassium or chloride is present. The precipitate was removed from the IL phase after centrifugation and was washed three times with absolute ethanol. A small volume of ethanol was kept with the precipitate to deposit it in the TXRF sample carrier and let it dry. Solid NMR, XRD and Energy dispersive X-ray (EDX) analysis might be considered as possible techniques to characterize further the nature of this precipitate.

Due to the possible presence of different unknown species in the system it may be difficult to propose an extraction mechanism for the system. The low platinum concentration in the system also makes it difficult to determine accurately the platinum speciation. However an investigation of distribution of the species using quantitative the ^{1}H and ^{19}F NMR, may give some insights about the extraction process.

5.2.2 Study of species distribution by NMR

The concentrations of the IL cation and anion were determined by the ERETIC digital method in the IL and aqueous phase after extraction in the presence of Pt(II) with a initial concentration of 5 mmol/kg. The results are shown in Figure 5.9.

Experimental Details *In the ^{1}H NMR, the ERETIC calibration sample was prepared with approximately 20 % w/w of betaine dissolved in ultrapure water. A sample of 1 mol/kg of LiTFSI dissolved in ultrapure water was used as ERETIC calibration ^{19}F NMR.*

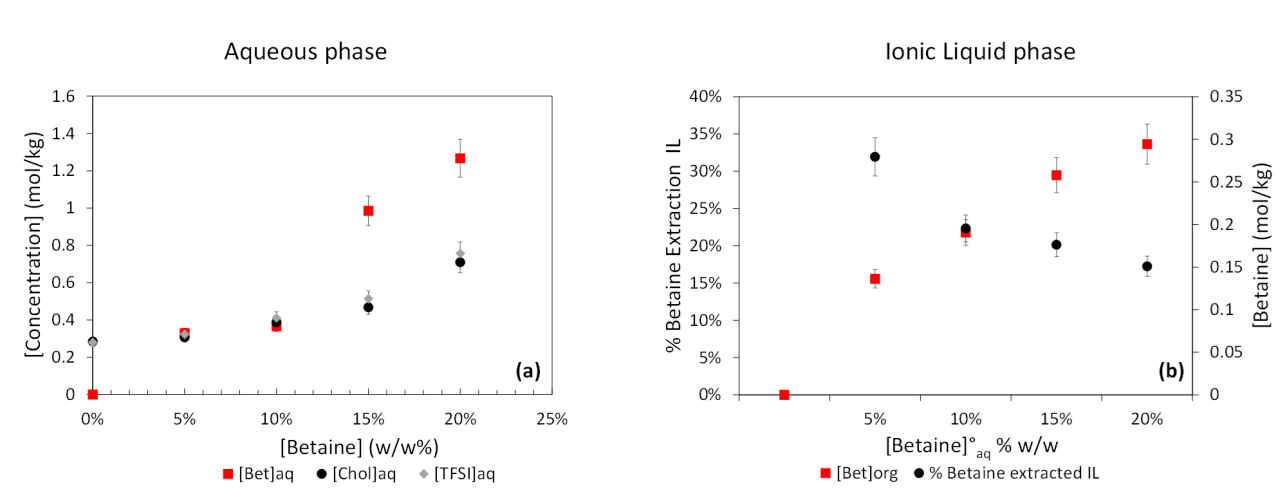

Figure 5.9: (a) Concentrations of the IL cation and anion and betaine in the aqueous phase. (b) Betaine concentration (right axis) and extraction percentage (left axis) in the IL phase. These concentrations were determined by ERETIC digital after extraction in the presence of a initial Pt(II) concentration of 5 mmol/kg and phase ratio 1:1.

The increase of the betaine concentration causes an loss of [Chol][TFSI] ions from the ionic liquid phase to the aqueous phase Figure 5.9(a). Thus, betaine increases the solubility of IL in the aqueous phase. These results are good agreement with the phase diagram § 4.3.1 presented on Chapter 4. This indicate that the presence of metal in this system might not have a significant impact in the system equilibrium composition after extraction processes. It is also possible to observe that even with the increase of betaine concentration in the aqueous phase, the extraction efficiency of betaine into the ionic liquid decreases, and the platinum extraction efficiency stabilizes with this decrease 5.9(b). The loss of the ionic liquid phase due to its solubility in the aqueous phase can affect the efficiency of the extraction process, and may need to be controlled to optimize efficiency. The unwanted loss of ionic liquid into the aqueous phase due to mutual solubility of the two phases can be avoided for example by controlling the acidity. Interactions of these species, IL cation, anion and betaine, can be further observed with two dimensional NMR experiments.

5.3 Conclusion

In this last chapter, we used the tools and methods developed on lithium to study the extraction of another critical metal, platinum. Two extraction systems according to the extraction state of the metal were designed and investigated.

We focused first on the homogeneous liquid-liquid extraction (HLLE) of Pt(IV) using the thermomorphic ionic liquid protonated betaine bis(trifluoromethylsulfonyl)imide [Hbet][TFSI]. We investigated the effect of Pt concentration in the aqueous phase, the influence of betaine concentration in the IL phase, and the selectivity between Pt and Pd since these two elements can be mixed in the waste stream. Our results showed that [Hbet][TFSI] was a more efficient extractant for Pt(IV) than [Chol][TFSI]/betaine. The extraction efficiency was higher at low Pt concentrations but decreased as the Pt concentration increased, eventually reaching a limit due to the loading capacity of the IL phase.We showed that stripping of the loaded IL can be performed with hydrochloric acid solutions. ^{195}Pt NMR chemical shifts were used to study the chemical environment of Pt in different conditions. It was possible to infer that the platinum is extracted as $[PtCl_6]^{2-}$ into the IL phase. Indicating that platinum could be extracted in an anion exchange mechanism.

The presence of betaine in the aqueous phase resulted in a shift in the Pt chemical shift to high resonances, suggesting a possible interaction between $[PtCl_6]^{2-}$ and betaine. The same is observed for ^{195}Pt in the IL phase. Diffusion experiments suggest the formation of a complex between $[PtCl_6]^{2-}$ and betaine in the IL phase. A study of selectivity between Pd and Pt showed selectivity from this system towards Pd. Opposite to the lithium system, the platinum system presented a potential for this metal extraction and other PGE. Further studies in the optimization parameter of systems could be conducted to enhance efficiency and selectivity in the extraction process. Potential future studies are the influence of phase ratio, as the proportion of the two immiscible phases can critically affect extraction efficiency and equilibrium. Similarly, the role of pH, and variations in pH levels can significantly alter metal speciation and its extractability. Furthermore, the dynamics of metal concentration in the feed solution could impact extraction kinetics. There is also a compelling case to study the synergistic effects, where combinations of extractants or other components might amplify extraction efficiency. These studies can help elucidate mechanism of extraction in combination with NMR experiments. The platinum medium NMR sensitivity might impose some difficulties in studying these nuclei.

In further works, EXAFS studies would help to elucidate the coordination of Pt in the system. It would then be possible to confirm the transfer of platinum with the chloride coordination shell and assess the binding by betaine inferred from the NMR measurement. With these results, the understanding of the transfer mechanism only outlined in this preliminary study would be improved. Precipitation and crystallization of metal complexes followed by solid NMR, XRD, and computational methods, such as density functional theory (DFT), could improve the knowledge of complexes formed during extraction.

We also studied the extraction of Pt(II) with [Chol][TFSI] and betaine. The presence of betaine significantly improved the extraction efficiency, reaching 80 % at a betaine concentration of 15 % w/w. However, the system exhibited the formation of a black precipitate in the absence of betaine, indicating the possibility of unknown species in the system. The formation of Pt(II)-betaine complexes appears to have a fundamental role in the extraction mechanism. The speciation of Pt(II) could not be observed due to

low concentrations then, EXAFS studies would elucidate the coordination of this metal in the system and a better understanding of the extraction mechanism. A future study of proton diffusion NMR in the system would give some insight into the dynamics and complex formation of the system. The metal complex formed in this system could also be investigated after crystallization.

NMR was also used to investigate the IL cation-anion and extractant distribution between the phases, and it showed that the addition of metal does not significantly change the phase behavior of the system. NMR spectroscopy proved to be a valuable tool for understanding the chemical environment and dynamics of the system. Further research is needed to optimize the extraction process and characterize the species involved to improve the efficiency of Pt extraction and the design of extraction systems.

Conclusions and Perspectives

In this research, a thorough exploration was conducted on the use of Nuclear Magnetic Resonance and other techniques to analyze extraction systems, with a particular focus on the applications of thermomorphic systems. We mainly concentrated our efforts on studying a sole metal per extraction system. While studying only one metal species has limitations, it provides valuable insights into the extraction process for specific metals. Additionally, some complex systems may not be suitable for the NMR technique due to paramagnetism, coordination, binding effects, etc. Studies with only one metal species lay the foundation for more comprehensive research that explores selectivity, multicomponent systems, and real-world applications in the future.

Chapter 3 highlighted the potential of the LOCSY technique in studying liquid-liquid extraction systems. Several observations were made in our exploration of biphasic liquid-liquid extraction systems using the LOCSY technique. Clear phase separation and interface regions in the NMR spectra were discernible across different nuclei. Concentration gradients and chemical shift disparities provided valuable insights into the composition and behavioral complexity of various systems. A methodology using in-situ agitation with gas bubbling in the NMR tube was presented, facilitating rapid and efficient system homogenization. This has potential ramifications for studying macroscopically unstable samples and introducing operando gas into liquid samples. Our investigation into the [Chol][TFSI]/aqueous phase system's phase separation during the cooling process and phase mixing during heating up revealed the potential of time-resolved localized spectroscopy in assessing the mass transfer rate between phases, enabling the extraction kinetics monitoring and optimization of extraction conditions.

In Chapter 4, our focus was drawn to the lithium liquid-liquid extraction process. Factors such as betaine concentration, IL/aqueous phase ratio, and initial lithium concentration were examined. The system with [Chol][TFSI] and betaine as extractant presented better efficiency. We also successfully compared the NMR ERETIC digital method and ICP-EOS measurements, confirming the former's suitability for determining lithium concentrations. Our NMR investigation unveiled the solvation nuances of Li^+ in dry [Chol][TFSI], studying the dynamic effects of the Li^+ concentration. In particular, a system's structural organization change is observed at high Li^+.

The complexities of lithium-ion dynamics, their solvation behavior, and the influences of the change in lithium dynamics in the IL were interpreted. The ternary system, comprising [Chol][TFSI], betaine, and water, was another crucial aspect of our research. Our efforts in constructing a phase diagram were fundamental in the characterization of the system's biphasic domain. DOSY measurements appointed essential insights into the system's dynamics. NOESY and HOESY experiments were essential in understanding the extraction system's behavior and organization. Betaine did not emerge as an ideal extractant for lithium ions. Our observations pointed out that the extraction of lithium ions revolved largely around water molecules. Finally, nanostructure investigation via SAXS techniques yielded structural insights. [Chol][D2EHP] and [Chol][TFSI] and betaine systems show aggregation, which could be pivotal in extraction processes, and it was possible to better understand the formation of these aggregates and determine some of their characteristic sizes.

While the challenges and complexities of lithium extraction in the chosen system were

evident, the chapter highlighted the immense potential and precision of NMR and SAXS in decoding and possibly enhancing extraction systems. The techniques and findings elucidated here pave the way for more refined and targeted research in lithium extraction.

The focus of Chapter 5 was on the homogeneous liquid-liquid extraction (HLLE) of Pt(IV) using thermomorphic ionic liquids. Notably, [Hbet][TFSI] showed enhanced efficacy in the extraction of Pt(IV) compared to [Chol][TFSI]/betaine. This investigation on the homogeneous liquid-liquid extraction (HLLE) of Pt(IV) employs the thermomorphic ionic liquid [Hbet][TFSI]. The ability of NMR spectroscopy was evident as it unraveled insights into the extraction mechanism. Through ^{195}Pt NMR shifts, we could infer the extraction of platinum as $[PtCl_6]^{2-}$ in the IL, probably complexing with betaine or protonated betaine, pointing towards an anion exchange mechanism. Betaine's presence altered the Pt chemical environment, suggesting an interplay between $[PtCl_6]^{2-}$ and betaine. Our diffusion experiments shed light on the dynamics, again revealing potential complex formation between $[PtCl_6]^{2-}$ and betaine within the IL phase. Remarkably, in mixing Pd and Pt, the system exhibited a selectivity towards Pd. This contrast with the lithium system highlights the promise this system holds for extracting platinum and other Platinum Group Elements (PGEs). To advance this field, exploring parameters for optimization would be investigated. As we expanded our focus to Pt(II) extraction using [Chol][TFSI] and betaine, betaine's fundamental role in increasing extraction efficiency was observed. Yet, in betaine's absence, a black precipitate was formed, hinting at unidentified coordination species in the system. While the role of Pt(II)-betaine complexes seems central to the extraction process, NMR could not study speciation due to concentration constraints. In encapsulating our findings, Pt extraction via thermomorphic ionic liquids was confirmed, although with paths for deeper explorations. NMR spectroscopy emerges as an important tool, shedding light on the system's chemical environment and dynamics.

Several perspectives are foreseen for future work. In Chapter 3, the utility of the LOCSY technique in understanding biphasic liquid-liquid extraction systems was shown. Looking ahead to further investigations, it will be pertinent to investigate the impact of heating within thermomorphic solvent extraction systems using the LOCSY approach. Initial experiments have unveiled the profiles of cholinium, betaine, and water. Using these concentration gradients, there is an opportunity to determine mutual diffusion coefficients within the analyzed system. A key area of exploration will be the use of time-resolved localized spectroscopy to study the rate of solute transitions between phases. This endeavor aims to deeply observe extraction kinetics and analyze any rate-limiting factor to improve extraction processes.

From a long-term perspective, time and space-resolved NMR LOCSY can monitor real-time molecular interactions and phase dynamics, leading to an enhanced comprehension of the underlying mechanisms governing extraction processes. This could pave the way for identifying and understanding transient intermediate phases or species and inhomogeneities within the mixture that may be crucial to extraction efficiency. This technique can also be valuable in optimizing mixer and settler designs to ensure uniform extraction conditions. Coupling LOCSY with temperature variation would enable the study of thermodynamic and kinetic aspects of extraction, elucidating the role of temperature-induced phase changes. The interfacial regions between the co-existing liquid phases, often the focus of important interactions, can be analyzed by exploring small spatial dimensions. Furthermore, this advanced technique could facilitate studies on the molecular diffusion rates between the phases, potentially identifying barriers to efficient mass transfer. Such

insights can guide the formulation of solvents with enhanced mass transfer characteristics. Integrating LOCSY with other modalities, like molecular simulations or computational fluid dynamics, would allow for the validation and refinement of theoretical models. These results can drive the design of extraction processes. Looking further, real-time monitoring of extraction under varied mechanical agitations, pressures, and other operational conditions using LOCSY could provide insights into the scalability and efficiency of extraction processes.

Based on the insights from Chapter 4, there's a clear path for exploring other potential extractants for lithium ions using NMR spectroscopy. A comprehensive screening of other molecules using NMR might yield better candidates with enhanced efficiency and a better understanding of already known successful extraction systems.

The nanostructures revealed by SAXS in thermomorphic systems can be studied more extensively. One could investigate how different structures are formed and their impact on extraction efficiency by tuning the compositions and conditions.

The findings in Chapter 5 showed that [Hbet][TFSI] holds promise for the extraction of Pt(IV). As well [Chol][TFSI] and betaine for the extraction of Pt(II). Further optimization of these systems could be studied, applying phase ratios, pH, metal concentration, addition of ligands studies, etc. Future EXAFS studies will be fundamental in decoding platinum coordination in the system.

EXAFS investigation, DRX, solid NMR of precipitates, and crystallized materials would assist in a better comprehension of the extraction process. Anion exchange mechanisms and the dynamics of such processes could be explored further using NMR with different nuclei. ^{15}N NMR can reveal the chemical environment of [TFSI], [Hbet], and betaine molecules, indicating interactions within the solution. The techniques offer invaluable insights into dynamics and mobility through relaxation times, hint at potential phase separations or heterogeneities in the system, and can detect solvent effects, primarily due to the presence of water. Furthermore, 2D NMR techniques might provide structural insights, and quantitative NMR can capture concentration details. These NMR studies provide a comprehensive understanding of the system's interactions, structure, and behavior.

While the research extensively utilized NMR spectroscopy, future works could integrate computational simulations, providing predictive insights and complementing the empirical findings in NOE and diffusion experiments. Molecular dynamics simulations, in particular, could visualize interactions at the atomic level, enhancing our understanding of extraction processes and supporting interpretations of the system, which could be supplemented by more local studies for the solvation of ions.

In liquid-liquid extraction with already known systems, NMR is a helpful tool to investigate the complex details of the system's efficiency and characteristics. Parameters such as chemical shifts shed light on the molecular environment and assist in identifying individual components within phases. Furthermore, by studying concentration gradients, one can evaluate the spatial distribution of solutes, thereby understanding the efficacy of extraction at a granular level. Relaxation times provide essential information about molecular dynamics. Diffusion coefficients, as measured by diffusion-ordered spectroscopy (DOSY), offer insights into the migration rates of molecules and their ease of transitioning between phases. A quantifiable measure of the extraction process can be deduced by analyzing the peak intensities, which correlate directly with concentrations.

When evaluating new extraction systems through NMR, several factors come into play.

The definition of the interface between two co-existing phases becomes fundamental. NMR visually represents this phase separation and chemically characterizes the interface. An even deeper investigation into the molecular dynamics at the interface reveals the behavior of molecules at this boundary, a crucial insight for any extraction system. Time-resolved NMR measurements can illuminate the system's kinetics, showcasing the speed at which equilibrium is achieved or investigative potential rate-limiting steps. Furthermore, with some systems displaying temperature-sensitive behaviors, NMR can monitor alterations occurring due to temperature variations. Lastly, for a better understanding, techniques such as Nuclear Overhauser Effect Spectroscopy come into play, highlighting the intermolecular interactions and providing a glimpse into the driving forces of the extraction process.

Given the global emphasis on sustainable processes, a rigorous environmental and life cycle assessment (LCA) of HLLE techniques is crucial. This includes considering carbon footprint, water usage, waste production, and IL recycling. This approach will optimize HLLE systems not only for efficiency but also for sustainability. Specific attention should be given to the ecological implications of the TFSI-based systems, and possible replacement studies for fluorinated compounds could be motivated.

In conclusion, the current results highlight the immense potential of NMR spectroscopy in investigating metal extraction systems. The ability to refine methodologies, delve deeper into specialized research areas and combine with other analytical methods positions NMR as a helpful tool for studying metal extraction processes' complex chemistry and kinetics. These thesis studies form a base for subsequent investigations focused on enhancing metal extraction efficiencies and highlight the significance of NMR techniques in advancing this field of research.

Annexes

Appendix A

Methods

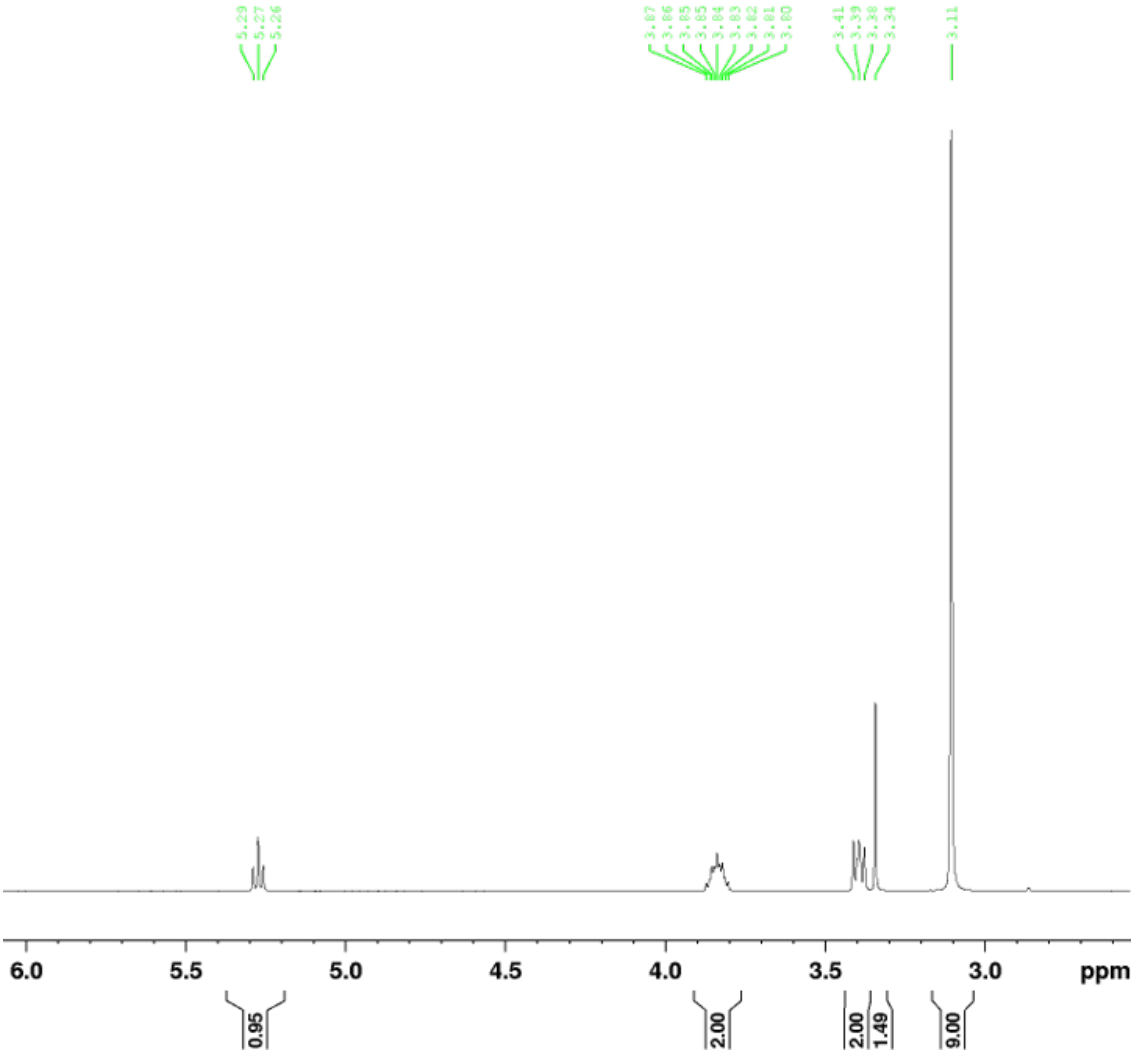

Figure A.1: $_1$H NMR spectrum of [Chol][TFSI] in DMSO. (500 MHz, TMS): δ = 5.29 (t, 1H), 3.84 (m, 2H), 3.39 (m, 2H), 3.10 (s, 9H).

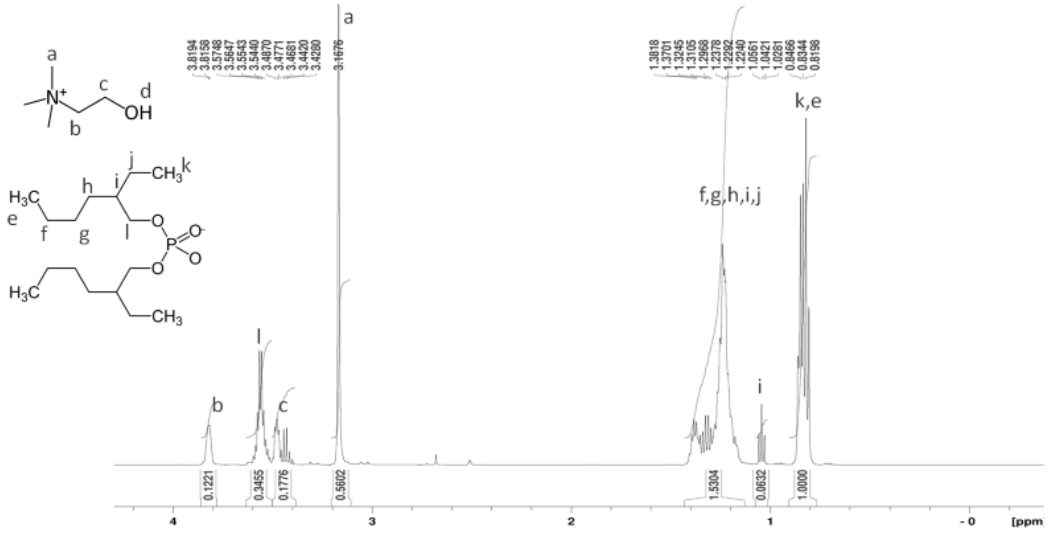

Figure A.2: ^{1}H NMR spectrum of [Chol][D2EHP] in DMSO. ^{1}H NMR (500 MHz, [D6]DMSO, TMS): δ = 0.80-0.81 (m, 12H, 4CH3), 0.91 - 0.91 (m, 12H, 4CH_3), 1.19-1.44 (m, 32H, 16CH_2), 1.59 (m, 2H, 2CH), 3.63 (m, 4H, 2OCH_2) 3.81 (m, OCH_2), 3.47 (m, NCH_2), 3.16 (s, 3NCH_3).

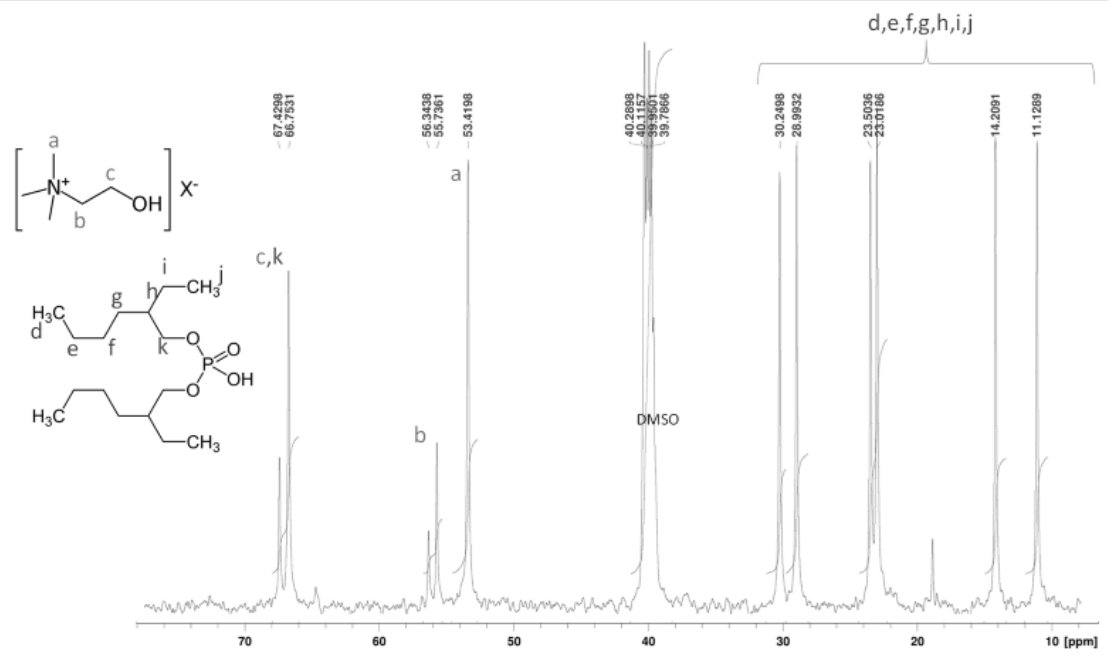

Figure A.3: ^{13}C NMR spectrum of [Chol][D2EHP] in DMSO.^{13}C NMR (500 MHz, [D6]DMSO, TMS):11.12 (4CH_3), 13.66 (2CH_3), 14.01 (2CH_3), 19.71 (4CH_2), 23.14 (2CH_2), 23.32 (2CH2), 24.07 (4CH_2), 29.06 (2CH3), 30.12 (2CH_2), 40.43 (2CH), 58.70 (3NCH_3), 53.41 (OCH_2), 56.35 (NCH_2), 67.27 (2OCH_2)

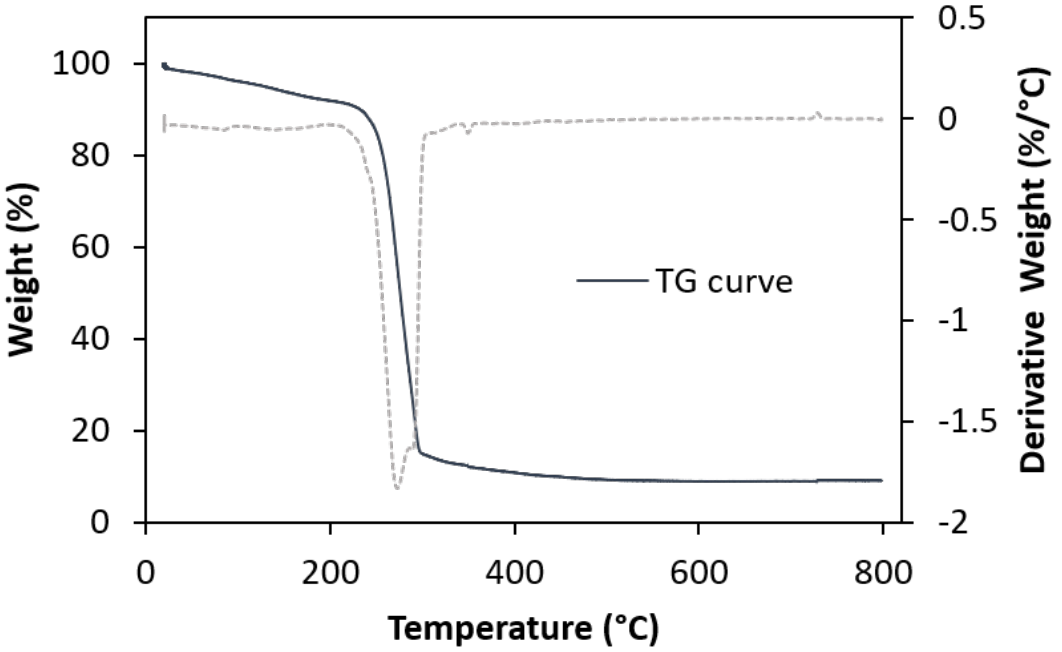

Figure A.4: Thermal gravimetric analysis (TGA) of [Chol][D2EHP] (20°C to 800 °C, 2 °C/min, in N_2 atmosphere).

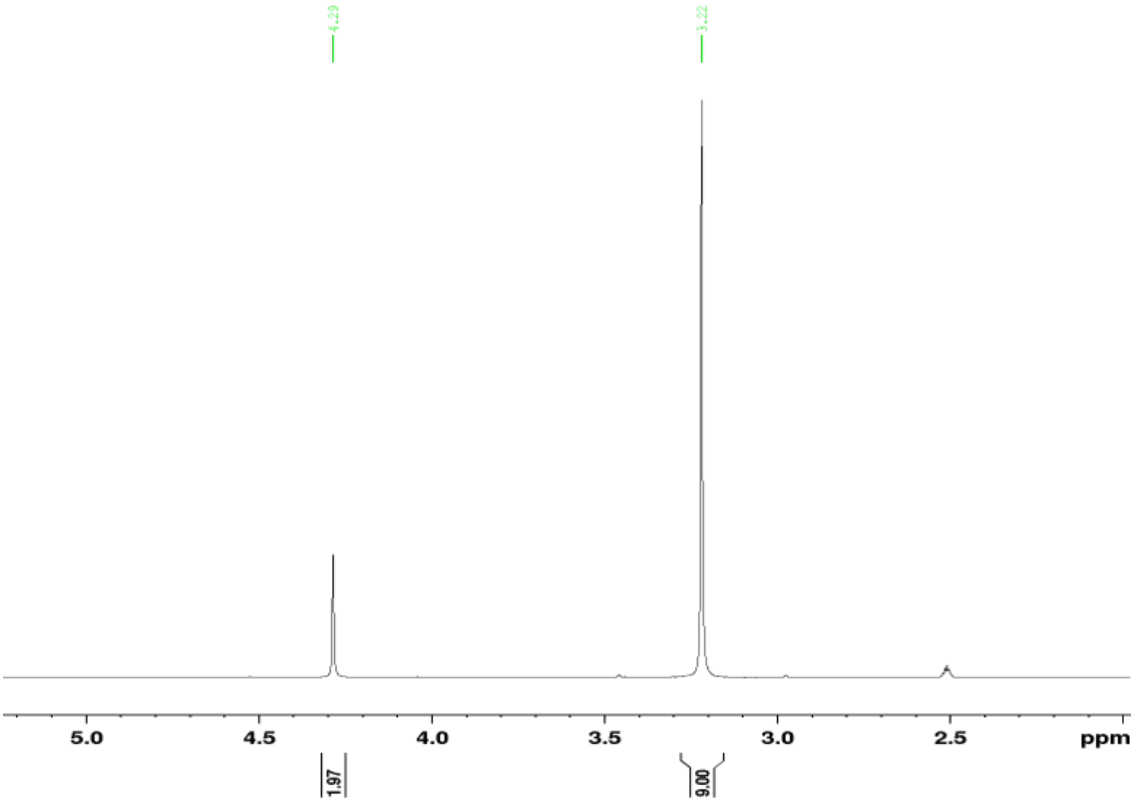

Figure A.5: ^{1}H NMR spectrum of [Chol][DHEHP] in DMSO. (500 MHz, [D6]DMSO, TMS): δ = 4.29 (s, 2H), 3.22 (s, 9H).

Appendix B

Small-angle X-ray scattering (SAXS)

In Small-Angle X-ray Scattering (SAXS), a sample is exposed to an X-ray beam, and the intensity of the scattered X-rays is measured as a function of the scattering angle, 2θ, and presented in Figure B.1. Before reaching the sample, the X-rays must propagate with a minimal amount of angular divergence to interact with the sample at the same relative angle. When the X-rays reach the sample they are scatter by the electrons.

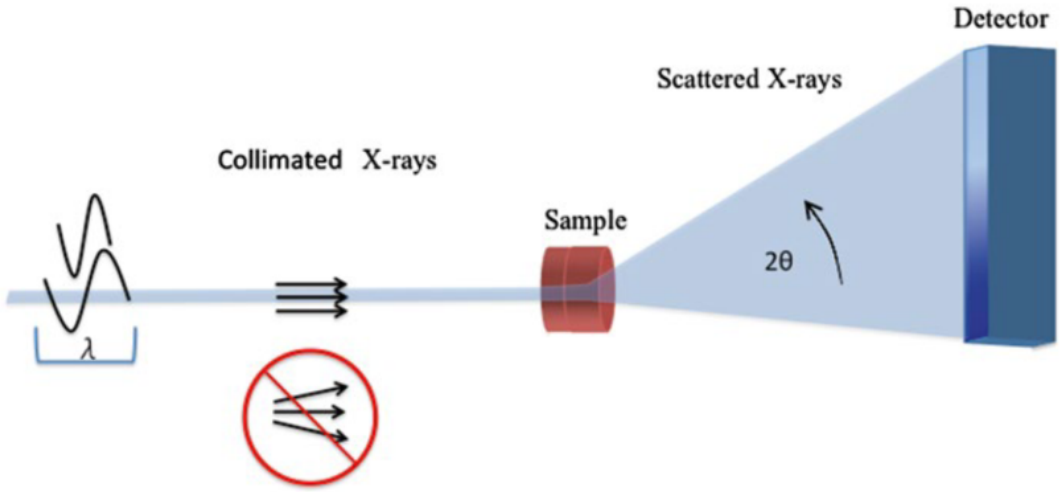

Figure B.1: A basic scheme depicts a standard SAXS experiment, illustrating the incoming and scattered X-rays interacting with a sample [40].

In the context of ILs, such organization may be intrinsic to the IL due to the cation, anion, or aggregation of amphiphilic molecules in ILs [40]. This structural order can be assessed by determining the recurring distance of the phases, or d. This order is directly observable in the SAXS pattern as "peaks" in the $I(2\theta)$ curve. These peaks signify the distance, d, of the structured arrangement according to Bragg's Law:

$$d = \frac{n\lambda}{2\sin\theta} \tag{B.1}$$

where λ is the X-ray wavelength and n is an integer. The scattered intensity is collected on the detector in the form of a 2D image. In order to convert the 2D image into a 1D curve, a radial integration is performed for different values of scattering vectors q Thus we obtain the scattering curve representing the scattered intensity as a function of q. This equation has proven valuable in exploring ILs through SAXS. For $n = 1$, this equation can also be expressed as:

$$d = \frac{2\pi}{q} \tag{B.2}$$

where q is the magnitude of the scattering vector at the peak center. However, it should be emphasized that while Bragg's law gives direct distances, d, it does not provide insight

into the origin of the order. Despite this, it is frequently used in SAXS in ILs due to its simplicity and universal application, even when more precise models might be suitable. An example is the analysis of ordered micelles' inter-micelle distance, where an analytical solution for modeling the SAXS data is already available.

Appendix C

Total Reflection X-rays Fluorescence (TXRF)

Total Reflection X-ray Fluorescence (TXRF) is an analytical technique that allows the detection and quantification of trace elements in a sample. It is based on the principle of total reflection of X-rays and subsequent stimulation of fluorescence radiation followed by an energy-dispersive X-ray detection [226, 227].

This technique is very similar to Energy Dispersive X-ray Fluorescence (EDXRF) but the position of the incident beam differs since the sample is inclined at a very low angle with respect of the incident X-ray beam ($\sim 0.1°$). The the X-ray beam is then in the condition of total reflection on the surface of the sample. This total reflection yields 3 significant advantages [228]:

- the background signal is smaller
- the sample is excited by both the incident and the reflected beam giving a higher fluorescence.
- the detector can be very close to the sample ($\sim$ 5 mm) enabling a more efficient collection of the fluorescence.

In a typical TXRF experiment, the sample is applied on a reflector and an X-ray beam with a well-defined wavelength is directed towards it at a very small angle, typically less than the critical angle for total reflection. As a result, the beam travels a long path within the sample, stimulating fluorescence radiation. This fluorescence is characteristic of the elements present in the sample and can be detected and analysed to determine the composition of the sample. Since the incident beam undergoes total reflection, the background signal is significantly reduced, resulting in a high signal-to-noise ratio and enabling detection of trace elements.

In the realm of optics, the phenomenon of total reflection occurs when light transitions from a medium with a higher refractive index to one with a lower refractive index, causing the light to be reflected back into the denser medium (see Fig. 14). This effect is observed when the angle of incidence upon the interface is smaller than a particular critical angle, given by:

$$\alpha_{\text{crit}} = \arccos\left(\frac{n_1}{n_2}\right) \tag{C.1}$$

where α_{crit} represents the critical angle for total reflection, n_1 is the refractive index of the less optically dense material, and n_2 is the refractive index of the denser material [229].

Based on elements sensitivities, different quantification models can be realized. In the method of quantification with an internal standard is incorporated into the sample. It's crucial that this element is absent in the initial sample. This mode of quantification is

suitable for liquid samples, digested samples, and suspensions. The concentration of the corresponding elements is determined by the following equation.

$$C_{\mathrm{i}} = \frac{C_{\mathrm{IS}} \cdot N_{\mathrm{i}} \cdot S_{\mathrm{IS}}}{N_{\mathrm{IS}} \cdot S_{\mathrm{i}}} \tag{C.2}$$

In the equation, $\mathrm{C_i}$ indicates the concentration of the element under analysis. $\mathrm{C_{IS}}$ is concentration of the internal standard. $\mathrm{N_i}$ represents the net pulse number within the measurement spectrum of the element to be analyzed. $\mathrm{N_{IS}}$ denotes the net pulse number within the measurement spectrum of the internal standard. $\mathrm{S_i}$ is the relative sensitivity of the element i. Finally, $\mathrm{S_{IS}}$ is the relative sensitivity of the internal standard element.

Appendix D

French Summary: Etude de l'extraction de métaux dans les Liquides Ioniques Thermomorphiques par spectroscopie RMN

D.1 Introduction

L'extraction liquide-liquide (LLE) joue un rôle crucial dans la voie hydrométallurgique pertinente pour le recyclage des métaux critiques. Les liquides ioniques (IL) sont apparus comme un substitut adéquat aux solvants organiques volatils traditionnellement utilisés dans ces procédés. Ceci est attribué à leurs caractéristiques moins toxiques, ininflammables et à faible volatilité par rapport à leurs homologues conventionnels. Dans ce cadre, les IL thermomorphes peuvent être appliqués pour l'extraction liquide-liquide homogène (HLLE), comme présenté dans la Figure D.1. Ce processus exploite les attributs uniques de miscibilité dépendant de la température de ces IL avec des solutions aqueuses [39, 72]. La miscibilité complète des phases constitutives qui en résulte efface la barrière d'interface du système. La plupart des recherches sur les LLE ont tendance à se concentrer exclusivement sur les espèces métalliques dans les phases aqueuses. Cependant, la spectroscopie par résonance magnétique nucléaire (RMN) apparaît comme un outil puissant capable d'étudier toutes les espèces impliquées dans le processus, telles que le liquide ionique, l'extractant, l'eau et les noyaux métalliques spécifiques. L'étude présentée ici fournit des outils visant à approfondir la compréhension du système d'extraction, pour améliorer son efficacité.

Cette thèse est structurée en chapitres distincts comme suit:

- Le premier chapitre propose une revue concise de l'état de l'art concernant l'application des liquides ioniques dans l'extraction par solvant pour le recyclage des métaux.
- Le deuxième chapitre décrit la synthèse des IL, le protocole expérimental HLLE, la théorie RMN et l'utilisation de la spectroscopie par résonance nucléaire pour l'étude de systèmes similaires.
- Le troisième chapitre introduit la spectroscopie localisée pour étudier les processus d'extraction liquide-liquide.
- Dans le quatrième chapitre, l'extraction possible du lithium d'une solution aqueuse à l'aide d'un système thermomorphique est explorée.
- Le cinquième chapitre présente une étude de l'extraction liquide-liquide du platine

dans les systèmes thermomorphes.

- La thèse se termine par un résumé général résumant les principaux résultats de la recherche et les orientations futures potentielles.

L'objectif principal de cette thèse est de développer des méthodologies pour élucider les processus d'extraction des ions métalliques par les liquides ioniques (ILs) dans le cadre du recyclage utilisant des extractions liquide-liquide, visant une base empirique pour l'optimisation de ces processus. Une difficulté majeure est la compréhension des mécanismes de solvatation des ions métalliques dans les ILs et la détermination des rôles de la phase aqueuse et de l'extractant. Bien que des progrès aient été réalisés dans la caractérisation de ces systèmes, des lacunes subsistent. Cette recherche propose une approche étudiant tous les participants (solvants, contre-ions, extractants) lors de l'extraction liquide-liquide. L'utilisation de techniques de résonance magnétique nucléaire (RMN) permet l'observation des extractants solvants, principalement via les noyaux d'hydrogène, de carbone et de fluor, offrant une surveillance simultanée de toutes les molécules, y compris l'eau, l'extractant, le cation, et l'anion des ILs. La RMN, outil puissant couramment utilisé, est employée pour sonder les dynamiques et structures locales des matériaux [85–88]. La thèse explore des outils spécifiques pour les systèmes d'extraction, incluant la spectroscopie localisée (LOCSY), la RMN quantitative, des expériences basées sur l'effet Overhauser nucléaire (NOE) et de la diffusion RMN (DOSY). Enfin, la thèse se concentre sur l'extraction métallique utilisant des liquides ioniques thermomorphes, cherchant une compréhension approfondie des processus d'extraction par solvant.

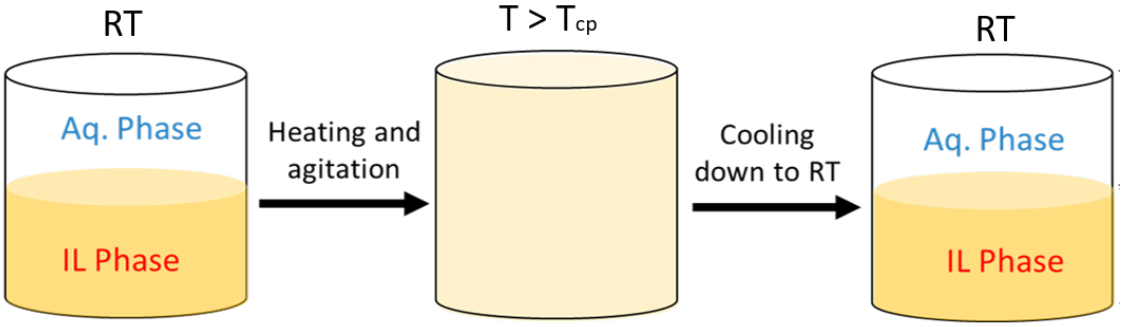

Figure D.1: Schéma simplifié homogène d'extraction liquide-liquide pour système IL/phase aqueuse avec un UCST(Upper Critical Solution Temperature).

D.2 Chapitre 2: Liquides ioniques : synthèse et méthodes RMN pour les Liquides Ioniques

En conclusion, ce chapitre présente les méthodes de synthèse des liquides ioniques et l'utilisation des méthodes de Résonance Magnétique Nucléaire (RMN) dans leur analyse. La synthèse de plusieurs liquides ioniques, [Chol][TFSI], [Chol][D2EHP], et [Chol][TFSI], a été détaillée. Leurs structures chimiques sont illustrées sur le Figure D.2 et D.3 Ces synthèses spécifiques jettent les bases d'expériences plus complexes et de la compréhension des liquides ioniques. Le protocole d'expériences d'extraction liquide-liquide avec des liquides ioniques thermomorphes a été présenté, mettant en évidence la préparation de phases liquides ioniques et aqueuses. Le chapitre a exploré les principes et les applica-

tions de la Résonance Magnétique Nucléaire dans le contexte des liquides ioniques. Un aperçu des principes de la RMN, de la relaxation, de la RMN quantitative et des expériences pour sonder la structure et la dynamique a été fourni, soulignant la pertinence des méthodes de RMN pour l'analyse des liquides ioniques. Notamment, la présentation d'expériences spécifiques telles que l'expérience de récupération d'inversion, NOESY, HOESY et DOSY souligne le rôle important de la RMN dans l'étude des liquides ioniques. Dans l'ensemble, le chapitre organise certaines bases pour d'autres études et expériences dans cette thèse, montrant la préparation de systèmes liquide/liquide et élucidant les utilisations et avantages potentiels de la RMN dans le contexte de l'étude des liquides ioniques, et en particulier de l'extraction liquide-liquide thermomorphique ionique liquides.

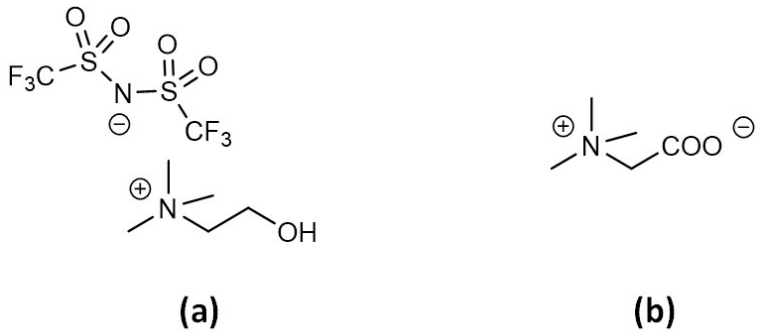

Figure D.2: Structure chimique de (a) [Chol][TFSI] et (b) betaine.

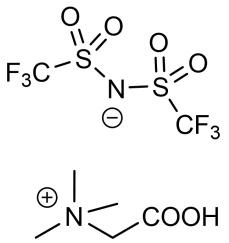

Figure D.3: Structure chimique de [Hbet][TFSI].

D.3 Chapitre 3: LOCalized SpectroscopY (LOCSY) comme outil pour l'étude de l'extraction liquide-liquide

La technique LOCSY a été appliquée pour étudier les systèmes d'extraction liquide-liquide biphasiques [129]. Une séparation de phase claire et des régions d'interface ont été observées dans les spectres RMN de différents noyaux. Des gradients de concentration et des différences dans les déplacements chimiques ont été identifiés, fournissant des informations sur la composition et le comportement de différents systèmes. Un exemple d'application le la sequence LOCSY est illustré à la Figure D.4.

Dans les enquêtes ultérieures, il est important de donner la priorité à la préparation et à la manipulation appropriées des échantillons afin de minimiser les artefacts et d'améliorer la reproductibilité des données.

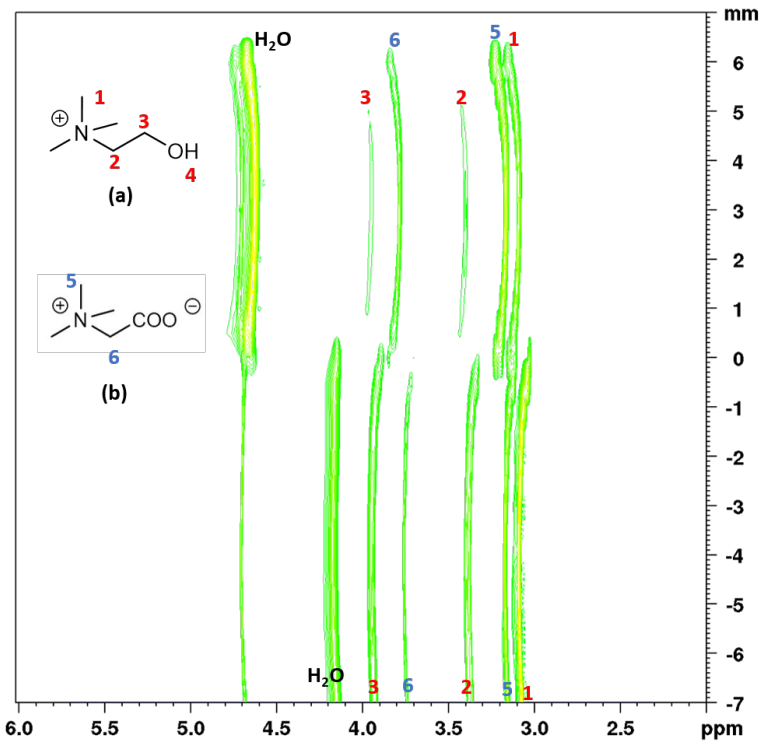

Figure D.4: Spectre 2D ^{1}H LOCSY du système biphasique composé de [Chol][TFSI], de bétaïne et de H_2O. Le pic autour de 4,7 ppm correspond à D_2O dans le tube capillaire.

Le processus d'extraction liquide-liquide homogène nécessite généralement un chauffage et une homogénéisation. Cependant, la mise en œuvre d'une configuration d'agitation in situ utilisant des bulles de gaz à l'intérieur du tube RMN peut permettre une homogénéisation rapide et efficace du système. La méthode a été validée par des expériences de RMN sélectives en tranches, démontrant qu'une homogénéisation propre peut être obtenue dans un court laps de temps. Cette approche offre des applications potentielles pour l'étude d'échantillons macroscopiquement instables ou l'introduction de gaz operando dans des échantillons liquides. Le processus d'homogénéisation facilite et accélère l'homogénéisation et l'insertion de gaz dans le spectromètre. Cependant, l'amélioration du flux de gaz dans le système améliorerait le procédé. Pour améliorer les interprétations des résultats spatialement résolus en cas de besoin, des études sur les effets des bulles de gaz dans la position du tube et du liquide pourraient être envisagées pour la configuration actuelle.

La séparation des phases pendant le processus de refroidissement a été étudiée pour le système [Chol][TFSI]/phase aqueuse. Les déplacements chimiques et les intensités maximales ont montré des variations lorsque le système est passé de 80 ° C à la température ambiante. Le processus de sédimentation était plus prononcé dans la phase liquide ionique, avec des changements d'intensité significatifs observés.

La bétaïne a montré une affinité plus élevée dans les deux phases, tandis que la teneur en eau a diminué dans la phase liquide ionique. Après 100 minutes, aucun changement significatif n'a été observé dans les intensités maximales. Les formes de raies déformées dans les spectres ont été attribuées à des effets de calage et de déphasage non optimaux.

Enfin, LOCSY a été menée pour étudier le système lors du chauffage dans un système

d'extraction par solvant thermomorphique. Les profils du cholinium, de la bétaïne et de l'eau ont été obtenus grâce à l'expérience. Les gradients de concentration obtenus avec la méthode pourraient être utilisés pour déterminer la diffusion mutuelle du système étudié. La spectroscopie localisée résolue en temps peut être appliquée pour étudier le taux de transfert de soluté d'une phase à l'autre. Cela permet de surveiller la cinétique d'extraction pour identifier les étapes limitant la vitesse d'optimisation des conditions d'extraction.

Le raffinement des techniques de traitement des données pour supprimer les artefacts ou les méthodes de déconvolution avancées pour améliorer la résolution spectrale et la sensibilité pourraient être considérés comme des perspectives pour améliorer encore la technique LOCSY. En outre, les données obtenues à partir d'expériences de spectroscopie localisée peuvent être utilisées pour valider et améliorer les modèles informatiques et les simulations de systèmes d'extraction par solvant. Cela aide à acquérir une compréhension globale des processus.

Les exemples de ce chapitre donnent un aperçu des applications potentielles de la séquence LOCSY, mettant en valeur sa capacité à étudier les systèmes d'extraction. Ces découvertes peuvent contribuer à une meilleure compréhension des systèmes thermomorphiques et de leurs applications dans les procédés d'extraction par solvant.

D.4 Chapitre 4: Extraction liquide-liquide du lithium à l'aide de liquides ioniques thermomorphiques

Dans ce chapitre, nous avons exploré la quantification de l'efficacité d'extraction et les effets de divers paramètres dans l'extraction du lithium à l'aide de liquides ioniques thermomorphiques. L'étude a porté sur la solvatation de Li^+ dans du [Chol][TFSI] pur et sur l'étude de systèmes ternaires comprenant du [Chol][TFSI], de la bétaïne et de l'eau. La structure et la dynamique de la phase LI utilisée dans HLLE ont également été analysées. La spectroscopie RMN a été le principal outil utilisé dans ces investigations. De plus, la nanostructure des systèmes a été examinée à l'aide de la technique de diffusion des rayons X aux petits angles (SAXS).

La première section de ce chapitre s'est concentrée sur l'évaluation de l'effet de différents paramètres sur l'efficacité d'extraction. Nous avons examiné l'influence de la concentration en bétaïne, du rapport LI/phase aqueuse et de la concentration initiale en métal sur le processus d'extraction pour le système [Chol][TFSI] saturé en eau en présence de bétaïne comme extractant. Les résultats ont montré que la concentration de bétaïne, le rapport de phase ainqi que la concentration initiale de lithium influençaient l'efficacité de l'extraction. Compte tenu des paramètres utilisés dans les séries individuelles, une bétaïne de concentration de 24 %, un rapport de phase de 3:1 et une concentration initiale de lithium de 0,6 mg/g ont été obtenus comme les meilleures conditions pour une extraction positive du lithium. D'autres investigations ont exploré [Chol][D2EHP] comme extractant potentiel, mais il a montré une efficacité d'extraction du lithium inférieure à celle obtenu avec la bétaïne. Cet extractant présente une solubilité élevée dans l'eau, ce qui contribue à sa perte dans la phase aqueuse et à des rendements inférieurs. Simultanément, un autre objectif de cette section est de comparer la méthode RMN ERETIC pour la quantification du lithium avec les mesures ICP-EOS. La comparaison entre les deux techniques montre que la méthode ERETIC est adaptée pour accéder aux concentrations du lithium.

Dans la deuxième section, nous explorons l'étude RMN de la solvatation de Li^+ dans le

[Chol][TFSI] sec. Des mesures de temps de relaxation longitudinale (T_1) et des expériences de diffusion ont été réalisées pour mieux comprendre le comportement de solvatation des ions Li^+ dans ce LI. Les noyaux de toutes les espèces impliquées sont observés. En analysant les temps de relaxation longitudinale, on observe une réduction progressive de la valeur de T_1 et de la mobilité de ces espèces à mesure que la concentration en lithium et que la viscosité augmentent. Cependant, à un certain point, la dynamique change plus lentement que la fréquence de Larmor, indiquant une transition vers un régime où la mobilité atteint une valeur limite malgré de nouvelles augmentations de la concentration en lithium et de la viscosité. L'influence de la liaison hydrogène dans le LI est également observée à travers l'augmentation des temps de relaxation par rapport aux autres protons. Les résultats de ^{7}Li-T_1 peuvent indiquer un changement significatif dans la dynamique de rotation locale du lithium en raison de la formation de différentes structures à des concentrations de lithium faibles et élevées. Au-delà d'une certaine concentration, les anions TFSI sont partagés entre plusieurs lithium et créent un réseau labile. Les ions lithium peuvent alors sauter d'un site à l'autre. Ces sauts augmentent la mobilité du lithium qui conduit à une augmentation du T_1 [183], illustrée à la Figure D.5.

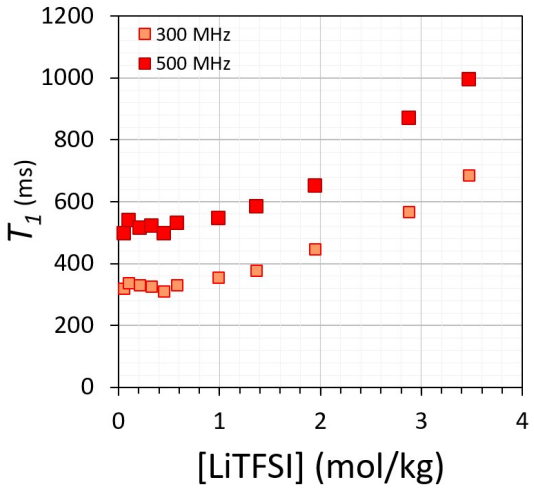

Figure D.5: ^{7}Li T_1 temps de relaxation longitudinale à 300 MHz et 500 MHz en fonction de la molalité du LiTFSI dans le liquide ionique sec [Chol][TFSI].

De plus, les mesures DOSY indiquent un effet substantiel de la concentration de LiTFSI dans la diffusion de toutes les espèces impliquées, suite à une décroissance similaire du coefficient d'auto-diffusion à mesure que la concentration de lithium augmente.

Nous avons aussi exploré l'étude RMN des systèmes d'extraction, en nous concentrant principalement sur le système ternaire comprenant de la [Chol][TFSI], de la bétaïne et de l'eau (Figure D.6). Un diagramme de phase a été construit pour comprendre le comportement du système, et des expériences NOESY et HOESY ont été menées pour sonder les interactions intermoléculaires.

L'utilisation de la RMN permet de déduire la formation de liaisons H avec le cation choline et l'eau et d'observer l'échange intermoléculaire entre le proton hydroxyle et l'eau, confirmé par les expériences HOESY et DOSY [82]. De plus, les expériences HOESY impliquent que les ions Li^+ sont solvatés par l'eau lors de l'extraction et la proximité du cation et de l'anion du LI. On observe également des interactions intramoléculaires entre la bétaïne et la choline. Les expériences DOSY confirment l'effet substantiel de l'eau sur

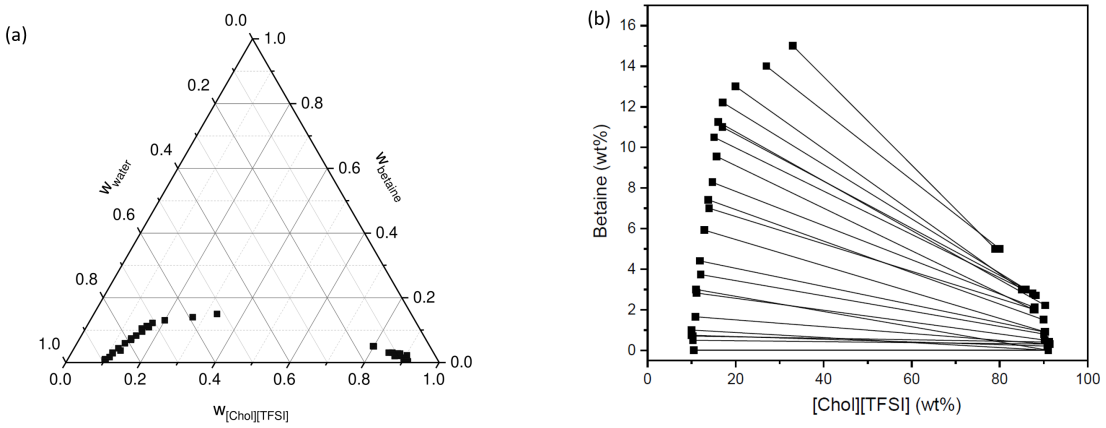

Figure D.6: (a) Diagramme de phase ternaire et (b) bidimensionnel avec tie-lines pour [Chol][TFSI]/bétaïne(ZW)/eau à 25 °C.

la diffusion du système. Aussi, la faible influence de la bétaïne et du lithium est observée sur la diffusion du système.

Sur la base de notre analyse des résultats, nous pouvons déduire que la bétaïne n'est pas un extractant approprié pour les ions lithium. La RMN du ^{7}Li dans les deux LI phases, avec ou sans présence de bétaïne, permet de constater que l'environnement chimique des ions lithium ne change pas significativement par rapport au lithium dans l'eau. De plus, l'environnement chimique dans le LI et la bétaïne ne présente pas de changements significatifs en présence de lithium. Les expériences NOE nous permettent aussi d'observer que les ions lithium sont extraits entourés de molécules d'eau. L'extraction observée pourrait être principalement due aux distributions des composants observées dans le diagramme en phase. Plus le transfert de masse d'eau est important, plus l'efficacité d'extraction observée pour notre système [Chol][TFSI]/bétaïne est élevée. Ce type de mécanisme d'extraction pourrait être une des raisons expliquant la difficulté d'interprétation des résultats basés sur des études hydrométallurgiques traditionnelles.

Nos résultats révèlent que le système d'extraction du Li n'est pas particulièrement efficace. La distribution du lithium dans la phase LI est sous-optimale par rapport à sa distribution dans l'eau. L'amélioration de cette distribution est possible en introduisant de la bétaïne, qui augmente la miscibilité entre les phases. En conséquence, le LI commence à refléter les propriétés de l'eau. Cependant, il existe une limitation essentielle : l'éventuelle miscibilité totale des deux phases. Au niveau microscopique, ce comportement provient de l'affinité prononcée du lithium pour l'eau, le rendant prédominant dans la phase LI au sein de sa sphère de solvatation. Les méthodes RMN valident cette solvatation en la différenciant de celle observée pour le lithium sans eau, telle qu'explorée dans les systèmes. Pour l'amélioration du système, la voie à suivre consiste à proposer une phase d'extraction LI qui présente une plus forte affinité pour le lithium que l'eau mais conserve une miscibilité limitée avec lui.

Des études complémentaires avec la RMN de l'azote et du chlore seraient intéressantes pour mieux comprendre les systèmes [Chol][TFSI]/bétaïne/eau/LiCl. La RMN ^{15}N peut révéler l'environnement chimique des molécules de [TFSI] et de bétaïne, indiquant les interactions au sein de la solution. La RMN du chlore peut fournir des informations sur la

distribution des ions chlorure dans le système et capturer les changements qui pourraient suggérer des interactions avec d'autres molécules du système. De plus, les techniques de RMN 2D pourraient fournir des informations structurelles et la RMN quantitative pourraiet déterminer les concentrations des espèces concernées.

Sur la base des résultats présentés dans ce chapitre, la RMN peut être utilisée pour sélectionner des extractants et des diluants dans les systèmes d'extraction liquide-liquide et étudier des systèmes innovants d'extraction liquide-liquide du lithium [212–214] Dans d'autres études, il faudrait faire des experiences des expériences de RMN avec, par exemple, l'extractant [Chol][D2EHP], en particulier, des expériences NOE et de diffusion pour mieux évaluer ce LI en tant qu'extractant possible et promouvoir une amélioration supplémentaire du système pour surmonter les problèmes observés avec cet extractant dans la présente étude.

Bien que les limitations de l'extraction liquide-liquide du lithium soient observées dans le système d'extraction étudié dans ce travail, on peut considérer que la RMN est une technique appropriée pour étudier les systèmes d'extraction au lithium. La sensibilité de ce noyau permet une mise en œuvre relativement facile d'une série d'expériences RMN différentes qui, combinées à différents noyaux, peuvent donner des informations importantes sur le processus d'extraction. Les techniques utilisées dans ce travail peuvent être appliquées à des systèmes d'extraction de lithium déjà connus et avoir une meilleure compréhension de ces systèmes, qui pourraient être utilisés pour la conception dnouveau système d'extraction.

La dernière partie de ce cahapitre impliquait l'étude de la nanostructure du système à l'aide du SAXS. Les structures de [Chol][D2EHP] et [Chol][TFSI] ont été analysées, et il est possible de déterminer le comportement et les longueurs de corrélation des agrégats ou des fluctuations de concentration dans le système. En outre, l'effet de la bétaïne sur la nanostructure de [Chol][TFSI] a été examiné. Les expériences SAXS nous ont permis de mieux comprendre l'organisation structurelle des systèmes étudiés. Cette technique permet d'observer certains phénomènes, comme l'agrégation ou les fluctuations de concentration, qui pourraient jouer un rôle essentiel dans les procédés d'extraction. Une perspective future serait de corréler les observations du SAXS avec les expériences de RMN, par exemple, avec NOE et les expériences de diffusion.

En conclusion, ce chapitre explore l'extraction du lithium à l'aide de liquides ioniques thermomorphiques. L'étude met en lumière les effets des paramètres sur l'efficacité d'extraction, la caractérisation du système ternaire et le comportement de solvatation. Les investigations RMN nous ont permis de mieux comprendre les interactions moléculaires et la structure du système, tandis que les techniques SAXS ont fourni des informations sur la nanostructure.

D.5 Chapitre 5: Extraction liquide-liquide du platine à l'aide de liquides ioniques thermomorphiques

Dans ce dernier chapitre, nous avons utilisé les outils et méthodes développés sur le lithium pour étudier l'extraction d'un autre métal critique, le platine. Deux systèmes d'extraction selon l'état d'oxydation du métal ont été conçus et étudiés.

Nous nous sommes d'abord concentrés sur l'extraction homogène liquide-liquide (HLLE) du Pt(IV) à l'aide du liquide ionique thermomorphique protoné bétaïne

bis(trifluorométhylsulfonyl)imide [Hbet][TFSI]. Nous avons étudié l'effet de la concentration de Pt dans la phase aqueuse, l'influence de la concentration de bétaïne dans la phase LI ainsi que la sélectivité entre Pt et Pd puisque ces deux éléments peuvent être mélangés dans le flux de déchets. Nos résultats ont montré que [Hbet][TFSI] était un Milieu extractant plus efficace pour Pt(IV) que [Chol][TFSI]/betaine. L'efficacité d'extraction était plus élevée à de faibles concentrations de Pt mais diminuait à mesure que la concentration de Pt augmentait, atteignant finalement une limite en raison de la capacité de charge de la phase IL. Nous avons montré que le *stripping* du LI chargé peut être effectué avec des solutions d'acide chlorhydrique. La spectroscopie RMN a été utilisée pour mieux comprendre le processus d'extraction. Les déplacements chimiques de la RMN du ^{195}Pt ont été utilisés pour étudier l'environnement chimique du Pt dans différentes conditions. Il a été possible de déduire que le platine est extrait sous forme de $[PtCl_6]^{2-}$ dans la phase LI comme le montrent les isotopomères du pic Pt de la figure D.7, ils sont caractéristiques du $[PtCl_6]^{2-}$ [221]. Ce qui nous amène à penser que le platine pourrait être extrait dans un mécanisme d'échange d'anions.

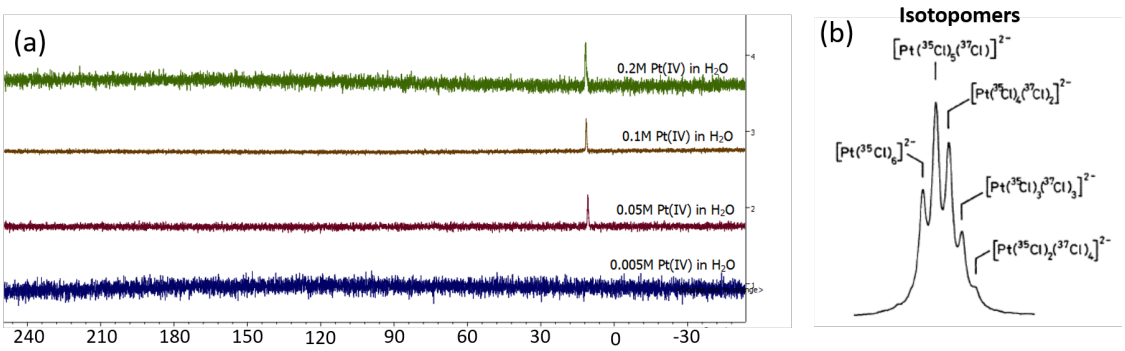

Figure D.7: Spectres de ^{195}Pt de solutions aqueuses avec des concentrations croissantes de Pt.

La présence de bétaïne dans la phase aqueuse a entraîné un déplacement du déplacement chimique du Pt vers des résonances élevées, suggérant une interaction possible entre $[PtCl_6]^{2-}$ et la bétaïne. La même chose est observée pour ^{195}Pt dans la phase LI. Les expériences de diffusion nous conduisent à penser qu'il y a la formation d'un complexe entre $[PtCl_6]^{2-}$ et la bétaïne dans la phase LI. Une étude de sélectivité entre Pd et Pt a montré une sélectivité de ce système vers le Pd. Contrairement au système lithium, le système platine présentait un potentiel pour l'extraction de ce métal et d'autres PGE. D'autres études sur le paramètre d'optimisation des systèmes pourraient être menées pour améliorer l'efficacité et la sélectivité du processus d'extraction. Les études futures potentielles portent sur l'influence du rapport de phases, car la proportion des deux phases non miscibles peut affecter de manière critique l'efficacité et l'équilibre de l'extraction. De même, le rôle du pH et des variations de pH peuvent modifier considérablement la spéciation des métaux et son extraction. L'étude de la diffusion du Pt dans le LI avec une sonde à haut gradient est l'une des perspectives de futurs travaux pour mieux comprendre la dynamique du système ainsi que le mécanisme d'extraction. Dans des travaux ultérieurs, des études EXAFS aideraient à élucider la coordination du Pt dans le système. Il serait alors possible de confirmer le transfert du platine avec la couche de coordination de chlorure et d'évaluer la liaison par la bétaïne déduite par les mesures de RMN. Avec ces résultats, la compréhension du mécanisme de transfert seulement décrit dans cette

étude préliminaire serait améliorée. La précipitation et la cristallisation des complexes métalliques suivies par la RMN du solide, la DRX et des méthodes de calcul, telles que la théorie de la fonctionnelle de la densité (DFT), pourraient améliorer la connaissance des complexes formés lors de l'extraction.

Nous avons également étudié l'extraction du Pt(II) avec [Chol][TFSI] et la bétaïne. La présence de bétaïne a significativement amélioré l'efficacité d'extraction, atteignant 80 % avec une concentration de bétaïne de 15 % w/w. Cependant, le système présentait la formation d'un précipité noir en l'absence de bétaïne, indiquant la possibilité d'espèces inconnues dans le système. La formation de complexes Pt(II)-bétaïne semble avoir un rôle fondamental dans le mécanisme d'extraction. La spéciation de Pt(II) n'a pas pu être observée en raison de faibles concentrations alors, des études EXAFS permettraient d'élucider la coordination de ce métal dans le système et une meilleure compréhension du mécanisme d'extraction. Une étude future de la RMN de diffusion de protons dans ce système donnerait un aperçu de la dynamique et de la formation du complexe metallique. Le complexe métallique formé dans ce système pourrait également être étudié après cristallisation.

La RMN a également été utilisée pour étudier la distribution cation-anion du LI et de l'extractant entre les phases. Celle-ci a montré que l'ajout de métal ne modifie pas de manière significative le comportement de phase LI du système. Une optimisation supplémentaire des paramètres d'extraction peut être étudiée dans le système avec des études de sélectivité. En conclusion, notre étude donne un aperçu de l'extraction liquide-liquide du Pt à l'aide de liquides ioniques thermomorphiques. La spectroscopie RMN s'est avérée être un outil précieux pour comprendre l'environnement chimique et la dynamique du système. Des recherches supplémentaires sont nécessaires pour optimiser le processus d'extraction et caractériser les espèces impliquées afin d'améliorer l'efficacité de l'extraction du Pt et la conception des systèmes d'extraction.

D.6 Conclusion

Dans cette recherche, nous avons mené une exploration approfondie sur l'utilisation de la Résonance Magnétique Nucléaire (RMN) et d'autres techniques pour analyser les systèmes d'extraction, en mettant particulièrement l'accent sur les applications des systèmes thermomorphiques. Notre étude s'est principalement focalisée sur un seul métal par système d'extraction. Malgré les limites de cette approche, elle offre une compréhension précieuse du processus d'extraction pour des métaux spécifiques. Cependant, certains systèmes complexes pourraient ne pas être adaptés à la RMN à cause de facteurs tels que le paramagnétisme et les effets de coordination.

Dans le chapitre 3, nous avons mis en évidence le potentiel de la technique LOCSY pour étudier les systèmes d'extraction liquide-liquide. Nous avons fait plusieurs observations sur ces systèmes biphasiques, identifiant clairement les séparations de phase dans les spectres RMN. Une méthodologie utilisant l'agitation in-situ a été introduite, offrant une homogénéisation efficace du système.

Chapitre 4 concerne le processus d'extraction liquide-liquide du lithium. Plusieurs facteurs ont été examinés, tels que la concentration de bétaïne et le rapport phase IL/aqueuse. Les mesures de RMN ERETIC ont confirmé la pertinence de la RMN pour déterminer les concentrations de lithium. Nous avons également observé des nuances importantes

concernant la solvatation du Li^+. Des investigations supplémentaires via le SAXS ont apporté des informations structurelles précieuses.

Le Chapitre 5 a porté sur l'extraction homogène liquide-liquide du Pt(IV) en utilisant des liquides ioniques thermomorphiques. [Hbet][TFSI] s'est révélé particulièrement efficace pour l'extraction du Pt(IV). La RMN a permis de décoder le mécanisme d'extraction, montrant un échange d'anions possible. De plus, des expériences de diffusion ont révélé la formation potentielle du complexes entre $[PtCl_6]^{2-}$ et la bétaïne. De plus, le système a montré une sélectivité en vers le Pd, suggérant son potentiel pour extraire d'autres éléments du groupe du platine.

En conclusion, les résultats actuels mettent en évidence l'immense potentiel de la spectroscopie RMN dans l'étude des systèmes d'extraction de métaux. D'autres études pourraient approfondir l'efficacité et la caractérisation de systèmes d'extraction déjà connus, tout en évaluant de nouveaux systèmes. Les nanostructures observées par SAXS dans les systèmes thermomorphiques pourraient être davantage étudiées, permettant d'examiner la formation de différentes structures. Pour le Pt(IV), l'exploration d'autres paramètres d'optimisation pourrait être menée. De plus, l'intégration de simulations computationnelles pourrait offrir des perspectives prédictives pour des expériences NOE et de diffusion.

Appendix E

Publications

Publications from this work

Antonio De Souza Braga Neto, Baptiste Rigaud, Guillaume Mériguet, Anne-Laure Rollet, Juliette Sirieix-Plénet, Efficient method for in situ agitation of liquids directly inside NMR spectrometer, MethodsX, Volume 11, 2023, 102254, ISSN 2215-0161, https://doi.org/10.1016/j.mex.2023.102254.

Bibliography

[1] European Commission. Directorate General for Internal Market, Industry, Entrepreneurship and SMEs. *Study on the EU's List of Critical Raw Materials (2020): Final Report.* Publications Office, 2020.

[2] Leena Grandell, Antti Lehtilä, Mari Kivinen, Tiina Koljonen, Susanna Kihlman, and Laura S. Lauri. Role of critical metals in the future markets of clean energy technologies. *Renewable Energy*, 95:53–62, 2016. ISSN 0960-1481. doi: 10.1016/j.renene.2016.03.102.

[3] Gavin Harper, Roberto Sommerville, Emma Kendrick, Laura Driscoll, Peter Slater, Rustam Stolkin, Allan Walton, Paul Christensen, Oliver Heidrich, Simon Lambert, Andrew Abbott, Karl Ryder, Linda Gaines, and Paul Anderson. Recycling lithium-ion batteries from electric vehicles. *Nature*, 575(7781):75–86, 2019. doi: 10.1038/s41586-019-1682-5.

[4] Nihan Karali and Nihar Shah. Bolstering supplies of critical raw materials for low-carbon technologies through circular economy strategies. *Energy Res. Social Sci.*, 88:102534, 2022. doi: 10.1016/j.erss.2022.102534.

[5] Glen T. Nwaila, Yousef Ghorbani, Steven E. Zhang, Hartwig E. Frimmel, Leon C. K. Tolmay, Derek H. Rose, Phumzile C. Nwaila, and Julie E. Bourdeau. Valorisation of mine waste - Part I: Characteristics of, and sampling methodology for, consolidated mineralised tailings by using Witwatersrand gold mines (South Africa) as an example. *Journal of Environmental Management*, 295:113013, October 2021. ISSN 0301-4797. doi: 10.1016/j.jenvman.2021.113013.

[6] European Commission. Joint Research Centre. *Towards Recycling Indicators Based on EU Flows and Raw Materials System Analysis Data: Supporting the EU 28 Raw Materials and Circular Economy Policies through RMIS.* Publications Office, 2018.

[7] United States Geological Survey. Mineral Commodity Summaries 2023: Us geological survey. 2023. URL https://pubs.usgs.gov/periodicals/mcs2023/mcs2023.pdf.

[8] Dwight C. Bradley, Lisa L. Stillings, Brian W. Jaskula, LeeAnn Munk, and Andrew D. McCauley. *Lithium.* U.S. Geological Survey, 2017. doi: 10.3133/pp1802K. Code Number: 1802-K Code: Lithium Publication Title: Lithium Reporter: Lithium Series: Professional Paper IP-051901.

[9] Pratima Meshram, B.D. Pandey, and T.R. Mankhand. Extraction of lithium from primary and secondary sources by pre-treatment, leaching and separation: A comprehensive review. *Hydrometallurgy*, 150:192–208, 2014. doi: 10.1016/j.hydromet.2014.10.012.

[10] Ernest Worrel and Markus Reuter. *Handbook of Recycling.* Elsevier, 2014. ISBN 978-0-12-396459-5. doi: 10.1016/C2011-0-07046-1.

[11] Michael L. Zientek. Critical Mineral Resources of the United States—Economic and Environmental Geology and Prospects for Future Supply Platinum-Group Elements. Professional Paper, U.S. Geological Survey, 2017.

[12] Jan Alexander. Platinum. In *Handbook on the Toxicology of Metals*, pages 1175–1208. Elsevier, 2015. doi: 10.1016/B978-0-444-59453-2.00052-4.

[13] Ana Paula Paiva, Francisco Vega Piedras, Pedro G. Rodrigues, and Carlos A. Nogueira. Hydrometallurgical recovery of platinum-group metals from spent auto-catalysts – Focus on leaching and solvent extraction. *Sep. Purif. Technol.*, 286:120474, 2022. doi: 10.1016/j.seppur.2022.120474.

[14] Jingjing Li, Lanlan Li, Ranran Yang, and Jianling Jiao. Assessment of the lifecycle carbon emission and energy consumption of lithium-ion power batteries recycling: A systematic review and meta-analysis. *J. Energy Storage*, 65:107306, 2023. doi: 10.1016/j.est.2023.107306.

[15] Jan Rydberg, editor. *Solvent extraction principles and practice*. Dekker, 2. ed., rev. and expanded edition, 2004. ISBN 978-0-8247-5063-3.

[16] Vladimir S Kislik. *Solvent extraction: classical and novel approaches*. Elsevier, 2011. doi: 10.1016/C2010-0-65805-6.

[17] Wen Xuan, Antônio De Souza Braga, and Alexandre Chagnes. Development of a Novel Solvent Extraction Process to Recover Cobalt, Nickel, Manganese, and Lithium from Cathodic Materials of Spent Lithium-Ion Batteries. *ACS Sustainable Chem. Eng.*, 10(1):582–593, 2022. doi: 10.1021/acssuschemeng.1c07109.

[18] C. Hanson. *Recent Advances in Liquid-Liquid Extraction*. Elsevier, October 2013. ISBN 978-1-4831-5166-3.

[19] Mark L. Dietz. Ionic Liquids as Extraction Solvents: Where do We Stand? *Sep. Sci. Technol.*, 41(10):2047–2063, 2006. doi: 10.1080/01496390600743144.

[20] Magdalena Regel-Rosocka and Katarzyna Materna. Ionic Liquids for Separation of Metal Ions and Organic Compounds from Aqueous Solutions. In *Ionic Liquids in Separation Technology*, pages 153–188. Elsevier, 2014. doi: 10.1016/B978-0-444-63257-9.00004-3.

[21] Diana Cholico-Gonzalez, Alexandre Chagnes, Gérard Cote, and Mario Avila-Rodriguez. Separation of Co(II) and Ni(II) from aqueous solutions by bis(2,4,4-trimethylpentyl)phosphinic acid (Cyanex 272) using trihexyl(tetradecyl)phosphonium chloride (Cyphos IL 101) as solvent. *Journal of Molecular Liquids*, 209:203–208, September 2015. ISSN 01677322. doi: 10.1016/j.molliq.2015.05.048.

[22] A. Matthew Wilson, Phillip J. Bailey, Peter A. Tasker, Jennifer R. Turkington, Richard A. Grant, and Jason B. Love. Solvent extraction: The coordination chemistry behind extractive metallurgy. *Chem. Soc. Rev.*, 43(1):123–134, 2014. doi: 10.1039/C3CS60275C.

[23] Douglas R. MacFarlane, Mega Kar, and Jennifer Pringle. *Fundamentals of Ionic Liquids: From Chemistry to Applications*. Wiley-VCH Verlag GmbH & Co. KGaA, 2017. doi: 10.1002/9783527340033.

[24] Natalia V. Plechkova and Kenneth R. Seddon. Applications of ionic liquids in the chemical industry. *Chem. Soc. Rev.*, 37(1):123–150, 2007. doi: 10.1039/B006677J. Publisher: The Royal Society of Chemistry.

[25] Nur Nadiatul Hidayah and Sumaiya Zainal Abidin. The evolution of mineral processing in extraction of rare earth elements using liquid-liquid extraction: A review. *Miner. Eng.*, 121:146–157, 2018. doi: 10.1016/j.mineng.2018.03.018.

[26] Robin D. Rogers and Kenneth R. Seddon. Ionic liquids–solvents of the future? *Science*, 302 (5646):792–793, 2003. doi: 10.1126/science.1090313.

[27] Ksenia S Egorova, Alexandra V Posvyatenko, Sergey S Larin, and Valentine P Ananikov. Ionic liquids: Prospects for nucleic acid handling and delivery. *Nucleic Acids Res.*, 49(3):1201–1234, 2021. doi: 10.1093/nar/gkaa1280.

[28] Andrew P. Abbott and Katy J. McKenzie. Application of ionic liquids to the electrodeposition of metals. *Phys. Chem. Chem. Phys.*, 8(37):4265–4279, 2006. doi: 10.1039/B607329H. Publisher: The Royal Society of Chemistry.

[29] Jonathan G. Huddleston, Heather D. Willauer, Richard P. Swatloski, Ann E. Visser, and Robin D. Rogers. Room temperature ionic liquids as novel media for 'clean' liquid–liquid extraction. *Chem. Commun.*, pages 1765–1766, 1998. doi: 10.1039/A803999B.

[30] Juan Wang, Boxuan Li, Jing Tang, Li Qiu, Xin Qiao, Na Xu, and Hu Yang. Ionic Liquid Pilocarpine Analog as an Antiglaucoma Drug Candidate. *ACS Pharmacol. Transl. Sci.*, 2022. doi: 10.1021/acsptsci.2c00024.

[31] Barbara Kirchner, editor. *Ionic Liquids*, volume 290 of *Topics in Current Chemistry*. Springer, Berlin, Heidelberg, 2010. doi: 10.1007/978-3-642-01780-3.

[32] David Dupont. *Rare Earth and Critical Metal Recycling Using Ionic Liquid Technology*. PhD thesis, KU Leuven - Faculty of Science, 2016.

[33] Magdalena Regel-Rosocka and Katarzyna Materna. Ionic Liquids for Separation of Metal Ions and Organic Compounds from Aqueous Solutions. In *Ionic Liquids in Separation Technology*, pages 153–188. Elsevier, 2014. doi: 10.1016/B978-0-444-63257-9.00004-3.

[34] Oscar Cabeza. Properties and Green Aspects of Ionic Liquids. In *Ionic Liquids in Separation Technology*, pages 1–93. Elsevier, 2014. doi: 10.1016/B978-0-444-63257-9.00001-8.

[35] Dongbin Zhao, Yongcheng Liao, and Ziding Zhang. Toxicity of Ionic Liquids. *CLEAN – Soil Air Water*, 35(1):42–48, 2007. doi: 10.1002/clen.200600015.

[36] Bieke Onghena. *Ionic liquid solvent extraction for the recovery of rare earths and cobalt*. PhD thesis, KU Leuven - Faculty of Science, 2018.

[37] Marisa C. Buzzeo, Russell G. Evans, and Richard G. Compton. Non-Haloaluminate Room-Temperature Ionic Liquids in Electrochemistry—A Review. *ChemPhysChem*, 5(8):1106–1120, 2004. doi: 10.1002/cphc.200301017.

[38] Tom Vander Hoogerstraete, Bieke Onghena, and Koen Binnemans. Homogeneous liquid-liquid extraction of rare earths with the betaine-betainium bis(trifluoromethylsulfonyl)imide ionic liquid system. *Int. J. Mol. Sci.*, 14(11):21353–21377, 2013. doi: 10.3390/ijms141121353.

[39] Tom Vander Hoogerstraete, Bieke Onghena, and Koen Binnemans. Homogeneous Liquid–Liquid Extraction of Metal Ions with a Functionalized Ionic Liquid. *J. Phys. Chem. Lett.*, 4(10):1659–1663, 2013. doi: 10.1021/jz4005366.

[40] Joshua A. Hammons, Jan Ilavsky, and Fan Zhang. Small-Angle X-Ray Scattering of Ionic Liquids. In Angel A. J. Torriero, editor, *Electrochemistry in Ionic Liquids*, pages 169–213. Springer International Publishing, Cham, 2015. doi: 10.1007/978-3-319-13485-7_6.

[41] Daphne Depuydt, Wim Dehaen, and Koen Binnemans. Docusate Ionic Liquids: Effect of Cation on Water Solubility and Solvent Extraction Behavior. *ChemPlusChem*, 82(3):458–466, 2017. doi: 10.1002/cplu.201600592.

[42] Filipa M. Maia, Oscar Rodríguez, and Eugénia A. Macedo. Relative hydrophobicity of equilibrium phases in biphasic systems (ionic liquid+water). *J. Chem. Thermodyn.*, 48:221–228, 2012. doi: 10.1016/j.jct.2011.12.025.

[43] David Dupont and Koen Binnemans. Recycling of rare earths from NdFeB magnets using a combined leaching/extraction system based on the acidity and thermomorphism of the ionic liquid [Hbet][Tf_2N]. *Green Chem.*, 17(4):2150–2163, 2015. doi: 10.1039/C5GC00155B.

[44] Peter Nockemann, Ben Thijs, Stijn Pittois, Jan Thoen, Christ Glorieux, Kristof Van Hecke, Luc Van Meervelt, Barbara Kirchner, and Koen Binnemans. Task-Specific Ionic Liquid for Solubilizing Metal Oxides. *J. Phys. Chem. B*, 110(42):20978–20992, 2006. doi: 10.1021/jp0642995.

[45] M. Canle L., María Isabel Fernández Pérez, and Juan Arturo Santaballa. Physicochemical Basis of IL Effects on Separation and Transformation Processes. In *Ionic Liquids in Separation Technology*, pages 95–106. Elsevier, 2014. doi: 10.1016/B978-0-444-63257-9.00002-X.

[46] Rafael M. Rios-Vera, Juliette Sirieix-Plénet, Laurent Gaillon, Cécile Rizzi, Mario Ávila-Rodríguez, Gerard Cote, and Alexandre Chagnes. Physicochemical properties of novel cholinium ionic liquids for the recovery of silver from nitrate media. *RSC Advances*, 5 (95):78268–78277, 2015. ISSN 2046-2069. doi: 10.1039/C5RA14101J.

[47] Thi Phuong Thuy Pham, Chul-Woong Cho, and Yeoung-Sang Yun. Environmental fate and toxicity of ionic liquids: A review. *Water Res.*, 44(2):352–372, 2010. doi: 10.1016/j.watres.2009.09.030.

[48] Zheng Li, Bieke Onghena, Xiaohua Li, Zidan Zhang, and Koen Binnemans. Enhancing Metal Separations Using Hydrophilic Ionic Liquids and Analogues as Complexing Agents in the More Polar Phase of Liquid–Liquid Extraction Systems. *Ind. Eng. Chem. Res.*, 58(34): 15628–15636, 2019. doi: 10.1021/acs.iecr.9b03472.

[49] Camiel H.C. Janssen, Norma A. Macías-Ruvalcaba, Martha Aguilar-Martínez, and Mark N. Kobrak. Metal extraction to ionic liquids: The relationship between structure, mechanism and application. *Int. Rev. Phys. Chem.*, 34(4):591–622, 2015. doi: 10.1080/0144235X.2015.1088217.

[50] Pavel A. Yudaev and Evgeniy M. Chistyakov. Ionic Liquids as Components of Systems for Metal Extraction. *ChemEngineering*, 6(1):6, 2022. doi: 10.3390/chemengineering6010006.

[51] Guillaume Zante, Abderrazak Masmoudi, Rémi Barillon, Dominique Trébouet, and Maria Boltoeva. Separation of lithium, cobalt and nickel from spent lithium-ion batteries using TBP and imidazolium-based ionic liquids. *J. Ind. Eng. Chem.*, 82:269–277, 2020. doi: 10.1016/j.jiec.2019.10.023.

[52] Chenglong Shi, Hongxia Li, Bing Liu, Yaru Qin, and Guixiu Song. Solvent extraction of lithium from aqueous solution using an ammonium ionic liquid. *J. Mol. Liq.*, 304:112756, 2020. doi: 10.1016/j.molliq.2020.112756.

[53] Chenglong Shi, Yan Jing, Jiang Xiao, Xingquan Wang, and Yongzhong Jia. Liquid-liquid extraction of lithium using novel phosphonium ionic liquid as an extractant. *Hydrometallurgy*, 169:314–320, 2017. doi: 10.1016/j.hydromet.2017.02.015.

[54] Chenglong Shi, Yan Jing, and Yongzhong Jia. Solvent extraction of lithium ions by tri-n-butyl phosphate using a room temperature ionic liquid. *J. Mol. Liq.*, 215:640–646, 2016. doi: 10.1016/j.molliq.2016.01.025.

[55] Daolin Gao, Xiaoping Yu, Yafei Guo, Shiqiang Wang, Mingming Liu, Tianlong Deng, Yuwei Chen, and Nelson Belzile. Extraction of lithium from salt lake brine with triisobutyl phosphate in ionic liquid and kerosene. *Chem. Res. Chin. Univ.*, 31(4):621–626, 2015. doi: 10.1007/s40242-015-4376-z.

[56] Gregorius Rionugroho Harvianto, Seok-Hyeon Kim, and Chang-Sik Ju. Solvent extraction and stripping of lithium ion from aqueous solution and its application to seawater. *Rare Met.*, 35(12):948–953, 2016. doi: 10.1007/s12598-015-0453-1.

[57] Solvay SA. CYANEX® 936P. https://www.solvay.com/en/product/cyanex-936p, 2021.

[58] Yoko Pranolo, Zhaowu Zhu, and Chu Yong Cheng. Separation of lithium from sodium in chloride solutions using SSX systems with LIX 54 and Cyanex 923. *Hydrometallurgy*, 154: 33–39, 2015. doi: 10.1016/j.hydromet.2015.01.009.

[59] Licheng Zhang, Lijuan Li, Dong Shi, Xiaowu Peng, Fugen Song, Feng Nie, and Wensheng Han. Recovery of lithium from alkaline brine by solvent extraction with β-diketone. *Hydrometallurgy*, 175:35–42, 2018. doi: 10.1016/j.hydromet.2017.10.029.

[60] Bina Gupta and Indu Singh. Extraction and separation of platinum, palladium and rhodium using Cyanex 923 and their recovery from real samples. *Hydrometallurgy*, 134–135:11–18, 2013. doi: 10.1016/j.hydromet.2013.01.001.

[61] Stéphanie Boudesocque, Aminou Mohamadou, Alexandra Conreux, Béatrice Marin, and Laurent Dupont. The recovery and selective extraction of gold and platinum by novel ionic liquids. *Sep. Purif. Technol.*, 210:824–834, 2019. doi: 10.1016/j.seppur.2018.09.002.

[62] Sébastien Génand-Pinaz, Nicolas Papaiconomou, and Jean-Marc Leveque. Removal of platinum from water by precipitation or Liquid–Liquid extraction and separation from gold using ionic liquids. *Green Chem.*, 15(9):2493, 2013. doi: 10.1039/c3gc40557e.

[63] Matthieu Gras, Lucien Duclos, Nicolas Schaeffer, Vijetha Mogilireddy, Lenka Svecova, Eric Chaînet, Isabelle Billard, and Nicolas Papaiconomou. A Comparison of Cobalt and Platinum Extraction in Hydrophobic and Hydrophilic Ionic Liquids: Implication for Proton Exchange Membrane Fuel Cell Recycling. *ACS Sustainable Chem. Eng.*, page 10, 2020.

[64] Frederik H. Kriel, Gregor Holzner, Richard A. Grant, Stephen Woollam, John Ralston, and Craig Priest. Microfluidic solvent extraction, stripping, and phase disengagement for high-value platinum chloride solutions. *Chem. Eng. Sci.*, 138:827–833, 2015. doi: 10.1016/j.ces.2015.08.055.

[65] Roberta Santos Marinho, Julio Carlos Afonso, and José Waldemar Silva Dias da Cunha. Recovery of platinum from spent catalysts by Liquid–Liquid extraction in chloride medium. *J. Hazard. Mater.*, 179(1-3):488–494, 2010. doi: 10.1016/j.jhazmat.2010.03.029.

[66] Masahiko Matsumiya, Yueqi Song, Yusuke Tsuchida, Hisashi Ota, and Katsuhiko Tsunashima. Recovery of platinum by solvent extraction and direct electrodeposition using ionic liquid. *Sep. Purif. Technol.*, 214:162–167, 2019. doi: 10.1016/j.seppur.2018.06.018.

[67] Ana Méndez, Carlos A. Nogueira, and Ana Paula Paiva. Recovery of Platinum from a Spent Automotive Catalyst through Chloride Leaching and Solvent Extraction. *Recycling*, 6(2): 27, 2021. doi: 10.3390/recycling6020027.

[68] Nicolas Papaiconomou, Lenka Svecova, Céline Bonnaud, Loïc Cathelin, Isabelle Billard, and Eric Chainet. Possibilities and limitations in separating Pt(IV) from Pd(II) combining imidazolium and phosphonium ionic liquids. *Dalton Trans.*, 44(46):20131–20138, 2015. doi: 10.1039/C5DT03791C.

[69] B. Raju, J. Rajesh Kumar, Jin-Young Lee, Hyuk-Sung Kwonc, M. Lakshmi Kantam, and B. Ramachandra Reddy. Separation of platinum and rhodium from chloride solutions containing aluminum, magnesium and iron using solvent extraction and precipitation methods. *J. Hazard. Mater.*, 227–228:142–147, 2012. doi: 10.1016/j.jhazmat.2012.05.025.

[70] Irina S. Rudik, Olesya N. Katasonova, Olga B. Mokhodoeva, Tatiana Anatolievna Maryutina, Boris Ya. Spivakov, and I. V. Ilyukhin. Separation of Pt(IV), Pd(II), and Rh(III) from Chloride Solutions by Multistage Extraction Using Nitrogen-Containing Extractants. *Inorg. Mater.*, 56(14):1374–1378, 2020. doi: 10.1134/S0020168520140125.

[71] Koen Binnemans and Peter Tom Jones. Ionic Liquids and Deep-Eutectic Solvents in Extractive Metallurgy: Mismatch Between Academic Research and Industrial Applicability. *J. Sustainable Metall.*, 9(2):423–438, 2023. doi: 10.1007/s40831-023-00681-6.

[72] Bieke Onghena, Jeroen Jacobs, Luc Van Meervelt, and Koen Binnemans. Homogeneous liquid–liquid extraction of neodymium(III) by choline hexafluoroacetylacetonate in the ionic liquid choline bis(trifluoromethylsulfonyl)imide. *Dalton Trans.*, 43(30):11566–11578, 2014. doi: 10.1039/C4DT01340A.

[73] Tom Vander Hoogerstraete, Bieke Onghena, and Koen Binnemans. Homogeneous liquid–liquid extraction of rare earths with the betaine—betainium bis(trifluoromethylsulfonyl)imide ionic liquid system. *Int. J. Mol. Sci.*, 14(11):21353–21377, 2013. ISSN 1422-0067.

[74] Clio Deferm, Bieke Onghena, Tom Vander Hoogerstraete, Dipanjan Banerjee, Jan Luyten, Harald Oosterhof, Jan Fransaer, and Koen Binnemans. Speciation of indium (iii) chloro complexes in the solvent extraction process from chloride aqueous solutions to ionic liquids. *Dalton Trans.*, 46(13):4412–4421, 2017.

[75] Daphne Depuydt, Liwang Liu, Christ Glorieux, Wim Dehaen, and Koen Binnemans. Homogeneous liquid–liquid extraction of metal ions with non-fluorinated bis (2-ethylhexyl) phosphate ionic liquids having a lower critical solution temperature in combination with water. *Chem. Commun.*, 51(75):14183–14186, 2015.

[76] David Dupont and Koen Binnemans. Antimony recovery from the halophosphate fraction in lamp phosphor waste: A zero-waste approach. *Green Chem.*, 18(1):176–185, 2016. doi: 10.1039/C5GC01746G.

[77] Aristidis N. Anthemidis and Kallirroy-Ioanna G. Ioannou. Recent developments in homogeneous and dispersive liquid–liquid extraction for inorganic elements determination. A review. *Talanta*, 80(2):413–421, 2009. doi: 10.1016/j.talanta.2009.09.005.

[78] Achim Schaadt and Hans-Jörg Bart. Coalescence Extraction - A Benign Extraction Tool. *Chem. Eng. Technol.*, 26(4):469–472, 2003. doi: 10.1002/ceat.200390070.

[79] Yuki Kohno, Shohei Saita, Yongjun Men, Jiayin Yuan, and Hiroyuki Ohno. Thermoresponsive polyelectrolytes derived from ionic liquids. *Polym. Chem.*, 6(12):2163–2178, 2015. doi: 10.1039/C4PY01665C.

[80] Katsuo. Murata, Yu. Yokoyama, and Shigero. Ikeda. Homogeneous liquid-liquid extraction method. Extraction of iron(III) thenoyltrifluoroacetonate by propylene carbonate. *Anal. Chem.*, 44(4):805–810, 1972. doi: 10.1021/ac60312a009.

[81] Yangyang Wang, Shuwen Chen, Ronghao Liu, Lixin Zhang, Wenfeng Xue, and Yanzhao Yang. Toward green and efficient recycling of Au(III), Pd(II) and Pt(IV) from acidic medium using UCST-type ionic liquid. *Sep. Purif. Technol.*, 298:121620, 2022. doi: 10.1016/j.seppur.2022.121620.

[82] Peter Nockemann, Koen Binnemans, Ben Thijs, Tatjana N. Parac-Vogt, Klaus Merz, Anja-Verena Mudring, Preethy Chirukandath Menon, Ravindran Nair Rajesh, George Cordoyiannis, Jan Thoen, Jan Leys, and Christ Glorieux. Temperature-driven mixing-demixing behavior of binary mixtures of the ionic liquid choline bis(trifluoromethylsulfonyl)imide and water. *J. Phys. Chem. B*, 113(5):1429–1437, 2009. doi: 10.1021/jp808993t.

[83] Kotoe Sasaki, Koichiro Takao, Tomoya Suzuki, Takahiro Mori, Tsuyoshi Arai, and Yasuhisa Ikeda. Extraction of Pd(II), Rh(III) and Ru(III) from HNO_3 aqueous solution to betainium bis(trifluoromethanesulfonyl)imide ionic liquid. *Dalton Trans.*, 43(15):5648–5651, 2014. doi: 10.1039/C4DT00091A.

[84] Bieke Onghena and Koen Binnemans. Recovery of Scandium(III) from Aqueous Solutions by Solvent Extraction with the Functionalized Ionic Liquid Betainium Bis(Trifluoromethylsulfonyl)Imide. *Ind. Eng. Chem. Res.*, 54(6):1887–1898, 2015. doi: 10.1021/ie504765v.

[85] Ralf Giernoth. NMR spectroscopy in ionic liquds. *Top. Curr. Chem.*, 290:263–83, 2010. doi: 10.1007/128_2008_37.

[86] Paul M Bayley, J A N Novak, and Maria Forsyth. NMR Studies of Ionic Liquids. In Natalia V. Plechkova and Kenneth R. Seddon, editors, *Ionic Liquid UnCOILed Critical Expert Overviews*, pages 13–37. John Wiley & Sons, 2012.

[87] Krishnan Damodaran. Recent NMR Studies of Ionic Liquids. *Annu. Reports NMR Spectrosc.*, 88:215–244, 2016. doi: 10.1016/bs.arnmr.2015.11.002.

[88] Viviane Overbeck and Ralf Ludwig. NMR Studies of Protic Ionic Liquids. *Annu. Reports NMR Spectrosc.*, 95:147–190, 2018. doi: 10.1016/bs.arnmr.2018.05.002.

[89] James Keeler. *Understanding NMR Spectroscopy*. Wiley, 2002.

[90] Peter Hore. *Nuclear Magnetic Resonance*. Oxford Chemistry Primers. Oxford University Press, Oxford, New York, 2 edition, 2015. ISBN 978-0-19-870341-9.

[91] Takatsugu Endo, Mamoru Imanari, Hiroko Seki, and Keiko Nishikawa. Effects of Methylation at Position 2 of Cation Ring on Rotational Dynamics of Imidazolium-Based Ionic Liquids Investigated by NMR Spectroscopy: [C $_4$ mim]Br vs [C $_4$ C $_1$ mim]Br. *The Journal of Physical Chemistry A*, 115(14):2999–3005, April 2011. ISSN 1089-5639, 1520-5215. doi: 10.1021/jp200635h.

[92] J.J. Allen, S.R. Bowser, and K. Damodaran. Molecular interactions in the ionic liquid emim acetate and water binary mixtures probed via NMR spin relaxation and exchange spectroscopy. *Physical Chemistry Chemical Physics*, 16(17):8078–8085, 2014. ISSN 1463-9076. doi: 10.1039/c3cp55384a. Cited By :23.

[93] Anne-Laure Rollet and Catherine Bessada. NMR Studies of Molten Salt and Room Temperature Ionic Liquids. *Annu. Reports NMR Spectrosc.*, 78:149–207, 2013. doi: 10.1016/B978-0-12-404716-7.00004-3.

[94] Sabine Bouguet-Bonnet, Mehdi Yemloul, and Daniel Canet. New Application of Proton Nuclear Spin Relaxation Unraveling the Intermolecular Structural Features of Low-Molecular-Weight Organogel Fibers. *Journal of the American Chemical Society*, 134(25):10621–10627, June 2012. ISSN 0002-7863. doi: 10.1021/ja303679z.

[95] F. Malz and H. Jancke. Validation of quantitative NMR. *J. Pharm. Biomed. Anal.*, 38(5): 813–823, 2005. doi: 10.1016/j.jpba.2005.01.043.

[96] Serge Akoka, Laurent Barantin, and Michel Trierweiler. Concentration Measurement by Proton NMR Using the ERETIC Method. *Anal. Chem.*, 71(13):2554–2557, 1999. doi: 10.1021/ac981422i.

[97] Nathalie Michel and Serge Akoka. The application of the ERETIC method to 2D-NMR. *J. Magn. Reson.*, 168(1):118–123, 2004. doi: 10.1016/j.jmr.2004.02.006.

[98] Luk Van Lokeren, Rainer Kerssebaum, Rudolph Willem, and Pavletta Denkova. Eretic implemented in diffusion-ordered nmr as a diffusion reference: a clarification. *Magn. Reson. Chem.*, 49(3):137–139, 2011. doi: https://doi.org/10.1002/mrc.2719.

[99] Serge Akoka and Michel Trierweiler. Improvement of the ERETIC method by digital synthesis of the signal and addition of a broadband antenna inside the NMR probe. *Instrum Sci. Technol.*, 30(1):21–29, 2002. doi: 10.1081/CI-100108768.

[100] Genoveffa Nuzzo, Carmela Gallo, Giuliana D'Ippolito, Adele Cutignano, Angela Sardo, and Angelo Fontana. Composition and quantitation of microalgal lipids by ERETIC ^{1}H NMR method. *Marine Drugs*, 11(10):3742–3753, 2013. ISSN 1660-3397. doi: 10.3390/md11103742.

[101] Pei-Lan Ding, Li-Qin Chen, Yang Lu, and Yong-Guo Li. Determination of protoberberine alkaloids in rhizoma coptidis by ERETIC 1H NMR method. *J. Pharm. Biomed. Anal.*, 60: 44–50, 2012. doi: 10.1016/j.jpba.2011.10.030.

[102] Hermann Weingärtner. NMR studies of ionic liquids: Structure and dynamics. *Curr. Opin. Colloid Interface Sci.*, 18(3):183–189, 2013. doi: 10.1016/j.cocis.2013.04.001.

[103] Ralf Giernoth, Andreas Bröhl, Martin Brehm, and Yves Lingscheid. Interactions in ionic liquids probed by in situ NMR spectroscopy. *J. Mol. Liq.*, 192:55–58, 2014. doi: 10.1016/j.molliq.2013.07.010.

[104] Albert W. Overhauser. Polarization of Nuclei in Metals. *Phys. Rev.*, 92(2):411–415, 1953. doi: 10.1103/PhysRev.92.411.

[105] Rudraksha Dutta Majumdar. *A nuclear magnetic resonance spectroscopic Investigation of the molecular structure and aggregation behavior of asphaltenes.* PhD thesis, University of Lethbridge. Faculty of Arts and Science, 2015.

[106] David Neuhaus and Michael P. Williamson. *The Nuclear Overhauser effect in structural and conformational analysis.* Methods in Stereochemical Analysis. Wiley-VCH Inc, 2000. ISBN 0-471-24675-1.

[107] Sándor Boros, Zoltán Gáspári, and Gyula Batta. Accurate NMR Determinations of Proton–Proton Distances. In *Annual Reports on NMR Spectroscopy*, volume 94, pages 1–39. Elsevier, 2018. doi: 10.1016/bs.arnmr.2017.12.002.

[108] Christian F. Pantoja, Markus Zweckstetter, and Nasrollah Rezaei-Ghaleh. Dynamical component exchange in a model phase separating system: An NMR-based approach. *Phys. Chem. Chem. Phys.*, 24(10):6169–6175, 2022. doi: 10.1039/D2CP00042C.

[109] Dheiver Santos, Maria Santos, Andersson Barison, Hasan Uslu, Dipaloy Datta, and Silvana Mattedi. Protic ionic liquid + water interactions studied by 1D NOESY NMR spectroscopy. *J. Mol. Struct.*, 1186:137–143, 2019. doi: 10.1016/j.molstruc.2019.03.017.

[110] Norman E. Heimer, Rico E. Del Sesto, and W. Robert Carper. Evidence for spin diffusion in a H,H-NOESY study of imidazolium tetrafluoroborate ionic liquids. *Magn. Reson. Chem.*, 42(1):71–75, 2004. doi: 10.1002/mrc.1318.

[111] Vanya Kurteva, Maria Atanassova, and Isabelle Billard. NMR study on the possible interactions between imidazolium based ionic liquids and extractants widely applied in solvent extraction and separation of f-ions. *J. Solution Chem.*, 44(12):2416–2430, 2015. doi: 10.1007/s10953-015-0420-3.

[112] Devendrababu Nama, P.G. Anil Kumar, Paul S. Pregosin, Tilmann J. Geldbach, and Paul J. Dyson. 1H, 19F-HOESY and PGSE diffusion studies on ionic liquids: The effect of co-solvent on structure. *Inorg. Chim. Acta*, 359(6):1907–1911, 2006. doi: 10.1016/j.ica.2005.09.015.

[113] Yves Lingscheid, Sven Arenz, and Ralf Giernoth. Heteronuclear NOE Spectroscopy of Ionic Liquids. *ChemPhysChem*, 13(1):261–266, 2012. doi: 10.1002/cphc.201100622.

[114] Tzi-Yi Wu, Hao-Cheng Wang, Shyh-Gang Su, Shr-Tusen Gung, Ming-Wei Lin, and Cheng-Bo Lin. Aggregation influence of polyethyleneglycol organic solvents with ionic liquids $BMIBF_4$ and $BMIPF_6$. *J. Chin. Chem. Soc*, 57(1):44–55, 2010. doi: 10.1002/jccs.201000008.

[115] Pierre-Alexandre Martin, Fangfang Chen, Maria Forsyth, Michaël Deschamps, and Luke A. O'Dell. Correlating Intermolecular Cross-Relaxation Rates with Distances and Coordination Numbers in Ionic Liquids. *J. Phys. Chem. Lett.*, 9(24):7072–7078, 2018. doi: 10.1021/acs.jpclett.8b03021.

[116] Charles S. Johnson. Diffusion ordered nuclear magnetic resonance spectroscopy: Principles and applications. *Prog. Nucl. Magn. Reson. Spectrosc.*, 34(3-4):203–256, 1999. doi: 10.1016/S0079-6565(99)00003-5.

[117] R. Huo, R. Wehrens, J.van Duynhoven, and L.M.C. Buydens. Assessment of techniques for DOSY NMR data processing. *Anal. Chim. Acta*, 490(1-2):231–251, 2003. doi: 10.1016/S0003-2670(03)00752-9.

[118] William S. Price. Pulsed-field gradient nuclear magnetic resonance as a tool for studying translational diffusion: Part 1. Basic theory. *Concepts Magn. Reson.*, 9:299–336, 1998. doi: 10.1002/chin.199750339.

[119] Edward O. Stejskal and John E. Tanner. Spin Diffusion Measurements: Spin Echoes in the Presence of a Time-Dependent Field Gradient. *J. Chem. Phys.*, 42(1):288–292, 1965. doi: 10.1063/1.1695690.

[120] D.H. Wu, A.D. Chen, and Charles S Johnson. An Improved Diffusion-Ordered Spectroscopy Experiment Incorporating Bipolar-Gradient Pulses. *J. Magn. Reson. A*, 115:260–264, 1995. doi: 10.1006/jmra.1995.1176.

[121] Valérie Mazan and Maria Boltoeva. Insight into the ionic interactions in neat ionic liquids by Diffusion Ordered Spectroscopy Nuclear Magnetic Resonance. *J. Mol. Liq.*, 240:74–79, 2017. doi: 10.1016/j.molliq.2017.05.021.

[122] Valérie Mazan and Maria Boltoeva. Insight into the ionic interactions in neat ionic liquids by Diffusion Ordered Spectroscopy Nuclear Magnetic Resonance. *J. Mol. Liq.*, 240:74–79, 2017. doi: 10.1016/j.molliq.2017.05.021.

[123] Valérie Mazan and Maria Boltoeva. Aqueous acidic solution - ionic liquid biphasic system: An original investigation by diffusion ordered spectroscopy nuclear magnetic resonance. *J. Mol. Liq.*, 269:684–693, 2018. doi: 10.1016/j.molliq.2018.08.086.

[124] Mehdi Yemloul, Emilie Steiner, Anthony Robert, Sabine Bouguet-Bonnet, Florent Allix, Brigitte Jamart-Grégoire, and Daniel Canet. Solvent Dynamical Behavior in an Organogel Phase As Studied by NMR Relaxation and Diffusion Experiments. *The Journal of Physical Chemistry B*, 115(11):2511–2517, March 2011. ISSN 1520-6106, 1520-5207. doi: 10.1021/jp200281f.

[125] Valérie Mazan and Maria Boltoeva. Aqueous N–H acid bis(trifluoromethylsulfonyl) imide solution - [C4mim][Tf_2N] ionic liquid biphasic system: An original investigation by diffusion ordered spectroscopy nuclear magnetic resonance. *J. Fluorine Chem.*, 245:109782, 2021. doi: 10.1016/j.jfluchem.2021.109782.

[126] Raquel V. Barrulas, Tiago G. Paiva, and Marta C. Corvo. NMR methodology for a rational selection of ionic liquids: Extracting polyphenols. *Sep. Purif. Technol.*, 221:29–37, 2019. doi: 10.1016/j.seppur.2019.03.077.

[127] Deyu Li, Ivan Keresztes, Russell Hopson, and Paul G. Williard. Characterization of Reactive Intermediates by Multinuclear Diffusion-Ordered NMR Spectroscopy (DOSY). *Acc. Chem. Res.*, 42(2):270–280, 2009. doi: 10.1021/ar800127e.

[128] Marcileia Zanatta, Víctor U. Antunes, Cláudio F. Tormena, Jairton Dupont, and Francisco P. Dos Santos. Dealing with supramolecular structure for ionic liquids: A DOSY NMR approach. *Phys. Chem. Chem. Phys.*, 21(5):2567–2571, 2019. doi: 10.1039/C8CP07071G.

[129] Claire Mantel, Pierre-Alain Bayle, Sabine Hediger, Claude Berthon, and Michel Bardet. Study of liquid-liquid interfaces by an easily implemented localized NMR sequence. *Magn. Reson. Chem.*, 48:600–606, 2010. doi: 10.1002/mrc.2628.

[130] Luiz H. K. Queiroz Júnior, Antonio G. Ferreira, and Patrick Giraudeau. Optimization and practical implementation of ultrafast 2D NMR experiments. *Quím. Nova*, 36(4):577–581, 2013. doi: 10.1590/S0100-40422013000400016.

[131] Laetitia Rouger, Benoît Charrier, Serge Akoka, and Patrick Giraudeau. Implementing ultrafast 2D NMR experiments on a bruker avance spectrometer, 2017. URL https://api.semanticscholar.org/CorpusID:24178794. CEISAM, Université de Nantes.

[132] T R Brown, B M Kincaid, and K Ugurbil. NMR chemical shift imaging in three dimensions. *Proceedings of the National Academy of Sciences*, 79(11):3523–3526, June 1982. ISSN 0027-8424, 1091-6490. doi: 10.1073/pnas.79.11.3523.

[133] Holly F. Brink, Michael D. Buschmann, and Bruce R. Rosen. NMR chemical shift imaging. *Comput. Med. Imaging Graphics*, 13(1):93–104, 1989. doi: 10.1016/0895-6111(89)90081-5.

[134] Truman R. Brown. Practical applications of chemical shift imaging. *NMR Biomed.*, 5(5): 238–243, 1992. doi: 10.1002/nbm.1940050508.

[135] Nicolas Dubouis, Chanbum Park, Michaël Deschamps, Soufiane Abdelghani-Idrissi, Matej Kanduč, Annie Colin, Mathieu Salanne, Joachim Dzubiella, Alexis Grimaud, and Benjamin Rotenberg. Chasing Aqueous Biphasic Systems from Simple Salts by Exploring the LiTFSI/LiCl/H_2O Phase Diagram. *ACS Cent. Sci.*, 5(4):640–643, 2019. doi: 10.1021/acscentsci.8b00955.

[136] Lauren E. Marbella, Stefanie Zekoll, Jitti Kasemchainan, Steffen P. Emge, Peter G. Bruce, and Clare P. Grey. ^{7}Li NMR chemical shift imaging to detect microstructural growth of lithium in all-solid-state batteries. *Chem. Mater.*, 31(8):2762–2769, 2019. doi: 10.1021/acs.chemmater.8b04875.

[137] Jörg Lambert, Roland Hergenröder, Dieter Suter, and Volker Deckert. Probing Liquid-Liquid Interfaces with Spatially Resolved NMR Spectroscopy. *Angew. Chem. Int. Ed.*, 48 (34):6343–6345, 2009. doi: 10.1002/anie.200901389.

[138] Marina M. Seitkalieva, Vadim V. Kachala, Ksenia S. Egorova, and Valentine P. Ananikov. Molecular Extraction of Peptides in Ionic Liquid Systems. *ACS Sustainable Chem. Eng.*, 3 (2):357–364, 2015. doi: 10.1021/sc500770v.

[139] Jean-Nicolas Dumez. Spatial encoding and spatial selection methods in high-resolution NMR spectroscopy. *Prog. Nucl. Magn. Reson. Spectrosc.*, 109:101–134, 2018. doi: 10.1016/j.pnmrs.2018.08.001.

[140] Y N Mitrev. Slice selective NMR approach for investigation of distribution phenomena in biphasic samples. *Bulg. Chem. Commun.*, 49:65–69, 2017.

[141] W. Kozminski. Application of Spatially Resolved NMR Spectrostopy for High Resolution Spectra of Heterogeneous Samples. *Pol. J. Chem.*, 74:1185–1189, 2000.

[142] Christian F. Pantoja, Jose A. Bolaños, Andrés Bernal, and Julien Wist. Mutual Diffusion Driven NMR: A new approach for the analysis of mixtures by spatially resolved NMR spectroscopy: Mutual Diffusion Driven NMR. *Magn. Reson. Chem.*, 55(6):519–524, 2017. doi: 10.1002/mrc.4561.

[143] Baptiste Rigaud, Imane Senoussaoui, Anne-Laure Rollet, Juliette Siriex-Plénet, and Guillaume Mériguet. Étude de l'extraction liquide-liquide d'ions métalliques par les liquides ioniques *via* la spectroscopie RMN localisée. Poster presentation, 21^{e} Congrès du GERM, Oléron, France, 2019.

[144] Christian F. Pantoja, Y. Mauricio Muñoz-Muñoz, Lorraine Guastar, Jadran Vrabec, and Julien Wist. Composition dependent transport diffusion in non-ideal mixtures from spatially resolved nuclear magnetic resonance spectroscopy. *Phys. Chem. Chem. Phys.*, 20(44):28185–28192, 2018. doi: 10.1039/C8CP05539D.

[145] Malgorzata Anna Wisniewska and John Georg Seland. Investigating structure-dependent diffusion in hydrogels using spatially resolved NMR spectroscopy. *J. Colloid Interface Sci.*, 533:671–677, 2019. doi: 10.1016/j.jcis.2018.08.112.

[146] Jörg Lambert, Roland Hergenröder, Dieter Suter, and Volker Deckert. Probing Liquid-Liquid Interfaces with Spatially Resolved NMR Spectroscopy. *Angew. Chem. Int. Ed.*, 48 (34):6343–6345, 2009. doi: 10.1002/anie.200901389.

[147] David Dupont, Daphne Depuydt, and Koen Binnemans. Overview of the Effect of Salts on Biphasic Ionic Liquid/Water Solvent Extraction Systems: Anion Exchange, Mutual Solubility, and Thermomorphic Properties. *J. Phys. Chem. B*, 119(22):6747–6757, 2015. doi: 10.1021/acs.jpcb.5b02980.

[148] Cynthia J. Hartzell, Szu-Wei Yang, Roderic A. Parnell, and David E. Morris. Sequestration of the Tributyl Phosphate Complex of Europium Nitrate in the Clay Hectorite: A ^{31}P NMR Study. *J. Phys. Chem.*, 99(12):4205–4210, 1995. doi: 10.1021/j100012a048.

[149] Boris Gouilleux, Nichlas Vous Christensen, Kirsten G. Malmos, and Thomas Vosegaard. Analytical Evaluation of Low-Field ^{31}P NMR Spectroscopy for Lipid Analysis. *Anal. Chem.*, 91(4):3035–3042, 2019. doi: 10.1021/acs.analchem.8b05416.

[150] Min Sun, Shijun Liu, Yunran Zhang, Mei Liu, Xin Yi, and Jiugang Hu. Insights into the saponification process of di(2-ethylhexyl) phosphoric acid extractant: Thermodynamics and structural aspects. *J. Mol. Liq.*, 280:252–258, April 2019. ISSN 01677322. doi: 10.1016/j.molliq.2019.02.025.

[151] Deepak U. Bapat and Vishwanath H. Dalvi. Molecular Insights into Water Clusters Formed in Tributylphosphate–Di-(2-ethylhexyl)phosphoric Acid Extractant Systems from Experiments and Molecular Dynamics Simulations. *J. Phys. Chem. B*, 123(7):1618–1635, 2019. doi: 10.1021/acs.jpcb.8b10831.

[152] Po-Ching Lee, Chi-Wang Li, Jie-Yuan Chen, Ying-Sheng Li, and Shiao-Shing Chen. Dissolution of D2EHPA in liquid–liquid extraction process: Implication on metal removal and organic content of the treated water. *Water Res.*, 45(18):5953–5958, November 2011. ISSN 00431354. doi: 10.1016/j.watres.2011.08.054.

[153] Brevard Christian and Granger Pierre. *Handbook of high resolution multinuclear NMR*. John Wiley & Sons, 1981.

[154] Antonio De Souza Braga Neto, Baptiste Rigaud, Guillaume Mériguet, Anne-laure Rollet, and Juliette Sirieix-Plénet. Efficient method for in situ agitation of liquids directly inside NMR spectrometer. *MethodsX*, 11(June):102254, 2023. doi: 10.1016/j.mex.2023.102254.

[155] Mara G. Freire, Pedro J. Carvalho, Ramesh L. Gardas, Isabel M. Marrucho, Luís M. N. B. F. Santos, and João A. P. Coutinho. Mutual Solubilities of Water and the $[C_n mim][Tf_2N]$ Hydrophobic Ionic Liquids. *J. Phys. Chem. B*, 112(6):1604–1610, 2008. doi: 10.1021/jp7097203.

[156] Merinda F. Volia, Evgeny E. Tereshatov, Valérie Mazan, Charles M. Folden, and Maria Boltoeva. Effect of aqueous hydrochloric acid and zwitterionic betaine on the mutual solubility between a protic betainium-based ionic liquid and water. *J. Mol. Liq.*, 276:296–306, 2019. doi: 10.1016/j.molliq.2018.11.136.

[157] Christian F. Pantoja, Jose A. Bolaños, Andrés Bernal, and Julien Wist. Mutual Diffusion Driven NMR: A new approach for the analysis of mixtures by spatially resolved NMR spectroscopy: Mutual Diffusion Driven NMR. *Magn. Reson. Chem.*, 55(6):519–524, 2017. doi: 10.1002/mrc.4561.

[158] Chenglong Shi, Hongxia Li, Bing Liu, Yaru Qin, and Guixiu Song. Solvent extraction of lithium from aqueous solution using an ammonium ionic liquid. *J. Mol. Liq.*, 304:112756, 2020. doi: 10.1016/j.molliq.2020.112756.

[159] Basudev Swain. Recovery and recycling of lithium: A review. *Sep. Purif. Technol.*, 172: 388–403, 2017. doi: 10.1016/j.seppur.2016.08.031.

[160] Ya Li, Jiugang Hu, Mingbo Fu, Jia Tang, Linlin Dong, and Shijun Liu. Investigation of intermolecular interactions of mixed extractants of quaternary phosphonium or ammonium chlorides and bis(2,4,4-ethylhexyl)phosphoric acid for metal separation. *RSC Advances*, 6 (62):56772–56779, 2016. ISSN 2046-2069. doi: 10.1039/C6RA07813C.

[161] Xiaoqi Sun and Kristian E. Waters. Development of Industrial Extractants into Functional Ionic Liquids for Environmentally Friendly Rare Earth Separation. *ACS Sustainable Chem. Eng.*, 2(7):1910–1917, 2014. doi: 10.1021/sc500255n.

[162] Kikuko Hayamizu, Yuichi Aihara, Hiroe Nakagawa, Toshiyuki Nukuda, and William S. Price. Ionic conduction and ion diffusion in binary room-temperature ionic liquids composed of [emim][bf4] and libf4. *J. Phys. Chem. B*, 108(50):19527–19532, 2004. doi: 10.1021/jp0476601.

[163] Isabella Nicotera, Cesare Oliviero, Wesley A. Henderson, Giovanni B. Appetecchi, and Stefano Passerini. NMR Investigation of Ionic Liquid-LiX Mixtures: Pyrrolidinium Cations and $TFSI^-$ Anions. *J. Phys. Chem. B*, 109(48):22814–22819, 2005. doi: 10.1021/jp053799f.

[164] Yuria Saito, Tatsuya Umecky, Junichi Niwa, Tetsuo Sakai, and Seiji Maeda. Existing condition and migration property of ions in lithium electrolytes with ionic liquid solvent. *J. Phys. Chem. B*, 111(40):11794–11802, 2007. doi: 10.1021/jp072998r.

[165] Kikuko Hayamizu, Seiji Tsuzuki, Shiro Seki, Yasutaka Ohno, Hajime Miyashiro, and Yo Kobayashi. Quaternary ammonium room-temperature ionic liquid including an oxygen atom in side chain/lithium salt binary electrolytes: Ionic conductivity and ^1H, ^7Li, and ^{19}F NMR studies on diffusion coefficients and local motions. *J. Phys. Chem. B*, 112(4): 1189–1197, 2008. doi: 10.1021/jp077714h.

[166] Marcelo J. Monteiro, Fernanda F. C. Bazito, Leonardo J. A. Siqueira, Mauro C. C. Ribeiro, and Roberto M. Torresi. Transport coefficients, raman spectroscopy, and computer simulation of lithium salt solutions in an ionic liquid. *J. Phys. Chem. B*, 112(7):2102–2109, 2008. doi: 10.1021/jp077026y. URL https://doi.org/10.1021/jp077026y. PMID: 18220384.

[167] Seiji Tsuzuki, Kikuko Hayamizu, and Shiro Seki. Origin of the low-viscosity of [emim][(fso2)2n] ionic liquid and its lithium salt mixture: Experimental and theoretical study of self-diffusion coefficients, conductivities, and intermolecular interactions. *J. Phys. Chem. B*, 114(49):16329–16336, 2010. doi: 10.1021/jp106870v. PMID: 21080680.

[168] My Loan Phung Le, Fannie Alloin, Pierre Strobel, Jean-Claude Leprêtre, Carlos Pérez del Valle, and Patrick Judeinstein. Structure-properties relationships of lithium electrolytes based on ionic liquid. *J. Phys. Chem. B*, 114(2):894–903, 2010. doi: 10.1021/jp9098842. URL https://doi.org/10.1021/jp9098842. PMID: 20039688.

[169] Marcelo J. Monteiro, Fernanda F. Camilo, Mauro C. C. Ribeiro, and Roberto M. Torresi. Ether-bond-containing ionic liquids and the relevance of the ether bond position to transport properties. *J. Phys. Chem. B*, 114(39):12488–12494, 2010. doi: 10.1021/jp104419k. URL https://doi.org/10.1021/jp104419k. PMID: 20839836.

[170] C. J. F. Solano, S. Jeremias, E. Paillard, D. Beljonne, and R. Lazzaroni. A joint theoretical/experimental study of the structure, dynamics, and Li+ transport in bis([tri]fluoro[methane]sulfonyl)imide [T]FSI-based ionic liquids. *J. Chem. Phys.*, 139(3): 034502, 07 2013. doi: 10.1063/1.4813413.

[171] Hassan Srour, Mounir Traïkia, Bernard Fenet, Hélène Rouault, Margarida F Costa Gomes, Catherine C. Santini, and Pascale Husson. Effect of nitrile-functionalization of imidazolium-based ionic liquids on their transport properties, both pure and mixed with lithium salts. *Journal of Solution Chemistry*, 44(3):495–510, 2015. doi: 10.1007/s10953-014-0280-2. URL https://doi.org/10.1007/s10953-014-0280-2.

[172] Patrick Judeinstein, Mehdi Zeghal, Doru Constantin, Cristina Iojoiu, and Benoit Coasne. Interplay of structure and dynamics in lithium/ionic liquid electrolytes: Experiment and molecular simulation. *J. Phys. Chem. B*, 125(6):1618–1631, 2021. doi: 10.1021/acs.jpcb.0c09597. URL https://doi.org/10.1021/acs.jpcb.0c09597. PMID: 33535754.

[173] H. P. Khanh Ngo, E. Planes, C. Iojoiu, P. Soudant, A.-L. Rollet, and P. Judeinstein. Transport properties of alkali/alkaline earth cations in ionic-liquid based electrolytes. *J. Ionic Liq.*, 2(2):100044, 2022. doi: https://doi.org/10.1016/j.jil.2022.100044.

[174] Tzi-Yi Wu, Lin Hao, Chung-Wen Kuo, Yuan-Chung Lin, Shyh-Gang Su, Ping-Lin Kuo, and I-Wen Sun. Ionic conductivity and diffusion in lithium tetrafluoroborate-doped 1-methyl-3-pentylimidazolium tetrafluoroborate ionic liquid. *Int. J. Electrochem. Sci.*, 7(3):2047–2064, 2012. doi: https://doi.org/10.1016/S1452-3981(23)13862-4.

[175] Luis Aguilera, Shizhao Xiong, Johan Scheers, and Aleksandar Matic. A structural study of LiTFSI–tetraglyme mixtures: From diluted solutions to solvated ionic liquids. *Journal of Molecular Liquids*, 210:238–242, October 2015. ISSN 01677322. doi: 10.1016/j.molliq.2015.04.053.

[176] Moon Young Yang, Boris V. Merinov, Sergey V. Zybin, William A. Goddard III, Eun Kyung Mok, Hoe Jin Hah, Hyea Eun Han, Young Cheol Choi, and Seung Ha Kim. Transport properties of imidazolium based ionic liquid electrolytes from molecular dynamics simulations. *Electrochem. Sci. Adv.*, 2(2):e2100007, 2022. doi: https://doi.org/10.1002/elsa.202100007.

[177] Xinming Xu, Long Su, Fei Lu, Zuobing Yin, Yanan Gao, Liqiang Zheng, and Xinpei Gao. Unraveling anion effect on lithium ion dynamics and interactions in concentrated ionic liquid electrolyte. *J. Mol. Liq.*, 361:119629, 2022. ISSN 0167-7322. doi: 10.1016/j.molliq.2022.119629.

[178] Keigo Kubota, Zyun Siroma, Hikaru Sano, Susumu Kuwabata, and Hajime Matsumoto. Diffusion of lithium cation in low-melting lithium molten salts. *The Journal of Physical Chemistry C*, 122(8):4144–4149, 2018. doi: 10.1021/acs.jpcc.7b11281. URL https://doi.org/10.1021/acs.jpcc.7b11281.

[179] Jean-Pierre Korb. Multiscale nuclear magnetic relaxation dispersion of complex liquids in bulk and confinement. *Progress in Nuclear Magnetic Resonance Spectroscopy*, 104:12–55, 2018. ISSN 0079-6565. doi: https://doi.org/10.1016/j.pnmrs.2017.11.001. URL https://www.sciencedirect.com/science/article/pii/S0079656517300353.

[180] Rainer Kimmich. *NMR Tomography, Diffusometry, Relaxometry*. Springer Berlin Heidelberg, 1997. ISBN 978-3-642-64465-8. doi: 10.1007/978-3-642-60582-6.

[181] Anne-Laure Rollet, Stéphanie Godier, and Catherine Bessada. High temperature nmr study of the local structure of molten laf3–af (a = li, na, k and rb) mixtures. *Phys. Chem. Chem. Phys.*, 10:3222–3228, 2008. doi: 10.1039/B719158H. URL http://dx.doi.org/10.1039/B719158H.

[182] Anne-Laure Rollet and Mathieu Salanne. Studies of the local structures of molten metal halides. *Annu. Rep. Prog. Chem., Sect. C: Phys. Chem.*, 107:88–123, 2011. doi: 10.1039/C1PC90003J. URL http://dx.doi.org/10.1039/C1PC90003J.

[183] N. Bloembergen, E. M. Purcell, and R. V. Pound. Relaxation Effects in Nuclear Magnetic Resonance Absorption. *Physical Review*, 73(7):679–712, April 1948. ISSN 0031-899X. doi: 10.1103/PhysRev.73.679.

[184] Helena Passos, Teresa B. V. Dinis, Emanuel V. Capela, Maria V. Quental, Joana Gomes, Judite Resende, Pedro P. Madeira, Mara G. Freire, and João A. P. Coutinho. Mechanisms ruling the partition of solutes in ionic-liquid-based aqueous biphasic systems – the multiple effects of ionic liquids. *Physical Chemistry Chemical Physics*, 20(13):8411–8422, 2018. ISSN 1463-9076, 1463-9084. doi: 10.1039/C8CP00383A.

[185] Maria Enrica Di Pietro, Mariagrazia Tortora, Cettina Bottari, Greta Colombo Dugoni, Roberto Vittorio Pivato, Barbara Rossi, Marco Paolantoni, and Andrea Mele. In Competition for Water: Hydrated Choline Chloride:Urea vs Choline Acetate:Urea Deep Eutectic Solvents. *ACS Sustainable Chem. Eng.*, 9(36):12262–12273, 2021.

[186] Emmanouil Veroutis, Steffen Merz, Rüdiger A. Eichel, and Josef Granwehr. Intra- and inter-molecular interactions in choline-based ionic liquids studied by 1D and 2D NMR. *J. Mol. Liq.*, 322:114934, 2021. doi: 10.1016/j.molliq.2020.114934.

[187] Masaru Matsugami, Ryohei Yamamoto, Takashi Kumai, Miho Tanaka, Tatsuya Umecky, and Toshiyuki Takamuku. Hydrogen bonding in ethanol–water and trifluoroethanol–water mixtures studied by NMR and molecular dynamics simulation. *J. Mol. Liq.*, 217:3–11, 2016. doi: 10.1016/j.molliq.2015.06.050.

[188] Michael Di Gioacchino, Fabio Bruni, and Maria Antonietta Ricci. Aqueous solution of betaine: Hydration and aggregation. *J. Mol. Liq.*, 318:114253, 2020. doi: 10.1016/j.molliq.2020.114253.

[189] Thomas C. W. Mak. Crystal structure of betaine monohydrate, $(CH_3)_3NCH_2COO{\cdot}H_2O$. *J. Mol. Struct.*, 220:13–18, 1990. doi: 10.1016/0022-2860(90)80095-2.

[190] Ida Zahrina, Kamarza Mulia, Arry Yanuar, and Mohammad Nasikin. Molecular interactions in the betaine monohydrate-polyol deep eutectic solvents: Experimental and computational studies. *J. Mol. Struct.*, 1158:133–138, 2018. doi: 10.1016/j.molstruc.2017.11.064.

[191] William M. Haynes. *CRC Handbook of Chemistry and Physics*. CRC Press, 2014. ISBN 978-1-4822-0868-9.

[192] Tatsuya Umecky, Toshiyuki Takamuku, Tomoya Matsumoto, Eiji Kawai, Masaya Takagi, and Toshitaka Funazukuri. Effects of Dissolved Water on Li^+ Solvation in 1-Ethyl-3-methylimidazolium Bis(trifluoromethanesulfonyl)amide Ionic Liquid Studied by NMR. *J. Phys. Chem. B*, 117(50):16219–16226, 2013. doi: 10.1021/jp409324k.

[193] Alain Chaumont and Georges Wipff. Solvation of Uranyl(II) and Europium(III) Cations and Their Chloro Complexes in a Room-Temperature Ionic Liquid. A Theoretical Study of the Effect of Solvent "Humidity". *Inorg. Chem.*, 43(19):5891–5901, 2004. doi: 10.1021/ic049386v.

[194] Peter Nockemann, Ben Thijs, Tatjana N. Parac-Vogt, Kristof Van Hecke, Luc Van Meervelt, Bernard Tinant, Ingo Hartenbach, Thomas Schleid, Vu Thi Ngan, Minh Tho Nguyen, and Koen Binnemans. Carboxyl-Functionalized Task-Specific Ionic Liquids for Solubilizing Metal Oxides. *Inorg. Chem.*, 47(21):9987–9999, 2008. doi: 10.1021/ic801213z.

[195] J. Jacquemin, P. Husson, A. A. H. Padua, and V. Majer. Density and viscosity of several pure and water-saturated ionic liquids. *Green Chem.*, 8(2):172–180, 2006. doi: 10.1039/B513231B.

[196] Maria Enrica Di Pietro, Kateryna Goloviznina, Adriaan Van Den Bruinhorst, Giselle De Araujo Lima E Souza, Margarida Costa Gomes, Agilio A. H. Padua, and Andrea Mele. Lithium Salt Effects on the Liquid Structure of Choline Chloride–Urea Deep Eutectic Solvent. *ACS Sustainable Chem. Eng.*, 10(36):11835–11845, 2022. doi: 10.1021/acssuschemeng.2c02460.

[197] Charles S. Johnson. Effects of Chemical Exchange in Diffusion-Ordered 2D NMR Spectra. *J. Magn. Reson., Ser. A*, 102(2):214–218, 1993. doi: 10.1006/jmra.1993.1093.

[198] Koji Saihara, Yukihiro Yoshimura, Soichi Ohta, and Akio Shimizu. Properties of Water Confined in Ionic Liquids. *Sci. Rep.*, 5(1):10619, 2015. doi: 10.1038/srep10619.

[199] Juan A. Aguilar, Ralph W. Adams, Mathias Nilsson, and Gareth A. Morris. Suppressing exchange effects in diffusion-ordered NMR spectroscopy. *J. Magn. Reson.*, 238:16–19, 2014. doi: 10.1016/j.jmr.2013.10.018.

[200] Carter W. Abney, Changwoo Do, Huimin Luo, Joshua Wright, Lilin He, and Sheng Dai. Controlling the Intermediate Structure of an Ionic Liquid for f-Block Element Separations. *The Journal of Physical Chemistry Letters*, 8(9):2049–2054, May 2017. ISSN 1948-7185, 1948-7185. doi: 10.1021/acs.jpclett.7b00755.

[201] Junpei Takeda, Yasunori Iwao, Masatoshi Karashima, Katsuhiko Yamamoto, and Yukihiro Ikeda. Structural Evaluation of the Choline and Geranic Acid/Water Complex by SAXS and NMR Analyses. *ACS Biomaterials Science & Engineering*, 7(2):595–604, February 2021. ISSN 2373-9878, 2373-9878. doi: 10.1021/acsbiomaterials.0c01324.

[202] R. Mhanna, R. Lefort, L. Noirez, and D. Morineau. Microstructure and concentration fluctuations in alcohol–Toluene and alcohol-Cyclohexane binary liquids: A small angle neutron scattering study. *Journal of Molecular Liquids*, 218:198–207, June 2016. ISSN 01677322. doi: 10.1016/j.molliq.2016.02.070.

[203] Nandhibatla V. Sastry, Nilesh M. Vaghela, Pradip M. Macwan, Saurabh S. Soni, Vinod K. Aswal, and Alain Gibaud. Aggregation behavior of pyridinium based ionic liquids in water – Surface tension, 1H NMR chemical shifts, SANS and SAXS measurements. *Journal of Colloid and Interface Science*, 371(1):52–61, April 2012. ISSN 00219797. doi: 10.1016/j.jcis.2011.12.077.

[204] Sylvain Prevost, Tobias Lopian, Maximilian Pleines, Olivier Diat, and Thomas Zemb. Small-angle scattering and morphologies of ultra-flexible microemulsions. *J. Appl. Crystallogr.*, 49 (6):2063–2072, 2016. doi: 10.1107/S1600576716016150.

[205] Leonard Salomon Ornstein and Frederik Zernike. Accidental deviations of density and opalescence at the critical point of a single substance. *Proc. K. Ned. Akad. van Wet.*, XVII(2):793–806, 1914.

[206] Alessio Sferrazza, Alessandro Triolo, Luisa M. Migneco, and Ruggero Caminiti. Synthesis and Small and Wide Angle X-Ray Scattering Characterization of L-Proline Based Chiral Ionic Liquids. *Curr. Org. Chem.*, 19(1):99–104, 2015. doi: 10.2174/1385272819666141211221640.

[207] T. Sukhbaatar, S. Dourdain, R. Turgis, J. Rey, G. Arrachart, and S. Pellet-Rostaing. Ionic liquids as diluents in solvent extraction: First evidence of supramolecular aggregation of a couple of extractant molecules. *Chem. Commun.*, 51(88):15960–15963, 2015. doi: 10.1039/C5CC06422H.

[208] André Guinier. La diffusion des rayons X sous les très faibles angles appliquée à l'étude de fines particules et de suspensions colloidales. *C.R. Hebd. Seances Acad. Sci.*, 206:1374–1376, 1938.

[209] Giovanni D'Arrigo and José Teixeira. Small-angle neutron scattering study of D $_2$ O–alcohol solutions. *J. Chem. Soc., Faraday Trans.*, 86(9):1503–1509, 1990. ISSN 0956-5000, 1364-5455. doi: 10.1039/FT9908601503.

[210] Ch. Venkateswara Rao, Alok Rout, and K. A. Venkatesan. Aggregation behavior of ionic liquid in molecular liquid medium: A dynamic light scattering study. *Separation Science and Technology*, 56(4):757–765, March 2021. ISSN 0149-6395. doi: 10.1080/01496395.2020.1734621.

[211] Sébastien Le Crom, Sandrine Dourdain, Stéphane Pellet-Rostaing, and Magali Duvail. Exploring the Aggregation Behavior of Extractant Molecules in Ionic Liquids: A Coupled Polarizable Molecular Dynamics and SAXS Study. *J. Phys. Chem. B*, 127(28):6408–6420, 2023. doi: 10.1021/acs.jpcb.3c02524.

[212] Patrick Baldoni-Andrey, Matthieu Jacob, Pierre Pedenaud, Guillaume De Souza, Pierre Callaud, and Bastien Dautriche. Breakthrough Technology for Produced Water Desalination. In *Day 3 Wed, November 09, 2016*, page D031S061R003, Abu Dhabi, UAE, 2016. SPE. doi: 10.2118/183131-MS.

[213] GeoLith's Li-Capt technology ensures zero-emission lithium extraction, 2022.

[214] Green and Clean Technology - Adionics. https://www.adionics.com/technology/, 2022.

[215] Kotoe Sasaki, Tomoya Suzuki, Takahiro Mori, Tsuyoshi Arai, Koichiro Takao, and Yasuhisa Ikeda. Selective Liquid–Liquid Extraction of Uranyl Species Using Task-specific Ionic Liquid, Betainium Bis(trifluoromethylsulfonyl)imide. *Chem. Lett.*, 43(6):775–777, 2014. doi: 10.1246/cl.140048.

[216] Christopher R. Day and Stephen A. Kempson. Betaine chemistry, roles, and potential use in liver disease. *Biochim. Biophys. Acta - General Subjects*, 1860(6):1098–1106, 2016. doi: 10.1016/j.bbagen.2016.02.001.

[217] W. A. Spieker, Jingjing Liu, Jeffrey T. Miller, Arthur Jeremy Kropf, and John R. Regalbuto. An EXAFS study of the co-ordination chemistry of hydrogen hexachloroplatinate(IV): 1. Speciation in aqueous solution. *Appl. Catal. A*, 232(1):219–235, 2002. doi: 10.1016/S0926-860X(02)00116-3.

[218] N. M. Rice, H. M.N.H. Irving, and M. A. Leonard. Nomenclature for liquid-liquid distribution (solvent extraction). *Pure Appl. Chem.*, 65(11):2373–2396, 1993. doi: 10.1351/pac199365112373.

[219] Mehrazin Omrani, Mathieu Goriaux, Yao Liu, Simon Martinet, Liliane Jean-Soro, and Véronique Ruban. Platinum group elements study in automobile catalysts and exhaust gas samples. *Environ. Pollut.*, 257:113477, 2020. doi: 10.1016/j.envpol.2019.113477.

[220] Brett M. Still, P. G. Anil Kumar, Janice R. Aldrich-Wright, and William S. Price. ^{195}Pt NMR—theory and application. *Chem. Soc. Rev.*, 36(4):665–686, 2007. doi: 10.1039/B606190G.

[221] Paul S. Pregosin. Platinum-195 nuclear magnetic resonance. *Coord. Chem. Rev.*, 44(2):247–291, 1982. doi: 10.1016/S0010-8545(00)80523-8.

[222] Jurjen Kramer and Klaus R. Koch. ^{195}Pt NMR Study of the Speciation and Preferential Extraction of Pt(IV)-Mixed Halide Complexes by Diethylenetriamine-Modified Silica-Based Anion Exchangers. *Inorg. Chem.*, 45(19):7843–7855, 2006. doi: 10.1021/ic0609655.

[223] Peter Nockemann, Ben Thijs, Kristof Van Hecke, Luc Van Meervelt, and Koen Binnemans. Polynuclear Metal Complexes Obtained from the Task-Specific Ionic Liquid Betainium Bistriflimide. *Cryst. Growth Des.*, 8(4):1353–1363, 2008. doi: 10.1021/cg701187t.

[224] José O. Hernandez and Eduardo A. Choren. Thermal stability of some platinum complexes. *Thermochim. Acta*, 71(3):265–272, 1983. doi: 10.1016/0040-6031(83)80059-8.

[225] A. K. Johnson and J. D. Miller. A kinetic study of the substitution reactions of the tetrachloroplatinate(II) ion with water and acetonitrile. *Inorg. Chim. Acta*, 16:93–96, 1976. doi: 10.1016/S0020-1693(00)91696-7.

[226] Hannes Aiginger and Peter Wobrauschek. A method for quantitative X-ray fluorescence analysis in the nanogram region. *Nucl. Instruments Methods*, 114(1):157–158, jan 1974. doi: 10.1016/0029-554X(74)90352-8.

[227] Reinhold Klockenkämper, Joachim Knoth, Andreas Prange, and Heinrich Schwenke. Total-reflection X-ray fluorescence spectroscopy. *Anal. Chem.*, 64(23):1115A–1123A, 1992. doi: 10.1021/ac00047a717.

[228] Sofía Riaño, Mercedes Regadío, Koen Binnemans, and Tom Vander Hoogerstraete. Practical guidelines for best practice on Total Reflection X-ray Fluorescence spectroscopy: Analysis of aqueous solutions. *Spectrochim. Acta Part B At. Spectrosc.*, 124:109–115, 2016. doi: 10.1016/j.sab.2016.09.001.

[229] Reinhold Klockenkämper and Alex von Bohlen. Fundamentals of X-Ray Fluorescence. In Reinhold Klockenkämper and Alex Von Bohlen, editors, *Total-Reflection X-Ray Fluorescence Analysis and Related Methods*, pages 1–78. John Wiley & Sons, Inc., Hoboken, New Jersey, December 2014. ISBN 978-1-118-98595-3 978-1-118-46027-6. doi: 10.1002/9781118985953.ch01.

Résumé : L'augmentation constante de la demande et du risque d'approvisionnement en métaux critiques encourage les efforts d'innovation en matière de recyclage. Ces métaux sont essentiels à la fonctionnalité des technologies vertes émergentes et présentent un risque d'approvisionnement. Par exemple, le lithium (Li) est essentiel à la production de batteries et sa demande tend à augmenter considérablement au cours des prochaines décennies. Le platine (Pt) est un métal précieux et stratégique du groupe du platine (MGP) qui est largement utilisé comme catalyseur dans l'industrie automobile pour le contrôle des émissions dans les convertisseurs catalytiques, ainsi que dans l'aviation, l'industrie pharmaceutique et plusieurs autres applications. Le recyclage des métaux critiques par voie hydométallurgique s'effectue principalement par une succession d'étapes : la lixiviation, l'extraction liquide-liquide et la récupération. L'extraction liquide-liquide est la répartition de solutés entre deux liquides non miscibles en contact. Les procédés industriels actuels utilisent de grandes quantités de solvants organiques volatils toxiques et d'extractants. Les liquides ioniques (LIs) représentent une alternative intéressante à ces solvants, au vu de leur faible pression de vapeur malgré leur viscosité élevée. Toutefois, les mécanismes d'extraction utilisant les liquides ioniques sont encore mal compris . La plupart des études sur le processus d'extraction liquide-liquide sont basées sur des techniques analytiques qui s'effectuent sur chacune des phases avant et après extraction et se focalisent principalement sur les espèces métalliques. L'extraction homogène liquide-liquide (HLLE) est une application des IL thermomorphiques. Ce processus tire parti de ces liquides, qui présentent un comportement de miscibilité avec les solutions aqueuses en fonction de la température. À l'état homogène, l'interface disparaît, il n'y a donc plus de barrière de diffusion lors de l'extraction. Ce travail se concentre sur les HLLE du lithium et du platine mais aussi sur la compréhension du mécanisme mis en jeu. Deux liquides ioniques thermomorphiques, le bis(trifluorométhylsulfonyl)imide de cholinium [Chol][TFSI] et le bis(trifluorométhylsulfonyl)imide de bétaïne [Hbet][TFSI], sont utilisés pour l'extraction de ces métaux. La spectroscopie RMN a été employée pour déterminer la spéciation des phases en contact et pour mesurer les concentrations dans le milieu et à l'interface, en utilisant la spectroscopie localisée (LOCSY). Celle-ci est aussi utilisée pour étendre la compréhension du processus d'extraction liquide-liquide puisque cette technique permet d'observer in situ les différentes espèces présentes dans le système, telles que l'extractant, le cation et l'anion du LI, et certain métaux en suivant différents noyaux, tels que 1H, 19F, 7Li et 195Pt. En outre, les interactions entre les espèces et les processus de diffusion ont également été étudiés par des expériences spécifiques telles que NOESY/HOESY, qui détectent les interactions entre les atomes proches dans l'espace mais non liés, et DOSY, qui détermine les coefficients de diffusion. Simultanément, les paramètres clés de l'efficacité de l'extraction liquide-liquide, tels que la concentration de l'extractant, le rapport de phase, la concentration en métal sont explorés. Cette approche permet d'approfondir la compréhension globale du processus de l'extraction dans les liquides ioniques.

Abstract: The constant increase in critical metals demand and supply risk promotes innovation efforts toward recycling. These metals are essential to the functionality of emerging green technologies and present a supply risk. For instance, lithium is essential for battery production, and its demand tends to increase considerably in the coming decades. Platinum is a precious and strategic platinum-group metal (PGM) that is extensively employed as a catalyst in the automotive industry for emission control in catalytic converters and also in aviation, the pharmaceutical industry, and several other applications. The hydrometallurgical recycling of critical metals is mainly carried out by a succession of stages: leaching, liquid-liquid extraction, and recovery. Liquid-liquid extraction is the distribution of solutes between two immiscible liquids in contact. The current industrial processes use large amounts of toxic volatile organic solvents and extractants. Ionic liquids (ILs) are a valuable alternative to replace volatile organic solvents since they are less toxic, flammable, and volatile than conventional solvents, although they can present high viscosity. However, the extraction mechanisms are not fully understood. Also, most studies of the liquid-liquid extraction process are based on analytical techniques used before and after extraction process and that focus mainly on the metallic species. Homogeneous liquid-liquid extraction (HLLE) is an application of thermomorphic ILs. This process takes advantage of these liquids, which exhibit temperature-dependent miscibility behavior with aqueous solutions. In the homogeneous state, the interface disappears, and there is no diffusion barrier for extraction. This work focuses on lithium and platinum HLLE and understanding the mechanism involved . Two thermomorphic ionic liquids, cholinium bis(trifluoromethylsulfonyl)imide [Chol][TFSI] and betaine bis(trifluoromethylsulfonyl)imide [Hbet][TFSI], are examined for the extraction of these metals. NMR spectroscopy bridges the knowledge gap in the liquid-liquid extraction process. This technique enables the observation of different species in the system, such as the extractant, the IL's cation, anion, and some metals, by tracking various nuclei, such as 1H, 19F, 7Li, and 195Pt. This allows for a better understanding of the system's composition, interactions between species, speciation, and more. Specifically, an NMR LOcalized SpectroscopY sequence (LOCSY) is employed to track the species' evolution, including their concentration in the bulk, speciation, and diffusion. To examine the system's dynamics and the molecular environment of the involved species, Diffusion Ordered Spectroscopy (DOSY) is applied to measure diffusion coefficients. NOESY and HOESY (Nuclear and Heteronuclear Overhauser Effect SpectroscopY) techniques capture through-space proximities between nuclei, furthering our understanding of the extraction mechanism. This allows observation of the interactions, providing insight into how these metals are extracted within the ionic liquids. Simultaneously, critical parameters impacting liquid-liquid extraction efficiencies, such as extractant concentration, phase ratio, and metal concentration, are explored. This comprehensive approach deepens our understanding of the extraction process into ionic liquids.